The soft-tissue restraints of the knee and its balancing capacity in total knee arthroplasty procedures

Von der Fakultät für Maschinenbau
der Gottfried Wilhelm Leibniz Universität Hannover
zur Erlangung des akademischen Grades
Doktor-Ingenieur
genehmigte Dissertation

von

Manuel Ferle, M.Sc.

2020

1. Referent: Prof. Dr.-Ing. Tobias Ortmaier
2. Referent: Prof. Dr.-Ing. Christof Hurschler

Tag der Promotion: 9.07.2020

Danksagung

Die vorliegende Arbeit entstand während meiner Tätigkeit als wissenschaftlicher Mitarbeiter im Labor für Biomechanik und Biomaterialien der Medizinischen Hochschule Hannover (MHH). An dieser Stelle möchte ich mich zunächst für die finanzielle Unterstützung der Deutschen Forschungsgemeinschaft vielmals bedanken. Mein besonderer Dank gilt Herrn Prof. Dr.-Ing. Christof Hurschler für seine Unterstützung und für die Möglichkeit mich auf dem Gebiet der orthopädischen Biomechanik stets völlig frei zu entwickeln. Zudem möchte ich mich gerne bei Herrn Prof. Dr.-Ing. Tobias Ortmaier für die wissenschaftliche Betreuung von Seiten der Leibniz Universität Hannover und die freundlichen, beratenden Gespräche bedanken.

Allen meinen ehemaligen KollegInnen aus dem Labor für Biomechanik und Biomaterialien sowie aus der orthopädischen Klinik der MHH am Annastift danke ich für die vertrauensvolle Zusammenarbeit der vergangenen Jahre. Besondere Erwähnung möchte ich noch für meine ehemaligen Bürokollegen Michael Schwarze und Bastian Welke finden, die mir für einen fachlichen Diskurs jederzeit zur Verfügung standen und wesentlich dazu beitrugen, dass der Spaß während der Arbeit nicht zu kurz kam.

Die vorliegende Dissertation hätte nicht gelingen können, ohne die starke seelische Unterstützung von Seiten meiner Familie. Dabei haben vor allem meine Frau Mariam Ferle und meine Tochter Flora gezeigt, was Opferbereitschaft heißt. Vielen lieben Dank für die Geduld, die immer wieder richtigen Worte wenn etwas einmal nicht so lief wie es sollte und das intensive, immer präsente Wir-Gefühl.

Zum Schluss möchte ich mich noch bei meinen Eltern Sonja und Alois Krämer bedanken. Bei allen Entscheidungen die ich auf dem Weg bis zum Abschluss dieser Arbeit gefällt habe, brachten sie mir stets tiefes Vertrauen entgegen. Ihr habt den Grundstein für diese Arbeit gelegt, vielen Dank.

Rosenheim, Juli 2020

Manuel Ferle

Zusammenfassung

Die totale Kniearthroplastik ist ein erfolgreiches operatives Behandlungsverfahren bei Patienten mit schwerer Kniegelenksarthrose. Dabei stellt die Wiederherstellung der Weichteilfunktion eine große Herausforderung dar. Abhängig von der Positionierung der Prothese, dem Implantationsverfahren und der Pathologie des Patienten ist eine Anpassung der Weichteilstrukturen erforderlich, um die Funktion des Kniegelenkes wieder herzustellen. Die Beurteilung und Anpassung des Weichteilmantels, das sogenannte Weichteilbalancing, stellt dabei einen subjektiven Prozess dar, der stark vom Operateur abhängig ist.

Die vorliegende Dissertation adressiert diese Herausforderungen und beschreibt basierend auf einer Meta-Analyse zur Nachgiebigkeit des natürlichen Kniegelenks quantitative Leitlinien für das Weichteilmanagement. Ein weiteres Ziel war zudem im Rahmen von *in-vitro* Untersuchungen zu klären, inwieweit das Lösen und Entfernen einzelner Weichteilstrukturen die Gelenknachgiebigkeit verändert und in welchem Maße ein Knie durch gezielte Resektion von Weichteilstrukturen balanciert werden kann. Darüber hinaus bilden *in-silico* Untersuchungen im Rahmen dieser Arbeit die Grundlage für ein numerisches Werkzeug, um die Funktion der Bänder besser zu verstehen und das Weichteilbalancing in Zukunft präoperativ besser planen zu können.

Die Untersuchungen der natürlichen Nachgiebigkeit des Kniegelenkes in verschiedenen Beugestellungen und Belastungsrichtungen im Rahmen einer Meta-Analyse zeigen eine starke Abhängigkeit der Gelenksnachgiebigkeit vom Beugewinkel. Desweiteren verdeutlichen die Ergebnisse eine starke Asymmetrie der Gelenknachgiebigkeiten beim Vergleich der Gelenktranslationen und-rotation in entgegengesetzten Richtungen innerhalb eines Freiheitsgrades. Die erhobenen Daten bieten dem Operateur quantitative Zielparameter für ein natürliches Weichteilbalancing in der Kniegelenksarthroplastik.

Die *in-vitro* Untersuchungen an 19 humanen Kniepräparaten zeigen, dass die Wiederherstellung der Weichteilfunktion des Knies nach einer Arthroplastik mit Hilfe des kinematischen Alignments alleine nicht erreicht werden kann. Die Verwendung einer Prothese die beide Kreuzbänder erhält, ist die einzige Möglichkeit die anteroposteriore Stabilität im Gleichgewicht zu halten. Um Varusdeformitäten zu korrigieren, erscheint die Balancierung des medialen Außenbandes als eine sichere Methode. Die Korrektur der Valgus Nachgiebigkeit kann durch Lösen des lateralen Außenbandes erreicht werden, was jedoch das Risiko einer Instabilität in Gelenkbeugung erhöht.

Im Rahmen dieser Arbeit konnten subjektspezifische Mehrkörpersimulationsmodelle entwickelt werden, mit denen die Nachgiebigkeiten des Kniegelenks, insbesondere im Bereich niedriger Beugungswinkel, gut reproduziert werden können. Das vorgestellte Verfahren zur Approximation der Bandansatzpunkte stellt eine zeitsparende Alternative zur Segmentierung der Ansätze aus MRT-Daten dar.

Schlagwörter:: Knie, Totalendoprothetik, Gonarthrose, Weichteilbalancing, Weichteilmantel, Mehrkörpersimulation, Bandansatz Approximation

Abstract

Total knee arthroplasty is a successful surgical treatment for patients with severe knee joint arthrosis. However, restoring soft-tissue function is a major challenge. Depending on the positioning of the prosthesis, the implantation procedure and the pathology of the patient, it is necessary to adjust the soft-tissue structures of the joint in order to restore the function of the knee. The assessment and adaptation of the soft-tissue envelope is a subjective process that is strongly dependent on the surgeon.

This dissertation addresses these challenges and seeks quantitative guidelines for soft-tissue management based on a meta-analysis of the laxity of the natural knee joint. A further aim of the present study was to clarify in the scope of *in-vitro* investigations to what extent the loosening and removal of individual structures alters joint laxity and how far the joint can be balanced by targeted resection of soft-tissue structures. In addition, *in-silico* investigations within the scope of this thesis form the basis for a numerical tool to better understand the function of the ligaments and to better plan soft-tissue balancing preoperatively in the future.

The investigations of the natural laxity of the knee joint in different flexion angles and loading directions by utilizing a meta-analysis show a strong dependency of the joint laxity on the flexion angle. Furthermore, the results show a distinct asymmetry of joint laxity when comparing translations in opposite directions within a certain degree of freedom. The data collected provide the surgeon with quantitative target parameters for natural soft-tissue balancing in knee arthroplasty procedures.

The *in-vitro* investigations on 19 human knee specimens show that the restoration of soft-tissue function of the knee after arthroplasty cannot be achieved by kinematic alignment alone. The use of a bicruciate-retaining knee arthroplasty is the only way to keep the anterior and posterior stability of the joint in balance. To correct varus deformities, balancing of the medial collateral ligament appears to be a safe method. Correction of valgus laxity can be achieved by partially or completely resecting the lateral collateral ligament, however this increases the risk of instability in joint flexion.

Within the scope of this work, subject-specific multi-body simulation models could be developed with which the laxity of the knee joint can be predicted, especially for low flexion angles. The presented procedure for the approximation of the ligament attachment sites represents a time-saving alternative to the segmentation of the attachments in MRI imgaes.

Keywords:: Knee, endoprosthetics, gonarthrosis, soft-tissue balancing, laxity, multi-body simulation, attachment site approximation

Anatomical terms of location

In the following, individual anatomical terms of direction and position are explained and visualized (Figure 0.1).

Anatomical terms	**Location or direction**
Anterior	Front, lying in front
Posterior	Rear, lying behind
Lateral	Lateral, lateral to the midline, to the side
Medial	Towards the center of the body
Superior	Lying on top, the upper one, the higher one
Inferior	Lower, lying below
Proximal	Located or running towards the center of the body
Distal	Located or running away from the center of the body
Frontal plane	Plane in the direction of the body's longitudinal axis, parallel to the forehead, front view
Transversal plane	Horizontal plane, divides the body in top and bottom
Sagittal plane	Plane oriented from back to front, divides the body median into two halves
Varus rotation	Angulation of the knee in the frontal plane, with the angle pointing away from the midline of the body
Valgus rotiationl	Angulation of the knee in the frontal plane, with the angle pointing towards the midline of the body
Internal rotation	Axial rotation of the tibia relative to the femur towards the medial side
Extern rotiationl	Axial rotation of the tibia relative to the femur towards the lateral side
Flexion	Angulation of the knee in the sagittal plane, bending of the joint by decreasing the angle between femur and tibia
Extension	0° of flexion, bending of the joint by increasing the angle between femur and tibia

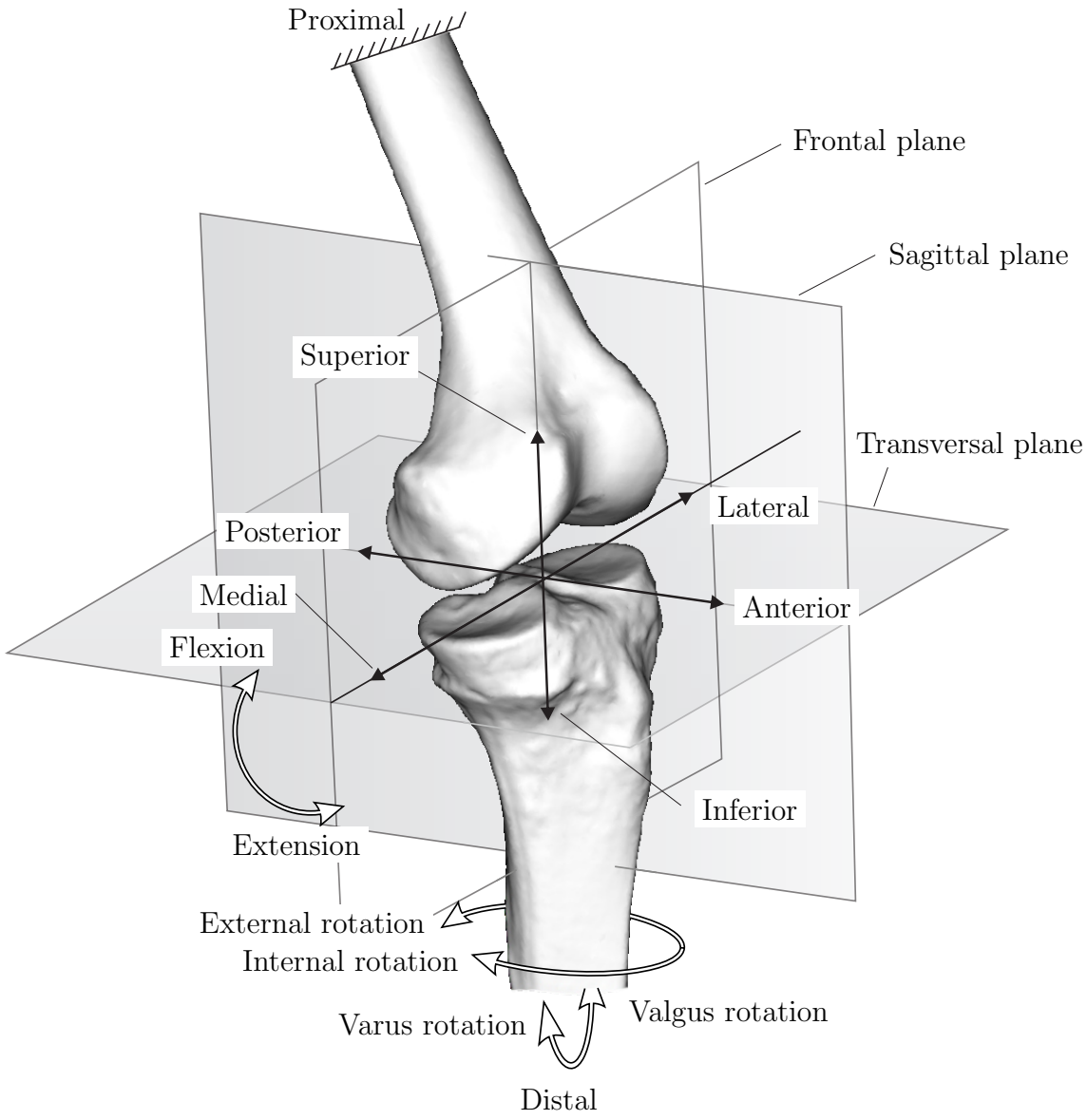

Figure 0.1: Anatomical terms describing locations, directions and motions in the human knee.

Nomenclature

Symbol	Description
$(\mathrm{CS})_\mathrm{S}$	Coordinate system of the sensor
$\boldsymbol{f}_\mathrm{S}$	Force vector of the sensor
$\boldsymbol{f}_{\mathrm{S_x}}$	x component of the force sensor with respect to $(\mathrm{CS})_\mathrm{S}$
$\boldsymbol{t}_\mathrm{S}$	Torque vector of the sensor
$\boldsymbol{t}_{\mathrm{S_x}}$	Torque around the x-axis with respect to $(\mathrm{CS})_\mathrm{S}$
${}^\mathrm{T}\boldsymbol{T}_\mathrm{S}$	Transformation matrix from $(\mathrm{CS})_\mathrm{S}$ to $(\mathrm{CS})_\mathrm{T}$
$\boldsymbol{x}_\mathrm{des}$	Desired position of the robot
$\boldsymbol{u}$	Position correction of the robot
$\boldsymbol{R}_i$	ith rotation matrix
$\boldsymbol{p}_i$	Translation vector
$\boldsymbol{y}$	Shift of the $(\mathrm{CS})_\mathrm{T}$ into the geometric rotational center
S_i	ith body in space
$\boldsymbol{q}_i$	Vector of position coordinates of S_i
$\boldsymbol{q}*$	Virtual positions
$\boldsymbol{v}_i$	Velocity of S_i
$\boldsymbol{r}_i$	Global position vector of the center of gravity of S_i
$\boldsymbol{p}_i$	Rotatation quaternion of S_i
$\boldsymbol{\omega}_i$	Angular velocity of S_i
$\Phi(\boldsymbol{q})$	Jacobian matrix with respect to position $\boldsymbol{q}$
$\boldsymbol{\gamma}$	the right-hand side of acceleration constraints
γ	right-hand side of acceleration constraints
Z	Objective functions
$\boldsymbol{C}$	Coefficient matrix of equilibrium equations
s_j	Muscle strength of the jth muscle
m_i	Mass of S_i
$\boldsymbol{I}$	Identity matrix
$\boldsymbol{J}$	Inertia tensor
$\boldsymbol{g}_i$	Sum of forces
$\boldsymbol{\alpha}_\mathrm{FDK}$	Guess of the joint position during FDK calculation
ϵ	Strain
l_0	Slack length
P	Pressure module
$\|\|\boldsymbol{x}\|\|_2$	Euclidean norm
ϕ	Radial basis function

Abbreviations

Abbreviation	Description
ACL	Anterior cruciate ligament
ALL	Anterolateral ligament
alPCL	Anterolateral bundle of the posterior cruciate ligament
amACL	Anteromedial bundle of the anterior cruciate ligament
CI	Confidence interval
dMCL	Deep medial collateral ligament
DOF	Degree of freedom
FDK	Force dependent kinematic
KRL	Kuka robot language
LAS	Ligament attachment site
LC	Lateral capsule
LCL	Lateral collateral ligament
MC	Medial capsule
MRI	Magnet resonance imaging
OPL	Oblique posterior ligament
PCL	Posterior cruciate ligament
plACL	Posterolateral bundle of the anterior cruciate ligament
pmPCL	Posteromedial bundle of the posterior cruciate ligament
POL	Popliteal oblique ligament
RTD	Robot based testing device
RBF	Radial basis function
RMSE	Root mean square error
RSI	Robot sensor interface
SD	Standard deviation
sMCL	Superficial medial collateral ligament
STL	Standard triangulation language
TKA	Total knee arthroplasty

Contents

1 General introduction and structure

With its distinctive asymmetrical design the knee is the biggest joint in all mammalian species. The sophisticated interplay of numerous ligament structures, tendons, muscles, cartilage structures and fat pads makes the joint a drive for complex movements and a damper at the same time. In the bipedal locomotion of the human beeing, the knee carries almost the full body weight and enables a stable standing position as well as a high degree of agility and mobility. However, the high loading and the complexity of the joint architecture also make the knee joint vulnerable to injuries and diseases. First and foremost, gonarthrosis, *i.e.* the arthritic disease of the joint surface of the knee, is a frequent cause of chronic pain and physical disability which also influences the psychological status of affected people and their families. This degenerative disease mostly affects elderly people, posing major challenges for the industrialized nations in view of their aging societies. Consequently, gonarthrosis is responsible for a significant and steadily increasing burden on the healthcare system all over the world. Thus researchers, engineers and surgeons are continuously working on treatment methods to overcome this disease. Since the 1960's the replacement of the diseased joint surface by use of technical materials has become the gold standard for treatment of the arthritic knee joint. This prostheses offer the return to a pain-free life and restored knee function with an implant survival rate of 15 years and more. However, the improvement in clinical outcome has stagnated in recent years. Still every 5th patient is dissatisfied with the result of the procedure suffering residual symptoms such as swelling, pain, instability or stiffness. Even increasingly better implants and modern computer-assisted implantation techniques which allow a precise implant alignment more than ever before could not improve functionality and patient satisfaction as expected. In addition, patients' expectations of knee endoprosthetics are constantly increasing. The patients nowadays not only want to move pain-free but also increasingly wish to return to their sport activities they did before arthrosis. As improved implant designs, implantation instruments and other efforts such as computer assisted surgical techniques did not solve this issues, the importance of anatomical aspects as well as the surgical technique became more apparent again. The integrity of the soft-tissue envelope which guides the joint, is essential for the functionality of the knee joint and satisfaction of the patient after total knee arthroplasty. An unbalanced knee may be responsible for symptoms instability, stiffness or unnatural feeling of the joint which is frequently reported. Thus, the adaption and restoration of the ligamentous structures and tendons is an essential step during knee joint arthroplasty. The soft-tissue tension is adjusted during surgery by partially and completely resecting individual soft-tissue structures. Although, based on theoretical considerations and clinical observations, more and more recommendations for soft-tissue balancing are suggested, there are still no quantitative target parameters as guideline for surgeons. Instead, the adjustment of the soft-tissue situation depends primarily on the surgeon's subjective assessment and personal experience. This lack of knowledge is the reason for this work.

On the following pages, the dissertation addresses the need for research in this field. Thus, quantitative target parameters for soft-tissue balancing in the total knee arthroplasty are

developed and the capacity of the soft-tissue envelope to rebalance the joint during knee arthroplasty procedures is analyzed. Furthermore, a numerical model is developed and investigated with which the complex structure of the knee joint can be systematically analyzed with respect to its restraints. This model is laying the foundation for a tool that may enable preoperative planning of soft-tissue management in the total knee arthroplasty, in the future.

Besides the introduction, the work is divided into 7 further chapters:

Chapter 2 introduces the theoretical background and basic information related to the topic of this thesis. In particular the anatomy and biomechanics of the knee joint as well as the aethiology, pathogenesis and the surgical treatment of the arthrotic disease are presented.

Chapter 3 describes the problem area which is addressed in this thesis, based on contemporary scientific literature data. Building on this, the objectives of this work are derived and presented.

Chapter 4 explains the way how the raised scientific questions and objectives are answered in this thesis.

Chapter 5 presents a meta-analysis of scientific literature of *in-vitro* experiments dealing with the laxity of the human knee. Differences in laxity depending on the angle of flexion in different directions were analyzed. In this context, the influence of experimental parameters on the measured joint laxity is presented.

Chapter 6 describes the experimental setup which was developed for biomechanical testing of the human knee joint. Furthermore, *in-vitro* investigations on human knee joints in order to evaluate the function of individual soft-tissue structures on joint laxity with respect to knee arthroplasty are presented.

Chapter 7 presents a numerical model of the knee joint which allows for subject-specific simulations of the knee laxity. A method for the approximation of ligament attachment sites is described. Furthermore, sensitivity analysis of several model parameters are shown. Finally, a description of the validation process of the model is given.

Chapter 8 summarizes the findings of this thesis and provides directions of further research related to this work.

2 State of the art

In order to understand the objectives addressed by this work, the following section describes the anatomy of the biological structures of the knee joint, its biomechanics and kinematics. Furthermore, a detailed description of the disease pattern of gonarthrosis and its treatment by means of an endoprosthetic treatment is provided. Thereby, the different types of prostheses, implantation techniques and implantation steps such as soft-tissue balancing are explained.

2.1 Anatomy of the knee joint

The knee is the middle joint of the lower extremity. It is one of the most complex and most strained joints in the human body. Three articulating bones and numerous soft-tissue structures, ligaments, tendons, cartilage structures, bursa and fat pads contribute significantly to the coordinated movement of the knee joint (Figure 2.1). In the following the individual structures of the knee and their functions are described in detail.

2.1.1 Articulating bones

The distal end of the femur and the proximal end of the tibial bone outline the main joint of the knee (art. femorotibialis). In distal view, the femoral condyles form two biconvex, bulging structures which slightly run together in ventral direction. The medial condyle is slimmer and more angled than the lateral counterpart. The two condyles are separated by the fossa intercondylaris at the dorsal end and by the facies patellaris at the ventral end. The sagittal curvature of the condyles is not constant; instead, the radius increases regularly from posterior to anterior. The two condyles and the intercondylar fossa are covered with hyaline articular cartilage. On the tibial side, the condyles are opposed by two reciprocally curved, medial concave, lateral convex, but incongruent and substantially flatter articular surfaces, which are separated from each other by a slight elevation in the centre. Anterior to the femorotibial joint, the patellofemoral joint forms an ancillary joint between the disc-shaped, sesamoid, bone (patella) in the tendon of the quadriceps (musculus femoris) and the trochlea of the distal femur. The upper two-thirds of the articulating patella surface are covered with 4-5 mm thick hyaline joint cartilage [114]. This posterior surface is divided lengthwise into two facets, each of which provides contact with the lateral or medial condyle of the femur. The facets are arranged at an angle of 120-140° [212] to each other and thus allow a stable gliding in the trochlea. The fibula, is a near to the knee joint located bone that lies laterally against the tibia. The fibula has no articulating function in the knee joint and little functional influence on the knee. Only individual ligament structures covering the knee joint start at the proximal end of the fibula.

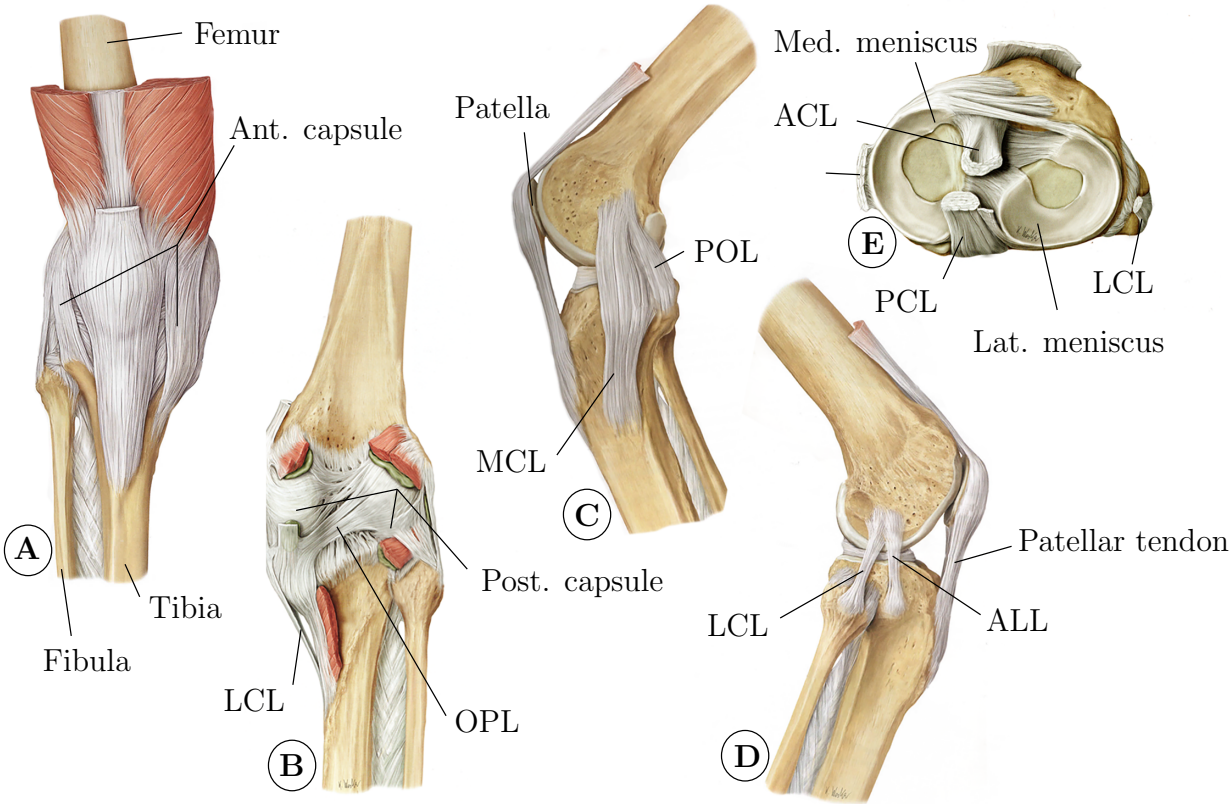

Figure 2.1: Anatomy of the capsule and ligament envelope of the knee joint in anterior (A), posterior (B), medial (C) and lateral view (D). In a transversal view (E) the menisci and the intra articular ligaments are shown. ACL: anterior cruciate ligament, ALL: anterior lateral ligament, LCL: lateral collateral ligament, MCL: medial collateral ligament, OPL: oblique popliteal ligament, PCL: posterior cruciate ligament, POL: posterior oblique ligament. Adapted from [213].

2.1.2 Ligaments and joint capsule

Both joints of the knee are covered by a shared joint capsule and lie in a unified articular cavity. Due to the limited guidance of the joint via the articulating surfaces of the femorotibial joint, stability and mobility is achieved through a strong ligament structure. A differentiation is made between extra- and intra-articular ligament structures.

The most important stabilizers amongst the intra-articular ligaments are the cruciate ligaments. Both structures are located in the middle of the knee and contribute significantly to the stabilization of the femorotibial joint. The cruciate ligaments protect the joint primarily against anterio-posterior and superio-inferior shear loads. These ligaments are tensioned differently depending on the flexion position of the knee. Anatomically, the anterior cruciate ligament (ACL) rises from the area intercondylaris anterior to the inner surface of the lateral condyle. Due to the wide attachment areas of the ACL and with regard to function, two bundles are distinguished in the literature [160]: the anteriomedial (amACL) and the posteriolateral (plACL). Opposite to the anterior, the posterior cruciate ligament (PCL) runs from the area intercondylaris posterior to the inner surface of the medial condylus femoris. This ligament is also functionally divided into two bundles: the anteriolateral (alPCL) and the posteriomedial (pmPCL) bundles. While the anterior

Table 2.1: Overview of the intra- and extra-articular ligaments in the human knee joint.

Extra-articular ligaments	Patellar tendon
	Medial longitudinal retinaculum (anterior capsule)
	Lateral longitudinal retinaculum (anterior capsule)
	Medial transversal retinaculum (anterior capsule)
	Medial transversal retinaculum (anterior capsule)
	Medial collateral ligament (MCL)
	Lateral collateral ligamend (LCL)
	oblique popliteal ligament (OPL)
	Posterior oblique ligament (POL)
	Anterolateral ligament (ALL)
Intra-articular ligaments	Anterior cruciate ligament (ACL)
	Posterior cruciate ligament (PCL)
	Anterior meniscomeniscal ligament
	Posterior meniscofemoral ligament

structures of the extra-articular ligaments essentially contribute to the guidance of the patella in the femoral patella facies, the lateral capsule-ligament structures ensure a stabilization against varus and valgus loading of the knee joint. Of the two main extra-articular structures, the medial collateral ligament (MCL) is the most pronounced. It originates at the medial epicondylus, extends in distal direction and attaches both directly under the tibial plateau and about 7-8 cm distally to the medial tibiae facies. Anatomically, the MCL is divided into two main bundles: the superficial MCL (sMCL) and the shorter, deep MCL (dMCL). The two medial ligaments can be shifted in relation to each other and are oriented differently. While the wider superficial ligament runs obliquely forward, about 15-20° to the tibial axis [244], the deep inner ligament continues to attach more dorsally to the tibia. On the opposite side of the joint there is the lateral collateral ligament (LCL). This starts at the lateral epicondylus and then continues to the caput fibulae where it is inserted super-laterally. Consequently, the LCL has no direct connection to the tibia [213]. The lateral ligament and also the medial ligaments show the highest tension when the knees are stretched and loosen in flexion. The posterior oblique ligament (POL) is attached to the posterior part of the MCL at the tibia, which extends obliquely over the intercondylar fossa and is attached super-laterally above the lateral condyle. The POL is particularly important for stabilization and meniscus protection during flexion [99]. The largest ligament at the posterior aspect of the knee joint, is the oblique popliteus ligament (OPL). This thin ligament is integrated into the posterior capsule and originating at the posterolateral aspect of the lateral femur condyle and running in inferomedial direction towards the distal tendon of the semimembranosus muscle [135]. In addition to these well known ligaments, another ligament has to be mentioned which was discovered within the last 10 years and has been discussed extensively in the scientific literature since then. The ligament called anteriolateral Ligament (ALL), runs along the lateral aspect of the

knee joint between femur and tibia. This anterior ligament originates in the lateral femur condyle of the LCL and runs down to the anterolateral side of the tibia [41].

2.1.3 Minisci

The meniscus medialis and lateralis are two crescent-shaped fibrocartilaginous structures located between the articular surfaces of the femur and the tibia. The menisci have a triangular geometry in cross section. The ends of the menisci are connected to the tibial plateau by four ligaments. The menisci compensate for the incongruencies of the joint surfaces of the knee, increasing the bearing surface and thus the load acting surface in the knee [244]. Although both minisci are attached to the tibia by means of ligament structures, they remain mobile on the tibial plateau and adopt slightly different positions depending on the rotation and flexion of the knee joint.

2.2 Basic biomechanics of the knee joint and its ligament structures

The mobility of the knee joint is essentially achieved by a complex interaction of bones, ligament structures, muscles and menisci. The mentioned soft tissue structures not only control the movement of the joint, they also absorb external loads acting on the lower extremities. However, the complex structure and the high load on the joint also make it vulnerable to diseases. An understanding of participating structures is a necessary prerequisite for comprehending the pathologies and therapeutic approaches associated with the knee joint. Biomechanical basics of the knee joint and its structures are described below.

2.2.1 Kinematic, laxity and loading of the knee joint

The knee joint is one of the most highly loaded joints in the human body. This is due to its position far below the centre of gravity of the body and due to the strong muscle structures surrounding the joint. In order to facilitate human mobility, the knee joint has three translational and three rotational degrees of freedom. The degrees of freedom of the knee are restricted by the surrounding soft tissue structures. The quantitative description of this property in clinical and experimental investigations is usually done by the parameter of joint laxity. This is defined as the reaction of the joint in the form of translations and rotations of the tibia relative to the femur as a result of a defined, non-destructive loading of the joint (typical values are within the range of 100 N and 10 Nm). The laxity of the joint within a degree of freedom can be summarized as the range of motion. The degree of freedom with the largest range of motion of about 145° is obtained with the flexion-extension motion of the knee [201]. If the joint is in maximum extension, it is locked and allows hardly any rotational degrees of freedom. As flexion increases, the varus-valgus rotation as well as the internal-external rotation become increasingly looser. In a 90° flexion position, the joint then allows an inner-outward rotation of about 40° and a varus-valgus rotation of 10°. In the course of the first 20° of flexion, the femoral condyles

roll on the tibial plateau. Undergoing a further flexion, the cruciate ligaments of the knee joint prevent a further pure rolling motion. Instead, the surfaces of the femorotibial joint roll and additionally slide onto each other [164]. Therefore, the knee joint movement is better known as a so-called roll-gliding motion. In summary, this kinematic property is expressed by a typical almost linear femorotibial translational movement during flexion of the joint from 0° to 90°, in which the tibia moves forward about 15 mm relative to the femur [55]. When the knee joint moves from a flexed position into the extension, an external rotation of the tibia of about 7° can be observed at the last 30° to the extension, the so-called screw-home mechanism [83]. In addition to femorotibial kinematics, patellofemoral kinematics should also be mentioned. Essentially, the patella is a kind of deflection pulley for the quadriceps muscle. Accordingly, the patellofemoral joint is particularly loaded during extension movements [98]. Seen from the front, the patella is centered between the condyles in full extension, slightly above the trochlea. The femoropatellar joint has the largest laxity in this position. Basically, the movement of the patella is strongly dependent on the active contraction of the quadriceps muscle [148]. By connecting the patella with the tibia via the patellar ligament, the patella follows the tibia during flexion and extension. Accordingly, a movement towards inferior during flexion and towards superior during extension can be observed. The contact surface of the femoropatellar joint increases with increasing flexion. Correspondingly, with rising flexion, the patella is more and more guided through the femoral trochlea, which essentially determines the movement trajectory of the patella [148].

For a long time only kinematics of the knee joint could be observed, the internal forces were largely unknown as basic kinematics can be measured non-invasively in contrast to the forces acting in the joint. For this reason, instrumented prostheses were developed with the help of which it is now possible to record the loads in the joint on a limited number of subjects. First axial load measurements were published by the working group around D'Lima [52, 53]. Three months after implantation of an instrumented knee prosthesis, an 80-year-old patient showed an axial load of up to 120 % of body weight. After a further nine months and an up to now strengthened musculature, loads of 280 % of the body weight could be determined. Accordingly, a large part of the joint load can be attributed to muscle activation. In recent years, Bergmann's working group has also investigated the load on the knee joint using instrumented prostheses [90]. For the first time, medio-lateral and anterio-posterior shear forces were recorded. This was shown to be subject to considerable fluctuations and range from 70 % to 390 % of body weight [117, 171]. In addition, the studies by Damm *et al.* confirmed the considerable axial load on the knee joint during normal gait and also showed that the knee joint is loaded with two loadpeaks of 210 % and 257 % body weight per gait cycle due to the heel strike and the toe off phase in the alternating gait [47].

2.2.2 Biomechanics of the ligaments

The main task of the ligaments in the knee joint is to ensure joint stability over the entire range of motion. Each of the numerous ligaments is to some extent responsible for stabilizing the joint in several degrees of freedom (DOFs) [245]. The ligament structures, which are essentially composed of nearly parallel bundles of collagen fibres and intermediate fibroblasts [192], differ greatly in length, width and strength within the knee joint.

The ligament attachments are compact in some cases and spread in others. Individual ligaments can usually be divided into several bundles, each of which is characterised by its parallel fibres. Although a ligament is described as an overall structure, under certain loads it can be seen that only parts of the fibre structures are stretched, others remain slack [61]. This indicates that the ligaments of the knee joint are much more complex structures than one would initially assume. This also becomes clear when ligaments are subjected to tensile stress. The human ligaments show a nonlinear, anisotropic force-displacement behavior especially at low loads of 50 N to 100 N and below. As the load increases, the stiffness of the ligaments increases until they then exhibit an almost linear material behavior under increased loads [61]. The mechanical characterization of individual ligament structures of the knee joint was and is the subject of research. The mechanical characteristics of the ligaments described in the literature are subject to large variations (Table 2.2). The reason for this is on the one hand the large variance of human tissue depending on factors such as age and sex, but on the other hand the variance is also due to the testing conditions: a load on a ligament based on physiology is only possible if the ligaments, including their anchoring in the bone, can be tested. If the ligament is detached from the bone anchors, it is very difficult to introduce forces into the ligament without changing the natural function of single bundles.

Table 2.2: Failure load and mean stiffness of the major ligaments of the knee reported by various authors.

Ligament	Failure load / N	Mean stiffness / (N/mm)
ACL	1207 ± 548 [225, 174, 247]	171 ± 91 [225, 84, 174, 247]
PCL	732 ± 146 [225, 84, 154]	203 ± 131 [225, 84, 88, 154]
dMCL	148 ± 66 [239, 202]	35 ± 10 [243, 239]
sMCL	546 ± 16 [239, 202]	66 ± 4 [243, 239]
LCL	404 ± 29 [225, 223, 162]	61 ± 34 [243, 225, 223, 162]
POL	256 ± 30 [239]	39 ± 16 [239]
ALL	175 ± 62 [118, 197]	23 ± 10 [118, 197]

Very few attempts have been made to directly measure ligament force by removing the bony attachment and coupling a tensiometer to the ligament (Figure 2.2). In the following, changes in the load of the respective ligament could be recorded depending on the flexion angle [155, 157, 195]. Since the ligaments were initially loosened for mounting the force transducer, the method is quite inaccurate and the initial force in the ligaments remains unknown. Accordingly, studies on length change are primarily the only literature available for the assessment of the load of individual ligaments. Individual findings in this regard are presented below:

For the anterior cruciate ligament, there are partly conflicting study results with regard to the length change of individual ACL bundles with flexion of the knee joint. In their *in-vitro* study, Girgis *et al.* showed a reciprocal function of the amACL and plACL bundle, with the am bundle beeing tight at high flexion and loose in extension and the pl bundle

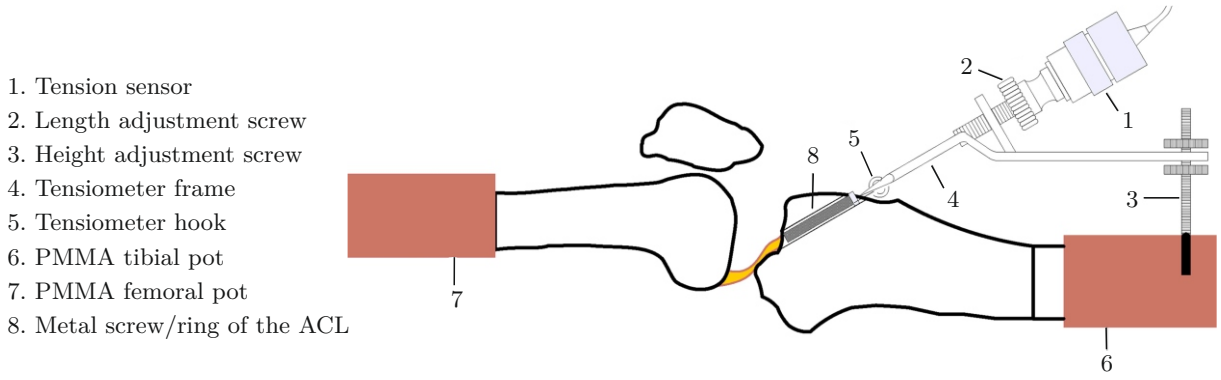

Figure 2.2: Schematic presentation of the tensiometer device that was used to measure *in-situ* forces in a ligament. Figure adapted from [195].

beeing tight in extension and loose in flexion [74]. In contrast, recent studies using MRI and 3D fluoroscopy imaging on five subjects showed that the length of the amACL from flexion to extension did not change significantly, whereas for the plACL a length change of 14 % (from extension to 90° flexion) with a significant decrease in the length of the anterior cruciate ligament could be observed, especially at flexion angles greater than 60°. The authors concluded that the posterior part of the ACL may have a more significant tension in extension than in flexion [140]. In their study, Li *et al.* examined not only the ACL but also the length change of the PCL during flexion and found a significant elongation of 31 % and 22 % of both PCL bundles (alPCL, pmPCL) by flexing the knee from 0° to 90° [140]. These changes in length therefore indicate a stronger tension of the ligament in flexion than in extension. Similarly, Hosseini *et al.* investigated length change patterns of single bundles of the LCL, sMCL and dMCL in eight subjects [96] when the knee joint was flexed from 0° to 120°. The investigations showed different length changes for the LCL, depending on the bundle. The anterior third of the ligament lengthened by 6 % with flexion, while the middle and posterior third of the ligament shortened by up to 3 % and 12%, respectively, during flexion. These studies therefore suggest that the anterior third of the LCL is tense in flexion while the middle and posterior bundle are most tense in extension. The investigations of the sMCL showed almost no change in length for the anterior third of the ligament with flexion up to 90° degrees, while the middle and posterior third of the sMCL shortened by 8 % and 15 %, respectively. Even greater differences between the individual bundles could be observed for the dMCL. While flexion up to an angle of 90° resulted in an increase in length of 17 % for the anterior third of the ligament, a decrease in length of 15 % was observed for the posterior third. The middle third of the dMCL, on the other hand, hardly changed in length. Also the length change pattern of the ALL during flexion from 0° to 90° was investigated on six cadaver specimens. The investigations showed an increasing length with increasing knee flexion of up to 12 % at 90° of flexion [259]. These investigations illustrate the complex function of individual ligament structures and give isolated indications of the tension situation within a ligament in the healthy knee joint.

2.3 Aetiology and pathogenesis of gonarthrosis

The present work is mainly focused on the treatment of the knee joint suffering from gonarthrosis. In this chapter the causes as well as the course of the disease of knee arthrosis are described in detail in order to explain the complexity of the disease and the background for the treatment of knee arthrosis by means of a knee endoprosthesis.

2.3.1 Definition of gonarthrosis

Gonarthrosis describes a slowly progressive, essentially non-inflammatory, degenerative disease of the knee joint [126]. Depending on the localization of the disease in the joint, a distinction is made between patellofemoral, femorotibial and patellofemorotibial osteoarthritis. Contrary to popular belief, osteoarthritis is not solely a disease of physiological wear and tear. On the other hand, the aetiology of osteoarthrosis is still unclear in many aspects and is often used today as a term for a heterogeneous group of diseases. Based on this, the following definition of osteoarthritis was developed in cooperation with the American Academy of Orthopedic Surgeons, which can also be used without restrictions for gonarthrosis [132]:

"Osteoarthritis is a group of overlapping distinct diseases, which may have different aetiologies but with similar biologic, morphologic, and clinical outcomes. The disease processes not only affect the articular cartilage, but involve the entire joint, including the subchondral bone, ligaments, capsule, synovial membrane, and periarticular muscles. Ultimately, the articular cartilage degenerates with fibrillation, fissures, ulceration, and full thickness loss of the joint surface."

2.3.2 Aetiology and pathogenesis

In recent decades, the view on the aetiology of osteoarthritis has changed from a joint disease that occurs as a result of wear and tear of the articular cartilage layer alone ("wear and tear" theory) to a complex metabolically active group of diseases with similar developmental pathways affecting the entire organ. The pathology of osteoarthrosis ranges from joint cartilage disease, changes in joint near bone which are manifested in osteophytic extensions and sclerotic thickening of the bone to pathological changes in the ligament and capsule structures. Some patients suffer from severe pain, while many patients with diagnosed osteoarthritis have no symptoms [137]. To this day, the causes of pain development in osteoarthritis are widely unknown [50]. However, a large number of pathological, biological, epidemiological and biomechanical studies have been able to identify key disease mechanisms over the last 20 years. According to the state of science, osteoarthrosis is a dynamic clinical picture which includes opposing degenerative as well as reparative processes [31]: As a result of an initial damaging process or mechanical trauma, all components of the entire organ participate in an adaptation reaction depending on the severity of the damage. This reaction is expressed, for example, by an increased metabolic activity of the cartilage in bone regeneration and remodelling [166]. The further course then depends on the success of the repair process and the severity of the damage and can present itself as a trigger for a further degenerative process as well as a compensative state. These triggers

are apparently influenced by biochemical, biomechanical, metabolic processes as well as environmental influences and predisposition [166]. The course of the disease can be highly individual, which might be the explanation for the strong heterogeneity of the disease and its symptoms. In this regard numerous epidemiological studies have uncovered systematic factors such as obesity, age or gender as well as mechanical and local factors such as joint position, trauma, soft-tissue or muscle tension as risk factors influencing osteoarthrosis [166].

The theories mentioned above can be applied to gonarthrosis without any restrictions. The joint specific aetiology of knee joint arthritis is distinguished by two basic disease processes: the idiopathic or primary gonarthrosis is less a result of a clearly attributable factor or trauma that sets the disease in motion, but rather arises under the influence of various risk factors that promote degeneration of the joint. Secondary gonarthrosis, on the other hand, is the result of clearly definable factors which within a primary event lead to direct or indirect degeneration, or damage to the joint cartilage or its extracellular matrix, which in a second step propagates to the development of oseteoarthritis as a result of destructive and reparative processes [166]. As the disease progresses, various mechanical, neurological, hormonal and biochemical mechanisms of action intermesh to further advance the disease: As a result of cartilage damage, abrasion particles of the cartilage in the form of detritus particles and free proteoglycans move into the joint space, and inflammation-promoting cytokines as well as proteases are released into the joint space by the body. These particles, proteins and enzymes then lead to an irritation of the synovial membrane, which then manifests itself in the form of swelling and pain up to effusion. This mechanism can then trigger further destruction cascades in interaction with cytokines and macrophages in which the cartilage matrix is further destroyed [121].

In the case of another mechanism, initial inflammation and cartilage destruction together with known risk factors such as obesity, axial joint misalignment or soft-tissue-related instability lead to an increased load on the subchondral bone which results in a remodeling reaction in the form of increasing bone density [126]. This is manifested by a deteriorated nutrition of the cartilage, the risk of neurotic bone resorption as well as reduced bone elasticity and thus increased mechanical stress on the cartilage [34]. The development of peripheral osseous protrusions, the so-called osteophytes, which are typical for osteoarthritis, are also frequently mentioned in this context. However, the cause of osteophyte formation is still unknown today. Descriptions of this bone formation as a compensatory reaction in the sense of a joint enlargement as a result of increased joint loads are controversial [126]. While the development of osteophytes is a clear indicator of age, observations in humans showed that cartilage damage alone is not directly related to osteophyte formation [10]. However, data also show that osteophytes in the knee joint can have a stabilizing effect in patients with osteoarthritis [188].

Other processes driving the disease are neuromuscular mechanisms. As a result of an initial inflammatory reaction in the joint, afferent neurons as well as intraarticular mechanoreceptors are inhibited. This is expressed in a reduced stimulus transmission and a change in neuronal muscle activation [178] and propreoception [235, 71, 177]. These neurological disorders increase the risk of falling and the risk of unnatural loading of the joint, which can easily lead to further injury of the joint surface. The interaction of the mentioned processes as well as the influence of numerous risk factors lead to a continuous progressive damage of the joint. Finally, pain and movement restrictions caused by this joint degen-

eration in the last consequence results in an artificial replacement of the joint surfaces in order to exchange large parts of the damaged tissue.

2.4 Total knee arthroplasty

Condylar knee arthroplasty in its current form describes the implant-based, partial or complete replacement of the sliding and bearing surfaces of the knee joint. With approximately 170,000 implantations in Germany per year [175], it is a very successful and meanwhile routinely performed surgical method to restore joint function as a result of osteoarthritis or massive fractures. The idea of arthroplasty goes back to the middle of the 19th century. In contrast to the current method, the main idea was to replace the diseased joint surfaces after an initial joint resection with biological tissue such as muscle or joint capsule inserted between the bone ends to allow the bone ends to heal [229]. Some of these treatments were described as successful, although the treatment results at that time are certainly not comparable with those of today's joint replacement operations. In 1928, Albee described the current problems of treatment in a published research article as follows: "These patients either had insufficient motion to satisfy them, or more often the degree of mobility was satisfactory but lateral instability was present and proved so troublesome as to offset the advantages of mobility" [7]. Based on these findings, technical materials made their way into knee joint arthroplasty in the 1950s. Numerous physicians and scientists experimented with polyamide tissues instead of biological soft-tissue [133]. However, the groundbreaking success was not achieved with this method. Parallel to these developments, initial efforts were made to replace joint surfaces destroyed by arthrosis with an endoprosthesis. For the first time, the concept of reconstructing the joint surfaces with resistant, biocompatible materials to restore joint function was developed. The first efforts with this concept were limited to hemiprosthetic solutions, *i.e.* implants that partially replaced only one of the joint surfaces of the knee with a polyethylen or metal implant. These treatment attempts also showed only moderate success, so that with further efforts in development the first complete joint replacement implants were developed in the 1950s [130]. As instability was registered as a major complication with earlier implants, a knee prosthesis with only one degree of rotational freedom was initially used [232]. These implants showed very good results immediately after the operation, but Wilson showed considerable implant loosening and thus implant failure already three years after implantation [242]. With the development of a semiconstrained total condylar desings in 1974 [1], the first serious successes were achieved in the treatment of osteoarthritis of the knee joint. This concept was based on the following basic principles, most of which have survived to this day [1]:

- Both joint surfaces are completely replaced.
- Straight, strictly defined bone incisions enable precise and safe implant placement.
- A concave design of the tibial component stabilizes the joint in the anterio-posterior direction and during axial rotation.
- The femoral and tibial components are partially conforming to give the joint the necessary degrees of freedom while avoiding point contact. The conformity provides a flat distribution of the load.

- The design of the implant components is based on the anatomy of the healthy joint in order to ensure the function of the soft-tissue envelope, the remaining ligaments and the musculature.
- The main part of the tibial component consists of polymer. The fixation is carried out by means of a central peg, which is inserted into the bone in order to absorb mainly acting moments and shear forces.
- Fixation of the implant components with bone cement in order to achieve a stable fixation with a broad load transfer.

2.4.1 Types of prosthesis

The initial total condylar concept of 1974 was slightly adapted in the following years to address the still existing complications such as implant loosening and instability (an abnormal increase in joint mobility) in total knee arthroplasty (Figure 2.3), [104]. The main implant variants of the recent years with their underlying philosophies are compared below:

Posterior-cruciate-retaining Bicruciate-retaining Hinged knee

Figure 2.3: Prosthesis with different type of restraints and different preservation of soft-tissue structures (Adapted from [3, 4, 2]).

Multiradius knee vs. single radius

One of the most important design criteria of modern knee arthroplasty is the relation of joint replacement to the anatomy of the healthy knee joint [106]. Multi-radius prosthesis designs take this into account in the sagittal design of the femoral component, which is characterized by a radius that changes several times according to the morphology of the distal femur. This design concept is intended to achieve a particularly natural soft-tissue tension of the soft-tissue envelope depending on the flexion of the joint, thus ensuring secure joint stability.
However, recent clinical and biomechanical studies suggest that prostheses with a multi-radius design are more prone to mid-flexion instability than other designs [110]. This

was particularly observed in prosthesis designs with strong, sudden changes in the radius. Contemporary multi-radius prosthesis designs are, therefore, now characterized by a fine gradation of the radii [43].
The multi-radius design is countered by the single-radius design, in which the sagittal contour of the femoral knee component is designed with a continuous radius in the range of motion of 10° to 110°. This design is based on biomechanical studies which show a locally fixed flexion-extensions axis in the kinematic view of the knee joint [95]. With regard to clinical functionality, the data is not yet clear, but individual studies indicate improved stability in mid-flexion compared to multi-radius designs [110].

Fixed bearing vs. mobile bearing

The majority of today's knee prostheses have a fixed bearing of the tibial polymer component (Figure 2.3). Therefore, the polymer inlay of the tibial implant is rigidly attached to the base plate anchored in the bone. One of the major complications in knee endoprosthetics, apart from stability, is the loosening of the implant and wear of the polymer joint surface. To counter this problem, implant types were developed with a polymer onlay that had one or two DOFs relative to the tibial base plate (Figure 2.4). The aim was to reduce the friction of the femoral component on the polymer inlay, reduce the shear stress on the bone-to-implant interface and enable higher mobility while maintaining the conformity of the prosthesis components. Some studies have also confirmed these biomechanical

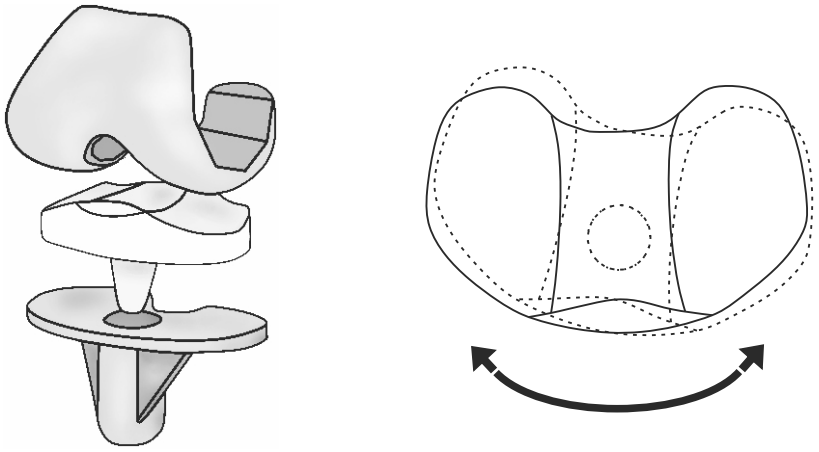

Figure 2.4: Schematic representation of the mobile bearing prosthesis concept.

advantages of this design philosophy [189]. Clinically, however, a so-called back-side wear phenomenon became apparent especially in the early development phase. The tibial polymer inlay showed a significant wear of the inlay back face (bearing surface) which in the further course led to a failure of the knee endoprosthesis. This problem was solved in later designs. Another disadvantage of the design was the observation of unphysiological roll forward behaviour of the knee prosthesis during flexion, instead of a physiological rollback [37].

Cruciate retaining vs. posterior stabilized

The supporting soft-tissue structures, especially the central intraarticular cruciate ligaments, are of great importance for the stability of the knee joint. Modern total knee

arthroplasty (TKA) therefore aims to insert the prosthesis as non-invasively as possible in order to preserve as many soft-tissue structures of the knee joint as possible (Figure 2.3). Since on the one hand the implant components require a large surface area for themselves, and on the other hand insertion and alignment of the implant by retaining the ACL is very challenging, almost for all implant designs available today the ACL has to be sacrificed to allow the insertion of the tibial prosthesis component. However, the posterior cruciate ligament can be retained with specialized cruciate retaining prosthesis designs. Nonetheless, an improve in the clinical outcome by preservation of the posterior cruciate ligament could yet not be confirmed [24].
In some cases, especially in patients with a weak soft-tissue situation or in patients who suffered from the sacrifice of the posterior cruciate ligament, a simple prosthesis design cannot achieve sufficient stability. There are two different posterior stabilizing approaches for these cases: On the one hand there is the possibility of using an inlay with a higher conformity, on the other hand implant designs exist which limit the knee stability mainly in the anterio-posterior direction by means of a central pin at the level of the posterior cruciate ligament as part of the tibial inlay.

Patient specific vs. generic

In order to change the kinematics and function of the knee joint as little as possible, it is a first step to replace the sliding surfaces of the knee joint as physiologically as possible with patient-specific prosthesis components. With the aid of geometric information from medical image data, computer-assisted procedures can be used to calculate the joint condition prior to the arthrotic disease and rebuild it with appropriately individualized prosthetic components [19, 141]. However, it is not possible to map the stabilizing function of the joint cartilage or the menisci with the technologies available today, which results in a discrepancy between the functionality of a physiological knee joint and individual prosthesis designs. Furthermore, the manufacturing process of such implants is time consuming and expensive. Nevertheless, current clinical and biomechanical studies which investigated this prosthesis concept have shown improved kinematical function compared to generic implant designs [258, 183].

Guided designs

In addition to semi constrained designs, total knee arthroplasty also includes significantly more closely guided joints in order to address the considerable problem of joint instability (Figure 2.3). The designs range from implants with conforming inlays which guarantee a higher stability of the joint, especially in the anterio-posterior direction, to hinge joints which restrict not only the mobility in the anterior-posterior direction but also in the varus-valgus direction. Some conservative variants of these guided joints also restrict motion in the internal and external rotation by coupling the femoral with the tibial component (Figure 2.3). An example of a joint with increased constraints is the so-called saddle joint, which has saddle-shaped geometries in the intercondylar region of the tibial inlay and corresponding bearings in the femoral component. This saddle joint allows stabilization of the joint depending on the flexion position.

Patients who, in addition to anterior-posterior instability, also exhibit wide open, uncontrolled varus-valgus instability can only be treated with a coupled prosthesis. With a

rotating hinge design, the rotational degree of freedom can be stabilized in the varus-valgus direction. However, the free internal and external rotation of the joint allows a more natural joint movement compared to the hinge joint with only one degree of freedom.

Biruciate retaining design

Besides joint surface replacement itself, maintaining or regaining joint stability is one of the main goals for the functional restoration of the arthrotically diseased knee joint. Therefore, the preservation of all ligament structures is considered ideal for knee arthroplasty. However, most available joint systems require the sacrifice of the anterior cruciate ligament to create space for the prosthesis and to allow proper implant alignment and fixation. In recent years, therefore, there have been repeated efforts to implement an implant design to preserve both cruciate ligaments. The first attempts on this approach were made with the introduction of unicompartmental knee prosthetics [21]. The unicompartmental arthroplasty procedure is thus designed for patients in whom only one condylar side of the joint is affected by arthrosis and accordingly only the replacement of the joint surface on one of the two condyles is performed, while the intercondylar area remains untouched. By applying this type of prosthesis to both the medial and lateral condyle, total knee arthroplasty can be achieved while preserving both cruciate ligaments. The main difficulty lies in implant placement, which must be carried out with particularly high accuracy to prevent implant loosening and wear as well as to ensure the function of the soft-tissue structures through a natural balance [200]. However, the complicated implantation represents the main limitation of this concept and has so far prevented its widespread application. With the introduction of robot-supported implantation procedures in knee endoprosthetics, in which three-dimensional surgical planning can be transferred to the situs with high precision, this implant concept receives increased attention.

2.4.2 Implantation techniques

Regardless of which of the above mentioned prosthesis concepts a patient is treated with, the implantation, more precisely, the implantation technique is crucial for the function, durability, pain relief and general outcome of knee arthroplasty [161, 159]. For this it is necessary to remove the area destroyed by the arthrosis by means of joint surface resections and to replace it with an artificial joint as well as to restore the function of the soft-tissue envelope responsible for the movement and stability of the joint. Today there are many highly specialized tools available for this purpose in order to enable the prosthesis to be implanted as accurately as possible. In addition to the purely mechanical resection tools, cutting blocks and implantation aids, computer- and robot-supported implantation techniques have for some time been making their way into knee arthroplasty with the aim of improving the accuracy of the implantation [111]. However, the main surgical steps are independent of the tools used and are described in more detail below:

The surgical approach, *i.e.* the structured opening of the joint, is the beginning of the operation and an important step towards a successful joint replacement. The aim of the surgical approach is to open the joint as gently as possible, in order to achieve sufficient exposure for the surgeon, and especially to protect the functionally important extensor apparatus and not to sustainably damage the patellar blood supply [179]. The current

literature discusses four basic approaches: medial parapatellar, medial midvastus, subvastus and lateral access. In addition, there are numerous other modifications of these four access types. An essential part of all these access routes is an anterior longitudinal incision through the skin, followed by a division of the underlying soft-tissue structures in order to obtain a clear view of the joint surfaces of the knee joint.

Following the opening of the knee joint, the first individual soft-tissue structures are resected. For instance, the Hoffa fatty body is removed to provide a better view of the knee joint, the anterior cruciate ligament is resected to make room for the implant, and the two menisci of the knee are removed as they are replaced by the implant. Using two to three femoral and a tibial bone incisions, the joint surfaces of the femorotibial joint are removed to prepare the implant-bone interface. The position and orientation of the bone incisions are based, on the anatomy of the knee joint and the dimensions of the implant and, on the other hand, on the reference axis used for alignment. There are different reference axes in knee arthroplasty:

Mechanical alignment

The mechanical alignment established decades ago, follows the goal of a stable joint with a neutral alignment of the knee with respect to the mechanical limb axis [18]. The mechanical limb axis is formed by a linear connection between the center of the femoral head and the center of the distal tibial joint surface of the ankle joint. Accordingly, the alignment of the prosthesis is independent of the individual varus-valgus alignment of the knee in order to systematically ensure a mechanically uniform restoration that prevents from strong asymmetric loading of the implant components. To quantify the amount of bony correction necessary to achieve neutral knee alignment, the mechanical axis can again be divided into two axes: the mechanical femoral axis runs from the center of the femoral head to the intercondylar notch of the distal femur. The mechanical tibial axis is formed by a linear connection between the center of the tibial plateau and the center of the upper ankle joint [149]. The angle between the two axes describes the degree of deformity of the knee joint [39]. In the healthy knee joint, the mechanical axis of the femur and the baseline of the knee joint, which is formed by a medio-lateral tangent to the condylar surface, span an angle of about 87°. Leg deformity is present in cases where the mechanical tibial axis does not coincide with the mechanical leg axis which is then corrected in mechanically aligned total knee arthroplasty. Therefore, the prosthesis components are aligned in the frontal plane 90° to the mechanical leg axis. In the transversal plane, the components are aligned according to the transepicondylar axis which is defined by the most prominent aspect of the lateral and the sulcus of the medial epicondyle (Figure 2.5), [18].

Kinematic alignment

In contrast to the mechanical alignment, the philosophy of kinematic alignment follows the idea of incorporating the individual anatomy of the patient into the implant positioning. The aim of this technique is to align the prosthesis as closely as possible to the kinematical axes [97]. The kinematic axes in knee arthroplasty differ significantly from the axes mentioned above. The kinematic axes describe the three-dimensional movement of the knee joint by mere orientation on the mechanics of the joint or anatomy of the individual bones. Three axes have to be mentioned here: the transversal condylar axis

which can be constructed from the connection of the midpoints of two circles fitted into the condyles; another transversal axis anterior, proximal and parallel to the condylar axis which describes the movement of the patella; a longitudinal axis which is perpendicular to the first two axes which describes the internal and external rotation of the joint [49]. The components are aligned along these axes. Accordingly, varus-valgus deformities are not corrected. This implantation concept is, therefore, not suitable for patients with severe deformities (Figure 2.5).

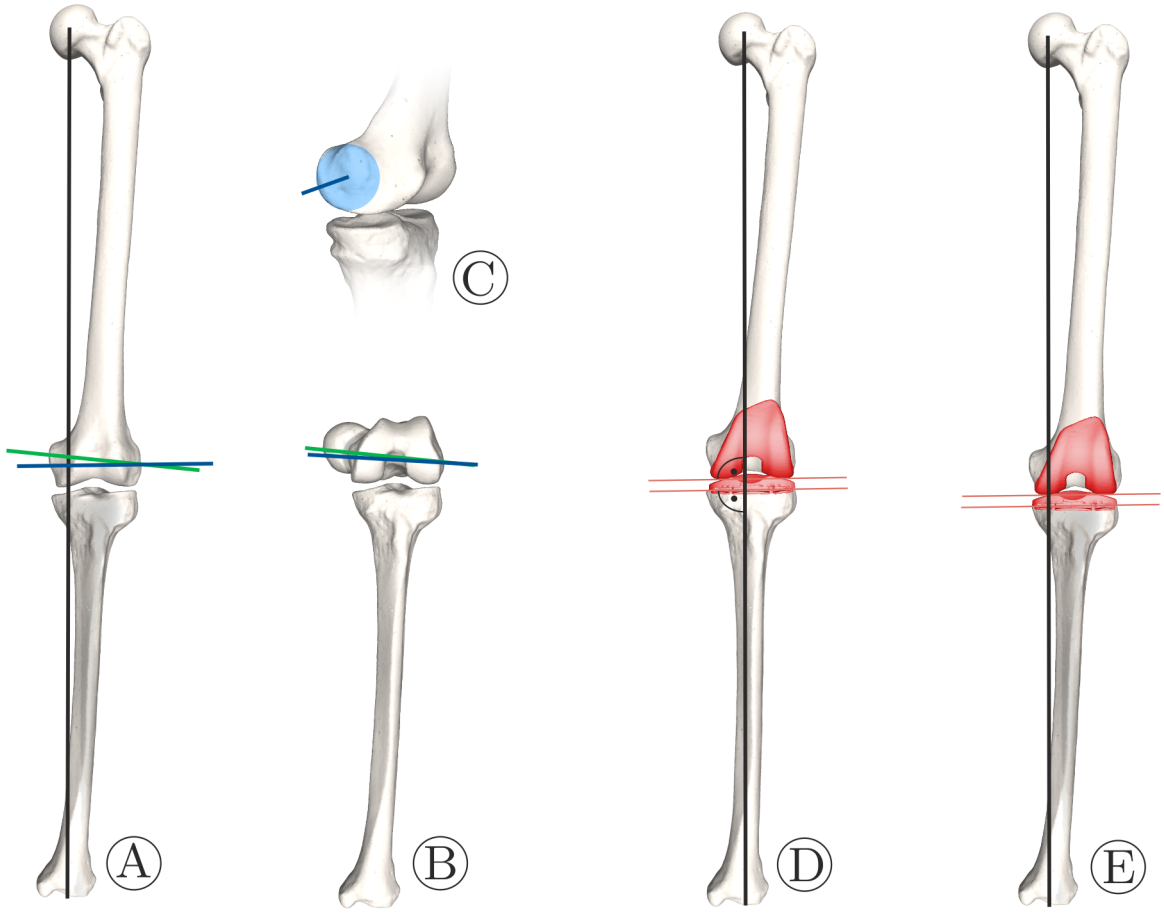

Figure 2.5: Representation of knee axis, used for implant alignment in total knee arthroplasty. A, B: frontal view of the lower limb in extension and 90° of flexion showing the mechanical (black), kinematic (blue), and epicondylar axis (green). C: kinematic axis built, based on cylinders fit into the condyles. D, E: mechanical and kinematic alignment of the implant components (red).

The choice of the alignment philosophy has a significant influence on the soft-tissue envelope. Accordingly, depending on the alignment technique, adjustments to the tension of individual tendon and ligament structures are necessary. These adjustment steps, which are essential for the subsequent outcome of the operation, are summarized under the term soft-tissue management or soft-tissue balancing [107]. Behind these terms hides basically the release of mainly ligament structures, but in particular also tendons with the aim to change the joint gap. Only in rare cases ligament structures are completely detached.

In most cases, only individual fibres or bundles of a ligament structure are released or attempts are made to reduce the ligament stiffness by means of small cuts in the ligament (so-called pie crusting technique). The decision on which of these many soft-tissue structures of the knee joint need to be partially released depends on the varus-valgus status of the joint, any pathological joint contractions, the implantation technique, the implant and the surgeon. Soft-tissue balancing is therefore a highly individual and critical step during the implantation of a knee prosthesis: Incorrect soft-tissue balancing leads to joint stiffness or instability, resulting in rapid functional loss of the entire joint [14, 68].

In order to get an overview of the soft-tissue situation during the operation and to objectively assess the effect of soft-tissue management, new instruments have been developed in recent years with which the joint can be tensioned or pressures within the joint can be measured: By means of spreaders and joint distractors, which are inserted into the joint space, a knee joint can be extended in order to evaluate the pretensioned joint space [214, 42]. Another option is to evaluate joint stability and soft-tissue function using distance blocks and sample inlays [21]. Recent developments should make the soft-tissue balance more quantifiable. Using instrumented tibial trial implant components, the joint pressures between lateral and medial femoral condyle as well as the tibial component can be recorded [204]. The soft-tissue structures are usually adjusted using the mentioned tools in extension and flexion after insertion of an implant template. After the soft-tissue situation has been adapted to the joint prosthesis, the implant components are finally fixed to the bone. In a final step, the joint capsule is closed again and the layers above are sutured.

3 Challenges and aims

As the descriptions in subsection 2.3.2 showed, arthrosis is a serious disease of the joints. In Germany about 12.4 million people are affected by this disease [63]. More than 50% of all patients diagnosed with osteoarthritis suffer from gonarthrosis [63]. In Germany alone, about 165,000 patients are, therefore, treated annually with primary total knee joint arthroplasty and the number of cases is steadily rising [175]. The mean age of these patients is 70 years at the time of surgery. However, statistics also show that patients are getting younger and younger [38]. Young and mobile patients, in particular, make high demands on joint arthroplasty, as they wish to return to physical exercise at home and at work, participate in social activities in general without restrictions in mobility or even resume the sport they exercised before the disease.

Current studies show, however, that about 20% of all patients with a knee joint prosthesis are dissatisfied with the treatment outcome [81]. The patients report one year post-operatively that the knee joint "does not feel normal", a lowered inducement for movement, swelling, stiffness, pain and generally poor knee function, for example during squatting, turning/shifting or moving laterally [173]. Also there are abnormalities in joint kinematics which are often seen in the clinical evaluation after knee arthroplasty such as mid-flexion instability or a missing screw home mechanism in joint extension [221, 85].

Despite the constant further development of prosthesis designs, which is also reflected in the numerous implant variants available today (subsection 2.4.1) and the constantly new and further developed tool technologies such as computer-assisted surgery, the number of dissatisfied patients could not be significantly reduced [33]. For this reason, the established surgical procedures for aligning the prosthesis components with the bone were recently challenged [97, 224]. The philosophy of mechanical alignment developed and widely used over decades and its modifications in which the prosthetic components are aligned perpendicular to the mechanical leg axis of the femur and tibia and the joint with its surrounding soft-tissue envelope is balanced in such a way that a symmetrical and equal joint gap is created in extension and flexion, allows for the implantation of the prosthesis with simple tools. At the same time it enables the correction of joint deformities (*i.e.* varus or valgus deformities), but it does not take the natural joint kinematics into account and may, therefore, change the function of the surrounding soft-tissue envelope (subsection 2.4.2). Motivated by studies from Anne M. Hollister's research group on the rotational axes of the healthy knee joint [95], Howell and Hull developed a novel alignment technique (kinematic alignment) with the aim of restoring the natural joint kinematics of the knee as well as possible and preserving both the natural alignment of the joint and the function of the soft-tissue envelope (subsection 2.4.2) [97]. The alignment of the femoral component is achieved according to the natural joint surface while attempting to restore the prearthritic condition. The alignment of the tibial component, on the other hand, is achieved by the vertical alignment of the anterior-posterior axis relative to the transverse axis of the femoral component, followed by an alignment of the centers of the tibial component with the center of the tibia [97].

This promising prosthesis concept considers the natural joint position and kinematics more than well-establish alignment techniques. In addition, much greater attention is paid to the restoration of the natural function of surrounding soft-tissue structures. The studies carried out to date to compare classical mechanical alignment with the new kinematic alignment technique paint a controversial picture. In some cases, kinematic alignment shows slightly better clinical results, but the results are far less clear than expected by the supporters of the technique [224]. The reason for this may be the limited study situation with currently only six prospective studies on the one hand, on the other hand this technique is currently still in a development phase. Thus, for example, there are currently no recommendations regarding the target group suitable for such an implantation procedure.

A consistent implementation of this philosophy also requires to provide a knee laxity when implanting the prosthesis that allows to reproduce natural knee joint kinematics. This, therefore, requires a more extensive evaluation and, if necessary, adaptation of the laxity of the joint through a systematic balancing of the soft-tissue envelope. Knowledge about soft-tissue balancing has been primarily obtained in the context of mechanically aligned total knee arthroplasty. Accordingly, many of these results cannot be transfered to derive balancing recommendations for kinematic alignment. Basic studies that deal with joint stability in arthroplasty without committing to a special alignment procedure are rare. Furthermore, it is currently unclear to what extent the declared aim of kinematic alignment to preserve the physiologic state of the soft-tissues as well as possible is a realistic goal, especially since individual structures must be removed in the course of the operation to make room for the prosthesis. Furthermore, there are currently no descriptions of joint laxity which are based on a large cohort. Thus, quantitative target parameters for balancing are missing. This presents new challenges for the soft-tissue balancing step. Critical here is the possible influence of individual structures on different directions of joint laxity as well as a possible interaction of different structures. The strong influence of numerous parameters such as the implantation technique or the implant alignment as well as anatomical parameters and individual pathological changes such as deformities of the joint make balancing very complex. For this purpose, a numerical model would be helpful to investigate the interaction of different ligament structures with respect to joint laxity. Such a model could then be used to derive a tool with which soft-tissue management can be planned preoperatively in the future based on medical imaging data.

This dissertation aims to address the described challenges in the knee arthroplasty with the following main objectives:

- to investigate the natural laxity of the knee joint with its asymmetries and dependencies on the flexion angle in order to develop target parameters for joint laxity in the total knee arthroplasty.
- to fundamentally investigating the restraints of the knee joint depending on the condition of the soft-tissue envelope with regard to knee arthroplasty and to analyse to what extent the joint can be balanced by targeted resection of soft-tissue structures.
- to develop a simulation model which enables the prediction of the joint laxity depending on subject-specific anatomy and soft-tissue condition in order to gain new insights for soft-tissue management in knee arthroplasty procedures and to create the basis for a computer-based tool for preoperative planning of soft-tissue management.

4 Scientific approach

In order to address the questions raised as well as possible, three different methods were applied in the context of this dissertation: a meta-analysis, an *in-vitro* investigation, as well as the development and validation of an *in-silico* model (Figure 4.1). The results from the different approaches can be used to mutually ensure the plausibility of the individual research results. In the following, the basic considerations for the individual solution approaches are presented.

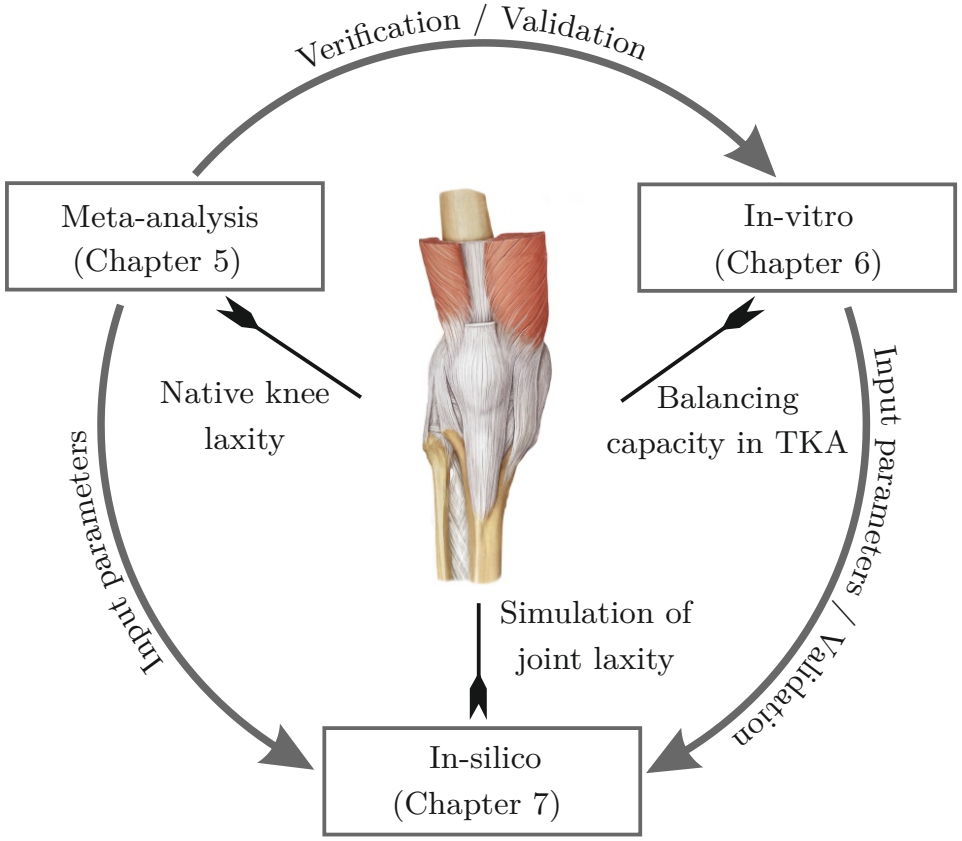

Figure 4.1: Schematic overview, illustrating the interlocking of the various methods used to address the aims of this dissertation. Drawing of the knee modified after [213].

In order to obtain reliable data on the laxity of the healthy, human knee joint, which are suitable for describing joint laxity in general and not just the characteristics of a small cohort, it is necessary to analyze the natural laxity of a large number of joints. Due to the limited number of specimens available, the associated ethical concerns and the immense effort required for such investigations, this cannot be achieved by own investigations of specimens. However, there are numerous publications in the literature in which the laxity of the healthy joint was recorded in individual directions. Therefore, all relevant, available literature data were collected in the context of this work and re-evaluated with the help of statistical methods in order to address the underlying problem.

Such a method is not suitable for analyzing the function of individual soft-tissue structures and their relevance for soft-tissue balancing in the knee arthroplasty, since very few data is available in the literature. Consequently, own investigations were used to address the underlying problem. For the investigations a new robot based biomechanic joint simulator was built and put into operation. The investigations of the joint laxity were performed by applying force and moment controlled loads in different directions. *In-vitro* investigations on knee specimens then made it possible to examine the function of individual soft-tissue structures with respect to the soft-tissue balancing in total knee arthroplasty. Single anatomical structures were dissected and the change in laxity of the knee joint in single direction was recorded.

Last, a new knee model was developed within the scope of this work in order to be able to numerically simulate the knee laxity. Since the movement within the joint is of special interest and in view of a later application for preclinical planning a short computing time and the possibility to integrate motion capture data is desirable, the decision was made to use a multibody simulation model. The advantage of this type of model compared to a finite element model is, that there are simulation platforms specially designed for biomechanical investigations with which a biomechanical model can easily be extended to include other joints and structures. By creating subject-specific data model, based on image data from specimens used in the *in-vitro* study, not only a indirect validation by a comparison to literature, but a direct one-to-one validation of the *in-silico* model could be achieved.

5 Soft-tissue laxity of the healthy knee joint

In the scientific literature there are numerous studies describing approaches to ensure the most efficient soft-tissue management possible in total knee arthroplasty. In these studies, the authors report the sequential order in which individual ligament structures should be partially released in order to achieve a balanced knee joint. The sequences described in the literature differ considerably in some cases [131]. Despite a lively discussion in research on this topic, total knee endoprostheses still fail today in part due to poor soft-tissue management [172]. One of the reasons for this is that to this day there are no commonly accepted guidelines regarding the desired soft-tissue tension of the knee joint. There are numerous guidelines for balancing itself, but there are still no guidelines that describe a desirable knee laxity in different directions for various flexion angles. Especially for modern, soft-tissue preserving techniques (*e.g.* kinematic alignment TKA), guidelines for soft-tissue tensioning based on examinations of the joint laxity on healthy knee joints seem suitable. In the scientific literature numerous studies exist, which deal with the determination of the soft-tissue laxity of the knee joint. In this context, the published literature can basically be distinguished in *in-vivo* and *in-vitro* investigations.

For *in-vivo* measurements different methods exist: these are mainly arthrometry, stress x-ray and radiostereometric analysis. In arthrometry, the knee laxity is determined by means of a device mounted around the knee joint of the patient. The device releases only defined DOFs and shifts the tibia relative to the femur in the desired direction under a pre-determined load. These non-invasive systems have the disadvantage that the measurements can be falsified by the soft-tissue movement (skin, fat, muscles) [217, 62]. A more accurate method which is not sensitive to the amount of soft-tissue present is the stress x-ray, in which the displacement of the tibia relative to the femur under load is recorded fluoroscopically [108]. The disadvantage of this method lies in the radiation exposure of the patient. For this reason, examinations with this method are mostly limited to a few flexion positions and testing directions. In addition, in most cases resulting knee motion is only captured in two dimensions, which can end in errors due to projection effects. One method with which a high resolution of the joint displacement in three-dimensional space can be recorded *in-vivo* is radiostereometric analysis [30]. For this method, small tantalum beads are inserted into the bones to be measured. The displacement of the joint under load can then be recorded three-dimensionally using two synchronously released x-ray sources, each of which records the joint from a different perspective. The obvious disadvantage of this method is its invasive nature, due to which only patients who have to be treated surgically can be considered for such examinations. Furthermore, only few clinics are equipped to perform radiostereometric imaging.

A much simpler and very effective method to measure the laxity of the healthy knee joint is the *in-vitro* examination. The examination of cadaveric joints coming from tissue donors allows a highly accurate assessment of joint laxity, the methods used in existing studies differ much less and there are no limitations due to the invasiveness of the application. Accordingly, *in-vitro* studies are particularly suitable for deriving the desired guidelines

for soft-tissue management of the knee joint. In the following, guidelines are to be worked out, by analysis of the existing scientific literature. The main focus is on summarizing knee laxity in anterior and posterior direction as well as in varus-valgus rotation and internal-external rotation. In this context, the asymmetry of the laxity values of antagonistic movements will also be investigated. Parts of these analysis were published in the Journal of Bone and Joint Surgery [60].

5.1 Materials and methods

The guidelines and recommendations of the Preferred Reporting Items for Systematic Reviews and Meta-Analysis statement (PRISMA) were taken into account in preparing this meta-analysis [220]. For the investigations, scientific databases were searched and all relevant studies were further analysed. Relevant data were extracted from the manuscripts, summarized and further analyzed. In the following the procedure is explained in more detail.

5.1.1 Literature search

In order to retrieve all relevant studies during the last 20 years (January 1st 1996 - December 31st 2016), the PubMed (https://www.ncbi.nlm.nih.gov/pubmed/) database and Web of Science (http://wokinfo.com/) were searched with combinations of the following keywords: biomechanical, knee, *in-vitro*, cadaveric, ligament, structures, laxity, soft-tissue, robot, robotic, simulator (Appendix A.1). The title list of this search was then analysed for relevant publications and the full text documents of those extracted. The following criteria were defined for the study selection:

- The knee laxity was examined on healthy joints.
- Laxity in at least one of the following directions was recorded: anterior, posterior, varus rotation, valgus rotation, internal rotation, external rotation.
- The joints were examined without simulation of the musculature.
- The data have been published in English language.
- The absolute values of the laxities determined in the studies were published in text form, tabular form or as a diagram.

5.1.2 Data extraction

The data were excerpted from the publications in a standardized way. The mean values and standard deviations of the laxity data were extracted for previously determined flexion positions. For the anterior and posterior translational directions the laxity data were recorded in full extension (0°), and 15°, 30°, 60° and 90° of flexion. The laxities in varus rotation, valgus rotation, internal and external rotation were recorded for the flexion positions full extension (0°), and 30°, 60° and 90° of flexion. For this purpose, the text of the

studies was examined and relevant data were transferred into a standardized table. If the data were available in tabular form, these data were also transferred to the standardized table. For publications where the laxity data was only available in the form of diagrams, the diagrams were enlarged to fill the screen and then saved in .png format. The diagrams were then digitally transcribed using freely available software (Engauge Digitizer, version 10.0). The accuracy of this method was examined by use of publications in which the data were presented both in the form of numerical values and in form of a diagram. The result was an accuracy of $< 0.1^\circ$ or < 0.1 mm per data point. In addition to the laxity data, further information regarding the specimens used and on the execution of the investigations was extracted from the publications. The following data were collected as far as it was possible: name of the lead author, year of publication, number of specimens, mean age of the donors, sex of the donors, specimen condition, storage temperature, thawing time, test rig design, definition of the coordinate systems used, forces/torques applied, DOFs of the testing setup. Boxplots of the pooled laxity data and laxities of analysis with the most often used testing method were generated for the six different testing directions. The latter were used to compare the data with own measurements, which were recorded with the same testing method (chapter 6).

5.1.3 Data analysis

The statistical software R (version 3.3.2 , R Foundation for Statistical Computing) [230] was used to further analyse the collected data. In order to carry out corresponding analyses, the packages "mice" (Multivariate Imputation by Chained Equations) [36] and "metafor" (A Meta-Analysis Package for R) [230] were also used. Before the data could be used for a meta-analysis, the data had to be further processed in order to prevent distortions caused by missing single values. For this reason, individual missing values in the data table were filled by means of an imputation procedure. The completeness of the data set before imputation was 80.5-86.8 %. A predictive mean matching model was used and fifteen imputations were processed to guarantee a stable imputation. In order to estimate the missing values, all other laxity data were used as predictors. In order to increase the reliability of the estimates, the type of testing setup, DOFs of the testing setup and amount of applied load were also used as predictors. In order of assessing the validity of the imputation, a sensitivity analysis was performed with the aim to assess the "missing at random" assumption. For further data analysis, a meta-analysis using a mixed-random-effects model was chosen. The decision was based on previous heterogeneity studies in which the heterogeneity between the studies was quantified by I^2 according to Higgins and Thompson [94]. Heterogeneity was then further investigated by subgroup analysis. For this purpose, the individual studies included were classified according to research groups. The different research groups were identified by the list of authors and the affiliation given in the study.

The main analysis was performed in the form of a three-level mixed-random-effects analysis with the aim to detect differences between the laxities (anterior, posterior, varus rotation valgus rotation, internal, and external rotation) depending on the flexion position. In addition, meta-analysis was used to investigate the asymmetry of the joint by determining the differences between the opposing movements (anterior-posterior, varus-valgus rotation internal-external rotation). For all analysis the mean laxity and standard deviations were

defined as the observed outcome. Type of testing setup, DOFs of the testing setup and applied loads served as covariates. For the statistical evaluation a significance level of $\alpha = 0.05$ was defined. For the presentation of the results mean values and 95 % confidence interval (CI) were given.

5.2 Results

The literature search in the databases resulted in a total of 1,117 hits. After reviewing the titles and abstracts, 115 relevant articles were identified. Thirty nine of these publications did not meet the inclusion criteria, according to which 76 studies with data totalling 865 knee joints were finally included in the meta-analysis (Figure 5.1, Appendix A.2). The level

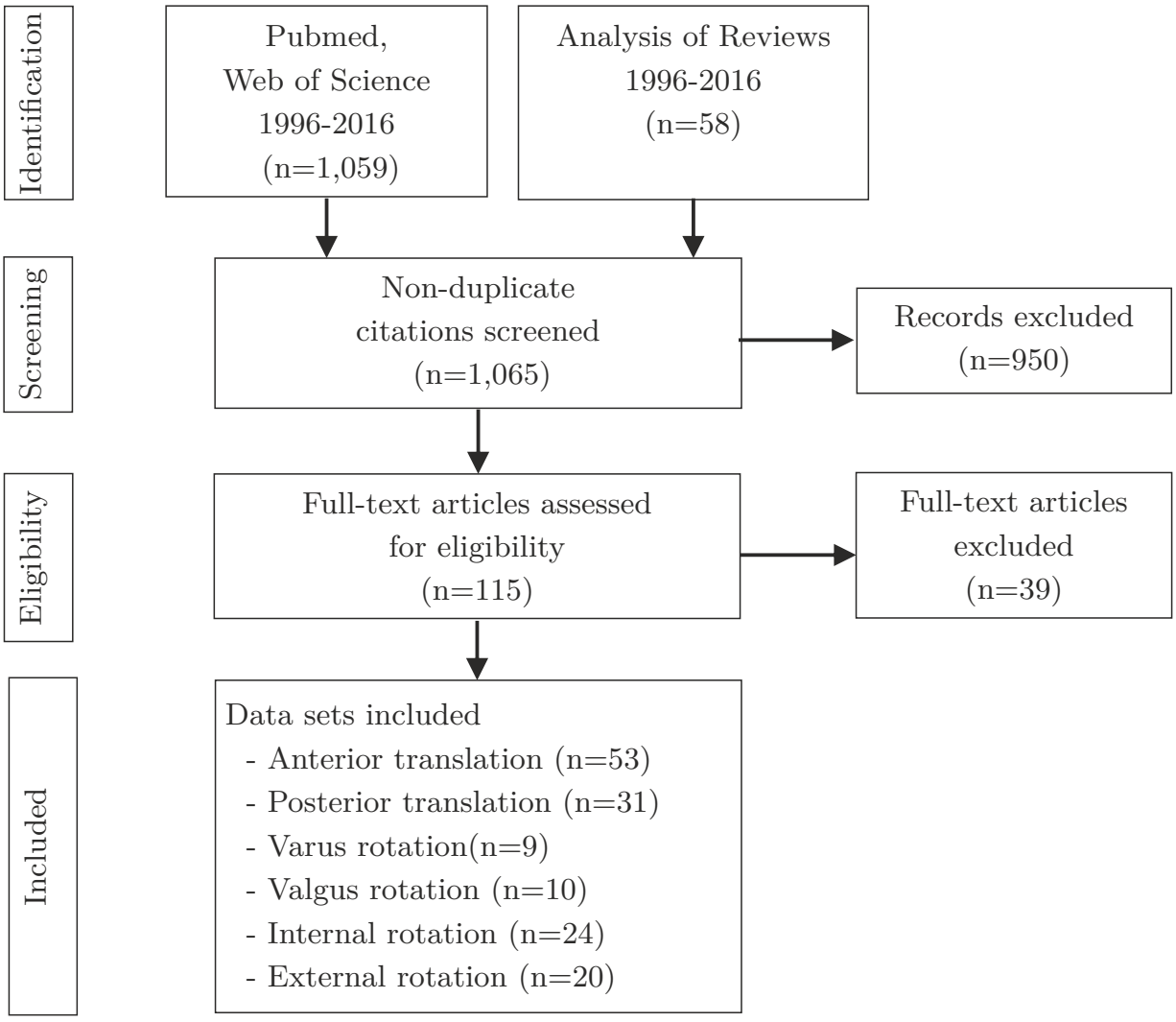

Figure 5.1: Flow of study selection for the meta-analysis showing the number of included and excluded studies (n = number of articles).

of detail of the experimental methods described in the publications differed considerably. The mean age of the tissue donors was therefore only stated in 61 %, the gender of the donors was only announced in 25 % of all included studies. However, the testing machine

used for the study was reported in 100 % and the amount of applied load in 99 % of the publications. Further details are summarized in the following table (Table 5.1).

Table 5.1: Summary of the experimental methods reported in the included studies.

Experimental methods	Number (%) of studies adequatly reporting experimental methods
Sample mean age	46 (61)
Sample range age	63 (83)
Sample sex	19 (25)
Sample situation	61 (80)
Sample storage temperature	52 (68)
Sample thawing time	58 (76)
Testing machine	76 (100)
Testing force	75 (99)
Location of coordinate Systems	28 (37)
Degrees of freedom	57 (75)

The load applied to evaluate the knee laxity differed between the publications and ranged from 45-150 N for the anterior and posterior direction. The applied loads in varus and valgus rotation were 3-10 Nm and 5-10 Nm, respectively. The axial rotation laxity was evaluated by applying torques of 4-10 Nm for internal rotations and 3-10 Nm for external rotations. In 76 % of all studies, a robot testing device was utilized to evaluate joint laxity, in 9.2 % a material testing machine and in 14.5 % a custom made testing device was used. Besides the amount of load and the type of testing device, the number of DOFs for the individual test scenarios differed between the included studies. In 67% of the studies only one DOF (flexion angle) and in 7% of studies two DOFs were restrained for the investigations. In one case each, three and five DOFs were restrained, respectively. 21% percent of the included studies did not report the restraints of motions in their testing protocol.

Heterogeneity in the included studies

The analysis of the heterogeneity between the included studies was without a further subgroup analysis in the lowest case I^2=85% for the external rotation and in the maximal case I^2=98 % for the valgus rotation. By means of a subgroup analysis the heterogeneity could be further assigned. Thus the heterogeneity between the research groups ranged from I^2<1 % for external rotation to I^2=53 % for anterior translation. Within the research groups similarly high values were observed, whereby the heterogeneity ranged from I^2=42 % for laxity data in anterior direction to I^2=85 % for external rotation laxity. Further details are summarized in the following table (Table 5.2).

Knee laxity at different flexion angles

The knee laxity changed in the knee joint depending on the angle of flexion between 0° and

Table 5.2: Overall amount of heterogenieity between the included studies (I^2) for the different testing directions. Heterogeneity between and within research groups are presented.

Testing direction	Global / %	Inter group / %	Intra group / %
Anterior translation	95	53	42
Posterior translation	96	50	46
Varus rotation	94	47	47
Valgus rotation	98	49	49
Internal rotation	90	28	62
External rotation	85	<1	85

90° in all investigated directions. The lowest laxity was observed at 0° flexion in all test directions except posterior translation and was 4.31 ± 1.45 mm in anterior translation, 5.51 ± 1.46 mm in posterior translation, 2.49 ± 1.05° in varus rotation, 3.00 ± 0.65° in valgus rotation, 10.98 ± 3.36° in internal rotation, and 11.66 ± 4.30° in external rotation. The following changes of the laxity could be observed in the individual directions:
The anterior laxity changed from 0° to 15° by 1.74 mm (95 % CI, 1.55, 1.92), from 15° to 30° by 0.81 mm (95 % CI, 0.58, 1.04), from 30° to 60° by -0.84 mm (95 % CI, -1.08, -0.59) and from 60° to 90° by -0.78 mm (95 % CI, -1.02, -0.54). Accordingly, the highest laxity could be observed with 7.38 ± 2.28 mm at 30°. All laxity values in anterior direction differed significantly from each other with flexion angle ($p<0.001$) except for the laxities at 15° and 60° which did not differ significantly from each other ($p=0.85$) (Figure 5.2, Table A.4, A.7).

The posterior laxity changed from 0° to 15° by 0.57 mm (95 % CI, 0.41, 0.973), from 15° to 30° by -0.02 mm (95 % CI, -0.18, 0.15), from 30° to 60° by -1.67 mm (95 % CI, -1.82, -1.52) and from 60° to 90° by 0.77 mm (95 % CI, 0.58, 0.95). All changes were significant ($p<0.001$) except between 15° and 30° ($p=0.84$). The highest laxity of 5.99 ± 1.71 mm could also be observed here at 30° flexion (Figure 5.2, Table A.4, A.8).

The greatest laxity in varus rotation was observed at 90° and was 4.92 ± 1.33°. The change of flexion angle resulted in an increase of laxity by 2.42° (95 % CI, 2.14, 2.71) from 0 to 30°, by -0.18° (95 % CI, -0.51, 0.15) from 30° to 60° and by -0.64° (95 % CI, -1.00, -0.28) from 60 to 90°. Laxity changed significantly in all cases ($p<0.001$) except when changing from 30° to 60° ($p=0.28$) (Figure 5.3, Table A.5, A.9).

Regarding valgus rotation, the highest laxity could be observed at 60° and was 6.96 ± 2.96°. The laxity changed with the FLexion from 0° to 30° by 3.47° (95 % CI, 2.14, 2.71), from 30° to 60° by -1.07° (95 % CI, -1.30, -0.85), and from 60° to 90° by 1.85° (95 % CI, 1.43, 2.26). The laxity change with flexion angle was significant in all cases ($p<0.001$) (Figure 5.3, Table A.5, A.10).

The laxity at internal rotation was highest at 60° with 19.39 ± 5.88°. From 0° to 30° the laxity changed by 6.56° (95 % CI, 5.93, 7.19, $p<0.001$), from 30° to 60° by -0.96 (95 %

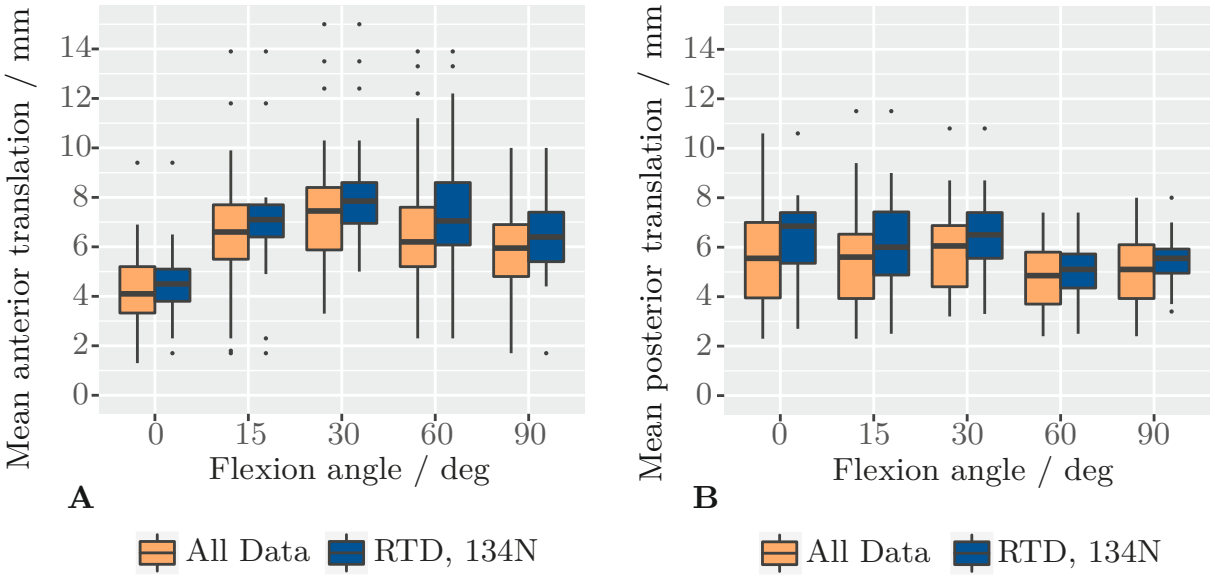

Figure 5.2: Tukey's box plots showing the knee laxity in anterior (A) and posterior (B) direction in dependence of the flexion angle from 0 to 90°. Presented are pooled data of all included studies (orange) and of the most often used testing method (blue): Robot Testing Device (RTD) as testing platform and 134 N as anterior/posterior load.

CI, -1.69, -0.23, p=0.01) and from 60 to 90° by -3.98° (95 % CI, -4.67, -3.27, p<0.001) (Figure 5.4, Table A.6, A.11).
Similar results could be observed for the laxity at external rotation. The highest laxity was 17.84 ± 5.71° at 90° flexion. The laxity increased steadily from 0° to 60° and increased from 0° to 30° by 4.96° (95 % CI, 4.12, 5.81), from 30° to 60° by 2.35° (95 % CI, 1.43, 3.26) significantly (p<0.001). The change from 60° to 90° by -0.89° (95 % CI, -1.87, 0.075) was not significant (p=0.075) (Figure 5.4, Table A.6, A.12).

Asymmetry in laxity of the knee joint

Regardless of the angle of flexion, differences in laxity between opposing directions in the single DOFs could be observed in almost all cases. The largest differences were for anterior posterior motion (p<0.001) at a flexion angle of 0° with values of ΔL=-2.64 mm (95 % CI, -2.95, -2.33), for varus-valgus rotation (p<0.001) at 30° with values of ΔL=-1.85 mm (95 % CI, -2.20, -1.50) and for internal-external rotation (p<0.001) also at 30° with ΔL=3.31 mm (95 % CI, 2.03, 4.56). The varus-valgus asymmetry at 0° and 90°, was low with -0.17° (p=0.041) and 0.10° (p=0.45°) (Table A.3).

5.3 Discussion

A better understanding of the laxity of the native knee joint is a fundamental requirement for effective soft-tissue management in total knee arthroplasty. To date, there are no quantitative guidelines that describe the general laxity of the knee joint on the basis of a larger cohort. Therefore, the aim of this meta-analysis was to collect the results of all knee

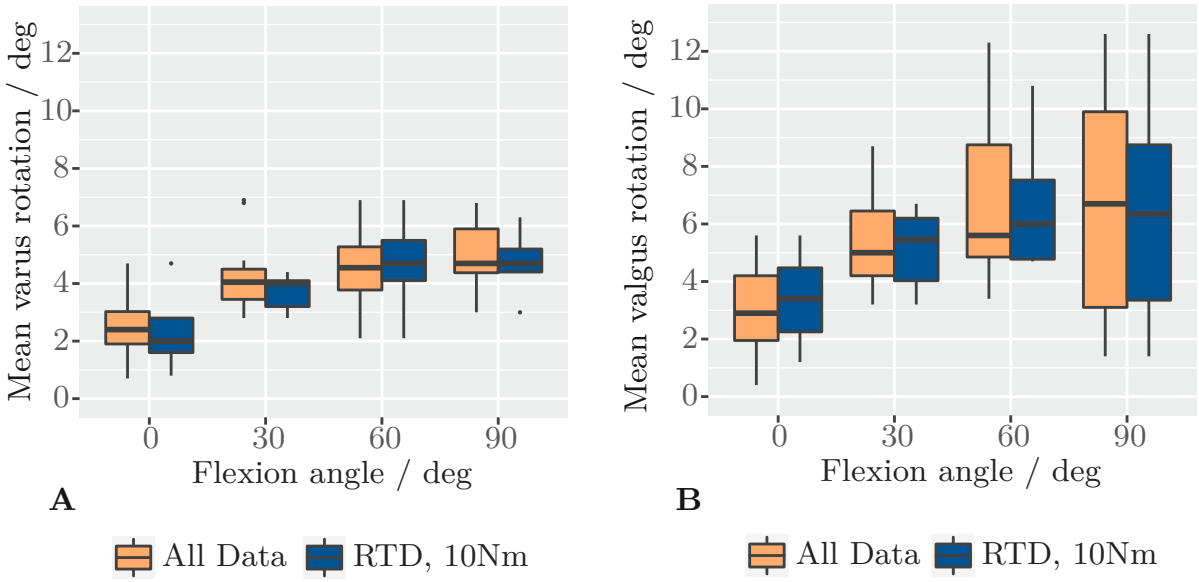

Figure 5.3: Tukey's box plots showing the knee laxity in varus (A) and valgus (B) rotation in dependence of the flexion angle from 0 to 90°. Presented are pooled data of all included studies (orange) and of the most often used testing condition (blue): Robot Testing Device (RTD) as testing platform and 10 Nm as varus/valgus torque.

laxities measured *in-vitro* for anterior translation, posterior translation, varus rotation, valgus rotation, internal rotation, and external rotation in order to extract guide values for native soft-tissue balancing. Since common soft-tissue management recommendations assume a symmetrical joint gap, another aim of this analysis was to determine the natural degree of symmetry or asymmetry of the joint between the opposite directions of a certain DOF. A third aspect of the analysis was to investigate the influence of the test conditions on the measurement result in order to be able to assess *in-vitro* measurements in the future. The analysis concludes that the laxity of the knee joint in the investigated directions differs greatly between the different flexion angles. In addition, the difference in laxity between anterior and posterior directions, varus and valgus rotation as well as internal and external rotation over a flexion range of 0-90° is significant. The investigations also showed that testing conditions in individual test directions influence laxity measurements.

The current procedure of soft-tissue balancing in total knee athroplasty is essentially limited to rudimentary recommendations for the symmetry of the joint space in most cases only for two flexion positions (0° and 90°). The assessment of the extent of laxity itself, even with the aid of modern balancing instruments, has so far been substantially based on the surgeon's assessments. This approach however cannot guarantee a complete restoration of the function of the soft-tissue envelope. Interestingly, the data collected with meta-analysis show that the joint gap in full extension and in 90° flexion has only a clinically insignificant asymmetry. At 30° and 60° flexion, however, a substantial asymmetry of the joint was found. In many cases, this leads to overstuffing or instability of the knee joint in flexion positions between 0° and 90° [58]. Based on the results of this analysis, soft-tissue balancing exclusively in 0° and 90° positions is not sufficient. Consequently, soft-tissue balancing in multiple flexion positions is recommended to prevent biomechanically unfa-

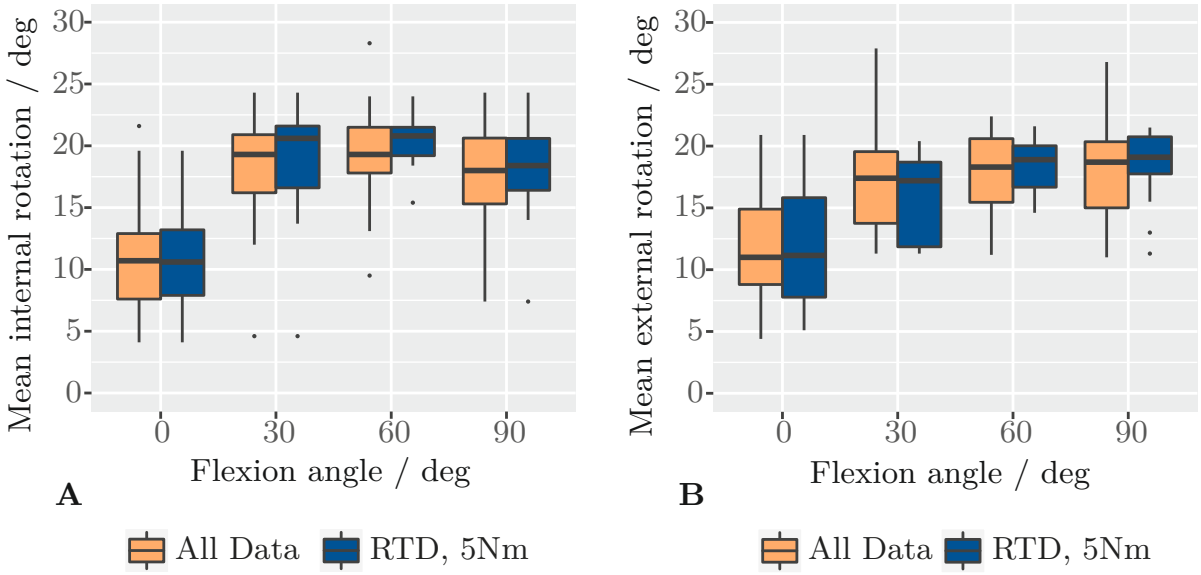

Figure 5.4: Tukey's box plots showing the knee laxity in internal (A) and external (B) rotation in dependence of the flexion angle from 0 to 90°. Presented are the pooled data of all included studies (orange) and of the most often used testing condition (blue): Robot Testing Device (RTD) as testing platform and 5Nm as internal/external rotation torque.

vorable conditions such as instability or high loading which can negatively influence the function of the joint. If the aim of modern joint arthroplasty is to restore the natural knee joint function, the collected data can serve as guidelines, for example to restore the natural soft-tissue tension when implanting a knee endoprosthesis using modern navigation systems or robot assistants [160]. With these technologies on the one hand, the change in knee laxity with respect to the flexion angle and on the other hand the natural asymmetry of the joint can be taken into account.

Another important finding was obtained by investigating the effect of testing methods on laxity. The testing modalities influenced the measurements only in single testing directions. The load applied to measure laxity only influenced the results in the posterior direction. The measurement of laxity in the anterior direction, on the other hand, seems to yield the same results regardless of a load between 45 N and 150 N. With regard to the influence of the load in the other directions, no meaningful statements can be obtained due to the low variance of the applied load between the studies. In this meta-analysis, the test setup only had an influence on the laxity measurements during internal rotation. The reason for this difference might be for example the test speed or the agility and accuracy of the controller. The testing methods also differed in the number of degrees of freedom released for investigation in the individual directions. However, an influence of the number of degrees of freedom was not observed in this study. The reason for this might probably be the low variance and the strongly different group size of the investigations with different degrees of freedom. In summary, it must be assumed that the test conditions of the included studies may have influenced the laxity measurements.

The heterogeneity studies also showed a considerable variance between the studies. The sub-group analysis also showed that on average 45 % of the heterogeneity was due to the

variance between research groups, while on average 55 % of the variance was found within a research group. The variance between the research groups may be due to different approaches to laxity testing, such as differences in test design or in the definition of coordinate systems used. While the variance within a working group is more likely due to the individuality of the used specimens and their preparation.
Nonetheless, this meta-analysis is also subject to some limitations. Currently there is no standardized process to assess the quality and to check for a possible publication bias in *in-vitro* studies. Therefore, the reporting of testing methods to quantify the reporting quality of the studies included in this meta-analysis was analyed. This showed that the physiological status of the knee joints used in the *in-vitro* studies was reported in only 80 % of all included studies. Accordingly, it cannot be completely ruled out that some of the data were obtained from joints with pathological joint laxity caused by a disease such as arthrosis-related flexion contracture or valgus deformity. Another limitation of this study is that only *in-vitro* data could be used for the analysis. Numerous studies have however shown that laxity measurements in *in-vitro* studies are comparable to *in-vivo* measurements [156, 218].

Concluding, the meta analysis provides mean pooled laxity data and laxity data based on the analysis with the most often used testing condition which can be used to validate new testing devices, experimental results, or to use for numerical modeling. To guarantee qualitative reporting, I recommend the following information to be reported in future studies investigating the laxities of the knee: range and mean age, sex, and condition (pathology) of the samples as well as type of the testing machine, applied loads, degrees-of-freedom of the setup, as well as a detailed description of the coordinate system used for data collection.

6 In-vitro analysis of the balancing capacity of the human knee in arthroplasty procedures

The removal of individual soft-tissue structures such as the two menisci and the ACL is a necessary step for the implantation of the majority of prostheses available on the market, to create space for a knee prosthesis and to allow for a proper alignment of the components. In this way the stabilizing function of these soft-tissue structures is already lost. In addition, depending on the implantation procedure, and the condition of the soft-tissue, further sometimes far-reaching changes in the function of the soft-tissue envelope are necessary to rebalance the joint.

With the development of new implant systems and implantation procedures, patients' and surgeons' expectations of the joint function provided with a knee prosthesis are growing. With regard to the postoperative soft-tissue structure of the knee joint and the implant design, the question arises to what extent a natural joint balance can be restored using a modern prosthesis design and a corresponding implantation technique?

By comparing the mechanical alignment technique with kinematic alignment technique, Maderbacher *et al.* showed in nine knee specimens that kinematic alignment allows to restore a more natural and physiological femorotibial kinematic. However, the results of the study still show considerable differences in knee joint kinematics after knee arthroplasty using kinematic alignment, especially between 20° and 70° flexion [152]. Similar results were obtained in a study by Stoddard *et al.* in which two different implant designs were investigated with regard to joint stability [221]. The authors conclude that the laxity of the knee joint after knee arthroplasty differs significantly from the laxity of a natural joint. It is still unclear whether the observed deviations in joint kinematics and joint stability between the knee with arthroplasty and the physiologic joint can be technically compensated, *i.e.* eliminated with the right implantation technique and a suitable knee implant. As a matter of principle the knee kinematic after knee arthroplasty essentially depends on the function of the postoperative soft-tissue constitution. The most important joint property in this regard is the joint laxity. The influence of individual ligament structures on the laxity of the knee joint has already been investigated in numerous studies. The majority of these biomechanical studies in this context investigated the laxity of the joint with regard to traumatic injuries (chapter 5). Still, there are several studies investigating the influence of individual soft-tissue structures on knee laxity with regard to knee arthroplasty. However, in these relevant studies, individual ligament structures were investigated following implantation of a knee prosthesis [40, 16, 17]. The results of these studies therefore depend on the implantation technique and the implant design. There are almost no basic studies independent of the implantation technique and implant design.

Therefore, the aim of this *in-vitro* study was to investigate the functional structure of the soft-tissue envelope in context of knee arthroplasty procedures. In particular, the joint laxity of the knee in anterior, posterior, inferior direction as well as in varus, valgus, internal-and external rotation, depending on the knee flexion and the condition of the

soft-tissue structures were investigated in order to clarify:

- to what extent the operative approach influences the laxity of the joint and thus distorts an *in-situ* balancing of the joint laxity,
- whether the structural anatomy of the knee joint allows in principle to restore the natural joint laxity after required tissue removals and releases of the menisci and ACL for prosthesis implantation, and to what extent the removal of the two structures influences the joint laxity,
- the influence of the release of individual soft-tissue structures potentially used for soft-tissue balancing on the laxity of the joint.

6.1 Materials and methods

For the biomechanical investigation of the knee joint, a robot-based testing device was set up. By using specially programmed testing protocols this system enables the defined loading of human knee joint specimens in different testing directions at various flexion positions in order to measure the laxity of the knee joint in a standardized way.
The following section presents details of the applied investigation methods. The components of the *in-vitro* setup, its control structures, robot programming, the coordinate systems used and the optical measurement system for recording geometry and kinematics are described in detail.

A further section reports the approach to determine the laxity of the knee depending on the soft tissue condition using human joint specimens. The individual aspects starting with the preparation of the specimens, the definition of the testing protocol, through to the implementation of the soft-tissue sections and releases and the statistical analysis are described.

6.1.1 Robot based knee simulator

The test bench developed within the scope of this work consists of a robot (KR 16-2, Kuka AG, Augsburg, Germany) including controller (KR C4, Kuka AG, Augsburg, Germany) and control unit (Smart Pad), a six component force-torque sensor (Delta Net, ATI Industrial Automation, Apex, USA), a specimen mounting tower as well as a peripheral computing unit.

The six-axis robot with serial, open kinematics has a nominal payload of 16 kg, a reach of 1611 mm and a repeat accuracy of $\pm$ 0.05 mm. The six components force-torque sensor is mounted at the end effector. The sensor has a sensing range of at least 660 N and 60 Nm at a resolution of at least 0.25 N and 7.5 $\cdot 10^{-3}$ Nm. The sensor flange has a mount for the tibia of the specimen. Opposite the robot is a custom made mounting tower, which is also equipped with a specimen mount to hold the femur of a specimen. Both specimen mounts are equipped with devices that enable the registration of coordinate systems by means of a probe tip and an optical measuring system. With these devices, reference coordinate systems of a potentially used optical measuring system can be matched with those of the

robot (Figure 6.1).

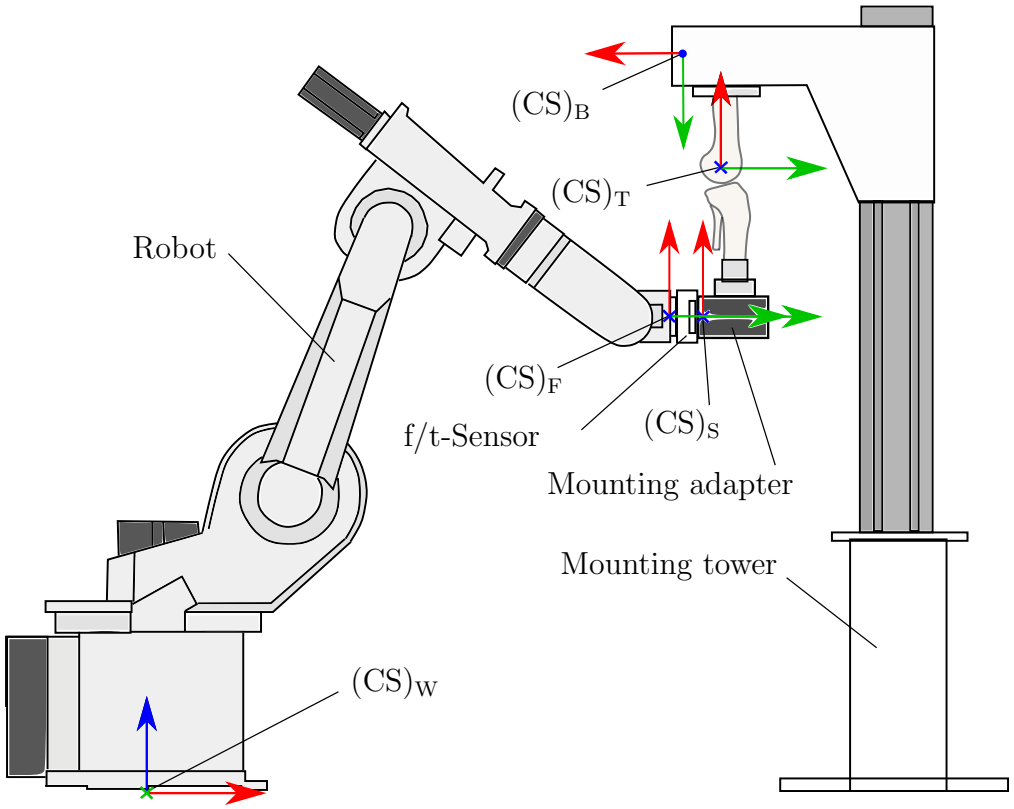

Figure 6.1: Overview of the testing setup including the robot with force-torque sensor (f/t-sensor), specimen mounting adapter at its wrist and the specimen mounting tower are shown. Furthermore, the defined coordinate systems (CS) are displayed: $(CS)_W$: World CS, $(CS)_B$: Base CS, $(CS)_T$: Tool CS, $(CS)_F$: Flange CS, $(CS)_S$: Sensor CS. Colors of the CS axis represent the directions: x (red), y (green), z (blue).

The different technical components (robot controller, smart pad, sensor, peripheral computing unit) communicate over EtherCat and Ethernet interfaces, *i.e.* they are connected via an Ethernet switch (Figure 6.2). The sensor data are fed into the Ethernet by an ATI Net box and made available to the robot controller via an EtherCAT (Beckhoff Automation GmbH, Verl, Germany) interface. The KUKA.RobotSensorInterface and KUKA.ForceTorqueControl technology packages enable sensor data to be integrated into the robot controller. This allows the robot to be moved in a force-torque controlled manner. Robot positions, forces, torques and other details required for testing can be transferred to an external computer with an Ethernet connection between the computer and the robot controller. The data is transferred in XML format using the KUKA.RobotSensorInterface technology package. This makes it possible to send data from the robot to the external processing unit and vice versa.

A stand-alone software environment based on the programming environment LabVIEW (version 2017, National Instruments, Austin, USA), which was set up on the peripheral computing unit, is used for online data recording and display. In addition, the software environment has additional functions for parametrizing the robot. The controlling of the robot itself and the execution of robot protocols is done via the Smart Pad of the robot. In order to be able to use the robot for biomechanical specimen testing, in certain work

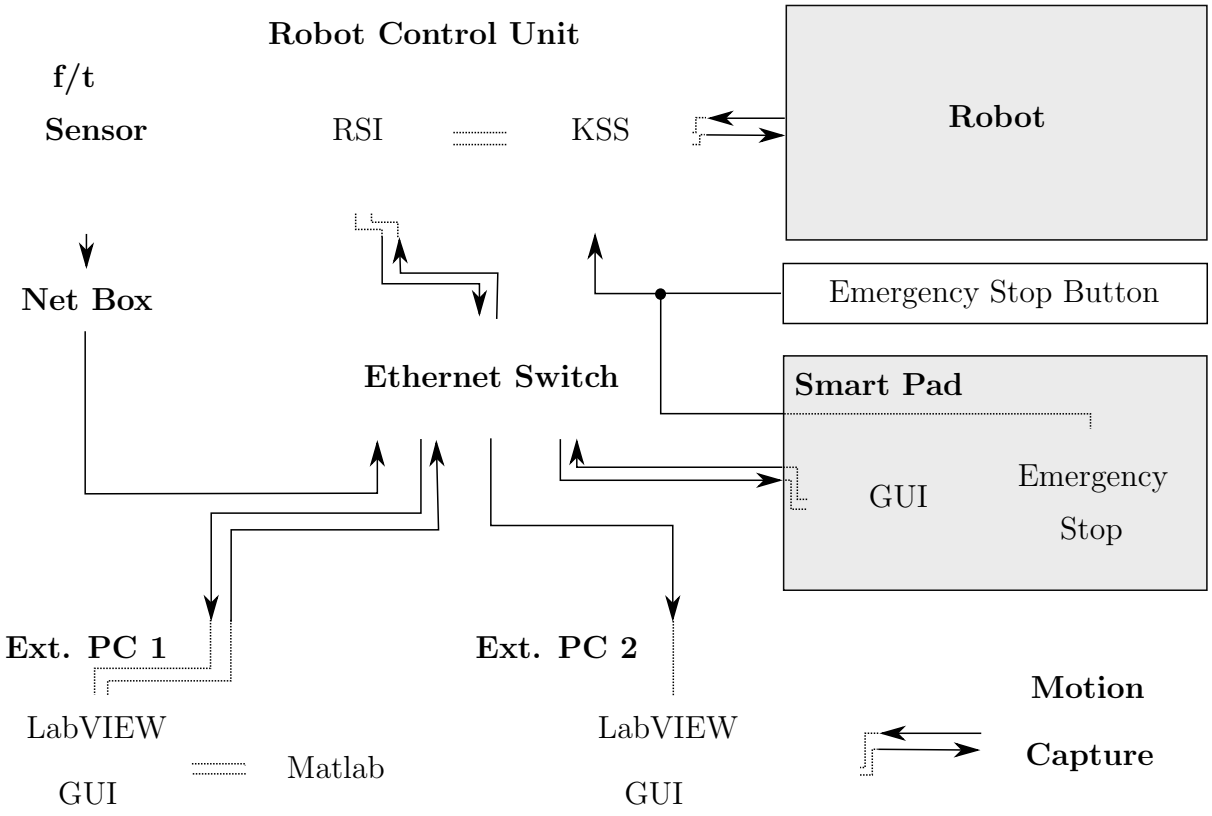

Figure 6.2: Overview of the system architecture showing the interconnection of the individual components for data exchange and processing.(RSI: Robot Sensor Interface, KSS: Kuka System Software, GUI: Graphical User Interface, Ext. PC: External Personal Computer)

steps it is necessary for the user to enter the workspace of the robot. This increases the risk of injury to the user. The system, therefore, has two separate emergency switches. One is located on the robot's control panel and another is separately accessible outside the work-space of the robot. In addition, the working area and safety area have been severely restricted on the controller side in order to reduce the risk of injury.

6.1.2 Coordinate systems

For a target-oriented movement of the robot arm, the system is equipped with different coordinate systems which, depending on the application, allow an easy coordination in six DOFs. In addition, coordinate systems can be individually created and defined. The following cartesian coordinate systems are defined (Figure 6.1):

- The world coordinate system $(CS)_W$, a space fixed coordinate system and origin coordinate system for the robot's base coordinate system. It is defined by default in the foot of the robot arm.
- The base coordinate system $(CS)_B$, usually a fixed coordinate system, defining the position of the mounting tower in the present setup relative to the $(CS)_W$.

- The flange coordinate system $(\mathrm{CS})_{\mathrm{F}}$ is located at the end of the flange of the robot wrist (last joint in the arm).
- The tool coordinate system $(\mathrm{CS})_{\mathrm{T}}$, is a coordinate system which lies in the working point of the tool. In the present application it is a specimen specific coordinate system which is defined in the geometric center of the specimen.

Furthermore, the force-torque sensor also has an independent sensor coordinate system $(\mathrm{CS})_{\mathrm{S}}$, which defines the directions and position of the measured force and torque vector:

$$ {}_{(\mathrm{S})}\boldsymbol{f}_{\mathrm{S}} = (f_{\mathrm{S_x}}, f_{\mathrm{S_y}}, f_{\mathrm{S_z}})^{\intercal} \quad \text{and} \quad {}_{(\mathrm{S})}\boldsymbol{t}_{\mathrm{S}} = (t_{\mathrm{S_x}}, t_{\mathrm{S_y}}, t_{\mathrm{S_z}})^{\intercal}, \quad \text{with} \quad {}_{(\mathrm{S})}\boldsymbol{f}_{\mathrm{S}}, {}_{(\mathrm{S})}\boldsymbol{t}_{\mathrm{S}} \in \mathbb{R}^3. \tag{6.1} $$

The elements of the force and torque vector correspond to the forces (f) and torques (t) along and around the axes of $(\mathrm{CS})_{\mathrm{S}}$.
Using appropriate transformations, the sensor coordinate system can be transferred to coincide with robot-specific coordinate systems such as the tool coordinate system to then capture the loads in the tool coordinate system. The force vector was transformed from $(\mathrm{CS})_{\mathrm{S}}$ to $(\mathrm{CS})_{\mathrm{T}}$:

$$ {}_{(\mathrm{T})}\boldsymbol{f}_{\mathrm{S}} = {}^{\mathrm{T}}\boldsymbol{R}_{\mathrm{S}(\mathrm{S})}\boldsymbol{f}_{\mathrm{S}} \quad \text{and} \quad {}_{(\mathrm{T})}\boldsymbol{t}_{\mathrm{S}} = {}^{\mathrm{T}}\boldsymbol{R}_{\mathrm{S}(\mathrm{S})}\boldsymbol{t}_{\mathrm{S}} + {}_{(\mathrm{T})}\boldsymbol{p}_{\mathrm{S}} \times {}_{(\mathrm{T})}\boldsymbol{f}_{\mathrm{S}} \quad \text{with} \quad {}^{\mathrm{T}}\boldsymbol{R}_{\mathrm{S}} \in SO(3), \tag{6.2} $$

with ${}_{(\mathrm{T})}\boldsymbol{p}_{\mathrm{S}}$ as the position vector of the $(\mathrm{CS})_{\mathrm{S}}$ origin.

6.1.3 Control architecture

A central part of the test setup is the force-torque control of the robot system. The integration of this technology using the packages provided by the manufacturer enables a simple activation and control of the force-torque control via the KUKA Robot Language (KRL) based robot scripts. The controller architecture for the sensor signal processing was designed using the Kuka's own graphical programming environment RSI Visual (v1.1.0.0, Kuka AG, Augsburg, Germany). A data flow (RSI context) was created using so-called RSI objects. An RSI object executes a certain functionality (*i.e.* addition, coordinate transformation) with its signal inputs and provides the result at the signal outputs. By interconnecting different objects, selected from a wide range, an RSI context was created to implement the force sensor data into the robot control which could then be loaded within the robot scripts. Within the robot script the data processing for the force-torque control, running parallel to the program flow of the robot control, can be switched on and off, depending on whether force-torque data is required or not [75]. Within the RSI context, Ethernet communication with the peripheral computing unit was also implemented to allow for external data recording or processing. For this purpose, an Ethernet object is available in RSI with which up to 64 input and output signals can be processed. The signals present at the inputs of the Ethernet object were sent to the peripheral processing unit. Data received from the peripheral processing unit were available at the outputs of the Ethernet object and made available for the RSI context. The communication between sensor, robot controller and peripheral processing unit was achieved via a real-time Ethernet connection. The data transmission was realized via a UDP/IP protocol. This allowed a complete signal processing in maximum 4 ms *i.e.* within one sensor cycle.

The influence of sensor data on the robot movement was realized within the RSI context. During an Ipo (input-process-output) cycle of the robot a Cartesian position correction can be calculated and add to the current target position. The movement corrections are added up, continuously. The new robot position is then calculated based on the displacement of the starting position and the correction value. The system allows to superimpose the sensor correction with a programmed path based movement of the robot. Depending on the testing protocol, the tool or base coordinate system can serve as the reference coordinate system for the correction.
The control architecture of the force-torque control consists of different elements (Figure 6.3). The forces $\boldsymbol{f}_{\text{act}}$ are measured via the force-torque sensor at the end effector of

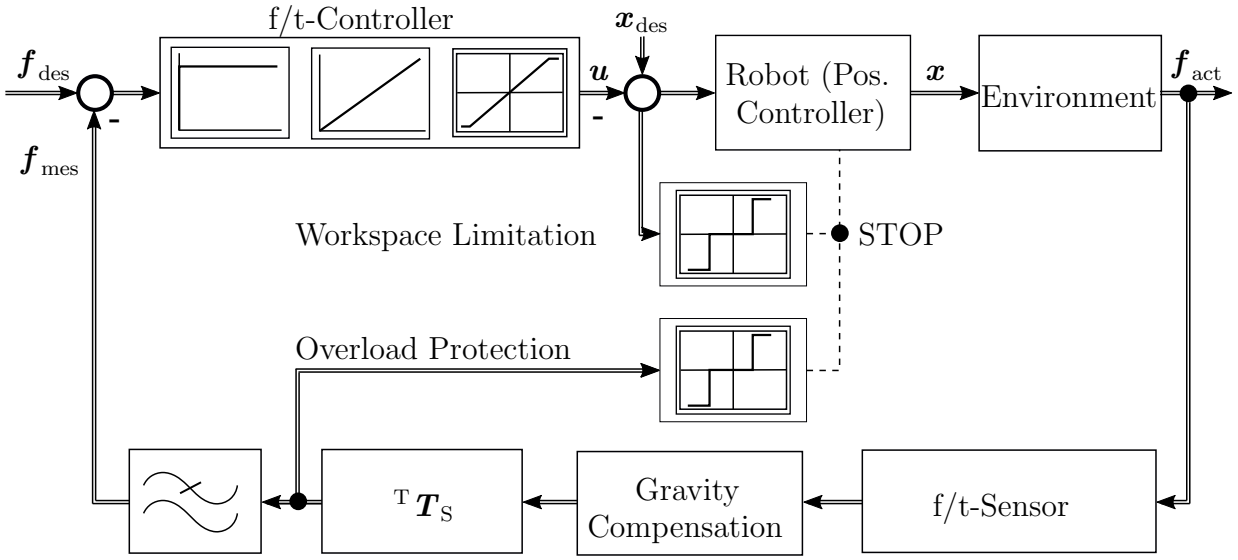

Figure 6.3: Force-torque (f/t) controller architecture of the robot based knee simulator. $\boldsymbol{f}_{\text{mes}}$: measured force/torque, $\boldsymbol{f}_{\text{des}}$: desired force/torque, $\boldsymbol{f}_{\text{act}}$: physical force/-torque acting, $\boldsymbol{x}_{\text{des}}$: desired position, $\boldsymbol{u}$: position correction, $^{\text{T}}\boldsymbol{T}_{\text{S}}$: load transformation from $(\text{CS})_{\text{S}}$ to $(\text{CS})_{\text{T}}$.

the robot. By a gravitation compensation the gravitational terms occurring due to the tool weight are being calculated out. For a tool with the mass m_{T} and the known local vector ${}_{(S)}\boldsymbol{s}_{\text{T}}$ of the center of gravity, the corrected forces ${}_{(S)}\boldsymbol{f}_{\text{comp}}$ and torques ${}_{(S)}\boldsymbol{t}_{\text{comp}}$ can be calculated by

$$ {}_{(\text{S})}\boldsymbol{f}_{\text{comp}} = {}_{(\text{S})}\boldsymbol{f}_{\text{S}} - {}_{(\text{S})}\boldsymbol{f}_{\text{grav}} \quad \text{with} \quad {}_{(\text{S})}\boldsymbol{f}_{\text{grav}} = {}^{\text{S}}\boldsymbol{R}_{\text{W}} \begin{pmatrix} 0 \\ 0 \\ -\text{m}_{\text{T}} g \end{pmatrix} \tag{6.3} $$

and

$$ {}_{(\text{S})}\boldsymbol{t}_{\text{comp}} = {}_{(\text{S})}\boldsymbol{t}_{\text{S}} - {}_{(\text{S})}\boldsymbol{f}_{\text{grav}} \times {}_{(S)}\boldsymbol{s}_{\text{T}}, \tag{6.4} $$

with g beeing the gravitational acceleration, ${}_{(\text{S})}\boldsymbol{f}_{\text{S}}$, ${}_{(\text{S})}\boldsymbol{t}_{\text{S}}$ the forces and torques recorded by the f/t-sensor and ${}_{(\text{S})}\boldsymbol{f}_{\text{S}}$, ${}_{(\text{S})}\boldsymbol{t}_{\text{S}}$ the forces and torques caused by the gravitation of the mounted tool. In the further course, the corrected forces and torques are transformed

into the tool coordinate system and further processed using a low-pass filter (PT_2 filter). The control error is then calculated between the desired load $\boldsymbol{f}_{\mathrm{des}}$ and the measured load $\boldsymbol{f}_{\mathrm{mes}}$. The subsequently operated force-torque controller contains a proportional and a integrational element which convert the control difference into an incremental correction of the position $\boldsymbol{u}$. In the following, the incremental correction is limited to a maximum acceptable threshold. The difference between the target position $\boldsymbol{x}_{\mathrm{des}}$ and the position correction $\boldsymbol{u}$ is passed on to the robot with integrated position control, which then influences the environment by moving to the calculated position $\boldsymbol{x}$. In addition, further safety precautions have been implemented: a work-space limitation restricts the approachable working points of the robot to a volume in the direct vicinity of the specimens to be tested. Exceeding this defined working area triggers a stop of the robot. The integration of a load monitoring also protects against the destruction of a mounted specimen on the one hand and against major damage to humans and the machine in the event of an undesired collision on the other. In case the load measured in the tool coordinate system $(\mathrm{CS})_{\mathrm{T}}$ exceeds a threshold value, the robot will stop its movement within 4 ms.

6.1.4 Robot scripts

The scripts to program the robot are implemented in the Kuka Robot Language (KRL). The scripts can be loaded and executed directly on the operating system of the robot. Within the program scripts the RSI context is implemented by means of a syntax, in which the signal processing of the force-torque sensor, the control architecture and the Ethernet communication with the peripheral computing unit is realized. The parametrization of the RSI context is done via KRL command lines that can be used to adapt individual attributes of the RSI objects. Furthermore, the processing of the RSI context can be activated and deactivated in the program sequence.

The programmatic implementation of the test protocols for biomechanical investigations of a human knee joint by use of the robot-based knee simulator can be divided into three program steps: specimen mounting, calculation of the geometric rotational center of the knee joint and biomechanical testing of the knee joint. These program steps are explained in more detail in the following:

Specimen mounting

For biomechanical examination of a knee joint, the femoral side of the specimen is attached to the mounting tower. With execution of the script for mounting the specimen, the robot performs a point-to-point (PTP) movement in the $(\mathrm{CS})_{\mathrm{S}}$ to a programmed position that is in close proximity to the tibia of the specimen. The robot is then attached to the tibial side of the knee joint. In order not to damage the knee joint, a force-torque controlled attachment of the robot was realized. This is done by means of a force-torque sensor based motion without further path specifications to the robot. The system is parametrized with a force torque specification of 0 N and 0 Nm in $(\mathrm{CS})_{\mathrm{S}}$. In addition, three translational DOFs as well as the rotational DOF around the y-axis are unconstrained. To constrain individual DOFs, the proportional gain for the corresponding direction is set to 0. After activating the force-torque control by switching on the RSI context, the user is able to manipulate the end effector of the robot in order to mount the specimen on the robot.

The program sequence ends after the specimen has been coupled with the robot and the RSI context has been deactivated.

Geometric rotational center of the knee joint

A specimen-specific coordinate system is essential in order to be be able to apply defined loads acting in the knee joint. A coordinate system based on anatomical landmarks is appropriate for this purpose. For the knee joint, the geometric rotation center is the best suitable location, as for a physiologic loading of the joint, forces and torques must be measured relative to the geometric center of the knee joint.

This was realized by a corresponding shift of the $(\mathrm{CS})_\mathrm{T}$ into the geometric center of rotation. The geometric center of rotation was estimated by successive, force-torque controlled movements of the knee joint with respect to in flexion rotation (around the ${}_{(\mathrm{T})}z$-axis), varus-valgus rotation (around the ${}_{(\mathrm{T})}y$-axis) and internal-external rotation (around the ${}_{(\mathrm{T})}x$-axis) with simultaneous application of an axial centering force of 20 N (along ${}_{(\mathrm{T})}x$). The rotations around the individual axes were applied until 20° of rotation or a torque of 5 Nm was reached. The forces and torques in all other DOFs were controlled to 0 N and 0 Nm. The control was performed in the Tool Coordinate System which was first shifted to the estimated position $\boldsymbol{c}_0$ of the rotational center.

The positions of $(\mathrm{CS})_\mathrm{T}$ with respect to $(\mathrm{CS})_\mathrm{W}$ were sent online to the peripheral computing unit via the RSI context. Using the developed software environment, the this position data were temporarily stored. Once the movements performed by the robot were complete, the center of rotation was calculated. This is defined as the point relative to the tibia that moves least during the movements. It can be calculated by minimizing the Euclidean distance of the given set of n positions ${}_{(\mathrm{W})}\boldsymbol{x}_1, {}_{(\mathrm{W})}\boldsymbol{x}_2, ..., {}_{(\mathrm{W})}\boldsymbol{x}_n \in \mathbb{R}^3$ and the average of all (N) positions $\boldsymbol{x}_\mathrm{avg}$ [100]. This applies to the positions:

$$\begin{pmatrix} {}_{(\mathrm{W})}\boldsymbol{x}_n \\ 1 \end{pmatrix} = {}^{\mathrm{W}}\boldsymbol{T}_\mathrm{T} \begin{pmatrix} {}_{(\mathrm{T})}\boldsymbol{x}_0 \\ 1 \end{pmatrix} \quad \text{with} \quad {}^{\mathrm{W}}\boldsymbol{T}_\mathrm{T} \in SE(3), \tag{6.5}$$

with ${}_{(\mathrm{T})}\boldsymbol{x}_0$ as the initial guess of the vector describing the position of the center of rotation relative to the $(\mathrm{CS})_\mathrm{T}$. After transformation ${}_{(\mathrm{W})}\boldsymbol{x}_n$ is entered into the following minimization function:

$$\underset{\boldsymbol{x}\in\mathbb{R}^3}{\arg\min} \sum_{n=1}^{N} \| {}_{(\mathrm{W})}\boldsymbol{x}_n - {}_{(\mathrm{W})}\boldsymbol{x}_\mathrm{avg} \|_2. \tag{6.6}$$

For efficiency reasons, the calculation is performed using a Matlab routine integrated into the LabVIEW code. The output of (6.6) ${}_{(\mathrm{W})}\boldsymbol{x}_\mathrm{min}$ is then transformed back to $(\mathrm{CS})_\mathrm{T}$, in order to obtain the vector ${}_{(\mathrm{T})}\boldsymbol{x}_\mathrm{min}$ which represents the desired shift of the tool coordinate system into the geometric rotational center of the joint. This vector is then transferred from the computer to the robot via the Ethernet interface. The robot script ends with the redefinition of the tool coordinate system after completion of the transfer of the calculated displacement.

Scripts for biomechanical joint testing

The robot script for the biomechanical testing of the knee joint was divided into a head script, modules and subprograms for reasons of clarity, structuring and efficiency. The head script *H_knee()* contains the complete user communication and parametrization of the test sequences. The module *m_knee()* contains the parametrization of the robot, the sensor and the force-torque control as well as the programmatic implementation of the individual test sequences. The module *m_move()* contains the program structures, which are responsible for a renewed run (playback) of the robot movement after a test increment (Figure 6.4).

The head script (*H_knee()*) is used to communicate with the user via a dialog that

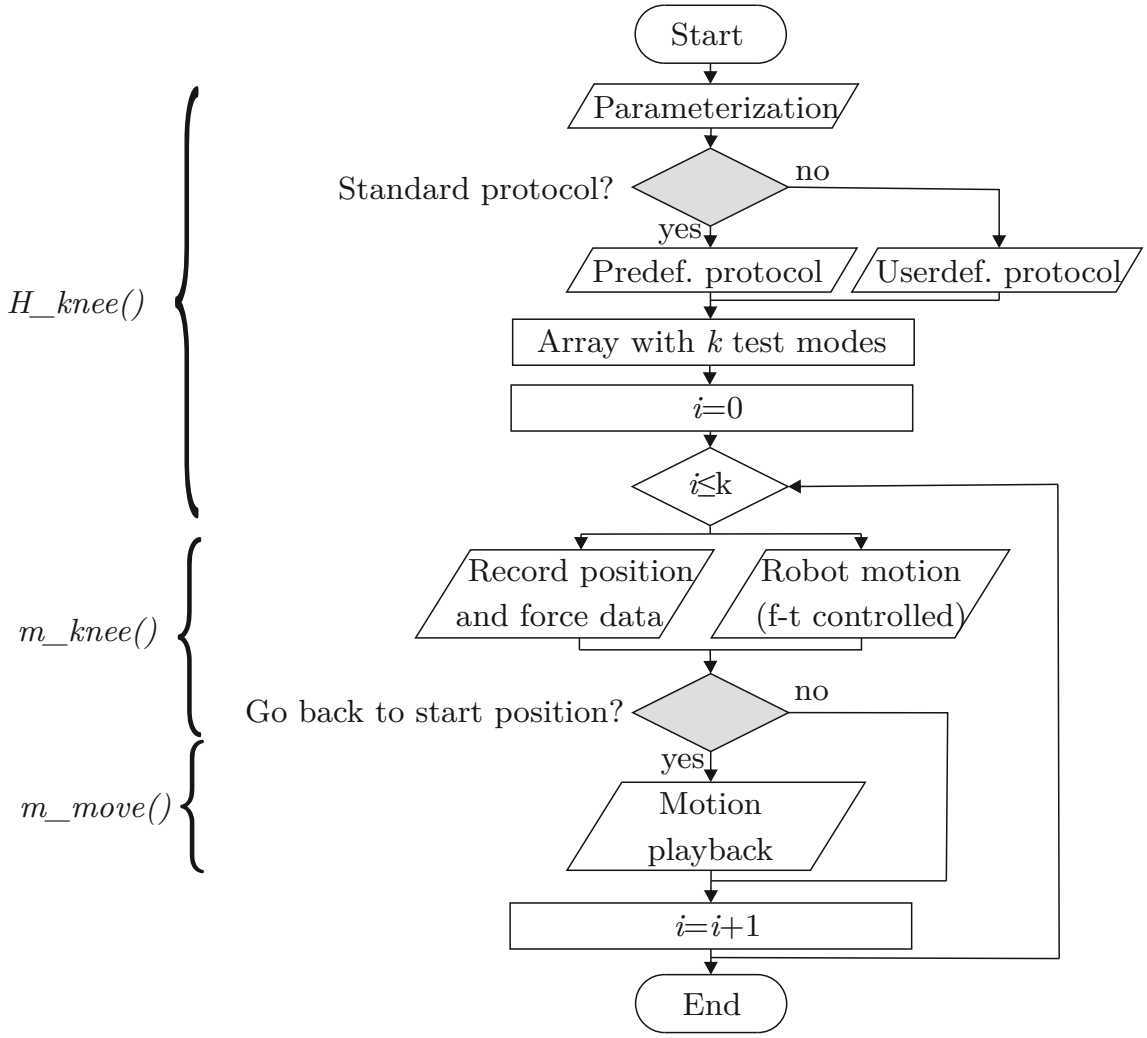

Figure 6.4: Flowchart showing the general structure of the program script used for the robot based biomechanical investigations of the human knee joint.

is realized by means of a graphical user interface on the Smart Pad of the robot. The parametrization of the test procedure is therefore carried out by a systematic query of test parameters relevant for testing. The query of the test sequence allows for the selection of a pre-programmed sequence for joint testing including the most important test directions are examined in flexion angles between 0° and 90°. In addition to the pre-programmed sequence, the user has the option of individually configuring a script. The user can select

from a list of load scenarios and robot movements and assemble these into a series of test steps.

By executing *m_knee()* the robot performs a corresponding force-torque controlled movement. In case the movement is a load test and not a pure instruction to change the flexion position, additionally to the module *m_knee()*, the module *m_move()* is executed before the the next iteration.

In the module *m_knee()*, the joint load is implemented according to the load type and direction selected in the head script. There are many test modes which can be selected via *H_knee()* (Table 6.1). While for the test modes applying a test load a pure force-torque control is active, the torque-based loads are carried out with a hybrid control, where beside the torque to be applied a programmed robot movement in the same direction is applied to keep the angular velocity constant until the target torque is reached. With the initiation

Table 6.1: Overview of the testing modes that can be applied on the knee joint for biomechanical testing. Type of test mode, loading condition in the single directions and degrees of freedom (DOFs) of the loading condition are shown for each case. Furthermore the movement task of the robot for the rotational testing modes is given.

	Loading condition / N							
Test mode	X	Y	Z	A	B	C	DOF	Movement task
No loading	0	0	0	0	0	0	6	-
Centering	20	0	0	0	0	0	5	-
Anterior translation	20	134	0	0	0	0	5	-
Posterior translation	20	-134	0	0	0	0	5	-
Medial translation	20	0	-134	0	0	0	5	-
lateral translation	20	0	134	0	0	0	5	-
Compression	200	0	0	0	0	0	5	-
Distraction	-200	0	0	0	0	0	5	-
Extension	20	0	0	-5	0	0	5	-A
Flexion	20	0	0	5	0	0	5	A
Varus Rotation	20	0	0	0	10	0	4	B
Valgus rotation	20	0	0	0	-10	0	4	-B
Internal rotation	20	0	0	0	0	5	4	C
External rotation	20	0	0	0	0	-5	4	-C
Extension 0	20	0	0	0	0	0	4	-A
Flexion 0	20	0	0	0	0	0	4	A
Internal rotation 0	20	0	0	0	0	0	4	C
External rotation 0	20	0	0	0	0	0	4	-C

of the robot movement, the joint is loaded according to the parametrization via the test mode. The robot motion ends when the desired load or motion is reached.

The head script is also used to optionally call *m_move()* after execution of the module *m_knee()*. This script is used to backtrack the movement made with *m_knee()* to get to the joint position that was set before loading the joint. The robot movement in this case is purely position controlled, with simultaneous monitoring of forces and torques to detect a possible load causing damage to the joint and to abort the movement, if necessary. The robot moves along the motion path of the previous task back to the starting position.

6.1.5 In-vitro investigation of the knee laxity in dependence on the soft-tissue situation

The laxity of the joint is expressed in the form of translations and rotations as a result of an applied load along or about a single DOF. In this way, *in-vitro* examinations were performed with regard to the total knee arthroplasty. First, the laxity of the knee joint between the individual preparation steps necessary for the implantation of the prosthesis was analyzed using an *in-vitro* approach. In addition, various ligaments and capsule structures were successively detached and the joint was tested for stability to evaluate the contribution of individual soft-tissue structures to joint balance. In different release paths, different primary stabilizers of the joint were completely released. Due to this irreversible adaptions of the knee joint during testing and the limited number of available joint specimens, only a limited number of release sequences could be tested. 24 human cadaver knee specimens were obtained for the study (ScienceCare, Phoenix, AZ, USA). The mean age of the donors was 71 ± 7 years and had a mean BMI of 28 ± 4 . The donors had no knee joint surgery or disease in their medical recordings. The cadaveric knee joints were stored at -22 °C. For biomechanical analysis the specimens were thawed for 24 hours at room temperature prior to testing. Specimens were biomechanically investigated by use of the *in-vitro* test setup (section 6.1).

Specimen preparation and mounting

In order to examine human knee specimens, they were prepared for testing as described in the following. When delivered, the specimens had a total length of approximately 60 cm; 30 cm were assigned to the femoral and the tibial side of the knee joint respectively. To be able to integrate the joints into the knee simulator, the joint ends needed to be prepared and embedded in brass cylinders. For this purpose, the muscle tissue was carefully removed from both sides at a distance of about 15 cm from the joint line and the bones were exposed. Ligamentous and capsule structures remained intact. The fibula was not needed to attach the femur to the robot. Accordingly, the fibula was fixed to the tibia 15 cm distal to the joint line with a screw and the remaining part of the bone was resected. The exposed bones were then freed from fat and fluids and embedded in brass cylinders using a cold curing three component resin (Rencast FC 52/53 Isocyanate, Polyol FC 53, Filler DT 982, Huntsman Corp., The Woodlands, USA). The cylinders were axially aligned with the longitudinal bone axis using an embedding device before the cylinders were filled with resin.

After the resin was cured, the specimens were attached to the experimental set-up. First,

the femoral end of the specimen was aligned and attached to the mounting tower. The femoral brass cylinder was placed in a cylindrical recess on the mounting tower and the knee joint was aligned before it was rigidly fixed by means of compressive screws. To align the joint, the specimen was moved with a hand-guided flexion from extension to 90° flexion. The flexion axis of the knee joint was then manually aligned parallel to the z-axis of the $(CS)_B$. To attach the tiba to the robot, the joint was put in extension and the robot was guided to the specimen by use of a active force-torque control and manipulation at the end effector by the user. The robot's mounting adapter also had a cylindrical recess in which the tibial side of the specimen was clamped. The use of force-torque control allowed the specimen to be mounted to the robot without any significant load being applied to the joint.

Testing conditions and protocol

The knee joints were tested at 0°, 30°, 60°, and 90° of flexion by subjecting the joint to seven loading cases: inferior, anterior and posterior force as well as varus, valgus, internal and external torque as described in Table 6.1. Prior to applicating the loading scenarios, a pure axial compressive load (Table 6.1) was applied while forces in the remaining five DOFs were minimized, to ensure tibiofemoral contact and a neutral resting position. Forces, torques, translations and rotations were recorded for each loading case. This test sequence was repeated for each specimen condition.

All joints were first tested in physiologic condition. The mean laxity of the joint was then determined for all flexion positions and loading conditions. The 24 specimens were then divided into four groups (six specimens per group, Figure 6.5). In order to obtain homogeneous groups with similar laxity distribution, the allocation of the specimens to the groups depended on the mean laxity. After completion of the grouping, the specimens were tested successively according to the sequence paths assigned (Figure 6.5). Thus, besides the physiological condition each of the specimens was examined in six further conditions, whereby the groups differed in only three conditions. The first three conditions (surgical approach, menisci resection, ACL release) were the same for all specimens.

Soft-tissue resection and release procedures

In order to investigate the influence of individual anatomical structures on joint stability, preparation methods had to be found that made it possible to transect individual tissue structures without affecting adjacent structures. Furthermore, it was important to ensure that the individual preparation steps were oriented as closely as possible to the operative procedure for implanting a knee prosthesis. The preparation steps performed are explained in more detail below.

- **Opening of the joint:** A medial surgical approach was chosen for the examinations. First, a central skin incision was made in superio-inferior direction, starting about 8 cm above the patella, centrally across the patella up to the medial side of the tibial tuberosity. The incision was made into the deep fascia and subcutaneous fat tissue to expose the quadriceps tendon proximally. A medial parapattelar approach was used to further open the joint. The incision was made along the medial edge of the quadriceps tendon up to the patella, further along the medial edge of the patella, and running out about 5 cm in a distal direction medially to the patellar tendon.

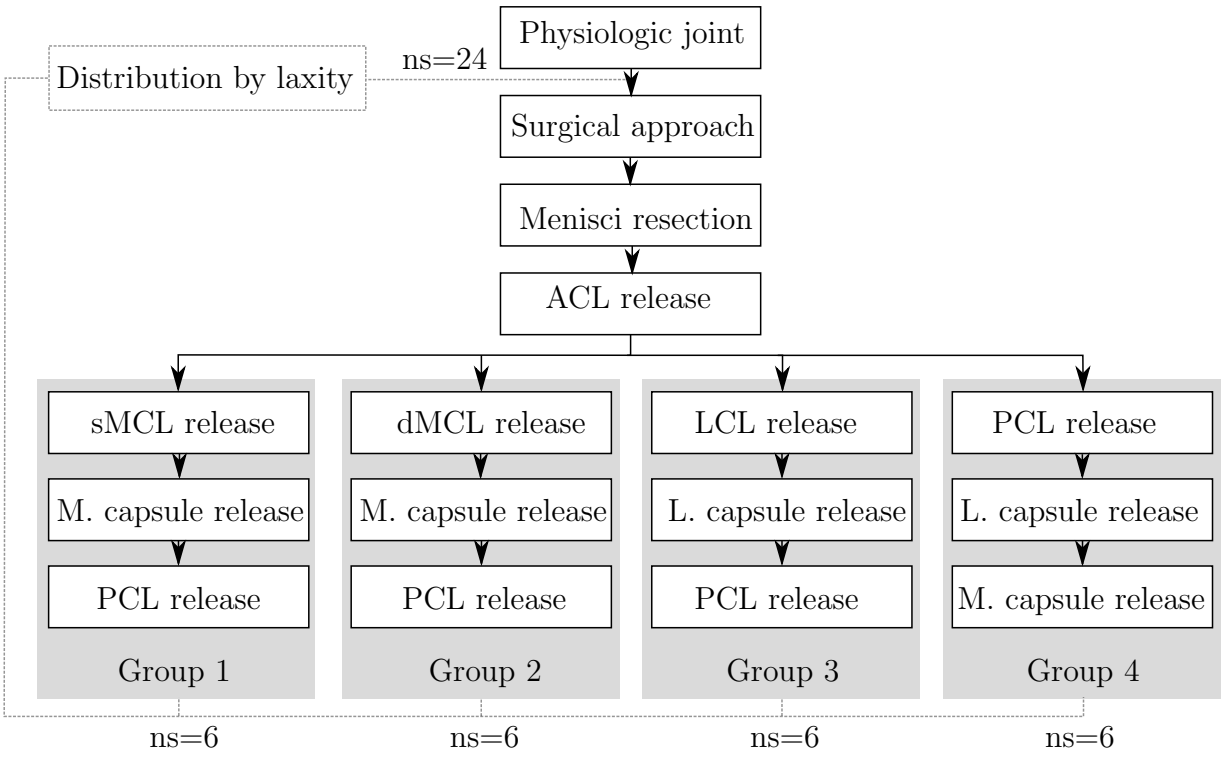

Figure 6.5: Soft-tissue resection and release sequences analyzed in the *in-vitro* study. The distribution of the specimens in four groups with differing sequence paths is shown (ns= number of specimens).

This incision provided access to the joint space. To prepare for further access, the infrapatellar fatpad was partially resected.

- **Resecting the lateral and medial meniscus:** To remove the menisci, the anterior menisci attachment sites were first detached. In the further course of the procedure, incisions were made to cut the meniscus attachments next to the surrounding capsular apparatus from anterior to posterior. With the help of bone rongeur forceps, the meniscus could be tensioned in anterior direction in order to loosen the posterior attachment of the menisci. The two menisci were then removed from the joint space.
- **Release of the ACL:** The tibial attachment of the ACL was loosened directly on the bone surface. In order to be able to more easily access the ligament, the joint was brought into 90° flexion.
- **Release of the PCL:** For the release of the PCL, the joint was brought into 90° flexion and the femoral attachment site of the ligament was detached close the bone surface.
- **Release of the sMCL:** The superficial medial ligament is attaches far inferior on the tibia. In order to obtain a clear view of the ligament, the anterior attachment of the joint capsule on the tibial side was first split by a longitudinal incision of about 3 cm in length in the middle, starting from the anterior edge of the tibial plateau in the direction of the tibial tuberosity. The medial capsule attachment was then carefully released along the edge of the tibia plateau until a clear view of the sMCL was possible. The ligament was then cut with a transverse incision.

- **Release of the dMCL:** Similar to the release of the sMCL, a longitudinal incision of the anterior tibial joint capsule was first made in order to then carefully loosen the joint capsule at the edge of the tibia plateau in a medial direction. With a clear view to the MCL, the attachment of the dMCL was first palpated directly at the edge of the tibia plateau, before the ligament was carefully loosened directly at the bone attachment. To palpate the ligament, the joint was brought into extension and a slight valgus stress was exerted on the joint. This made it possible to detect the ligament unambiguously.
- **Release of the LCL:** The LCL was initially palpated by a slight varus stress in the extension position. The ligament was then traced in the direction of the femoral attachment, within the joint capsule, and cut with a transverse incision.
- **Release of the posterior medial capsule:** At the beginning, the medial femoral condyle was identified from dorsal side. Afterwards, a 4 cm skin incision was made from the medial femoral condyle towards the medial epicondyle. The subcutaneous tissue was then carefully disected until the synovial recess was visible. A 2 cm medio-lateral incision was made on the posterior medial capsule.
- **Release of the posterior lateral capsule:** The incision of the lateral capsule was performed according to the descriptions of the release of the posterior medial capsule on the lateral side.

Statistical analysis

Statistical analysis of the data was performed using the software environment R (version 3.3.2, R Foundation for Statistical Computing). Differences between groups were analyzed by utilizing a repeated-measures analysis of variance, with specimen condition and flexion angle as the relevant factors. Significant findings were further analyzed with Tukey's post hoc test. The significance level was set to $\alpha = 0.05$. For relevant data, means with standard deviation (SD) are presented. Box plots were used to visualize the results: Whiskers represent the lowest and highest values within the 1.5 times inter quartile range of 1st and 3rd quartile, respectively. Dots represent outliers, defined as values beyond the whiskers.

6.2 Results

Flexion contracture was found in two of the specimens examined. These specimens were assigned to group 4 in the further course of the experiment. Until the release of the lateral capsule, these specimens could only be examined in 30°, 60° and 90° flexion.

6.2.1 Physiologic joint laxity in dependence on flexion angle

The post-hoc analysis revealed significant differences for the anterior joint laxity between 0° flexion and all other investigated positions 30° ($p<0.001$), 60° ($p<0.001$) and 90° ($p=0.001$), (Table B.1). The anterior laxity at 30° flexion was also significantly different from the anterior laxity measured at 90° flexion ($p<0.001$).

For posterior joint laxity, no significant differences between the flexion angles could be observed (p=0.082) (Figure 6.6).

The examination of inferior joint laxity (joint distraction) revealed significant differences

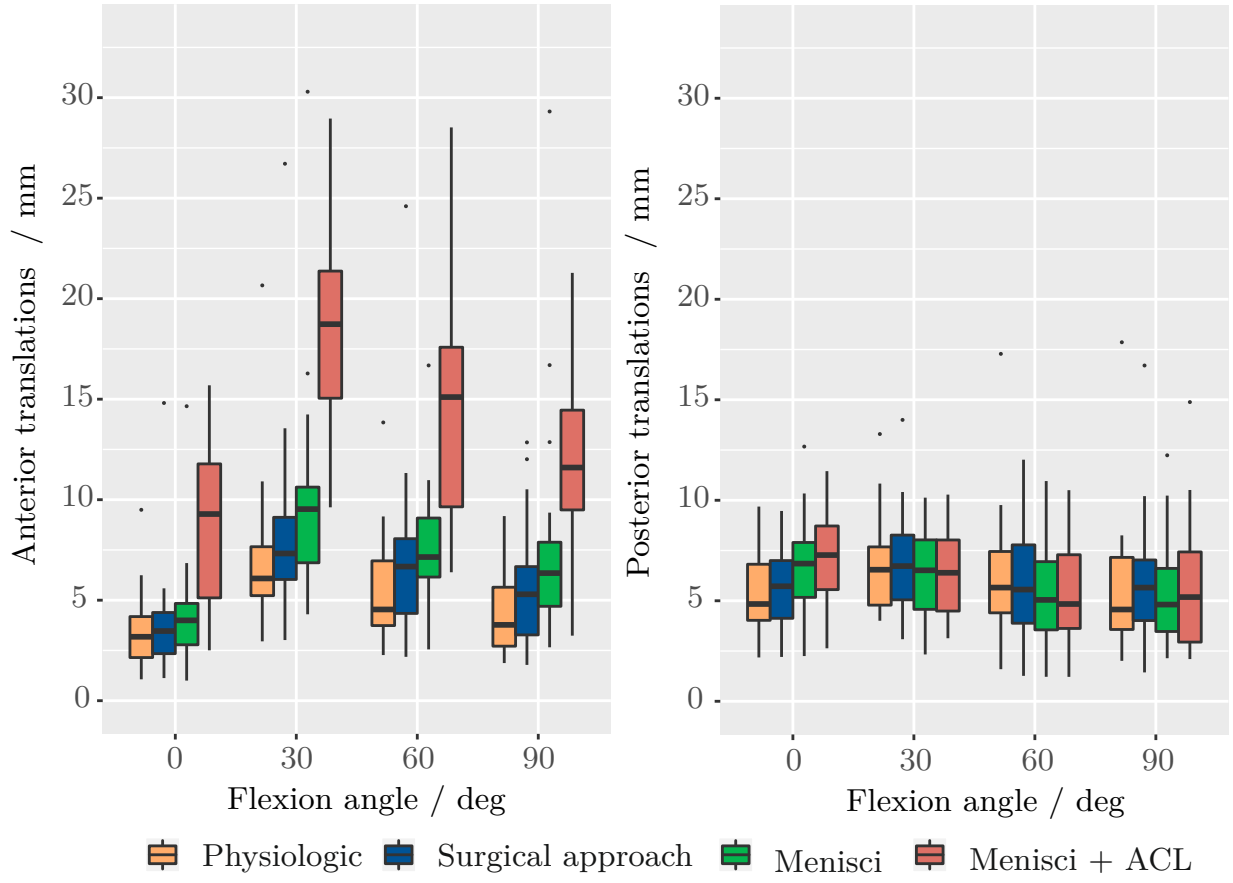

Figure 6.6: Box Plots showing the anterior (left) and posterior (right) laxities of the knee joint from 0° to 90° of flexion. Presented are the data of four different testing conditions: physiologic, after surgical approach, after resection of the menisci, after resection of the menisci and the ACL.

for inferior translation and coupled varus-valgus rotation, which occurs when an inferior load is applied. For inferior translation between 0° flexion and all other investigated positions there were significant differences (p<0.001). Furthermore, differences between 30° and 60° (p=0.045) as well as 30° and 90° (p=0.002) flexion were observed. The coupled varus-valgus rotation due to an inferior force at 0° flexion differed from the laxity values in 60° (p=0.005) and 90° (p<0.001) flexion. Furthermore, the laxity values at 30° flexion differed from those at 90° flexion, significantly (p<0.001) (Figure 6.7).

For varus laxity there were significant differences between all flexion angles tested (all p<0.002). Significant differences between the flexion angles could also be observed for valgus laxity. Thus the laxity values measured in 30°, 60° and 90° differed from those measured in 0° flexion (all p<0.001)(Figure 6.8).

Similar results could be found for the internal and external rotation. In both directions the laxity values at 0° flexion differed from those at 30°, 60° and 90° flexion (all p<0.001) (Figure 6.9).

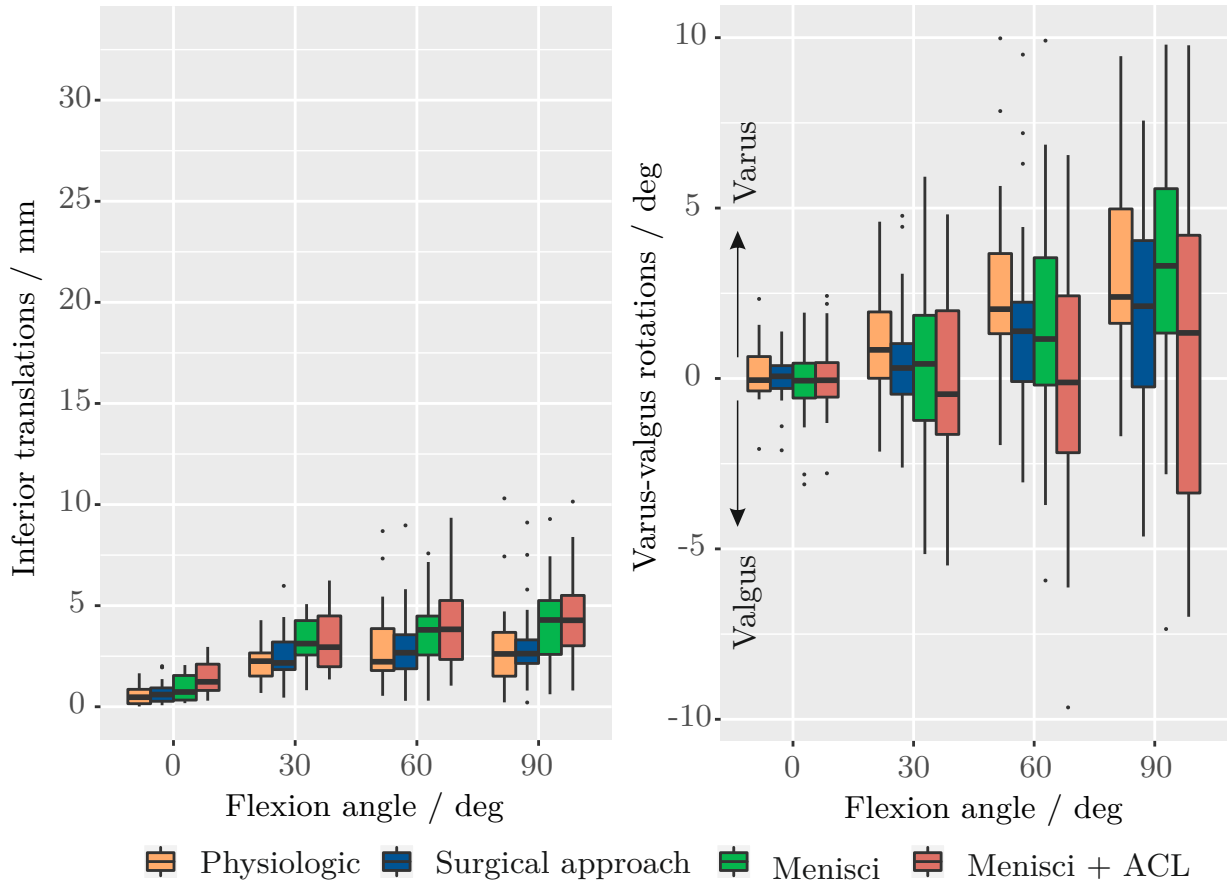

Figure 6.7: Box Plots showing the inferior joint laxity. Translations (left) and coupled varus-valgus rotations (right) of the knee joint from 0° to 90° of flexion are shown. Presented are the data of four different testing conditions: physiologic, after surgical approach, after resection of the menisci, after resection of the menisci and the ACL.

6.2.2 Joint laxity in dependence on soft-tissue condition

The laxity of the knee joint did not change significantly in any of the investigated directions due to the placement of the surgical approach ($p>0.16$), (Table B.2). Only the removal of the menisci had an influence on joint laxity (Table B.3). Compared to the physiological joint the laxity increased in anterior direction by up to 3.2 ± 4.1 mm in 90° flexion ($p<0.001$), in inferior direction by up to 1.1 ± 1.7 mm in 90° flexion ($p=0.02$), and in internal rotation by up to $20.6 \pm 17.6°$ also at 90° flexion ($p<0.001$). The removal of the ACL significantly increased the laxity of the knee joint compared to the physiological joint: by up to 10.0 ± 8.7 mm ($p<0.001$) in anterior direction and 30° flexion, by up to 1.2 ± 3.0 mm in 90° flexion ($p<0.001$) and up to $-3.6 \pm 4.4°$ ($p=0.02$) in inferior direction and 60° flexion, up to $4.6 \pm 5.9°$ in 90° flexion ($p=0.008$) in valgus rotation, and up to $21.6 \pm 16.7°$ ($p<0.001$) in internal rotation in 60° flexion (Table B.4). If one compares the laxity values after meniscus resection with the values after the additional resection of the cruciate ligament, only in the anterior direction the laxity increased significantly by up to 7.0 ± 9.7 mm in 30° flexion ($p<0.001$) (Table 6.2).

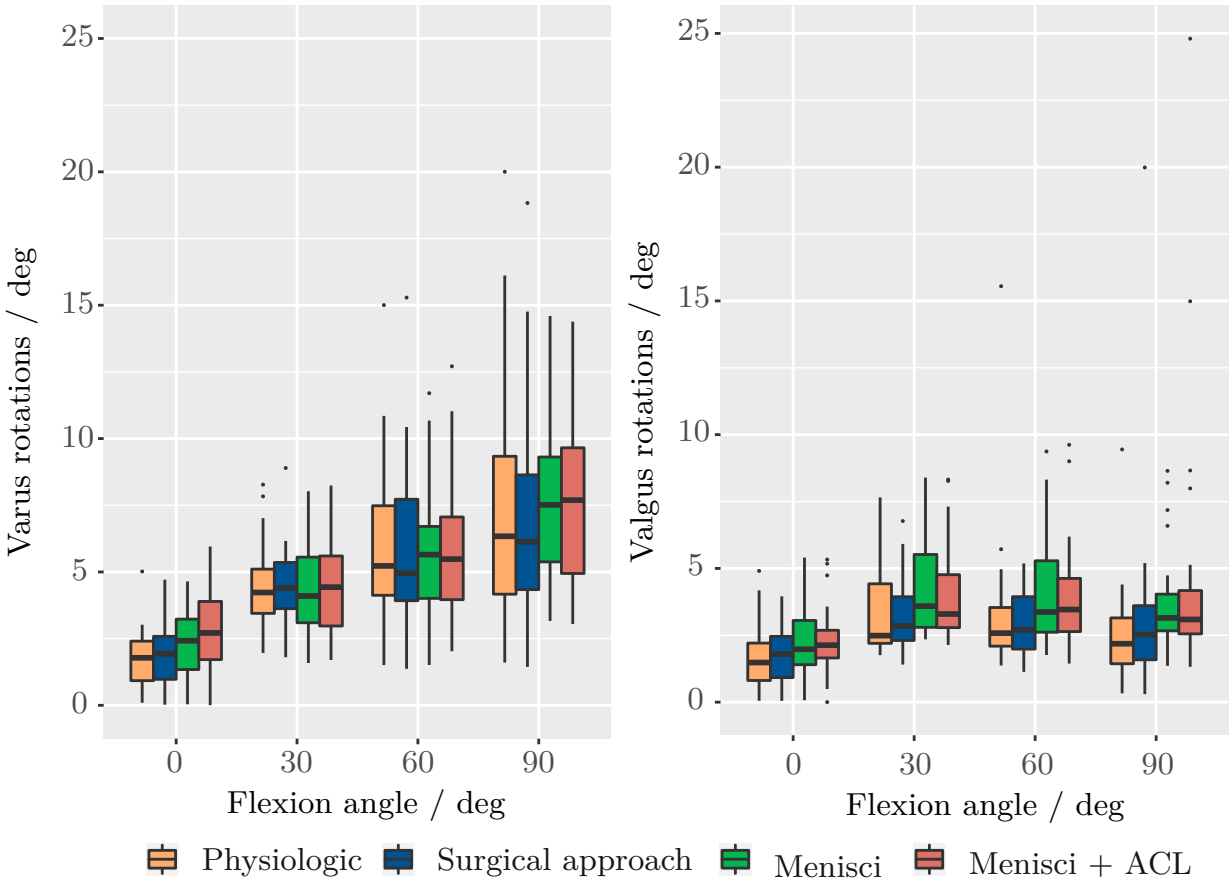

Figure 6.8: Box Plots showing the varus (left) and valgus (right) rotation laxities of the knee joint from 0° to 90° of flexion. Presented are the data of four different testing conditions: physiologic, after surgical approach, after resection of the menisci, after resection of the menisci and the ACL.

Group 1 resection sequence

None of the resection states (1. sMCL release, 2. medial capsule release, 3. PCL release) had a significant influence on anterior joint laxity ($p>0.26$), (Figure 6.10). Resection of the sMCL and subsequent resection of the medial capsule also had no effect. Only after resecting the PCL, the posterior laxity increased significantly compared to all previous resections (all $p<0.001$). In all other directions no significant differences could be observed between the investigated configurations with p values for the inferior laxity greater than 0.47 for the translations, and 0.68 for the coupled varus-valgus rotations (Figure 6.11), p values for the varus and valgus laxity greater than 0.99 and 0.55 as well as p values for the internal and external rotation laxity greater 0.26 and 0.47 (Figures 6.12, 6.13).

Group 2 resection sequence

In group 2 none of the investigated resection states (1. dMCL release, 2. medial capsule release, 3. PCL release) showed a significant influence on anterior joint laxity ($p>0.34$), (Figure 6.10). With regard to posterior laxity, resection of the dMCL and subsequent resection of the medial capsule showed no influence. Similar to group 1, posterior joint laxity increased significantly with PCL dissection compared to all previous resections (all

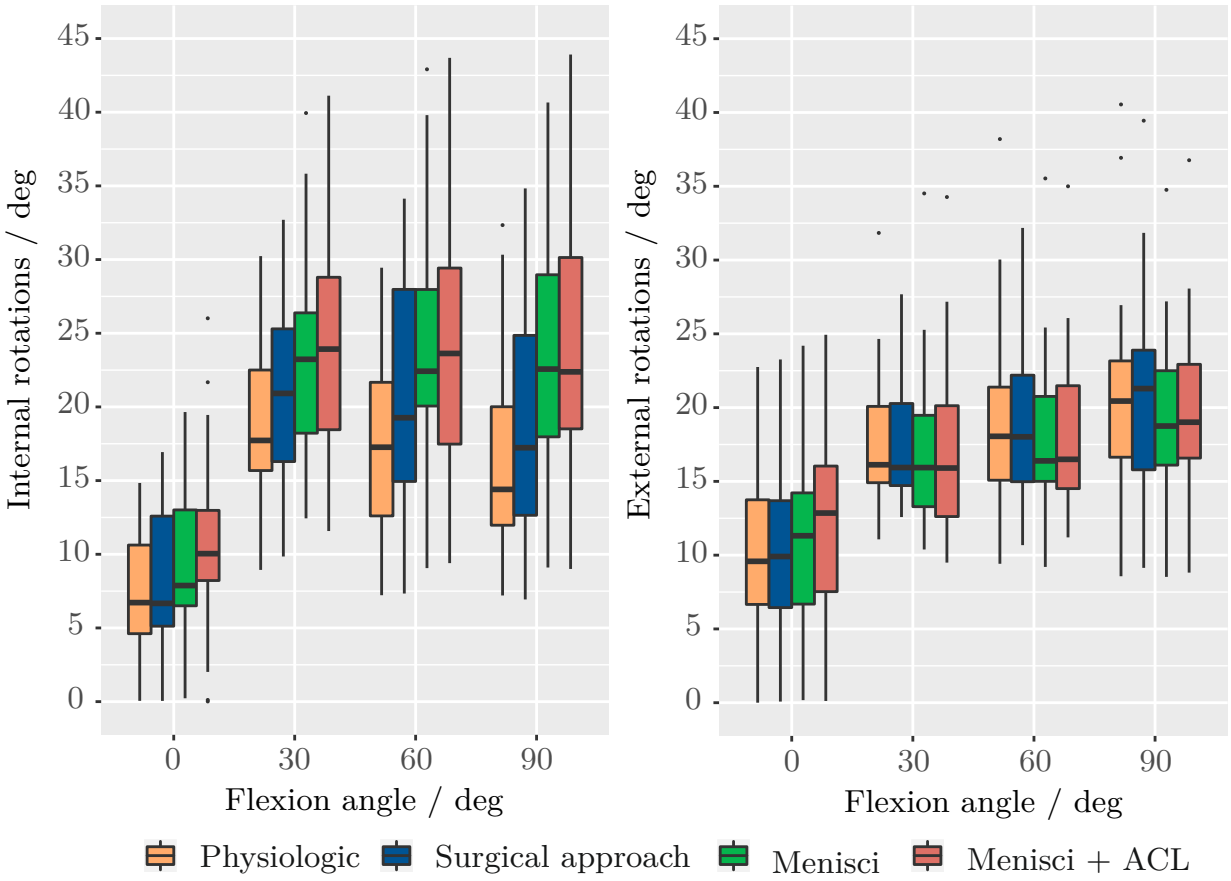

Figure 6.9: Box Plots showing the internal (left) and external (right) rotation laxities of the knee joint from 0° to 90° of flexion. Presented are the data of four different testing conditions: physiologic, after surgical approach, after resection of the menisci, after resection of the menisci and the ACL.

p<0.001), (Figure 6.10). While the inferior laxity, varus laxity and the internal rotation laxity of the joint did not differ significantly between the states (p>0.12, p>0.15, p>0.21), the valgus rotation showed significantly different values after transection of the PCL compared to the joint state after removal of menisci and ACL (p=0.015), (Figures 6.11, 6.12, 6.13). Furthermore, the external rotation laxity values were increased after resection of the dMCL (p=0.002) and subsequent resections of the medial capsule (p<0.001) and the PCL (p<0.001) compared to the state after transecting the ACL (Figure 6.13).

Group 3 resection sequence

Also in group 3 there were no significant differences between the examined resection states (1. LCL release, 2. lateral capsule release, 3. PCL release) for the anterior laxity (p>0.54). When considering posterior laxity, resection of the LCL and subsequent resection of the lateral capsule had no significant effect. Only cutting the PCL significantly increased joint laxity compared to the state after ACL resection (p=0.029), (Figure 6.10). For inferior joint laxity there was a tendency towards an increased translation after resecting the LCL (p=0.066) and a significant increase in translation after cutting the PCL (p=0.013) compared to the joint condition after cutting the ACL (Figure 6.11). Also the coupled varus-valgus rotation during the inferior laxity test shifted towards varus after resecting

Table 6.2: Differences in laxity comparing the native knee with the joint after menisci were resected and ACL was cut for all directions which showed significant differences between joint conditions.

	Differences in translations and rotations (mean $\pm SD$)				
Flexion / deg	Anterior / mm	Inferior / mm	Inferior / deg	Valgus / deg	Internal / deg
0	4.1 ± 5.2	0.6 ± 0.9	0.7 ± 1.3	2.3 ± 1.9	9.3 ± 8.8
30	10.0 ± 8.7	0.9 ± 1.6	2.3 ± 2.6	3.8 ± 3.5	19.1 ± 15.4
60	8.8 ± 8.6	0.9 ± 2.4	3.6 ± 4.4	3.7 ± 3.3	21.6 ± 16.7
90	7.5 ± 7.5	1.2 ± 3.1	3.1 ± 6.0	4.6 ± 5.8	21.3 ± 17.5

the lateral capsule (p=0.001) which was maintained after further resection of the PCL (p=0.002), (Figure 6.11). Similar changes could also be observed for varus laxity. After cutting the lateral capsule the joint laxity increased significantly (p=0.016) compared to the joint condition after transecting the ACL. The subsequent resection of the PCL then again increased the varus laxity compared to the state after cutting the ACL (Figure 6.12. For the valgus, internal and external rotation laxity there were no significant differences between the investigated states (p>0.99, p>0.23, p>0.57) (Figures 6.12, 6.13).

Group 4 resection sequence

None of the investigated resection states (1. PCL release, 2. lateral capsule release, 3. medial capsule release) had a significant influence on anterior joint laxity (p>0.17). The joint condition after cutting of the PCL showed an increased posterior laxity compared to the condition after transecting of the ACL (p=0.043), (Figure 6.10). With regard to posterior laxity, resection of the lateral capsule showed a significant increase compared to the joint condition after ACL release (p=0.003), (Figure 6.10). The subsequent resections of the medial capsule showed only a tendency to increased laxity compared to the joint condition after ACL release (p=0.064). For the inferior, varus, valgus as well as internal and external rotation laxities, no differences between the states could be observed (p=0.89, p=0.83, p=0.057, p=0.18, p=0.82) (Figures 6.11, 6.12, 6.13).

6.3 Discussion

In order to gain a basic understanding of the change in joint balance and laxity in knee arthroplasty procedures this study aimed to analyze the knee joint restraints with respect to flexion angle and soft-tissue condition in the seven most important loading directions by use of a robot based knee simulator. With regard to soft-tissue balancing we also aimed to analyze the influence of single ligament structures on the joint laxity to better understand balancing steps necessary to restore the native knee joint laxity as well as possible. To my knowledge this is the first study to systematically analyze the change in joint balance as a result of individual surgical steps necessary for implantation of a knee prosthesis.

The translations and rotations measured with the robot system are comparable to the laxity values described in the literature. This is shown by the comparison with the data determined in the meta-analysis for native joint laxity (chapter 5). The data measured *in-vitro* were almost exclusively within the standard deviation of the values from the meta-analysis. Only two values: the varus rotation in 90° flexion and the valgus rotation at 0° flexion were 2.4° and 1.2° below the mean values of the meta-analysis. These minor deviations may be explained by differences in the mean varus-valgus knee alignment of the specimens within the investigated cohort, compared to the data included in the meta-analyis.

The *in-vitro* investigations showed a strong dependence of laxity on the flexion angle in the physiologic knee joint, and thus further support the results from the meta-analysis. After opening of the joint, resection of the menisci and transecting of the ACL, these differences remained or were further amplified. The flexion gap, which could be evaluated by the examination of inferior joint laxity, showed similar results for both translation and coupled varus-valgus rotation with distraction of the joint between 0° and 90° flexion.

Surgical techniques such as gap balancing, which aim to homogenize joint laxity over the entire range of motion, ignore these strong variations in laxity and joint space. Consequently, such a technique requires a strong adaptation of the soft-tissue envelope especially in 0° flexion. This findings are supported by investigations of Gu et al. on virtual bone models comparing four different mechanical alignment techniques [78]. Balancing the joint tension in 0° and 90° flexion, therefore, involves the risk of balancing the joint in flexion too tightly, which according to Ghosh et al. results in movement restrictions for the patient and a joint with unnatural function and kinematics [72]. Recent clinical studies have also shown that the use of a kinematic alignment technique that takes greater account of the natural joint restraints of the knee leads to better pain reduction, function, restoration of the patellar kinematic, joint flexion, and a perceived more natural knee [56, 172, 120].

The current study showed that the re-examination of joint laxity after the joint was provided with a medial approach to the knee joint revealed no change compared to the healthy joint in any of the investigated directions. It has been demonstrated that, the retinaculum and other anteromedial capsule structures have exclusively a stabilizing effect on the patellofemoral joint, the stability of the femorotibial joint remains unaffected by these structures even in flexion. The evaluation of joint laxity is performed intra-operatively with the opened knee joint by the use of tools that support the surgeon in adjusting the soft-tissue tension. An influence of the surgical approach via the temporarily weakened structures on the joint stability would make the balancing process considerably more difficult, since the soft-tissue situation could only be estimated after closing the knee joint. The results of these investigations support the assumption that the intra-operative evaluation process of joint laxity with the joint open is representative for the joint stability of the knee joint in the closed state.

The removal of the menisci after opening of the joint showed a significant influence on joint laxity in anterior direction as well as on internal rotation. In addition, the removal of the menisci increased the joint space. These results are consistent with a clinical study in 4497 patients with primary ACL ligament reconstruction, which showed increased anterior instability after resection of the medial meniscus [46]. Several biomechanical studies also showed an increase in the anterior laxity of the femorotibial joint on specimens with deficient ACL in which one or both menisci were removed [199, 252]. Wang and Walker

showed the contribution of menisci to joint stability [233] in the context of a study on the rotatory laxity of the knee. This is confirmed by the results of this work, showing increased internal rotation (Figure 6.9). Reynolds *et al.* also showed the increase of the joint space after removal of the menisci which is in accordance to our findings [199], (Figure 6.7).
In addition to removing the menisci, cutting the ACL, as required for the majority of endoprostheses available today, increases joint laxity most in the anterior direction. This confirms the function of ACL as a primary anterior stabilizer. The compensation of an increased anterior laxity cannot be achieved by a corresponding balance of individual ligaments because the ACL is the only primary stabilizer of the knee joint in the anterior direction. Accordingly, this situation poses increased challenges to the implant and its positioning (*i.e.* the anterior-posterior alignment of the femoral component), to provide stability especially in joint flexion. Several studies described altered gait pattern of patients after knee arthroplasty, which is essentially characterized by lower gait speed, reduced step length, reduced knee flexion moment and a shortened stance phase, lower knee flexion and a gait pattern generally described in the literature as quadriceps avoidance gait, [207, 167, 23]. A very similar gait pattern is also described in patients with ACL injury [205, 125]. Furthermore, the literature [5, 176, 211] often describes the occurrence of flexion instability after joint arthroplasty. The loss of anterior stability, in particular the unproportinal increase in laxity through knee flexion and the increase in internal rotation laxity, may probably be decisive factors for the complications and changes in gait patterns described above.

Theere are only two ways to influence the increased laxities in the anterior direction: first, the adjustment of the implant geometry, such as the general design of the sagittal shape of the condyles (single and multi radii) as well as the conformity of the tibial insert. Second, the adjustment of the alignment of the prosthesis, for example with respect to the posterior femoral condyles to address the disproportionate increase in laxity at higher flexion angles, as well as the adjustment of the posterior tibial slope to counter the anterior instability, on the other hand. The adaptation of these parameters influences not only the anterior stability but also the stability and function of the joint in other directions. A change in the sagittal condyle geometry, such as a posterior reinforcement of the natural condyles, allows the reduction of joint laxity in flexion, but also unintentionally changes the tension of the posterior cruciate ligament. Increasing the conformity of the tibial inlay in relation to the femoral component also allows the reduction of the anterior laxity, but might limit the internal-external rotational ability of the joint, can negatively influence the maximum flexion of the joint and increases the risk of implant loosening due to the increased mechanical load on the tibial inlay. In addition, although the removal of the ACL showed the greatest effect in the anterior direction and with respect to internal rotation (Figures 6.6, 6.7), an increase in the asymmetry of the joint space was also observed (Figure 6.9). These are further factors that are difficult to compensate by the implant design or implant alignment.

The results of this study suggest that a complete restoration of physiological joint laxity can hardly be achieved with modern prosthesis designs, especially since very individual adjustments of the implant geometry would be necessary for each individual knee in order to balance the joint accordingly. In principle, there is a conflict in implant design between a necessary conformity in one direction and the resulting unwanted restriction of knee laxity in another direction. The application of modern alignment techniques, such as kinematic alignment, which is based on the natural joint geometry in order to preserve

the physiological joint laxity as well as possible, cannot compensate for the deficits of the soft-tissue envelope described above. Furthermore, the reconstruction of the natural joint laxity as accurately as possible also poses great challenges in terms of implant alignment accuracy which can probably only be met by computer or robot-based systems.

Precisely because of the above described dissatisfaction of many patients with the ACL sacrificing joint arthroplasty, the hope rests on a bi-cruciate retaining implant design. Studies on such prosthesis designs have shown contradictory results in the past. While some clinical studies reported superior results to ACL sacrificing designs [191, 190, 9], other studies showed no better functional results of this prosthesis design [109, 77]. The reason for this is not clear, but it is obvious that depending on the implantation technique the positive effect of the ACL obtained did not always manifest itself. Computer-assisted surgical procedures that allow more accurate implant positioning, combined with a more physiological implantation technique such as kinematic alignment, may in the future enhance the benefits of a bi-cruciate retaining design and possibly solve the problem of anterior instability, especially as the results of this study showed that menisci influence anterior laxity but only marginally compared to the ACL.

While arthrotic knee joints with a normal leg axis and no ligament or capsule contractions do not require a balancing of individual ligament structures, this is different for complicated joints with bony deformities or with contractures of ligament and capsule structures. In these cases, an implantation of the joint prosthesis without significant intervention in the soft-tissue structure is not sufficient. The further analyses of the joints in the four resection groups yielded significant insights into the balancing of such joints, although the specimens in the investigated cohort did not show these anomalies. Thus, for knees with varus deformity, it was shown that a release of the superficial MCL, contrary to the fears by some surgeons of a catastrophic increase in valgus instability, valgus laxity increased relatively slightly, so that in the tested cohort of six specimens the increase in laxity in this direction was not evaluated as significant. Similar results were found for the deep MCL. Here, the increase in laxity was not evaluated as significant (Figure 6.12). Another study with a larger sample size found a significant increase in valgus laxity of up to 6° for the resection of dMCL and sMCL [202]. In these studies, however, the MCL was cut without prior removal of the menisci and the ACL as performed in this thesis. The previous resection of the ACL already showed a significant increase in valgus laxity, possibly altering the function of the medial structures. The contrary to expectations small increase in laxity in valgus rotation is in line with the results of a prospective clinical study in which knee arthroplasty patients with a complete and partial MCL release were re-examined 6 and 12 months post-operatively. The authors conclude that transecting the complete MCL is a safe procedure for soft-tissue balancing in knee arthroplasty and does not lead to postoperative joint instability. Besides the varus-valugus laxity, the dMCL showed a strong influence on the rotation laxity. In contrast to the sMCL, the release of the dMCL leads to a strong increase of the external rotation laxity. This is in line with an *in-vitro* study by Izawa *et al.* [101], and by the short ligament length compared to the sMCL. To correct the soft-tissue situation as a result of varus deformity, the release of the sMCL is, therefore, preferable to the dMCL in order to better maintain the rotational stability of the joint.

To correct a valgus deformity, some research studies on soft-tissue balancing recommend the partial or complete release of the LCL [238]. The results of the present study confirm

a considerable increase of the varus laxity after release of the LCL by an average of 3° in 30° and 60° flexion and less than 2° in 0° and 90° flexion. Furthermore, the results showed a tendency towards a general enlargement of the joint space during distraction of the joint. An influence of the LCL on other DOF was not observed. Very similar results were found by Coobs *et al.*, in their biomechanical study, they reported an increase in varus laxity of 3° resp. 3.3° at 30° and 60° of flexion and 1.5° resp. 1.3° at 0° and 90° of flexion after sectioning the LCL [45]. This uneven increase in varus laxity, depending on the angle of flexion, may contribute to mid-flexion instability, which frequently occurs in the knee arthroplasty. This should be considered if a correction of valgus deformity is necessary.

The loosening of posterior capsular structures is generally favored to counter flexion contracture [215]. The investigations in this study showed an influence of the posterior capsule on the posterior joint laxity of the menisci and ACL deficient knees. This is shown by the investigations in group 4 where the medial and lateral capsule were resected (Figure 6.10). In the other groups the influence of the posterior capsule structure was not significant. This is probably due to the fact that in group 4 two specimens with flexion contracture were included in which the effect of the release is amplified by the contractile structures. Consequently, an increase in anterior-posterior laxity can be expected in the treatment of patients with flexion contracture. The preservation of the posterior cruciate ligament, therefore, seems to be particularly important in these patients in order to prevent instability of the joint, especially in flexion.

The posterior cruciate ligament is the primary stabilizer of the knee joint with respect to posterior joint stability. This is confirmed by the investigations carried out in the context of this study and is thus in line with the findings of Race and Amis who analyzed the isolated release of the PCL *in-vitro* [193]. The influence of this ligament was observed in the present study even after the numerous previous releases in the different release sequences. In addition, the transection of the cruciate ligament increased the joint gap during joint distraction. The PCL had a particularly strong influence on the release sequences in which the sMCL or dMCL were previously released. Accordingly, destabilization in the posterior direction after weakening of the medial structures appears to be completely compensated by the PCL. This influence of the medial structures on the posterior stability only becomes apparent with the release of the PCL. There are currently no comparable studies available. Since the different release sequences were examined on different groups of specimens, an influence of the samples cannot completely be excluded, so that this must be verified in future experiments. Since posterior laxity, similar to anterior laxity, cannot be rebalanced by adapting individual ligament structures, the PCL should be protected as well as possible during surgery to preserve this.

The present study is subject to some limitations which are listed below:
First of all, it should be mentioned that the study is a laboratory investigation and some differences in laxity compared to human subjects cannot be completely ruled out. However, several comparative studies showed that the *in-vitro* analysis on cadaveric knees are comparable with the measurements on living subjects [156, 218]. Accordingly, the results of this study should be of clinical relevance. Nevertheless, the results of the analysis refer exclusively to the passive stability of the knee joint. The stabilizing effect of individual muscle structures could not be considered. However, the intra-operative evaluation of knee laxity also takes place under passivated muscle tone, so that these values can be compared to a clinical setup. A further limitation is that the specimens are exclusively joints without

or with mild arthrosis. In the current study, the influence of pathologic changes of the joint structures due to severe arthrosis could not be considered in this study. Accordingly, it cannot be ruled out that a pathological joint behaves differently in the case of resection of individual structures. Patients of older age with limited joint stability are one example. Investigations in ths context are the goal of future investigations. In addition, different specimens had to be used to examine different release sequences, as the soft-tissue releases are destructive and irreversible changes to the joint were made. Although the grouping of the specimens was performed in such a way that the distribution was as similar as possible with regard to laxity and the overall number of specimens was high (24), an influence of the specimen groups on the results cannot be ruled out, despite a sample size of N=6 per group (1-4). It should also be mentioned that the measurement of the translations and rotations via the robot system is also subject to errors due to the applied load. This was evaluated in a series of tests with static weights and an external optical measuring system (NDI Optotrak Certus). The measurements showed compliance of the robot and thus a measurement error of 0.82 ± 0.22 mm with a load of 150 N on the end effector. Within the scope of the in-vitro study, an evaluation of the differences in translation and rotation as a result of a changed soft-tissue condition is carried out, therefore, these inaccuracies can be neglected here.

In conclusion, the investigations in this study support a preference of the kinematic alignment technique over the gap balancing technique. The strong dependence of the knee laxity on the flexion angle should be considered in order to preserve the natural joint function as much as possible. The evaluation of joint laxity with opened knee joint is adequate for the purposes of joint balancing. Restoration of the soft-tissue function of the knee after arthroplasty cannot be achieved with the kinematic alignment surgical technique alone. The use of a prosthesis that maintains both cruciate ligaments is the only way to maintain the anterior-posterior stability of the joint in balance. The compensation of the cruciate ligament function solely through the prosthesis design and implant alignment is unlikely. To correct varus deformity, MCL balancing appears to be a safe method. In order to maintain rotational stability as much as possible, the transection of the sMCL should be preferred to the dMCL. The correction of valgus laxity can be achieved by partially or completely transecting the LCL, however, this may increase the risk of mid-flexion instability. When correcting an extension deficit by loosening the posterior capsule structures, preservation of the PCL is particularly important to preserve posterior stability of the joint.

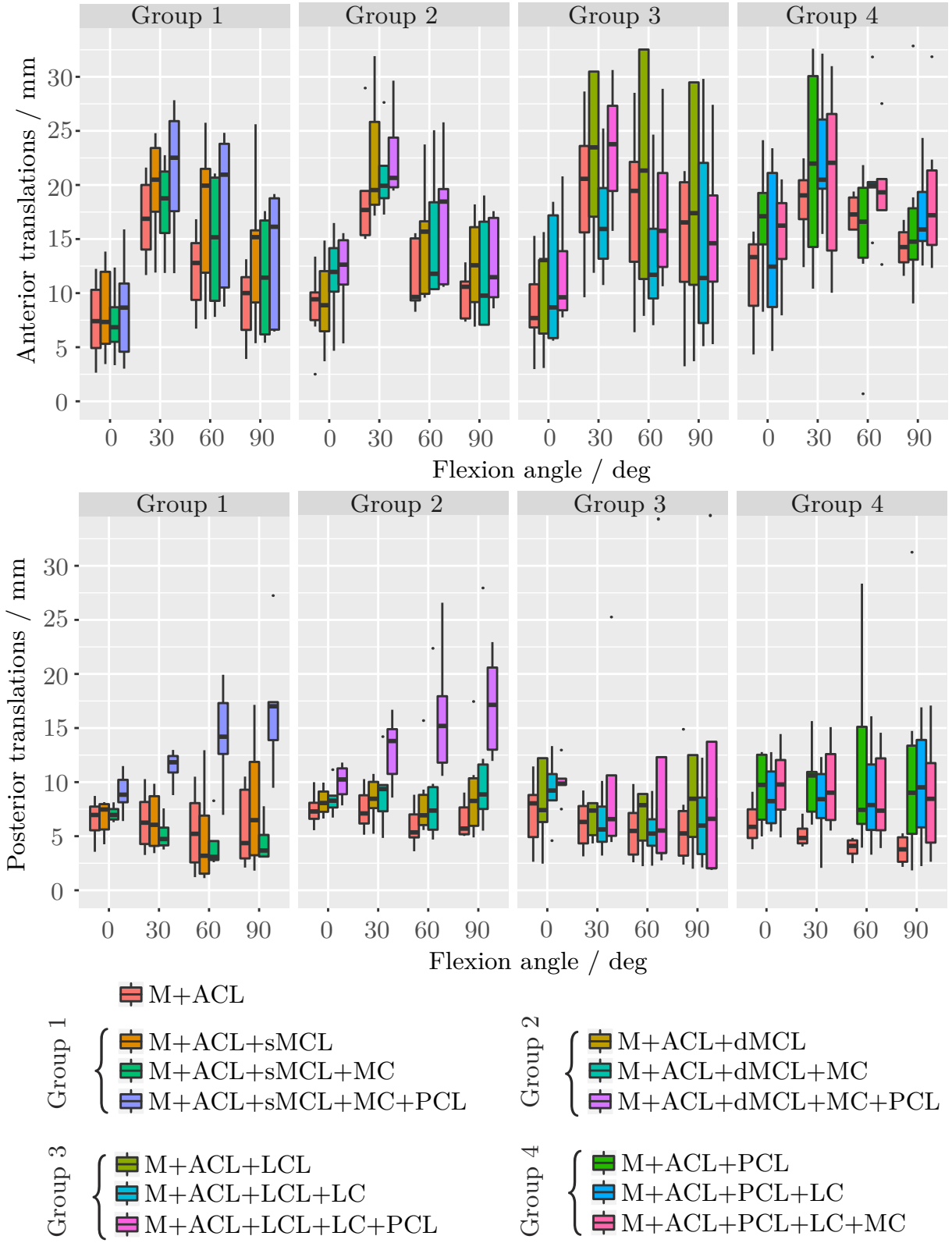

Figure 6.10: Box Plots showing the anterior (top) and posterior (bottom) laxities of the knee joint from 0° to 90° of flexion. Presented are the data of four different testing groups with three different conditions tested in each group. Laxities after resection of the ACL is provided for reference.

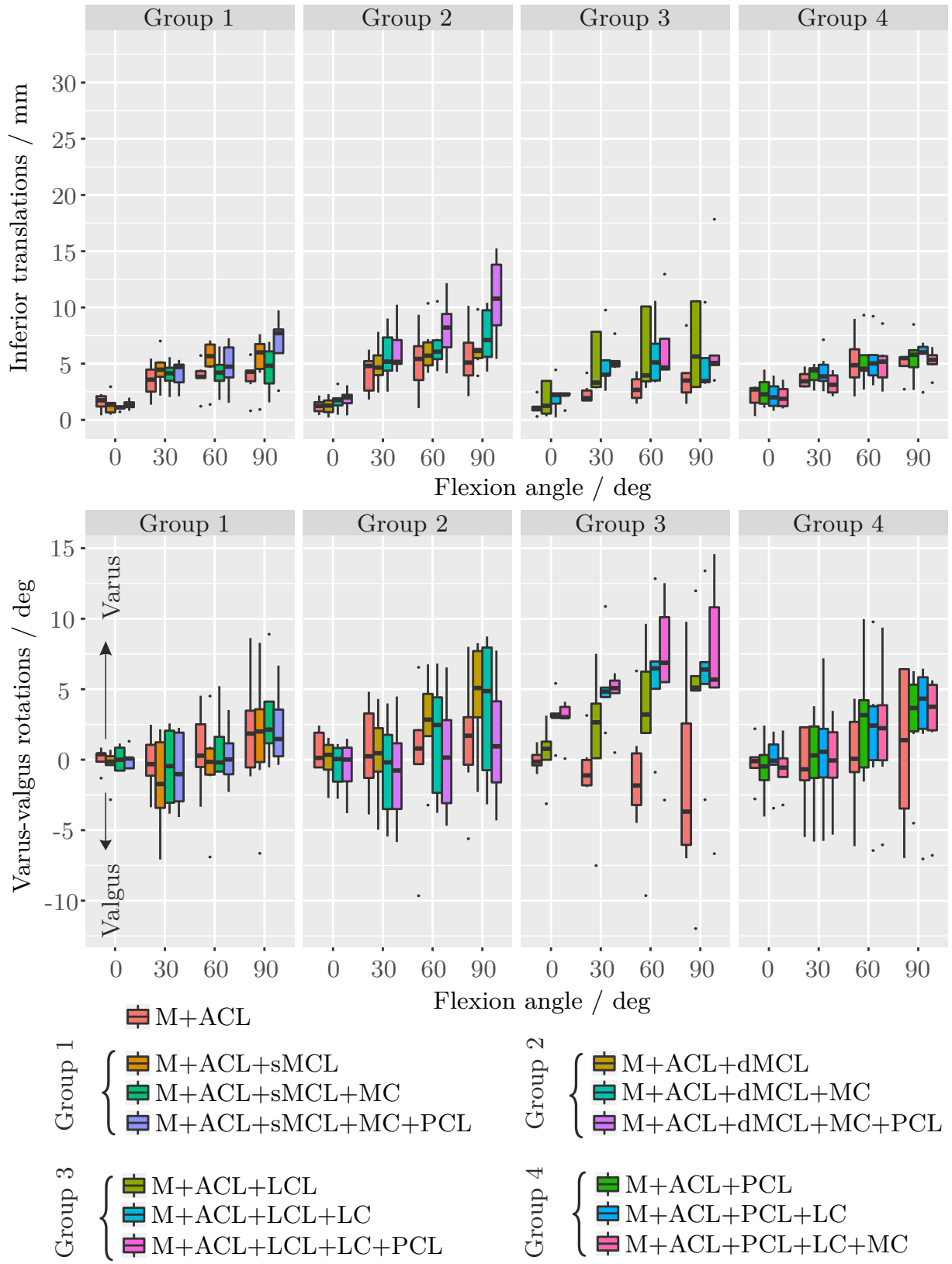

Figure 6.11: Box Plots showing the inferior translation (top) and coupled varus-valgus rotations (bottom) following the inferior laxity test of the knee joint from 0° to 90° of flexion. The data of four different testing groups with three different conditions tested in each group are presented. Laxities after resection of the ACL is provided for reference.

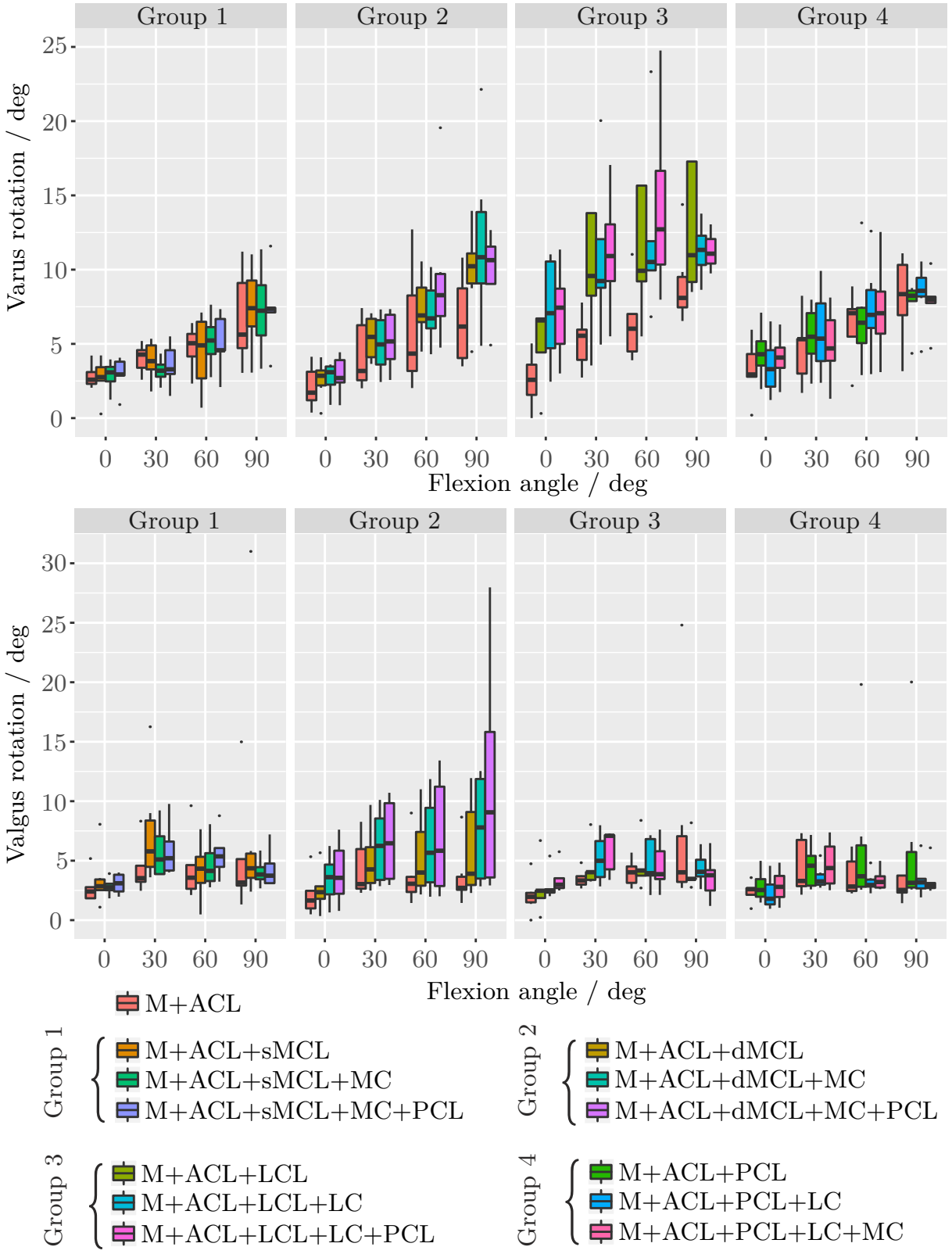

Figure 6.12: Box Plots showing the varus (top) and valgus (bottom) laxities of the knee joint from 0° to 90° of flexion. The data of four different testing groups with three different conditions tested in each group are presented. Laxities after resection of the ACL is provided for reference.

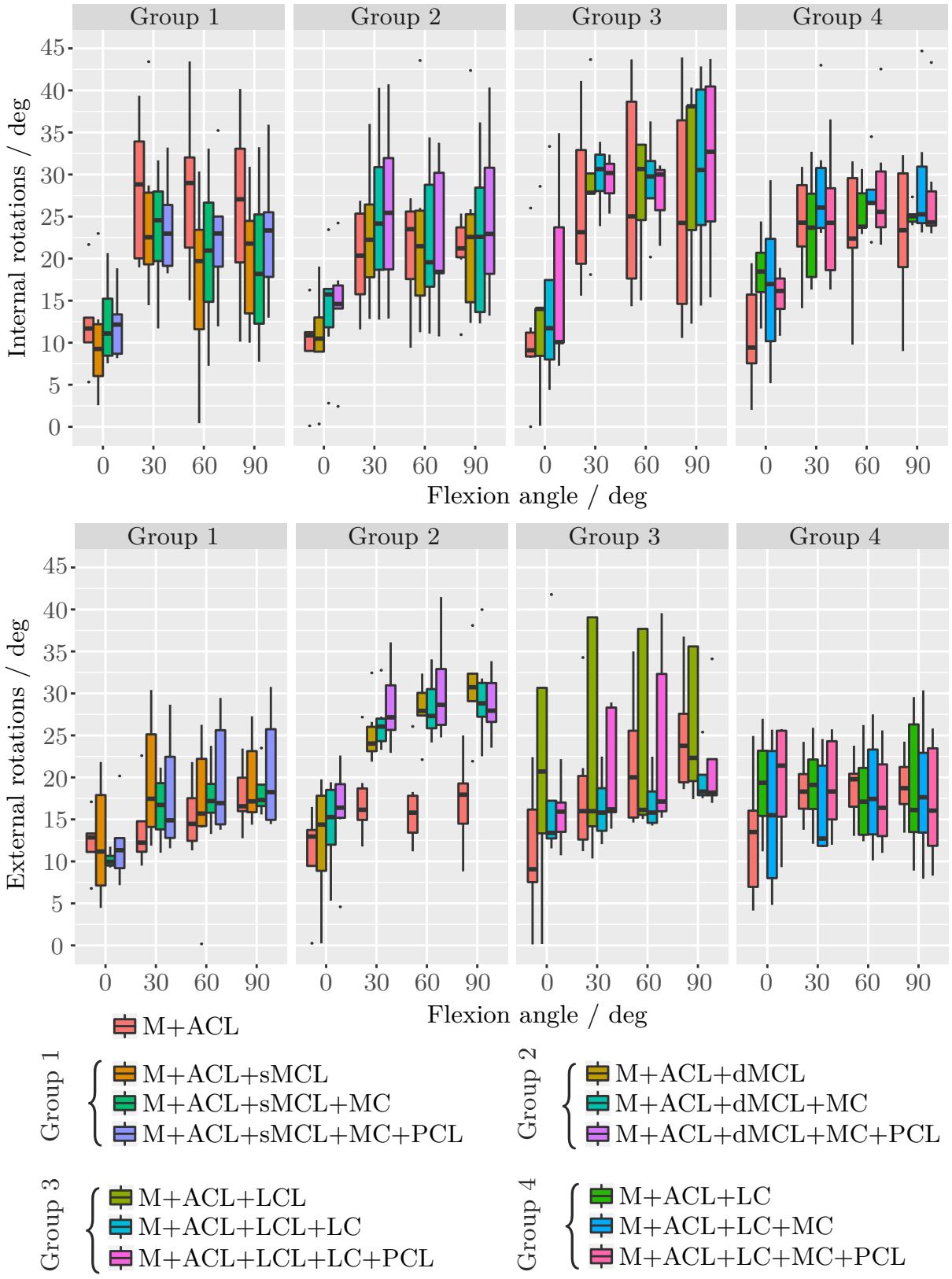

Figure 6.13: Box Plots showing the internal (top) and external (bottom) rotation laxities of the knee joint from 0° to 90° of flexion. The data of four different testing groups with three different conditions tested in each group are presented. Laxities after resection of the ACL is provided for reference.

7 Investigation of an in-silico model for laxity analysis of the knee joint

The restoration of joint function as a result of arthrosis of the knee is the primary goal in the knee arthroplasty. This includes on the one hand the replacement of the cartilage surface and the correction of possible axial misalignments and on the other hand the adaptation of the surrounding soft-tissue structures. The development of effective strategies for the adaptation of the soft-tissue envelope poses a particularly major challenge since no technical models exist that realistically represent the knee joint with its menisci, ligaments, tendons and muscles. The application of *in-vitro* methods as described in section 6.1 is, therefore, the only established possibility to investigate the function of single ligament structures to an extent that otherwise invasive methods on patients would be necessary. However, the *in-vitro* investigations on joint specimens are very limited due to high costs, ethical concerns and the limited availability of the specimens. Furthermore, *in-vitro* investigations are only suitable for obtaining basic knowledge, a clinical application of the methods in the sense of patient-specific analyses is not possible.

Computer simulation methods, which have become more and more important in recent years, may be able to resolve these limitations. *In-silico* methods are theoretically only limited by the available computing capacity. However, in practice, *in-silico* models are also severely limited by the lack of patient-specific parameters and geometries. By combining *in-vitro* findings such as the mechanical properties of individual soft-tissue structures (*e.g.* ACL, PCL, LCL *etc.*) with geometric information obtained from medical imaging, subject-specific models can be created that represent the functionality of the joint. In the past years different numerical models have been developed to investigate the laxity of the joint in different conditions [20, 70, 86, 89, 26, 79]. Most of these models are finite element models, in which the subject-specific bone geometry and ligament structures were partially reproduced. To date, only a few multi-body simulation models exist that have been developed for similar investigations. However, Guess *et al.* could show in a comparative study that investigations on joint laxity by means of a multi-body simulation can reduce the simulation time by four times compared to a finite element simulation with the same boundary conditions [80]. In addition, there are simulation platforms specially developed for biomechanical questions with which a multi-body model can be easily extended by further structures and joints.

Although some of the existing numerical models have been developed and described in publications, the authors failed to prove their validity [20, 70, 11]. In other studies, model validation was also described, but it is mostly limited to comparison with literature data, only sporadic comparisons in individual directions and joint positions, or only based on experimental data of one single subject [26, 59, 237]. Studies with proper one-to-one comparisons between simulation and experimental data on several subject-specific models are sparse. However, if the aim is to develop a numerical model for the extension of experimental trials or for clinical application, a detailed sensitivity analysis and validation in a

structured way as described in literature is essential [209]. Based on these simulation models described in the literature, the goal of the presented study was to develop a multibody model for the subject-specific simulation of the joint laxity of the knee. The model was evaluated on the basis of the existing *in-vitro* data with one-to-one comparisons in order to supplement the *in-vitro* investigations on the function of individual ligaments carried out in this thesis. On the other hand the simulation was created as a basis for a multibody model which can later be used to support the surgeon in surgical planning with regard to soft-tissue management of the knee arthroplasty. The objectives of these investigations were thus:

- to develop a multi-body model to simulate femorotibial joint laxity in which the essential anatomical structures and stabilizers of the knee are represented.
- to develop a work flow to transfer subject-specific information to an initially generated model.
- to investigate the sensitivity of the model by variation of individual model parameters.
- to verify and validate the simulation model on the basis of literature data and the results of *in-vitro* studies (section 6.2).

7.1 Materials and methods

In the following, the schema of the multibody simulation is described in general (subsection 7.1.1) before the knee model created in this thesis is explained in detail (subsection 7.1.5). Furthermore, the developed workflow for the generation of subject-specific models is reported including the segmentation and processing of MRI image data, import of subject-specific meshes and the approximation of ligament attachment sites by use of a radial basis function based morphing algorithm (subsection 7.1.3). In subsection 7.1.4 the methods used for the accuracy and sensitivity analysis are described. Finally the methods used for validation of the model are presented.

The multibody knee model developed in this thesis was built in the Anybody software environment (v.7.0, Anybody Technology, Aalborg, Denmark), a tool for musculoskeletal modeling of the human body. The system's own programming language Anyscript enables object-based programming of complex multibody models based on anthropometric data of the human anatomy. In addition to bones (rigid bodies), tendons, ligaments and muscles can be represented according to their biomechanical behavior.

7.1.1 Mathematical description of the multibody system

In Anybody, the movements of the bodies are described in Cartesian coordinate systems. The position ($\boldsymbol{q}_i$) and velocity ($\boldsymbol{v}_i$) of a body S_i in space relative to a global coordinate

system $(\mathrm{CS})_\mathrm{G}$ is defined by the coordinates

$$ {}_{(G)}\boldsymbol{q}_i = \begin{pmatrix} {}_{(G)}\boldsymbol{r}_i \\ {}_{(K)}\boldsymbol{p}_i \end{pmatrix} \quad \text{and} \quad {}_{(G)}\boldsymbol{v}_i = \begin{pmatrix} {}_{(G)}\dot{\boldsymbol{r}}_i \\ {}_{(K)}\boldsymbol{\omega}_i \end{pmatrix} \tag{7.1} $$

where ${}_{(G)}\boldsymbol{r}_i$ is the global position vector of the center of mass of S_i and ${}_{(G)}\dot{\boldsymbol{r}}_i$ its velocity; ${}_{(K)}\boldsymbol{p}_i$ is the rotation in the form of a quaternion and ${}_{(K)}\boldsymbol{\omega}_i$ is the angular velocity of S_i in the body fixed coordinate system $(\mathrm{CS})_\mathrm{K}$.
Positions and velocities of all bodies then are each collected as vectors in

$$ \boldsymbol{q} = \begin{pmatrix} {}_{(G)}\boldsymbol{q}_1{}^\mathsf{T} & {}_{(G)}\boldsymbol{q}_2{}^\mathsf{T} & \dots & {}_{(G)}\boldsymbol{q}_i{}^\mathsf{T} \end{pmatrix}^\mathsf{T} \quad \text{and} \quad \boldsymbol{v} = \begin{pmatrix} {}_{(G)}\boldsymbol{v}_1{}^\mathsf{T} & {}_{(G)}\boldsymbol{v}_2{}^\mathsf{T} & \dots & {}_{(G)}\boldsymbol{v}_i{}^\mathsf{T} \end{pmatrix}^\mathsf{T}. \tag{7.2} $$

The relations of the bodies to each other (joint) as well as their movements by kinematic drives can then be determined by non-linear holonomic constraint equations

$$ \Phi(\boldsymbol{q}, t) = \boldsymbol{0} \tag{7.3} $$

which are then solved numerically using a Newton-Raphson scheme. It should be noted that the system must be kinematically determined for the solution. In order to obtain the velocities and acceleration constraints of the bodies, the following velocity and acceleration constraints

$$ \Phi_{\boldsymbol{q}*}\boldsymbol{v} = -\boldsymbol{\Phi}_t \quad \text{and} \quad \boldsymbol{\Phi}_{\boldsymbol{q}*}\dot{\boldsymbol{v}} = \boldsymbol{\gamma}(\boldsymbol{q}, \boldsymbol{v}, t) \tag{7.4} $$

must be solved, with $\Phi_{\boldsymbol{q}*}$ corresponding to the Jacobi Matrix of the constrained equations regarding a virtual set of points $\boldsymbol{q}*$ that correspond to the velocities ($\boldsymbol{v}$). $\boldsymbol{\Phi}_t$ is the partial deviative of the constraint equations and $\boldsymbol{\gamma}$ the right-hand side of acceleration constraints, containing position- and velocity-dependent terms with respect to time. Thus all positions, velocities and accelerations of the individual bodies are known.
The musculoskeletal models of the human body in most cases also consider the musculature because they are the main drivers of human movement. The joints are strongly overdetermined by the many simultaneously acting muscles and to date it is unclear according to which criterion the central nervous system of the human being decides on the degree of activation of the individual muscles. In this case, the use of an optimization criterion to counter this situation [48]:

$$ \arg\min_f Z(\boldsymbol{f}_\mathrm{M}), \quad \text{with} \quad 0 \geq \boldsymbol{f}_{\mathrm{M},j} \geq \boldsymbol{s}_{\mathrm{M},j} \tag{7.5} $$

and the constraints

$$ \boldsymbol{C}\begin{pmatrix} \boldsymbol{f}_\mathrm{M} \\ \boldsymbol{f}_\mathrm{R} \end{pmatrix} = \boldsymbol{d} \quad \text{with} \quad \boldsymbol{C} = \begin{pmatrix} \boldsymbol{C}_\mathrm{M} & \boldsymbol{C}_\mathrm{R} \end{pmatrix} \tag{7.6} $$

where Z is the objective function of the muscle forces $\boldsymbol{f}_\mathrm{M}$ of j modeled muscles with the maximum muscle strength $\boldsymbol{s}_j$. The coefficients matrix $\boldsymbol{C}$ all unknown muscle forces ($\boldsymbol{f}_\mathrm{M}$ and joint reaction forces $\boldsymbol{f}_\mathrm{R}$) together with all known forces (applied loads and inertia forces) $\boldsymbol{d}$ form the dynamic equilibrium. The objective function applied in Anybody is based on the assumption that the human body always tries to minimize the maximum

activation of the individual muscles, so function Z can be represented as follows [48]:

$$Z(\boldsymbol{f}_{\mathrm{M}}) = \max\left(\frac{\boldsymbol{f}_{\mathrm{M},j}}{\boldsymbol{s}_j}\right). \tag{7.7}$$

With the determination of all positions, velocities and inclinations from 7.4, 7.6 can be set up. The left side of 7.6 can, therefore, be set up with the Newton/Euler equations of all bodies i, which in this case are defined as

$${}_{(K)}\boldsymbol{g}_i = \begin{pmatrix} m_i\boldsymbol{I}_3 & \boldsymbol{0} \\ \boldsymbol{0} & {}_{(K)}\boldsymbol{J}_i \end{pmatrix} \dot{\boldsymbol{v}}_i + \begin{pmatrix} \boldsymbol{0} \\ {}_{(K)}\boldsymbol{\omega}_i \times {}_{(K)}\boldsymbol{J}_{i(K)}\boldsymbol{\omega}_i \end{pmatrix} \in \mathbb{R}^6, \tag{7.8}$$

${}_{(K)}\boldsymbol{g}_i$ describes all forces and torques acting on the center of mass of the object, m_i the mass of the body, $\boldsymbol{I}_3$ the identity matrix and ${}_{(K)}\boldsymbol{J}_i$ the inertia tensor. By splitting the forces $\boldsymbol{g}_i$ into applied loads ($\boldsymbol{g}_{\mathrm{app},i}$), muscle loads ($\boldsymbol{g}_{\mathrm{M},i}$) and reaction forces ($\boldsymbol{g}_{\mathrm{R},i}$), the dynamic equilibrium equations 7.6 can be built:

$${}_{(K)}\boldsymbol{d}_i = {}_{(K)}\boldsymbol{g}_{\mathrm{app},i} - \begin{pmatrix} m_i\boldsymbol{I}_3 & \boldsymbol{0} \\ \boldsymbol{0} & {}_{(K)}\boldsymbol{J}_i \end{pmatrix} \dot{\boldsymbol{v}}_i - \begin{pmatrix} \boldsymbol{0} \\ {}_{(K)}\boldsymbol{\omega}_i \times {}_{(K)}\boldsymbol{J}_{i(K)}\boldsymbol{\omega}_i \end{pmatrix}. \tag{7.9}$$

With this inverse dynamic model, the reaction forces in the joints and the forces in the muscles can be calculated, but the joints are limited to a maximum of three rotational and no translational DOFs. However, to predict the joint laxity of the knee, a model of the femorotibial joint with six DOFs allowing to take translations and joint geometries into account, is necessary. For this reason the model has been extended with the so-called Anybody Force Dependent Kinematic (FDK) method in order to enable inverse dynamic analysis to calculate the load-related motion in individual directions. For this purpose some of the equations described above have to be extended. Furthermore, the theoretical and mathematical considerations for the integration of this method are described in more detail:

The method of the FDK is based on the assumption that the loading conditional movements in individual degrees of freedom (FDK DOFs) are small movements $\boldsymbol{\alpha}_{\mathrm{FDK}}$ and thus dynamic influences can be excluded [12]. Consequently, a quasi-static force equilibrium can be assumed to avoid temporal integration and the inverse dynamic model can be augmented with an iterative approach (Figure 7.1). With this scheme, the positions in the FDK DOFs are calculated so that forces in these DOFs are in static equilibrium for each time step in the simulation [12]:

In the first, an initial guess of the joint position $\boldsymbol{\alpha}_{\mathrm{FDK}}$ is used to run the inverse dynamic analysis considering the assumptions of $\dot{\boldsymbol{\alpha}}_{\mathrm{FDK}} = 0$ and $\ddot{\boldsymbol{\alpha}}_{\mathrm{FDK}} = \boldsymbol{0}$. For this, the description of the relationships between the bodies (7.4) must be extended according to the FDK DOFs $\Phi_{\mathrm{FDK}}(\boldsymbol{q})$:

$$\Phi_{\mathrm{FDK}}(\boldsymbol{q}) - \boldsymbol{\alpha}_{\mathrm{FDK}} = \boldsymbol{0}. \tag{7.10}$$

Furthermore, the linear velocity equations (7.4) must be extended by the FDK DOFs:

$$\Phi_{FDK,\boldsymbol{q}*}\boldsymbol{v} = \boldsymbol{0} \quad \text{and} \quad \Phi_{FDK,\boldsymbol{q}*}\dot{\boldsymbol{v}} = \boldsymbol{\gamma}_{\mathrm{FDK}}(\boldsymbol{q}, \boldsymbol{v}, t). \tag{7.11}$$

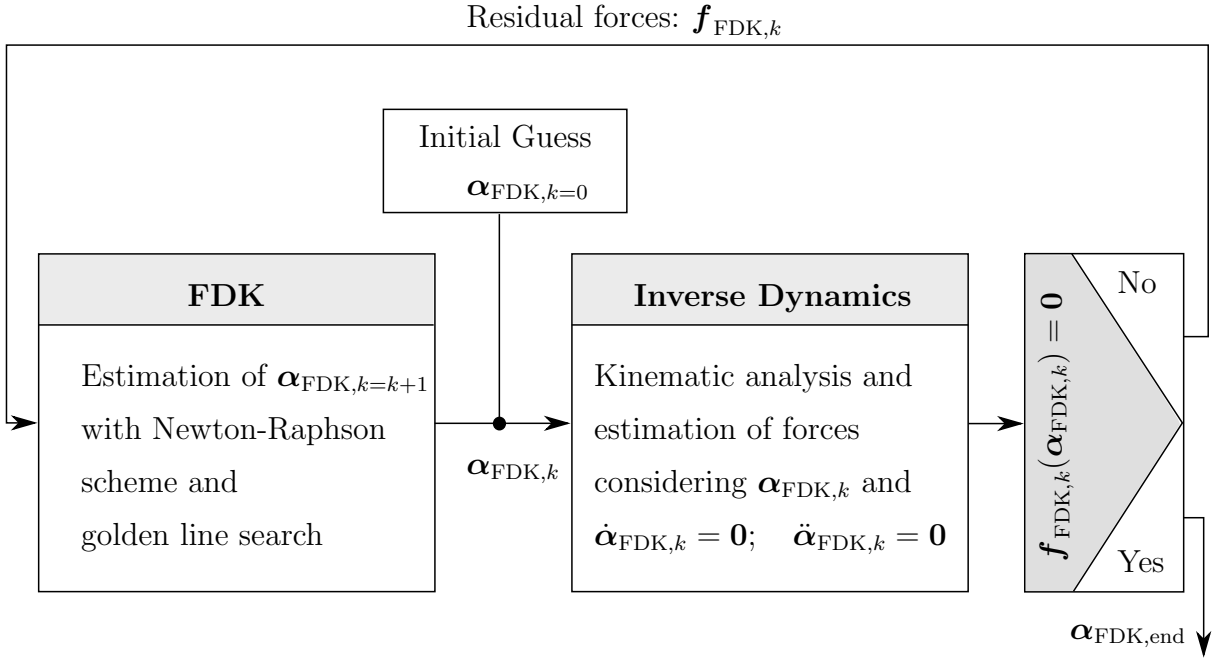

Figure 7.1: Schematic representation of the optimization cycle used to calculate the force dependent kinematics of the knee model.

Now the coefficient matrix including the component of the FDK residual forces can be set up and (7.6) can be reformulated accordingly:

$$\boldsymbol{C} \begin{pmatrix} \boldsymbol{f}_{\mathrm{M}} \\ \boldsymbol{f}_{\mathrm{R}} \\ \boldsymbol{f}_{\mathrm{FDK}} \end{pmatrix} = \boldsymbol{d} \quad \text{with} \quad \boldsymbol{C} = \begin{pmatrix} \boldsymbol{C}_{\mathrm{M}} & \boldsymbol{C}_{\mathrm{R}} & \boldsymbol{C}_{\mathrm{FDK}} \end{pmatrix}. \tag{7.12}$$

The inverse dynamic analysis then returns the forces in the system including the residual forces in the FDK DOFs.
The residual forces of the FDK DOFs form the input variable for the FDK solver. Using a modified Newton-Raphson method with a golden line search a new $\boldsymbol{\alpha}_{\mathrm{FDK}}$ is calculated with the goal [12]:

$$\boldsymbol{f}_{\mathrm{FDK}}(\boldsymbol{\alpha}_{\mathrm{FDK}}) = \mathbf{0}. \tag{7.13}$$

These iteration steps are repeated for a time step of the multibody simulation until a corresponding $\boldsymbol{\alpha}_{\mathrm{FDK}}$ is found or the iteration loop is terminated by an abort criterion.

7.1.2 Rigid-body knee model

The knee model developed in this work basically consists of five rigid bodies: three bones (femur, tibia, fibula) and two menisci (left and right). Especially the two main segments femur and tibia are surrounded and connected by numerous soft-tissue structures which are modeled in the form of non-linear springs. Each segment was assigned a mass and a

moment of inertia. The segments were positioned in relation to each other after a global reference coordinate system and the segments' own local coordinate systems were defined. A further coordinate system was created to apply loads to the motion segment (Figure 7.3). In this model, the fibula was firmly connected to the tibia and only serves to anatomically map the distal attachment site of the LCL. The two menisci are also firmly connected to the tibia. The geometric representation of the segments is realized by surface models of the rigid bodies which were loaded into the Anybody system in the form of *.stl files. For the bones, the geometries provided by the Anybody Repository (Twente Lower Extremity Model 2.1,AMMR, v.1.6.2) were used first. However, the repository does not have any meniscus models; for this reason, the generic surface models were replaced in a further step with models of a cadaveric knee used in this study. These models were generated from an image data set generated from magnet resonance imaging (MRI) sequences (see subsection 7.1.3). The two menisci were also segmented in order to be able to represent them in the simulation. In addition to the bones and menisci, the attachment sites of all ligament structures represented in this model were also segmented. The coordinates of the attachment sites were transferred to the model via reference frames. Since the ligaments of the knee joint sometimes have a width of several centimeters, individual attachment sites were divided into two or three reference frames in order to represent several bundles of a ligament and thus also the spatial expansion of a soft-tissue structure and to take into account the partly varying biomechanical function of a ligament. Accordingly, three fiber bundles each (anterior, intermediate, posterior) were generated for MCL, dMCL, and LCL, and two for ACL (anteromedial, mediolateral) and PCL (anterolateral, psteriomedial). The mechanical properties of the ligament and capsule structures were implemented using nonlinear springs. The ligament model of Blankevoort and Huiskes [28] was used which has three different areas, including a slack region, a non linear force-strain relationship for low strains and a linear relationship for higher strains.
Accordingly, the tensile force in the ligament f_{Lig} is defined as:

$$f_{\text{Lig}} = \begin{cases} \text{slack region:} & 0, & \epsilon < \epsilon_0, \\ \text{non linear region:} & \dfrac{k\epsilon^2}{4\epsilon_\text{l}}, & 0 \leq \epsilon \leq 2\epsilon_\text{l}, \\ \text{linear region:} & k(\epsilon - \epsilon_\text{l}), & \epsilon > 2\epsilon_1, \end{cases} \tag{7.14}$$

where k is the stiffness and ϵ is the strain in the ligament. The linear strain limit ϵ_l was set to 0.03 [35]. In Figure 7.2 an exemplary force-strain behavior of a ligament with respect to equation 7.14 is shown. The slack lengths l_0 of all modeled ligaments are being calibrated prior to the simulation at reference positions.

The following table (Table 7.1) summarizes the modeled ligament and capsule structures with their stiffness and the division into ligament fiber bundles: The modeling of a ligament by a direct connection of two ligament attachment sites disregards the redirection of soft-tissue structures frequently occurring in human anatomy by involved bone or cartilage surfaces. Such redirections can be considerable in the human body and in many cases have a major influence on the kinematics of a joint. In order to take such redirections into account, individual ligament structures were extended with a wrapping model. Anybody provides a kinematic measure in the form of a string for this purpose, which can be used to calculate the shortest distance between two attachment sites, taking into account any

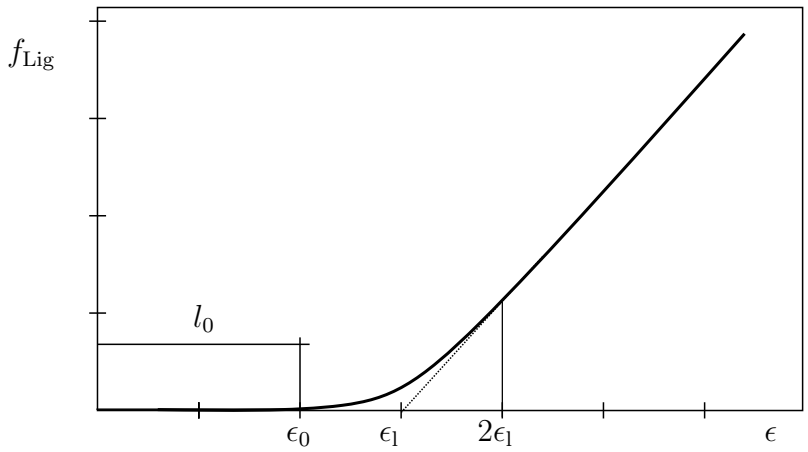

Figure 7.2: Force-strain relationship for the modeling of the mechanical behavior of the knee ligaments. $f^{(Lig)}$: ligament force; ϵ: strain; ϵ_0: zero strain limit; ϵ_1: linear strain limit; l_0: slack length.

surfaces between them. This kinematic measure can be coupled with nonlinear spring elements. The contact between string and surface is assumed to be friction-free. The shortest distance of the string is achieved by establishing a static equilibrium, *i.e.* the minimum potential elastic energy of the string. The contact between a surface and the string is solved iteratively until the displacement of the ligament tends towards zero. This kinematic measure can be realized with the imported surface models as well as with simple geometric primitives (spheres, cylinders) available in the Anybody environment. The wrapping over models (*e.g.* in STL format) as for example the bone models is on the one hand very computationally complex and on the other hand strongly dependent on the mesh size. For this reason, cylinder surfaces were generated in the knee model for all bony structures over which the ligaments travel: A cylinder was placed in the epicondyles on the femur side, with the cylinder axes parallel to the epicondylar axis and radius corresponding to the posterior portion of the epicondyle. This cylinder serves to deflect the posterior capsule structures. In addition, a further cylinder was placed in the area of the intercondylar groove to be able to guide the anterior cruciate ligament along the bone surface between the condyles if necessary. Two additional cylinders were modeled medially and laterally at the level of the tibial plateau to physiologically redirect the medial ligaments and the lateral ligament. In addition to the ligament structures, the modeled joints create the connection between the rigid bodies. The model has a total of twelve degrees of freedom. The femur as one of the two segments is firmly connected to the global coordinate system and thus fixed in space. The tibia, fibula and the two menisci are combined via the tibial segment and are thus firmly connected to each other. Five of the six DOFs of the segment are controlled by the FDK, the remaining DOF was equipped with a rotary driver to adjust the flexion position and movement of the joint by providing the angular position and velocity.

In order to include the joint surfaces in the calculations, the knee model was extended with surface contact models. The contact algorithm calculates the contact forces between femur and tibia by limiting penetration to the penetration depth d_i of the meshes in contact [12]. The contact forces are calculated using a linear volume approximation. The penetration volume V_i between two opposite triangles is calculated approximately using a cylinder with the length d_i and the base area A_i. Together with a pressure module P assigned to

Table 7.1: Summary of all modeled ligaments and capsule structures, presenting the division of single ligaments into ligament fiber bundles and the stiffness values of the structures.

Ligament/Capsule	Fiber bundle	Stiffness / (N/mm)
Superficial Medial Lateral Ligament (sMCL)	sMCLa	30
	sMCLi	30
	sMCLp	30
Deep Medial Lateral Ligament (dMCL)	dMCLa	14
	dMCLi	14
	dMCLp	14
Lateral Collateral Ligament (LCL)	LCLa	30
	LCLi	30
	LCLp	30
Anterior Cruciate Ligament (ACL)	amACL	75
	plACL	75
Posterior Cruciate Ligament (PCL)	alPCL	102
	pmPCL	102
Oblique Popliteal Ligament (OPL)	OPL	30
Posterior Oblique Ligament (POL)	POL	25
Anterior Lateral Ligament (ALL)	ALL	25
Medial Capsule (MC)	MC	12
Lateral Capsule (LC)	LC	12

the contact surface, the contact force can be calculated as follows:

$$F_i = \mathrm{P} V_i \quad \text{with} \quad V_i = A_i d_i. \tag{7.15}$$

The direction of the force corresponds to the surface normal of the respective triangle. In the present model this contact algorithm for the contact between femur and tibia as well as the femur and the two menisci was modelled. The pressure module for the femorotibial contact was modelled with $\mathrm{P}_{\mathrm{femtib}} = 5.0 \times 10^8 \, \frac{N}{m^3}$ and for the femoromeniscal contact with $\mathrm{P}_{\mathrm{femmen}} = 8.0 \times 10^7 \, \frac{N}{m^3}$ are assumed [12]. The calculated contact forces are then included in the calculation of the FDK in the form of external forces. A force tolerance of 1.0 N was applied as a stopping criterion for the FDK algorithm solving the equation 7.13. Any residual forces after solving the FDK are recorded as FDK error.

A reference coordinate system linked to the tibia was defined to represent applied loads relative to the knee joint. This coordinate system was placed based on the bony landmarks of the femur and the tibia. The origin was defined by the center of the two femoral

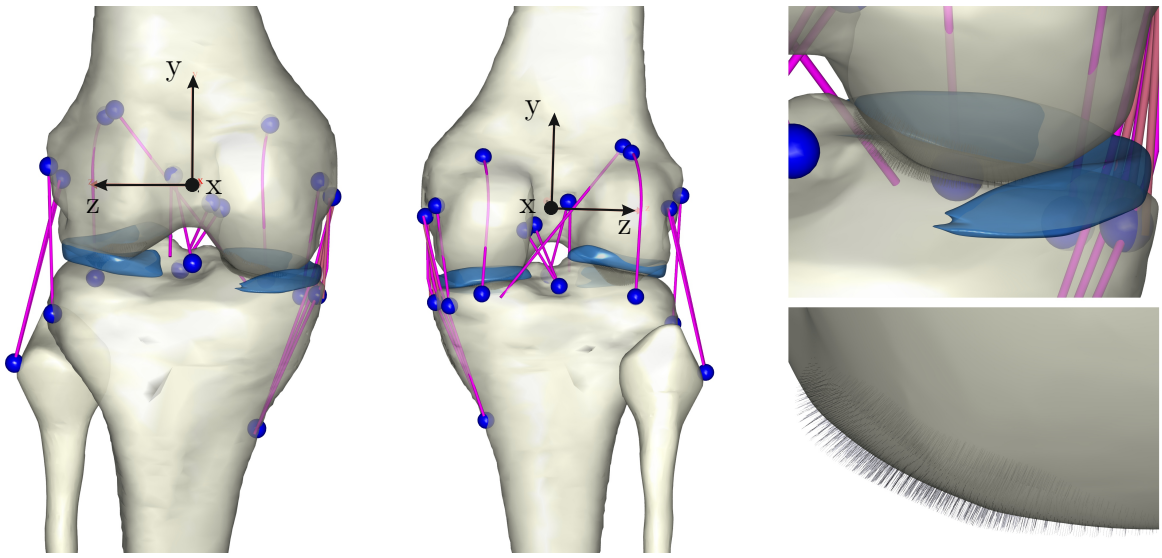

Figure 7.3: Representation of a subject-specific multibody model from the front (left) and from behind (middle). The reference coordinate System for the descriptions of the femorotibial motions is depicted. In addition, detailed representations of the femorotibial contact are given (right). The individual force vectors calculated with the penetration model can be seen.

epicondyles. A vector going through the lateral and medial femoral epicondyle pointing to the right defined the z-axis. The x-axis was defined by the vector perpendicular to z-axis and the long axis of the tibia pointing anteriorly. Finally, the vector perpendicular to the z- and x-axis defined the orientation of the y-axis (Figure 7.3).

7.1.3 Subject specific modeling

The laxity data of 865 knee joints summarized in chapter 5 very nicely illustrate the bandwidth in which the knee joint properties differ between individual subjects. In order to better plan the soft-tissue balancing to foresee the result more precisely, a tool is to be created on the basis of multibody simulation models so that the currently existing surgical planning steps can be extended by the aspect of soft-tissue management. This requires subject-specific models that can be created on the basis of information from medical imaging and take into account the individual anatomy of a joint. A work flow towards subject-specific models was developed that can be used in the future for the above-mentioned application scenario. In the context of this study, the individualization of the models was used to obtain an accurate *in-silico* representation of specimens examined in the *in-vitro* study. The individualization includes the subject-specific bone anatomy, the individual position and length of the ligaments and the individual mechanical properties of individual soft-tissue structures. In the following, the workflow with the individual work steps is described in more detail.

Magnetic resonance imaging

In order to obtain as much information as possible on the individual anatomy of a subject, the use of a three-dimensional cross-sectional technique was best suited for this purpose.

Since, in addition to the bone geometry, information on the soft-tissue structures with their insertion sites was also relevant, magnetic resonance imaging is the method of choice for obtaining layer images of a human knee joint. Within the scope of this work, ten individual models were created based on the anatomical data of ten cadavers used in the *in-vitro* experiments (chapter 6). Accordingly, the human knees were examined in a 3.0 Tesla scanner (Verio, Siemens Healthineers, Germany). The joints were scanned in extension position using a Tx/Rx 15-channel knee coil (Siemens Healthineers, Germany) to obtain high-resolution images. The sagittal PD weighted imaging sequence consisted of a 3D spoiled gradient-recalled acquisition with fat suppression (flip angle = 120°), repetition time = 1000 ms, echo time = 40 ms). The field of view was 172 × 180 mm and the image matrix 320 × 269, yielding a pixel size of 0.47 mm. 320 contiguous slices, 0.6 mm thick, were acquired in 30 minutes.

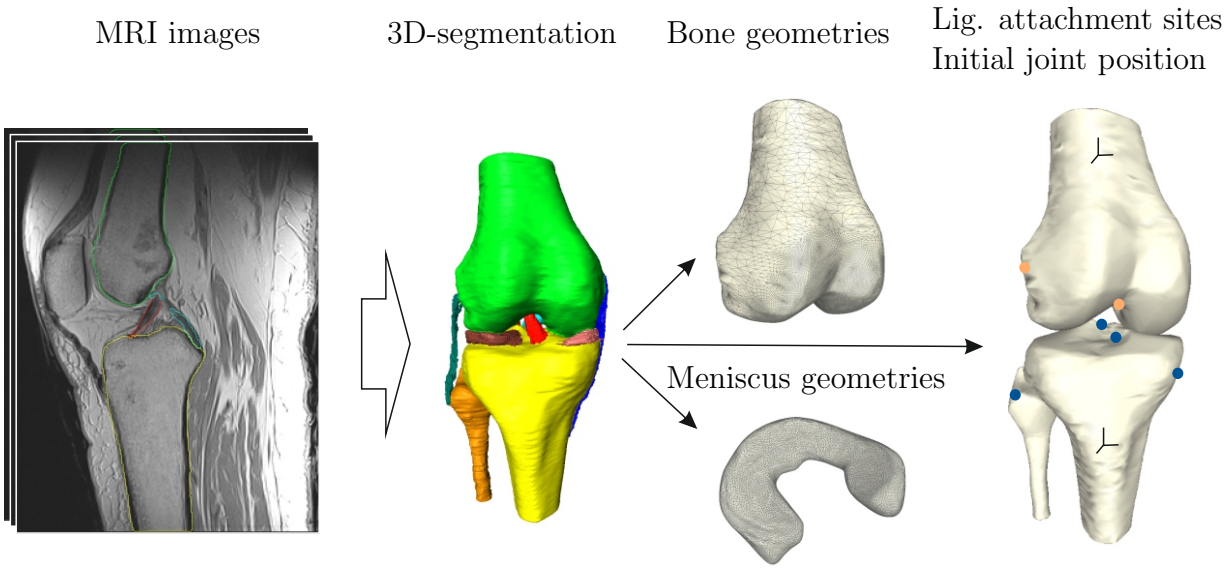

Figure 7.4: Schematic representation of the data extraction process from MRI data for the subject-specific modeling.

Segmentation and processing of image data

The aim of the segmentation was to convert the layer image data generated with the MRI scanner into 3D models in order to integrate them into the Anybody environment in the form of surface models (STL format). For this purpose the function of the Amira® (v5.3.3, FEI Visualization Sciences Group, Oregon, USA) software environment was used. The individual anatomical structures were each assigned their own label in all layers. Each label set was then exported as its own surface model. Due to the relatively low contrast difference between the anatomical structures to be separated and the heterogeneity of the contrasts within a structure (Figure 7.4), it was difficult to label the structures using segmentation tools such as threshold-based methods. For this reason, all structures in the individual layers were segmented manually. A particular challenge was the segmentation of individual ligament structures. Ligaments such as the ALL are tightly interwoven with surrounding soft-tissue structures, so that the ligament attachment sites could not be segmented for all ligaments modeled in the simulation model. In summary, the following

structures could be labeled:

- Distal Femur including cortical bone, cancellous bone and joint cartilage
- Proximal Tibia including cortical bone, cancellous bone and joint cartilage
- Proximal Fibula including cortical and cancellous bone
- Lateral and medial meniscus
- ACL, PCL, MCL and LCL

In addition to the ligament structures, a particular focus was placed on segmenting the joint surfaces as precisely as possible, since these were of considerable importance for the contact model in Anybody. With a smoothing function integrated in the segmentation software, the labels in the individual layers were regularized before the 3D segments were exported in the form of triangulated surfaces. With the help of the program library Meshlab (v.2016, Institute of Information Science and Technology-CNR, Italy) the number of triangular surfaces of the 3D segments of femur, tibia and fibula was first reduced and then the joint surfaces of femur and tibia were refined and smoothed with the software GOM Inspect (v.7, GOM GmbH, Germany).

Import of the meshes and adaption of the ligament attachment sites

In order to transfer the patient-specific bone and meniscus segments into the generic model, they first had to be slightly scaled to the size of the generic segments and the reference coordinate system of the object (STL) had to be transformed according to the generic segments. For such purposes an alignment function is available in the Meshlab program library. Before the two segments to be superimposed could be aligned using an iterative closest point algorithm, they first had to be aligned roughly manually. For this purpose, predefined landmarks were first marked on both meshes. The meshes could then be shifted and scaled via an alignment function so that the corresponding landmarks of the two meshes match as closely as possible. The generic mesh was defined as spatially fixed and the patient-specific mesh was shifted to the position of the generic mesh. The meshes scaled and transformed in this way could now be loaded into the created Anybody model without having to move or realign the individual elements of the model. However, this did not apply to the ligament attachment sites within a model, as these are very closely tied to the individual anatomy of the respective bone. In many cases, a simple transfer of the coordinates of the individual ligament attachments of the initial model to a patient-specific model would result in ligament attachments being distant from the bone surface due to the variances in the anatomy and thus not accurately representing reality. On the other hand, the segmentation and transfer of the ligament attachments from the MRI data is very time-consuming and only applicable for certain ligaments. For this reason, a morphing algorithm was implemented in the simulation model in addition to the segmentation of the ligaments (Figure 7.5), with which the ligament attachment points of the generic model could be transferred to the patient-specific meshes.

The morphing algorithm contains three interpolation functions, each for one of the three spatial directions, in the form of radial basis functions (RBF). These RBFs are used for the transformation of a set of given points (source landmarks) into a set of known subject-specific points (target landmarks). The individual determination of the ligament

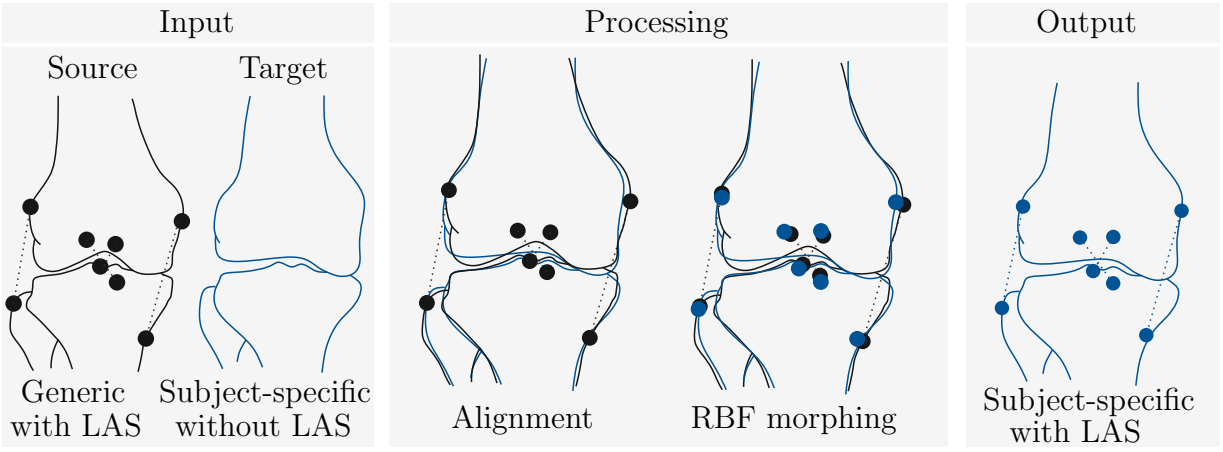

Figure 7.5: Schematic representation of the alignment and morphing process for approximation of subject-specific ligament attachment sites (LAS) using a closest point alignment and radial basis function (RBF) based mesh morphing technique.

attachment sites is done by use of the surface information of the bone meshes of a generic model (source) and of a individual subject (target). The approximation that is used for this purpose is defined by linear combinations of basis functions (ϕ) with respect to the Euclidean distance $||\boldsymbol{x}||_2$ for a given number of boundary nodes n in the following form:

$$f(\boldsymbol{x}) \approx \sum_{j=1}^{n} c_j \phi(||\boldsymbol{x} - \boldsymbol{x}_j||_2) + p(\boldsymbol{x}) \tag{7.16}$$

with the weighting factors c_j, the boundary nodes $\boldsymbol{x}_j = (x_j, y_j, z_j)^\intercal$ and a polynomial function p.
As radial basic functions different types are available for the approximation in this case:

$$\text{thin plate spline:} \quad \phi(r) = x^2 \ln(r), \tag{7.17}$$

$$\text{multiquadratic function} \quad \phi(r) = \sqrt{r^2 - a}, \; a < r^2, \tag{7.18}$$

$$\text{triharmonic function} \quad \phi(r) = r^3, \quad \text{with} \quad r = ||\boldsymbol{x} - \boldsymbol{x}_j||_2. \tag{7.19}$$

The definition of the grid points is done automatically. Therefore, a given number of points is seeded on the source surface and corresponding landmarks are found on the target surface by identifying closest vertices. The prerequisite for this is that the source and target mesh have already been registered to each other and that a good alignment prevails.
In order to achieve the best possible estimation with the morphing algorithm, the generic model used was trained on the basis of ten MRI data sets of the knee joint. The definition of the attachment sites of the model was shifted in such a way that the deviation between

the ligament attachments segmented from the MRI data and the attachments estimated with the RBF was minimized [8].

7.1.4 Accuracy and sensitivity analysis of the in-silico model

The accuracy and sensitivity investigations of the developed multibody model were conducted on the one hand to analyse the functionality of individual methods (*e.g.* RBF, FDK) applied in the model and on the other hand to work out the robustness of the model against changes of individual model parameters.
In the following, methods are described which were used to examine the accuracy of the ligament attachment site approximation using RBFs. In this context, the influence of the ligament attachment sites on the simulation result were also investigated. Furthermore, the following subsections describe the methods which were used to evaluate the influence of the initial position of the joint, the mesh size of the surface models as well as the pressure module of the femorotibial joint on the simulation results with regard to the related FDK approach.

Accuracy and sensitivity of the ligament attachment site approximation by use of radial basis functions

Since the quality of mesh morphing by RBF may depend on both the type of RBF and the number of boundary nodes, the sensitivity of the morphing function as a result of changes in these factors was first investigated. In order to quantify the quality of the ligament attachment site determination using RBF, the accuracy of the RBF was also determined for the single ligaments in the three spatial directions. The attachment sites of the MCL, LCL, PCL, and ACL were estimated for the femoral side of the knee joint using the three RBF types (7.19, 7.18, and 7.17) to investigate the attachment site estimation depending on the RBF function used. For all RBF types 800 automatically selected boundary nodes (subsection 7.1.3) have been defined as landmark points to construct the RBF transformation. In further investigations the femoral attachment sites were estimated using the thin plate spline function (7.17) on the basis of 50, 100, 200, 400, and 800 automatically selected boundary nodes.

To evaluate the quality of the ligament attachment site estimation, the Euclidean distances between the attachment sites were calculated for all configurations from the MRI data and the results from the RBF morphing. For the configuration with the thin plate spline as RBF type and 800 boundary nodes the differences of the attachment sites between MRI data and the RBF were evaluated in dependence of the three spartial directions.

Sensitivity of the force dependent kinematics as a function of the ligament attachment sites

The estimation of the ligament attachments by means of RBFs is naturally subject to an estimation error. This error may affect the results of simulations with the multibody model. In order to investigate how sensitive the knee model reacts to deviations of the ligament attachments, a probabilistic experiment based on the results from the accuracy evaluation of the attachment site approximation (subsection 7.2.1) was used to investigate

the influences of the ligament attachments on the joint translations and rotations as a result of an applied load.

For this purpose, a patient-specific, FDK multibody model with 5 DOFs as described in subsection 7.1.5 was used. An anterior drawer test was accomplished by simulating a steadily increasing load of up to 134 N, while the joint was kept centered. This was realized by simultaniously applying 20 N compression load in axial direction (y-axis). The flexion of the joint was held constant with the joint in 0° flexion position while all other DOFs were unconstrained.
For loading and parametrization of the model, execution of the simulation and collecting the results a script was written in the programming language Python (Python Software Foundation, Wilmington, Delaware, USA). The script based controlling of the multibody model on the one hand allowed for a systematical and efficient investigation of certain parameters and on the other hand allowed a parallelization of simulation processes. Parametrization of the model was implemented as follows:

Attachment sites of the ligaments derived from the MRI data were used as initial sites. The variation of the attachment site of each ligament was realized by creating 100 different positions for each attachment site with a maximum difference of 5 mm per direction relative to the initial sites. The variation was based on a cosine distribution as an approximation to the normal distribution to reproduce the distribution of the RBF based attachment site predictions relative to the reference position derived from MRI. The probability density function for the cosine distribution is:

$$f(x) = \frac{1}{2\pi}(1 + \cos x) \quad \text{for} \quad -\pi \leq x \leq \pi. \tag{7.20}$$

The calculated attachment sites were then randomly assigned to the model by utilizing a Latin hypercube sampling technique. Accordingly, 100 simulations were carried out. The following simulation steps were performed after parametrization of the model:

- Segments were set in its defined initial position.
- Ligament calibration: slack lengths for all ligaments were calculated with the joints in initial position at 0° of flexion.
- Inverse dynamic simulation: Solving the FDK based musculoskeletal model.
- Saving the output: Translations and rotations of the femur, positions of the ligament attachment sites and the error in the determination of the equilibrium of forces in the model at each simulation step (FDK error).

After completion of the simulation, for each parameter set the Euclidean distances between the investigated ligament attachment sites and the MRI-determined sites were calculated. In addition to the probabilistic experiments, the model was calculated using the ligament attachment sites determined from the MRI data and from the RBF.

The statistical software R (version 3.3.2, R Foundation for Statistical Computing) was used to further analyse the collected data. To analyse the correlation of the sum of the Euclidean distances of a given model configuration with the results of the simulation, a Pearson correlation was performed. Furthermore, to find ligament attachment sites whose positions have a great effect on the model results, the Euclidean distance of the attach-

ment relative to the MRI based target site for individual ligaments were correlated with the measured translations and rotations of the joint, again by calculating the Pearson correlation coefficient. An α value of 0.05 was set for all analysis. Additionally, a line plot for each parameter set was created, showing the translations and rotations of the joint in dependence of the simulation progress. Box plots for the change in position and rotation of the joint were created (Figure 7.11). Regarding the box plots, whiskers represent the lowest and highest values within the 1.5 times inter quartile range of 1st and 3rd quartile, respectively. Dots represent outliers, defined as values beyond the whiskers.

Sensitivity of the force dependent kinematics as a function of the mesh size

Since the triangular surfaces of the bone surface models are included in the calculation of the contact forces, an influence of the mesh refinement on the simulation results cannot be neglected. The sensitivity of the model to the change in mesh refinement was investigated as follows:

A patient-specific, FDK multibody model with 5 DOFs as already described in the previous section was used. The surface models of femur and tibia were varied with regard to the number of triangular surfaces using the Meshlab program library without changing the geometry in a meaningful way. The surface models were simplified using a Quadric Edge Collapse Decimation algorithm. The number of triangle surfaces of the two segments was reduced to 1/4, 1/8, and 1/16 of the original number, respectively, and saved as a surface model.
In the following, three models with mentioned mesh configurations were created in addition to the existing model. In accordance with the above investigations, an anterior drawer test was then agin simulated. During the simulation, the joint reactions were recorded in the form of translations and rotations. Furthermore, the FDK error was recorded. Subsequently, the translations and rotations of the joint were evaluated for all configurations.

Sensitivity of the force dependent kinematics as a function of the initial joint position

The initial joint position of the model is the starting point of the force calculations for the FDK and the inverse dynamics. This position is usually specified by the user of the simulation model. Different starting points may lead to different force relationships in the joint, therefore, an influence of this initial position on the simulation results cannot be excluded. To investigate this, probabilistic experiments were used similar to the sensitivity analysis for the ligament attachment sites. Also in this case, a patient-specific, FDK multi-body model with 5 DOFs as mentioned above was used. Again an anterior drawer test was simulated. For loading and parametrization of the model, execution of the simulation and collecting the results a Python script was written and executed.

The initial position of the joint was defined based on the MRI data of the subject-specific model. Specimens were scanned in full extension of the knee, by use of a knee coil. Accordingly, the MRI data are also available with the joint in extension position. By segmenting the bones in the same reference coordinate system, this joint position could be transferred to the model. Based on the MRI derived joint position, various initial positions were calculated with the aid of a cosine distribution (equation 7.20), whereby the maximum deviation corresponded to a displacement of 5 mm in anterior-posterior

and medial-lateral direction and a maximum rotation of 1.5° in varus-valgus and internal-external rotation. The displacement in superio-inferior direction was not varied, since in this DOF the positioning of the joint is clearly defined by the contact of the bone geometries. As preliminary experiments showed that a variation of the initial position quickly leads to a termination of the simulation, a total of 200 different initial positions were investigated. The calculated alterations in the single directions were then randomly assigned to the model again by utilizing a Latin hypercube sampling technique for 200 different initial positions. Subsequently, the model was subjected to the same simulation process as before.

Following the simulations, the translations and rotations of the individual configurations were evaluated. A line plot for each parameter set was created, showing the translations and rotations of the joint in dependence of the simulation progress. Box plots for the change in position and rotation of the joint were created.

Sensitivity of the force dependent kinematics as a function of the femorotibial pressure module

The contact model of the femorotibial joint is a central aspect of the FDK method in this multibody model. The calculation of the joint contact and the contact forces is done by means of a penetration model (subsection 7.1.5) with the pressure module as the decisive variable. Since the penetration of two bodies, as implemented in the model, does not occur in reality, no equivalent literature data exist for the parameter "pressure module". However, the manufacturer of the simulation environment provides guide values in order to obtain realistic simulation results which are in the range of 1.0×10^7 to 1.0×10^{10} $\frac{N}{m^3}$. To what extent the variation of this parameter influences the simulation results is completely unknown and in all likelihood dependent on the parameters of the simulation. For this purpose, these pressure module was varied in a sensitivity analysis. For this purpose, once more the patient-specific, FDK multibody model with 5 DOFs as mentioned above was used and again an anterior drawer test was applied. For loading and parametrization of the model, execution of the simulation and collecting the results a script was written in the programming language Python.
The variation of the pressure module of the femorotibial contact model was realized by creating 200 different values ranging from 1.0×10^8 to 1.0×10^9 $\frac{N}{m^3}$. The allocation of the random values was distributed by coincidence. The calculated pressure modules were then assigned by chance to the model by utilizing a Latin hypercube sampling technique. Accordingly, 200 simulations were carried out. The model went through the same simulation process as applied before.
After the simulations, the deviations in the translations and rotations were calculated.

7.1.5 Model validation and simulation of the knee laxity

Ten subject specific models created from MRI data (subsection 7.1.3) were used for the validation and simulation of the knee laxity. On the one hand, the model was validated indirectly by means of available literature data and on the other hand directly by means of the data collected in the *in-vitro* experiments. In the following, the experimental setup and the execution of the validations are described in detail.

As the sensitivity analysis demonstrated differences between MRI and RBF based ligament attachment sites (subsection 7.2.1), for further analysis sites were modeled based on MRI data and literature data for those which could not be located in the MRI images. Initial posture of the joints was defined to be in full extension. Positions of the bones in extension were derived from MRI data of the knees which were scanned in full extension (subsection 7.1.3). Each motion simulation was performed in 100 computational steps. A Python script was used for loading, parametrization, execution of the multibody knee models. Furthermore, the script was used for a detailed ligament calibration prior to laxity testing.

The ligament calibration consisted of three iterative calibration steps. Initially the slack lengths of all ligaments were set at 0° flexion. During each iteration a knee flexion motion from 0° to 90° was simulated and joint position as well as length changes of all modeled ligaments were recorded at 0°, 15°, 30°, 60° and 90°. After each flexion motion zero load lengths of the ligaments were set based on available literature: slack lengths of the dMCL and sMCL were defined to be at 30° [96, 180]. The LCL was defined to be slack at 30°[180]. Zero load lengths of the PCL was set at 15° [234] and of the ACL at 30° [155, 195, 57]. Slack length of the OPL, POL and ALL were all set at 15° [259]. Posterior-medial and -lateral capsule forces were defined to be zero at 15°.

After calibration of the ligaments, laxity of the joints was analysed at 0°, 15°, 30°, 60° and 90° of flexion. For testing of the joint restraints only the flexion angle was held constant, all other directions were allowed to move freely. Anterior, posterior, inferior translation laxity was evaluated by applying a load of 134 N, to the tibia in the respective direction. For the analysis of the varus and valgus rotational laxity, 10 Nm load were applied around the tibial x-axis. Internal and external rotation laxity was evaluated by applying 5 Nm in axial direction of the tibia. Additionally to the testing load a 20 N centering force along the axis of the tibia was applied to keep the femorotibial joint centered during testing. The laxities of the knee models were analysed for three different joint conditions: intact, after removal of the menisci and after an additional removal of the ACL bundles.

In the first step of validation, the flexion motion of the knee models after ligament calibration was analyzed. Two main kinematic parameters, the axial rotation of the tibia relative to the femur as well as anterior-posterior translation of the tibia relative to the femur better known as the femoral roll back during a flexion task from 0° to 90° were analyzed. For this purpose, five literature references were randomly selected, in which the mentioned parameters of knee joint kinematics were examined on healthy knees and the absolute values were available in the manuscript in the form of text, table or illustration [165, 145, 54, 32, 134]. The rotations and translations of the tibia relative to the femur during flexion were transcribed for flexion angles 0°, 10°, 20°, 30°, 45°, 60° and 90° and mean values and standard deviations were determined for each angle position. The literature data were then compared with the simulation results. In addition, the forces of the individual ligament structures and their length changes during flexion were evaluated.

In a second step of validation, the subject-specific model predictions of the native knee laxity in all tested directions and flexion angles were compared to the *in-vitro* investigations. As the subject-specific models were created based on the image data of knee specimens used in the *in-vitro* experiments, a direct one-to-one comparison for each single subject could be carried out. Accordingly, for the flexion angles 0°, 30°, 60°, and 90° the root mean square errors (RMSEs) between numerically calculated and experimentally

determined values were calculated.

7.2 Results

The outcome of the individual investigations are shown in the following sections. In the first four sections, the results of the sensitivity analyses of the *in-silico* model are described. Furthermore, the findings of the validation of the model by comparing the numerical predictions to literature data and the *in-vitro* data (section 6.2) are presented.

7.2.1 Accuracy and sensitivity analysis

The investigations showed no influence of the number of boundary nodes of the RBF on the algorithm for ligament attachment site approximations, and no significant dependence of the results on the type of radial basis function. The accuracy of the approximation ranged from 0.60 mm to 6.12 mm, depending on ligament and anatomical direction. The variation of the ligament attachment sites showed an influence on the calculated joint laxity. The sensitivity analysis also showed an influence of the mesh size and the initial position of the joint on the joint laxity. The femorotibial pressure module also influenced the calculated joint laxity. In the following, the results of the investigations are listed in detail.

Accuracy and sensitivity of the ligament attachment site estimation by use of radial basis functions

The investigations on the number of boundary nodes showed no influence on the accuracy of the attachment site approximation. The calculated differences between the Euclidean distances based on 50 and 800 boundary nodes was 0.010 mm for the ACL, 0.14 mm for the LCL, 0.07 mm for the MCL, and 0.07 mm for the PCL (Figure 7.6).
The different RBFs also showed no significant differences in the results for the approximation of the ligament attachment sites. The distance averaged over all Euclidean distances was 5.26 ± 0.31 mm for the calculation with the thin plate spline, 5.24 ± 0.32 mm for the triharmonic function and 5.24 ± 0.31 mm for the multiquadric function (Figure 7.7).
With the application of the thin plate spline RBF and 800 boundary nodes, the approximated attachments of ACL, LCL and MCL on the femur showed that they were spread around the respective attachment site determined by MRI. The largest deviations among these three ligaments were 1.11 ± 4.63 mm and 0.78 ± 2.85 mm in posterior direction for MCL and ACL, respectively, and 0.60 ± 3.40 mm in lateral direction for the LCL (Figure 7.8). For the PCL, on the other hand, there were larger deviations in all three directions: The deviation was 2.54 ± 2.03 mm in posterior, 2.84 ± 1.93 mm in superior, and 3.00 ± 2.70 mm in lateral direction.

Regarding the approximation of the tibial ligament sites, the largest deviations were found for the MCL. Here the deviations were 6.12 ± 5.43 mm in superior and 1.88 ± 2.38 mm in lateral direction compared to the sites derived from the MRI data. The largest deviations of the remaining ligaments were 1.70 ± 4.36 mm in posterior direction for the ACL, 1.06 ± 1.72 mm in superior direction for the PCL, and 0.90 ± 2.99 mm in inferior direction for the LCL (Figure 7.8).

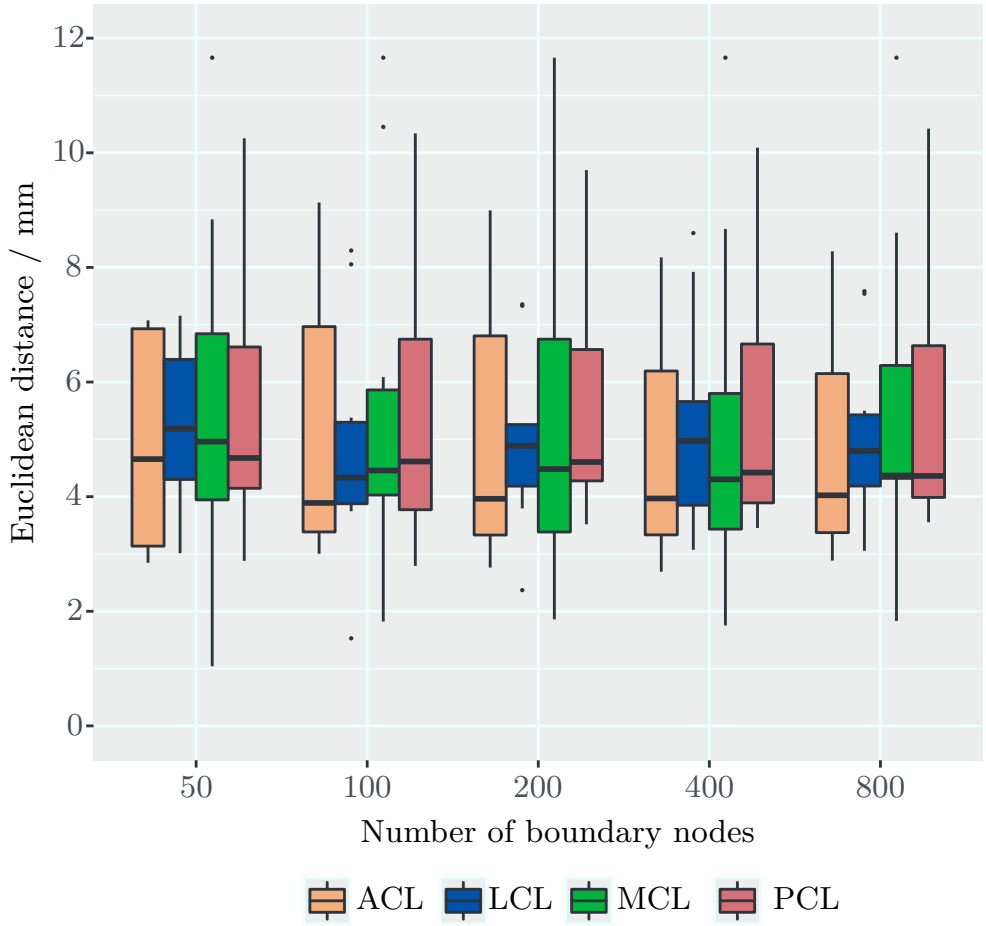

Figure 7.6: Box Plots showing the Euclidean distance between the location of a ligament attachment site estimated via MRI and approximated via a radial basis function based morphing algorithm. The number of boundary nodes were varied for approximation from 50 to 800 nodes. Presented are data for the femoral ligament attachment sites of the MCL, LCL, PCL, and ACL.

Sensitivity of the force dependent kinematics as a function of the ligament attachment sites

Of the 100 individual simulations, 78 could be evaluated, 22 simulations were aborted by the system due to calculation errors. The Euclidean distance of the successfully completed simulations, summed over all varied ligament attachment sites, was on average 5.26 ± 0.31 mm for the femur and 4.57 ± 1.83 mm for the tibia (Figures 7.9, 7.10).

In ten simulations the errors of the FDK model averaged more than 10 N (mean 225 ± 111 N). The lowest FDK error was 1.3 N. As a result of the first calculation step, the joint position of simulations with an FDK error greater than 10 N differed from simulations with a smaller FDK error by 0.6 mm in the x-direction, 0.8 mm in the y-direction, and 1.9 mm in the z-direction, as well as rotations of 0.8° around the x-axis, and -3.8° around the y-axis. The calculated joint translation in loading direction (x-axis) averaged over all simulations was 3.2 ± 1.9 mm. The translations ranged from -2.0 mm to 9.7 mm. For comparison, the translations calculated with the MRI and RBF based ligament attachment site estimations were 3.7 mm and 3.3 mm in the x-direction, respectively. Besides the translation in x-

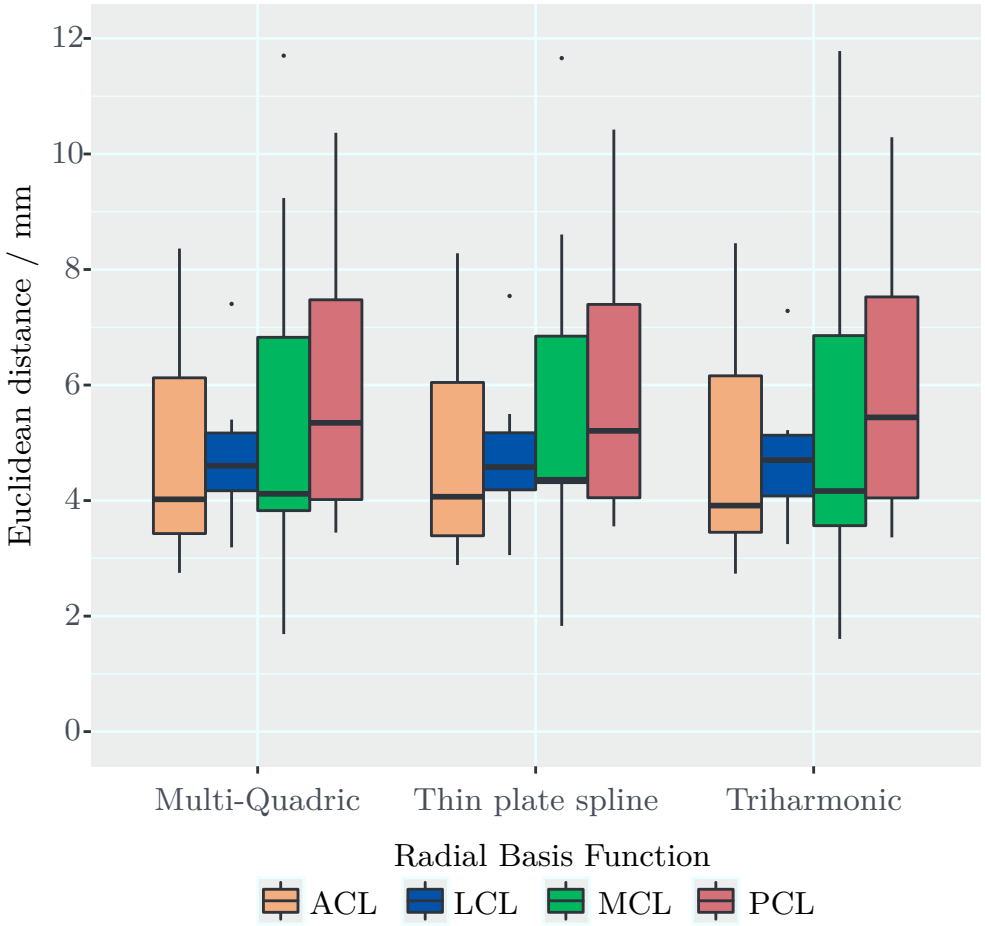

Figure 7.7: Box Plots showing the Euclidean distance between the location of a ligament attachment site estimated via MRI and approximated via a radial basis function based morphing algorithm. Different types of radial basis functions were investigated. 800 boundary nodes were used for all functions investigated. Presented are data for the femoral ligament attachment sites of the MCL, LCL, PCL, and ACL.

direction, there were lower translations in y- and z-direction with values of 0.2 ± 0.2 mm and 1.2 ± 1.1 mm. In addition to the displacements, rotations around the x- and y-axis also occurred with values of $0.5 \pm 0.6°$ and $-1.1 \pm 1.9°$, respectively. Especially the rotation around the y-axis varied between the simulations. The values ranged from $-5.6°$ to $3.2°$. Subdividing the calculated joint translations of the simulations with an FDK error greater than 10 N with those with a smaller FDK error, data reveal significant differences in four DOFs (Table 7.2): Comparing the simulations in which the ligament attachments were configured on the one hand by means of MRI and on the other hand by means of RBF methode, there were differences in the translations of 0.4 mm in x-direction, 0.1 mm in y-direction, and 1.2 mm in z-direction, as well as differences in the rotations of 0.6° and 1.6° around the x- and y-axis, respectively.

The correlation of Euclidean distances of individual ligament structures with the resulting translations and rotations of the joint showed significant correlations for the femoral attachment of the LCL and the translation in x- ($p = 0.021$) as well as in y-direction ($p = 0.017$), (Figure C.1). The corresponding tibial attachment site showed no influence on

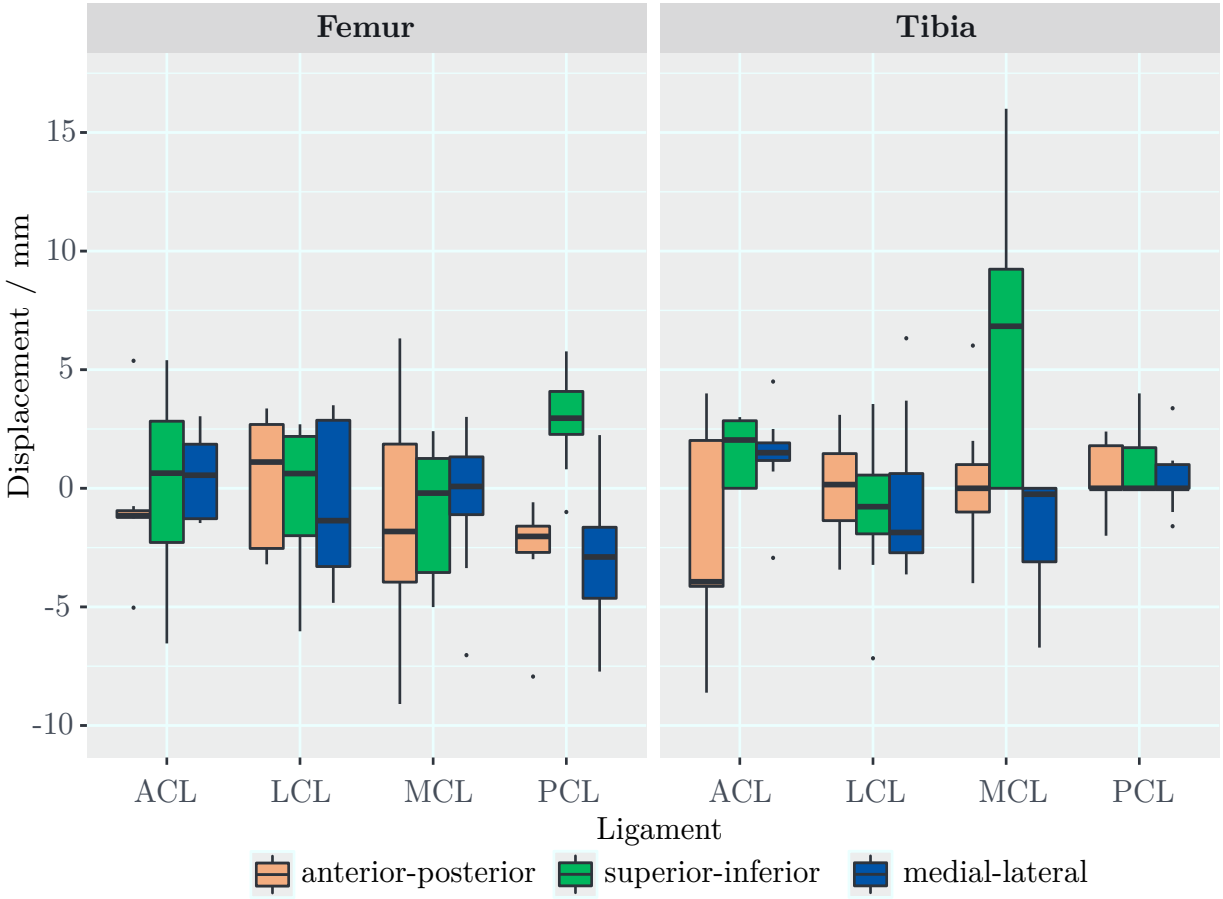

Figure 7.8: Accuracy of the radial basis function based approximation of the ligament attachment sites of the MCL, LCL, ACL, and PCL for the femur and the tibia. Differences in relation to the MRI based attachment site estimation in three directions are displayed.

joint laxity, (Figures C.3, C.4). The position of the femoral attachment site of the sMCL and dMCL correlated with the rotation about the y-axis ($p = 0.044$, $p = 0.037$), (Figure C.2). The position of the tibial attachment site influenced the shift in the z-direction ($p = 0.039$), (Figure C.3). The Euclidean distances of the attachment sites of ACL and PCL showed no significant correlation with the joint displacements and rotations ($p > 0.19$).

Sensitifity of the force dependant kinematics as a function of the mesh size

The refinement of the mesh showed an influence on the calculation results of the simulation model (Figures 7.12, 7.13). The joint positions differed already in the first calculation step between the simulations with differing mesh configuration. The reduction of the number of triangles to 1/16 led to difficulties in solving the contact model during the simulation. The results of the simulation for this case showed increased displacements and rotations for all five DOFs compared to all other mesh conditions. Compared to the initial model, the largest deviations were 4.3 mm, 3.0 mm, and 4.6 mm in x-, y-, z-direction as well as 2.6° and 6.2° around the x- and y-axis. Not before 12.5 % of the initial mesh density the simulation could be carried out without major problems during solving. Compared to the initial model, the translations in the x-, y- and z-directions deviated by 1.5 mm, 1.6 mm and 2.2 mm and the rotations around the x- and y-axis by 1.6° and 2.7°. The configuration

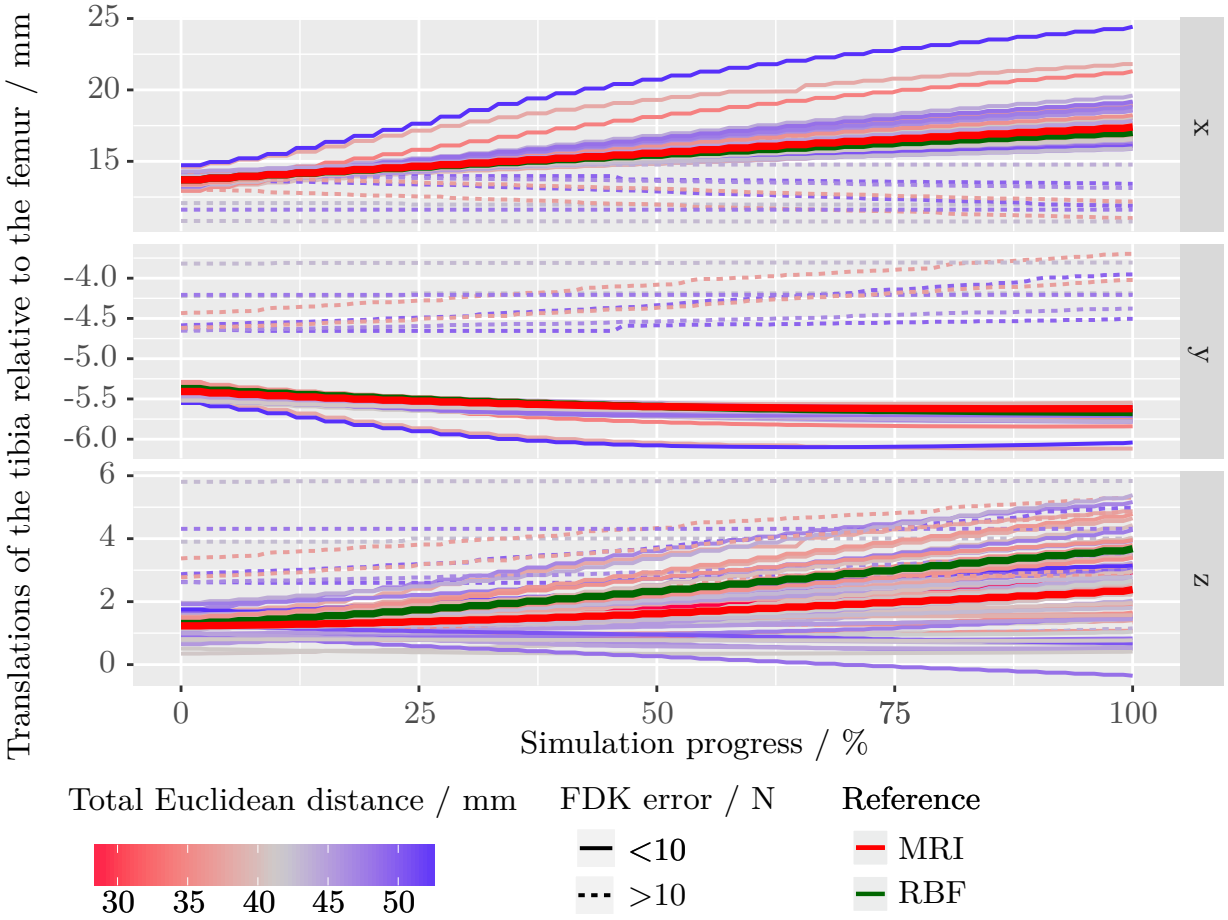

Figure 7.9: Line diagrams of the tibial position relative to the femur in dependence of the simulation progress simulating an anterior drawer test. 0 % progress corresponds to 0 N and 100 % to 134 N anterior load, respectively. Each line represents one simulation with a different ligament attachment site configuration of the MCL, LCL, ACL, and PCL. In addition, the results of simulations in which the ligament attachments were determined by MRI and radial basis function (RBF) are displayed.

with 25 % of the initial mesh density, showed no more differences in the simulation results compared to the initial model.

Sensitivity of the force dependent kinematics as a function of the initial joint position

Of the 200 individual simulations, only 39 were successfully completed. Eleven of them were finished with a mean force dependent kinematic error greater than 10 N (mean 299 ± 113 N). For these the translations in x-, y-, z-direction were 2.0 ± 2.5 mm, 0.4 ± 0.5 mm, -0.4 ± 3.6 mm and the rotations around the x- and y-axis $0.5 \pm 0.8°$ and $-3.1 \pm 3.3°$, respectively. For the remaining simulations with a mean force dependent kinematic error smaller than 10 N, the translations in x-, y-, z-direction were 4.5 ± 1.1 mm, -0.2 ± 0.1 mm, 1.1 ± 1.0 mm and the rotations around the x- and y-axis $0.4 \pm 0.8°$ and $-0.4 \pm 2.1°$, respectively.

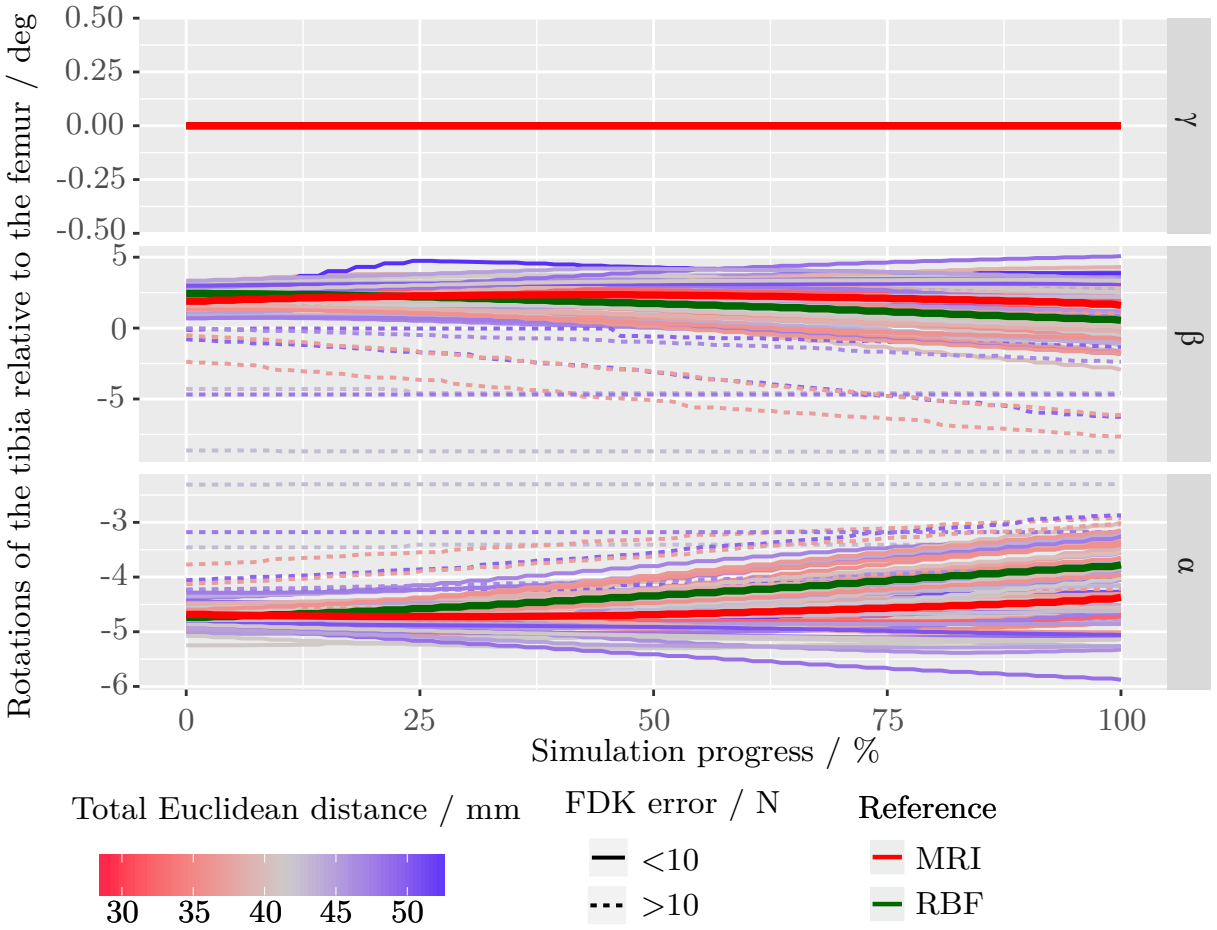

Figure 7.10: Line diagrams of the tibial rotation relative to the femur in dependence of the simulation progress simulating an anterior drawer test. α, β, γ represent the rotations about the x-, y-, z-axis, respectively. 0 % progress corresponds to 0 N and 100 % to 134 N anterior load, respectively. Each line represents one simulation with a different ligament attachment site configurationof the MCL, LCL, ACL, and PCL. In addition, the results of simulations in which the ligament attachments were determined by MRI and radial basis function (RBF) are displayed.

A comparison of the translations and rotations of all simulations with a low FDK error with the results in which the initial position was determined using the MRI data showed a maximum deviation of 3.5 mm in the loading direction (x-axis), (Figures 7.14, 7.15). A correlation of the measured translation in loading direction with the displacement of the initial joint position showed a significant correlation for the displacement in x-direction ($p < 0.0001$) as well as in z-direction ($p = 0.026$). Changes of the initial position by rotation around the x- and y-axis showed no significant influence ($p = 0.46$, $p = 0.23$).

Sensitivity of the force dependent kinematics as a function of the femorotibial pressure module

Only 42 of the 200 simulations with varying pressure module could be completed. The pressure module of the successfully finished simulations was in a range between 1.14 and $8.9 \times 10^8 \frac{N}{m^3}$. Considering the distribution of the pressure module values that could be

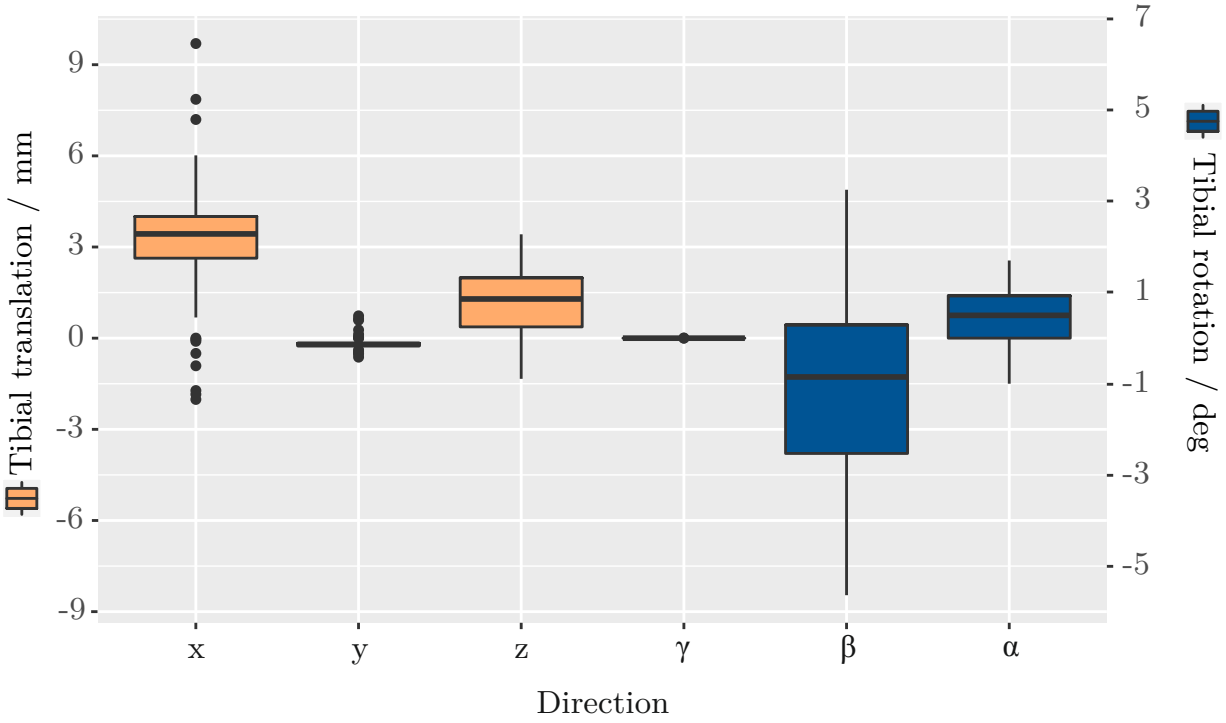

Figure 7.11: Box plots of translations (x, y, z) and rotations (α, β, γ) as responds to 134 N anterior drawer load. The plots include all simulations with differing ligament attachment site configuration.

Table 7.2: Mean translations and rotations as responds to 134 N anterior drawer load for simulations with FDK error less and greater than 10 N. α and β represent the rotations about the x-, and y-axis, respectively.

	Translations and rotations (mean $\pm SD$)				
FDK error	x / mm	y / mm	z / mm	α / deg	β / deg
<10 N	3.8 ± 1.3	-0.2 ± 0.1	1.3 ± 1.1	0.5 ± 0.6	-1.0 ± 1.8
>10 N	0.04 ± 1.5	0.2 ± 0.3	0.8 ± 0.9	0.4 ± 0.5	-2.1 ± 2.5

successfully calculated, only six simulations with results were within the range of 5.0 to $8.9 \times 10^8 \frac{N}{m^3}$. The largest deviations in the calculated joint movement were observed for the translation in loading direction (x-axis) with a range of 1.75 mm as well as for the rotation around the y-axis with a range of 2.36° (Figure 7.16).

7.2.2 Model validation and simulation of the knee laxity

Ligament calibration was successful for seven of the ten models. With the remaining three models, the flexion movements for the ligament calibration could not be completed due to the abort of the simulations. Also by repeated simulation tests, a renewed verification of the modeling itself and a slight variation of different model parameters like the pressure module or the initial position the simulations of the flexion movement could not be successfully completed. A ligament calibration for the three models was not possible.

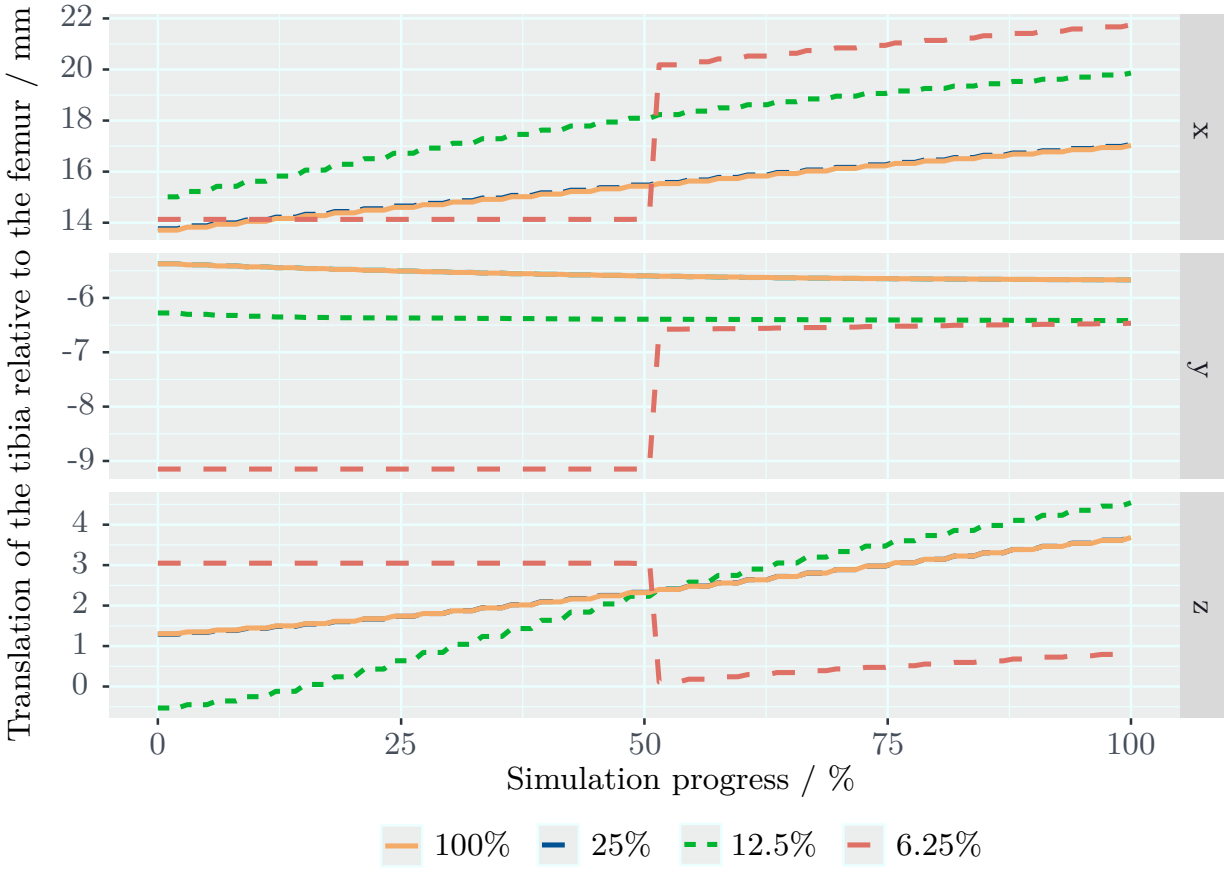

Figure 7.12: Line diagrams of the tibial position relative to the femur in dependence of the simulation progress simulating an anterior drawer test. 0 % progress corresponds to 0 N and 100 % to 134 N anterior load, respectively. Shown are the data of four different multi body models with differing mesh size of the femoral and tibial bone surface. 100 % mesh size represents the bone surface models used for all other simulations in this thesis.

Accordingly, the knee laxity was simulated and validated exclusively on only seven out of ten models. The numerical prediction of the knee laxity could not be calculated for all directions independent of the investigated soft-tissue condition. Both the valgus laxity and the internal rotation laxity could not be determined numerically due to failed calculations of the inverse dynamics or due to high force dependent kinematic errors.

Validation of the kinematic during joint flexion of the physiologic joint

A comparison of the anterior-posterior translation of the knee during a simulated flexion with literature data showed a basically similar outcome. In particular, a continuous, almost linear translation of the tibia or a rolling back of the femur relative to the tibia could be seen. Whereby based on the joint position at 0° flexion for the translation at 10° flexion a difference in the mean values of 0.8 mm and thus a 78 % lower value results from the simulation compared to the literature data (Figure 7.17). This percentage deviation also represents the largest difference between the data. Only in this flexion position the simulation results were not within the standard deviation of the literature data. The percentage deviations for the further angles were for the flexion angles of 20° 37 %, 30° 22 %,

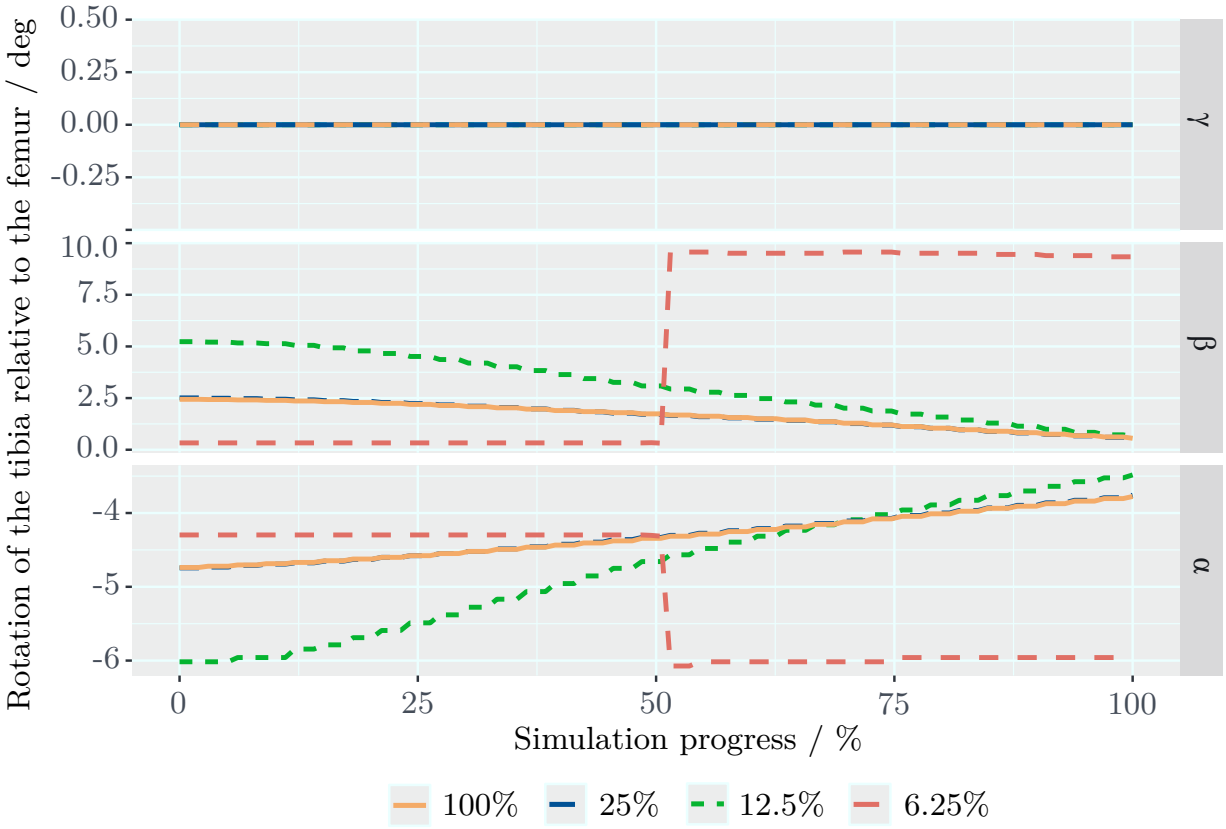

Figure 7.13: Line diagrams of the tibial rotation relative to the femur in dependence of the simulation progress simulating an anterior drawer test. α, β, γ represent the rotations about the x-, y-, z-axis, respectively. 0 % progress corresponds to 0 N and 100 % to 134 N anterior load, respectively. Shown are the data of four multibody models with differing mesh size of the femoral and tibial bone surface. 100 % mesh size represents the bone surface models used for all other simulations in this thesis.

45° 4 %, 60° 13 % and 90° 18 %. In summary, the RMSE for antero-posterior translation was 1.3 mm over all angles (Figure 7.17).

Larger differences were observed for the axial rotation of the tibia relative to the femur. Starting from the position at 0° flexion, there were moderate deviations of 16 % at 10°, 7 % at 20°, 13 % at 30° and 22 % at 45° flexion (Figure 7.18). For the higher flexion angles a further increase of 40 % at 60° flexion and up to 125 % at 90° flexion was observed. A steady increase of the standard deviation with progressing joint flexion could be observed in the literature data. So that only the numerically predicted rotations at 10° and 90° were outside the standard deviation of the literature values. In summary, the RMSE for internal rotation at flexion was 4.2° (Figure 7.18).

Ligament length changes during joint flexion of the physiologic joint

When examining the length changes of the individual ligament structures during the flexion movement, strong differences could be observed between the individual structures. All three bundles of the LCL shortened from a respective length of 55 ± 4 mm in extension to 90° flexion by 5 %, 9 %, and 14 % for the anterior, intermediate, and posterior bundle,

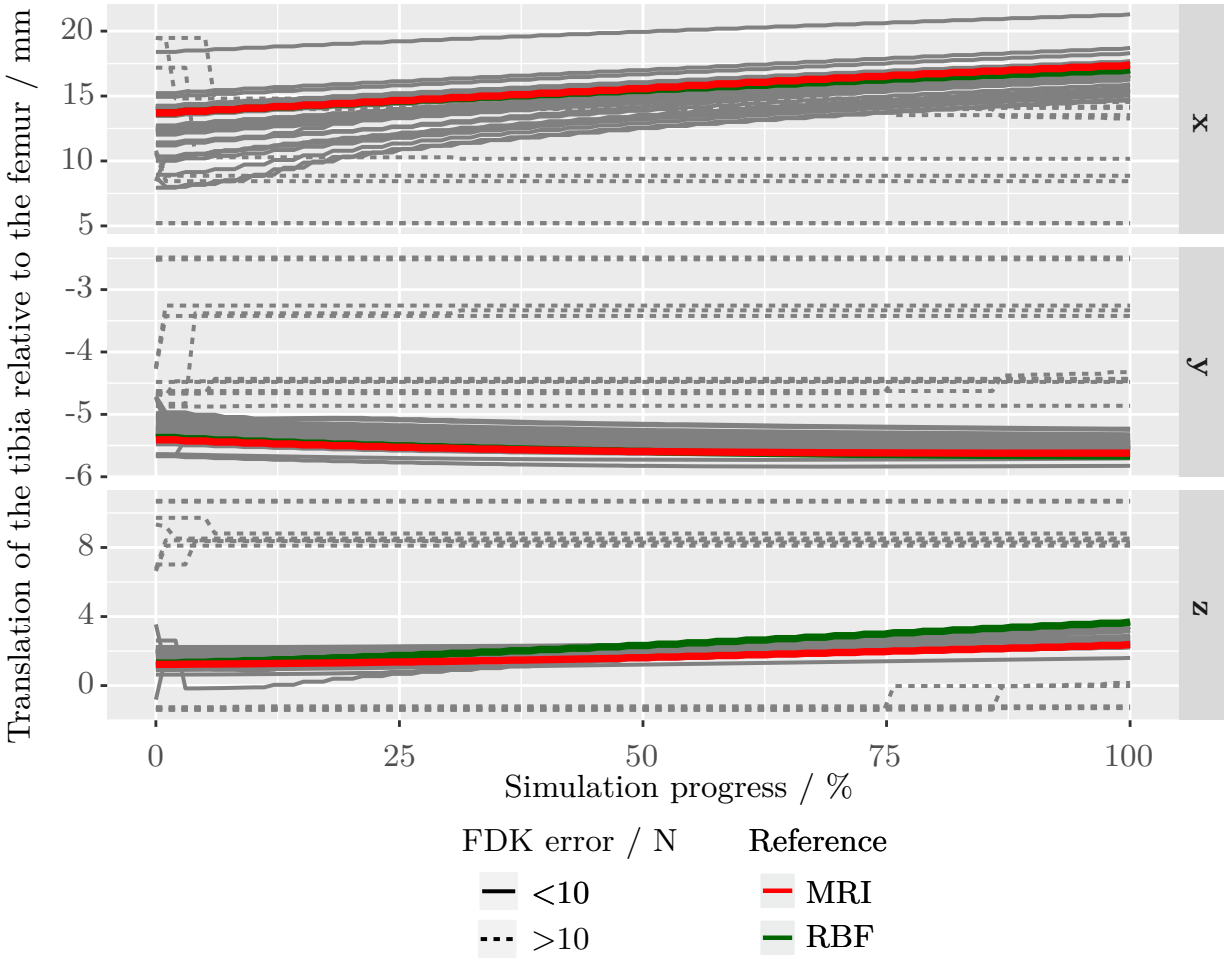

Figure 7.14: Line diagrams of the tibial position relative to the femur in dependence of the simulation progress simulating an anterior drawer test. 0 % progress corresponds to 0 N and 100 % to 134 N anterior load, respectively. Each line represents one simulation with a different initial positions of the femorotibial joint. In addition, the results of simulations with MRI based initial position in which the ligament attachments were determined by MRI and radial basis function (RBF) are displayed.

respectively (Figure C.7). The three bundles of the sMCL, on the other hand, extended in the course of flexion from 0° to 90°, starting from an initial length of 88 ± 8 mm, 86 ± 8 mm, and 85 ± 9 mm in extension by 10 %, 5 %, and 0 % for the anterior, intermediate, and posterior bundle, respectively (Figure C.5). Increases in length in the course of flexion from 0° to 90° could also be determined for all three bundles of the dMCL (Figure C.6). The increase was 28 %, 16 % and 5 %, respectively, with a length in extension of 32 ± 4 mm for the anterior, intermediate and posterior bundle, respectively. The length of the ACL increased from 0° to 90° flexion (Figure C.8). The anteromedial bundle lengthened from 25 ± 3 mm in extension by 4 %, the posterolateral bundle lengthened from 30 ± 3 mm by 10 %. Both the anterolateral as well as the posteromedial bundle of the PCL with a length of 34 ± 3 mm and 30 ± 3 mm in extension, also lengthened by 9 % each with increasing flexion (Figure C.9). The medial and lateral capsule portions shortened from 0° to 90° flexion by 66 %, 61 %; the length of the capsule portions at extension was 56 ± 4 mm and 56 ± 4 mm, respectively (Figure C.10). Loss of length could also be observed for the POL

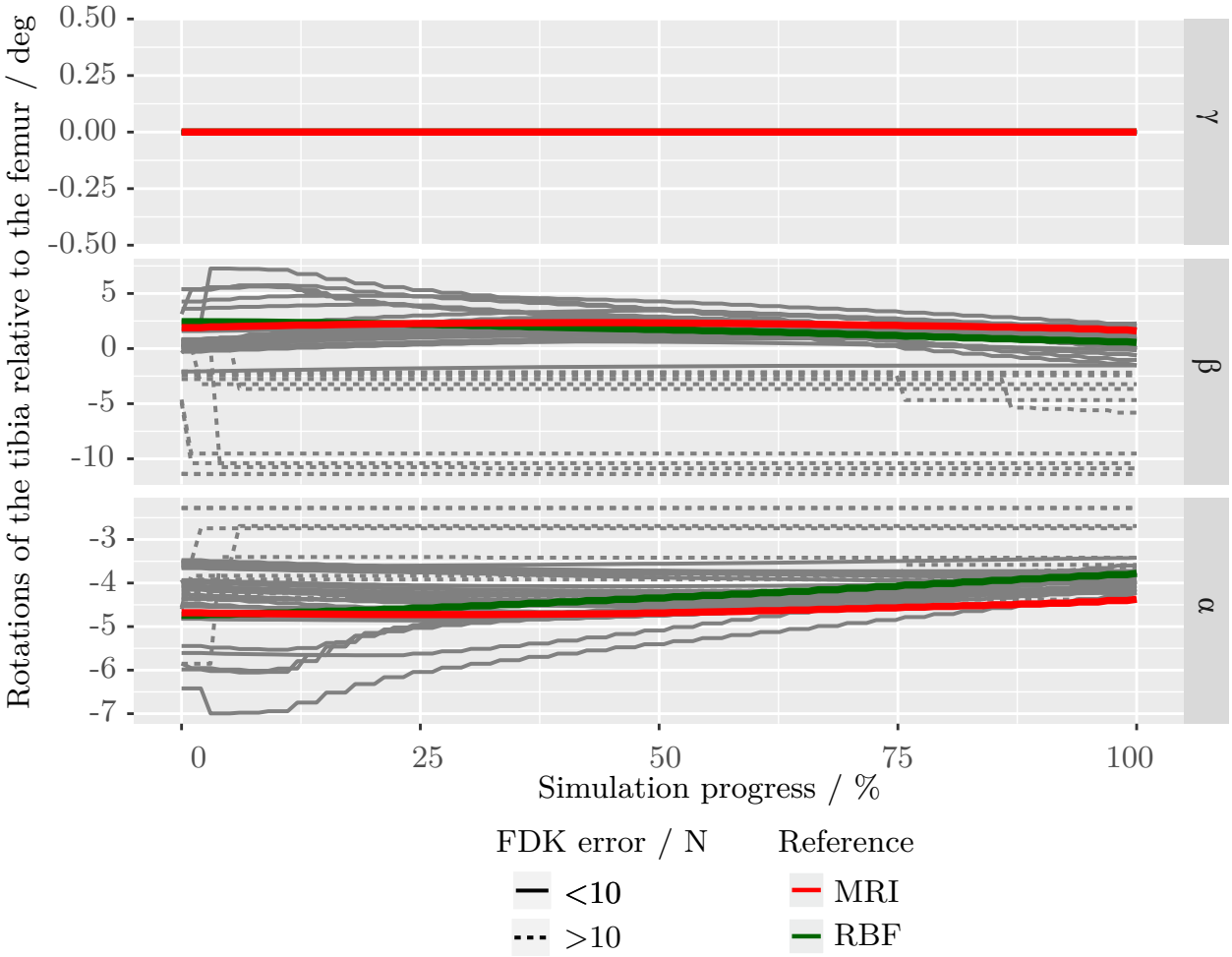

Figure 7.15: Line diagrams of the tibial rotations relative to the femur in dependence of the simulation progress simulating an anterior drawer test. 0 % progress corresponds to 0 N and 100 % to 134 N anterior load, respectively. Each line represents one simulation with a different initial positions of the femorotibial joint. In addition, the results of simulations with MRI based initial position in which the ligament attachments were determined by MRI and radial basis function (RBF) are displayed.

and OPL. The POL decreased from 38 ± 3 mm by 75 % (Figure C.11), the OPL decreased from 69 ± 4 mm by 70% (Figure C.12). The ALL on the other hand shortened from a length of 41 ± 2 mm in aspect ratio with increasing flexion by up to 17 % at 90° flexion (Figure C.13). By considering the forces, the ligament structures could be divided into two groups: The LCL, POL, OPL and the posterior capsule showed a maximum tensile force of 17 ± 1 N, 22 ± 17 N, 39 ± 12 N, and 39 ± 6 N in extension, while the sMCL, dMCL, ACL, PCL, and ALL each showed the greatest traction of 27 ± 11 N, 28 ± 10 N, 73 ± 5 N, 156 ± 43 N, and 81 ± 27 N in 90° flexion. Accordingly, the total tensile force exerted by the ligaments was 124 N in extension and 318 N in 90° flexion. The lowest tensile force could be observed with 18 N at 16° flexion.

Laxity prediction of the physiologic joint

The comparison of the numerically predicted joint laxity with the *in-vitro* results showed

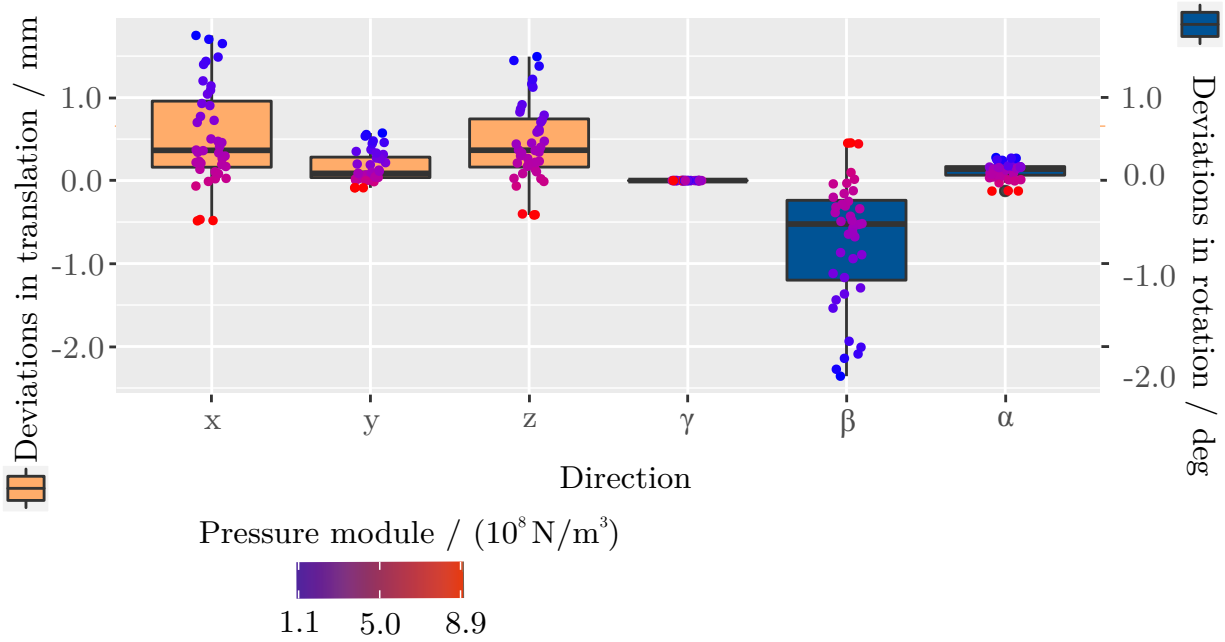

Figure 7.16: Boxplots showing the deviations in translations (x, y, z) and rotations (α, β, γ) in the single directions in dependence of the pressure module for simulations of an anterior drawer test.

differences greater than 25 % in all directions and flexion angles. In the following the numerical and percentage differences as well as the RMSEs between the *in-vitro* and *in-silico* laxity values are presented. The comparison of the results for the anterior joint laxity between *in-silico* and *in-vitro* examinations showed RMSEs in a range of 1.7 ± 1.1 mm (25 ± 13 %) at 30° flexion and 3.3 ± 2.2 mm (30 ± 23 %) for 60° flexion. The lowest percentage deviation for anterior laxity was observed at 30° flexion. For posterior laxity, similar RMSEs of 1.8 ± 2.4 mm for 0° and 6.9 mm (82 %) for 90° flexion were found. Whereby the posterior laxity at 90° flexion could only be successfully calculated in one of the models. The lowest percentage deviation was found with 26 ± 47 % for 0° flexion. The inferior joint laxity was numerically predicted lower than in the *in-vitro* studies. The RMSEs ranged from 0.4 ± 0.2 mm (49 ± 29%) for 0° flexion to 2.1 ± 1.4 mm (49 ± 29 %). The smallest percentage deviations of 49 ± 27 were found for 30° flexion. For coupled varus-valgus rotation in inferior joint laxity RMSEs were found in a range of 1.8 ± 2.4° for 0° flexion and 6.0 ± 1.6° for 90° flexion. For the varus joint laxity, RMSEs of 1.0 ± 0.9° (48 ± 31 %) for 0° of flexion and up to 6.9 ± 3.4° (84 ± 57 %) for 90° of flexion, corresponding to the highest percentage deviation, could be found. The lowest percentage deviation could be observed with 35 ± 28 % (RMSE 1.7 ± 1.1°) at 30° flexion. The results of the internal joint laxity differed when comparing the numerically and experimentally determined data with RMSEs from 6.5 ± 3.8° (56 ± 28 %) at 0° flexion to 12.7 ± 7.6° (74 ± 30 %) at 90° flexion which also corresponds to the highest percentage deviation. The lowest percentage deviation could be found with 46 ± 39 % (RMSE 9.2 ± 5.3°) at 30° flexion.

Laxity prediction of the joint after meniscus removal

The removal of the menisci in the numerical model resulted in only minor changes in laxity in almost all directions compared to the results in physiologic condition. Thus, the

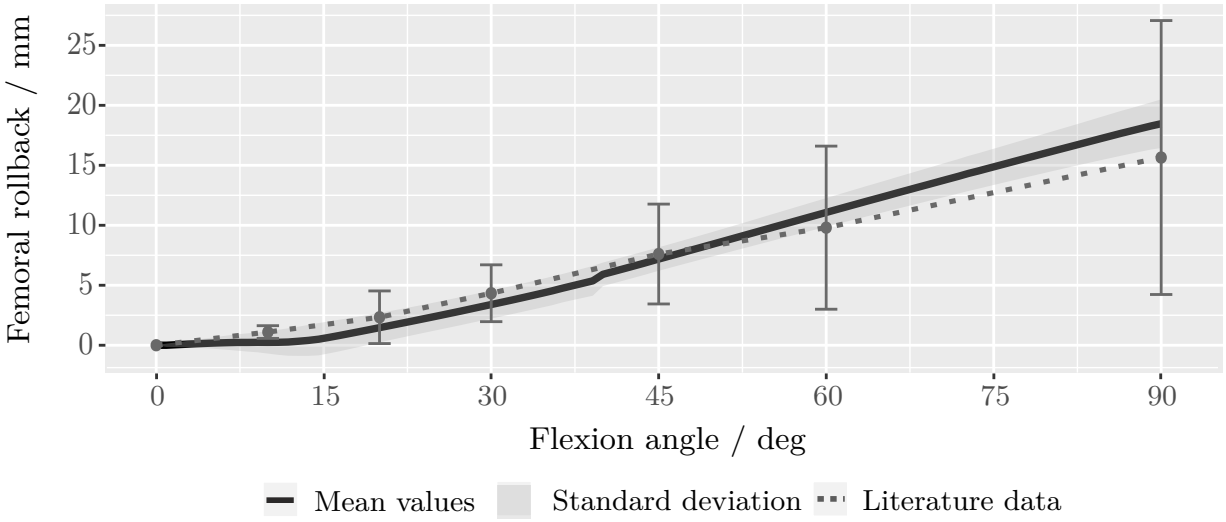

Figure 7.17: Anterior translation of the tibia relative to the femur during flexion motion from 0° to 90°. The solid line shows the mean values of the model predictions, standard deviation is given by the grey band. The doted line, with data points and whiskers shows the data from the literature [165, 145, 54, 32, 134].

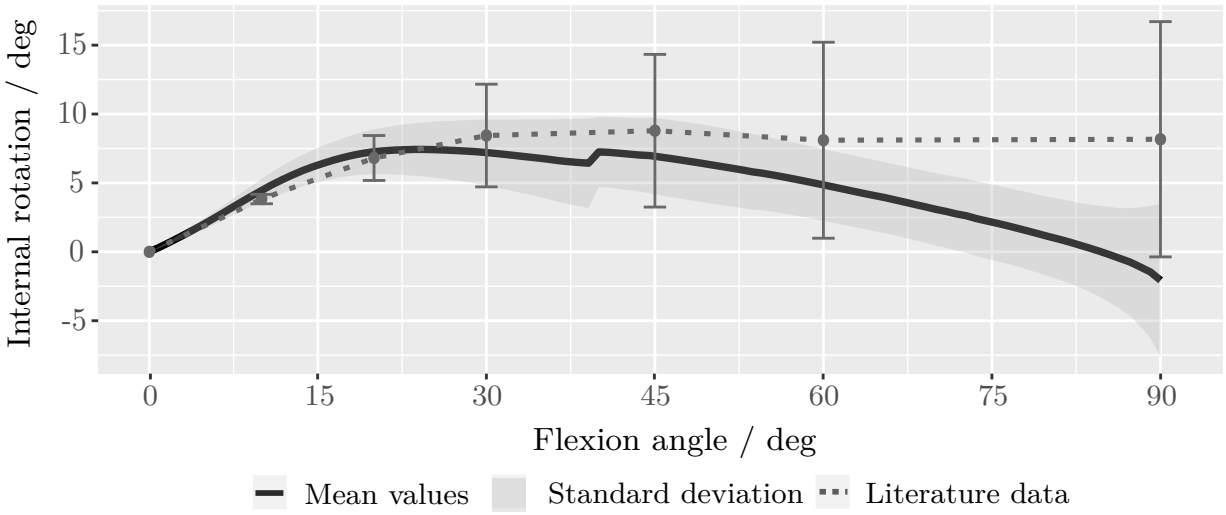

Figure 7.18: Internal rotation of the tibia relative to the femur during flexion motion from 0° to 90°. The solid line shows the mean values of the model predicitions, standard deviation is given by the grey band. The doted line, with data points and whiskers shows the data from the literature [165, 145, 54, 32].

largest difference of the anterior laxity was 0.3 ± 0.5 mm at 60° flexion and the posterior laxity 1.85 mm at 90° and 0.6 ± 0.6 mm at 15° flexion. For the inferior joint laxity the largest differences for the inferior translation were 0.2 ± 0.4 mm at 30° flexion and for the coupled varus-valgus rotation 0.1 ± 0.3° at 60° flexion. For the varus laxity the largest difference was 1.1 ± 2.0° at 30° flexion. Only for the internal rotation laxity larger differences could be observed: the differences were 2.5 ± 5.5°, 8.7 ± 10.9°, 14.2 ± 11.6°, 6.3 ± 7.4°, 3.6 ± 4.6° in 0°, 15°, 30, 60° and 90° flexion, respectively.

Laxity prediction of the joint after ACL transection

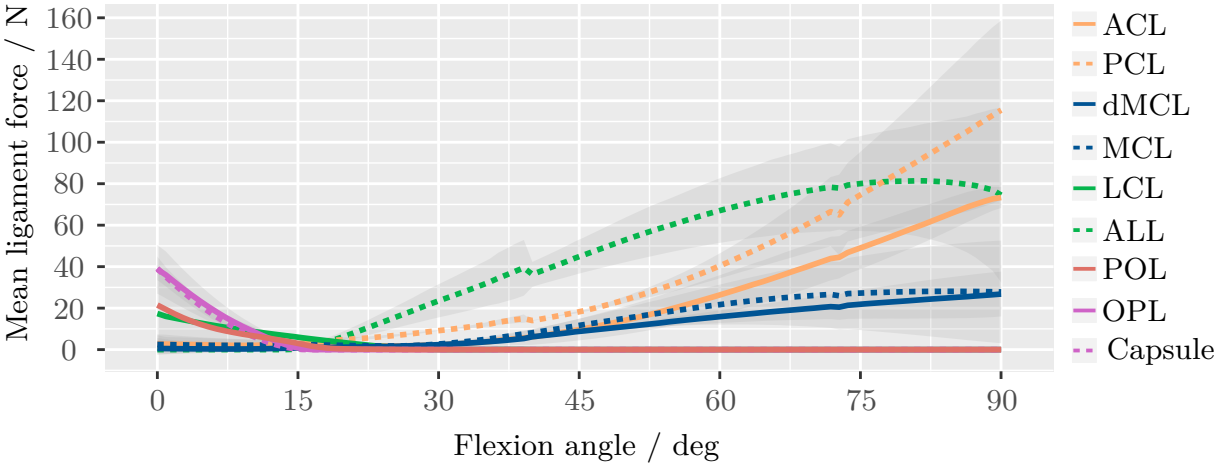

Figure 7.19: Mean Forces of single ligaments during flexion from 0° to 90°. Data of the sMCL, dMCL, LCL, ACL, PCL, POL, OPL, ALL and capsule are given. Grey bands present standard deviations.

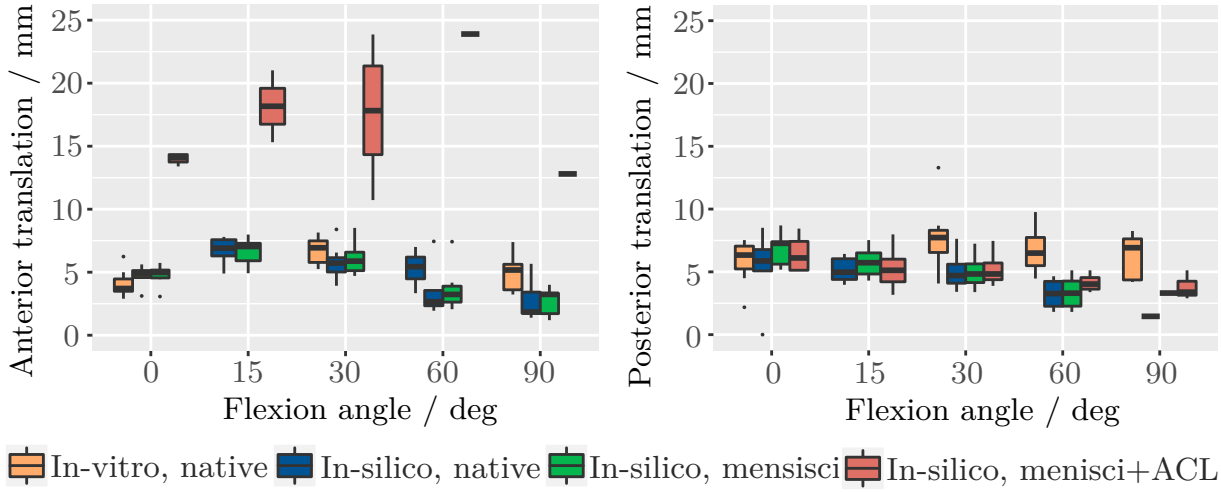

Figure 7.20: Box Plots showing the anterior (left) and posterior (right) laxities of the knee joint from 0° to 90° of flexion. Presented are the numerically determined laxities with the knee in physiologic condition and after removal of the menisci. Furthermore, the experimentally determined physiologic knee laxities of all subjects which were also numerically modelled, are presented.

After the respective removal of the anterior cruciate ligament from the subject-specific models, only five models could be successfully solved. The model reacted to an anteriorly directed load with an increased translation of 10.0 ± 2.3 mm at 0° flexion to 21.95 mm at 90° flexion, compared to the measurements in the native state. The anterior joint laxity for the flexion angles 60° and 90° could only be evaluated with one model. The posterior joint laxity increased only slightly after ACL removal in a range of 0.1 ± 0.2 mm at 30° flexion to 1.9 ± 2.2 mm at 90° flexion. The inferior translation due to an inferior force also increased only slightly in the model by 0.05 ± 0.29 mm at 15° flexion to 0.3 ± 0.3 mm at 90° flexion. The coupled varus-valgus rotation during inferior loading also changed to a range of $0.1 \pm 0.5°$ at 0° flexion to $0.8 \pm 0.7°$ at 30° flexion. The removal of the ACL with regard to the varus laxity showed a greater effect. Here an increase in the range of $0.7 \pm 1.3°$ with 0° flexion to $3.7 \pm 5.4°$ with 90° flexion could be observed. An even greater effect could

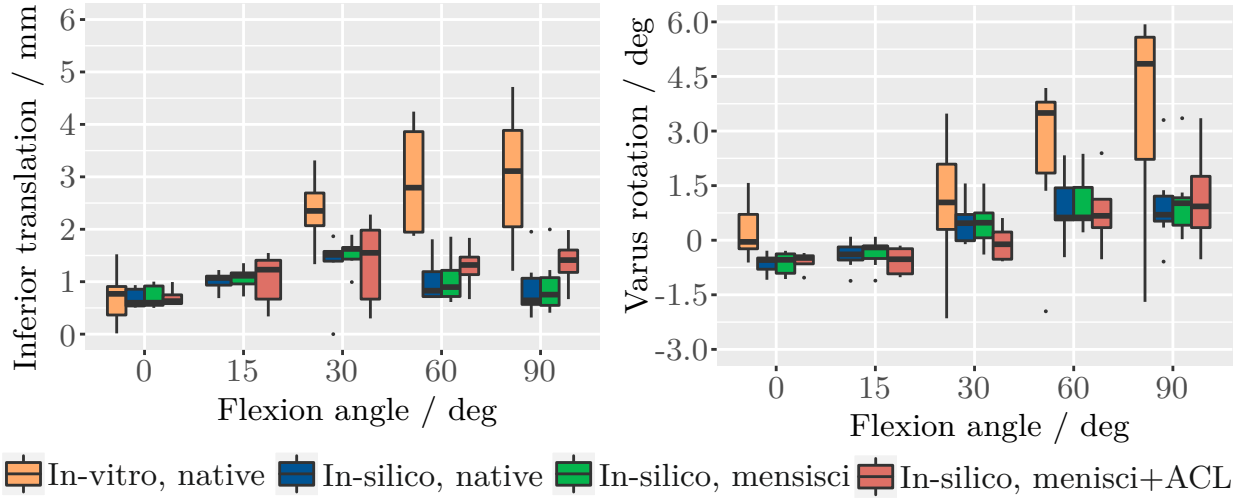

Figure 7.21: Box Plots showing the inferior translations (left) and coupled varus-valgus rotations (right) for the inferior joint laxities of the knee joints from 0° to 90° of flexion. Presented are the numerically determined laxities with the knee in physiologic condition and after removal of the menisci. Furthermore, the experimentally determined physiologic knee laxities of all subjects which were also numerically modelled, are presented.

be observed for the internal rotation joint laxity. The gain in joint laxity ranged from $2.8 \pm 5.0°$ at 90° to $12.6.8 \pm 11.9°$ at 30° flexion.

7.3 Discussion

A subject-specific model simulating the laxity of the knee joint could help to better understand the function of individual ligament structures of the knee joint. In addition, this could be used in the future to pre-operatively plan a required soft-tissue balancing procedure of the knee during total knee arthroplasty. The aim of this study was, therefore, to develop a simulation model of the knee in which subject-specific properties can be taken into account and with which the laxity of the knee joint can be calculated as a function of the soft-tissue situation. Furthermore, the aim of this work was to analyze the simulation model with regard to the sensitivity of the model to the changes of individual model parameters and to examine it with regard to a later clinical applicability.

Ten subject-specific multibody simulation models were created based on MRI data from ten of the knee specimens examined *in-vitro*. Due to model instability during ligament calibration only seven models could finally be used for further analysis. The numerical prediction of joint laxity was an essential goal of the modeling in this thesis. A calculation of the laxity was not possible for all directions due to the model instability. This problem could not be solved even after adaptation of numerous parameters. An exact cause for the direction-dependent model instability could not be identified in the context of the present work and is a goal of future investigations.

Due to the low contrast range of the images, the segmentation of the bone geometries from the MRI data could only be performed with manual and thus very time- and resource-

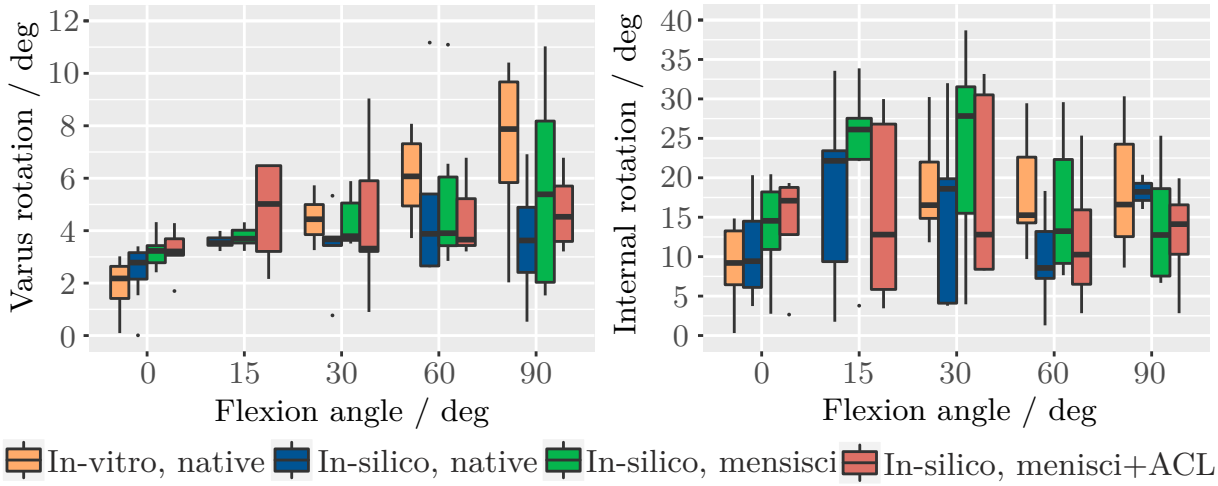

Figure 7.22: Box Plots showing the varus (left) and internal rotation (right) laxities of the knee joint from 0° to 90° of flexion. Presented are the numerically determined laxities with the knee in physiologic condition and after removal of the menisci. Furthermore, the *in-vitro* determined physiologic knee laxities of all subjects which were also numerically modelled, are presented.

consuming techniques. This is critical with regard to clinical application. Manual segmentation techniques are not suitable for such an application and would have to be performed by semi-automatic or automatic segmentation techniques [144]. Furthermore, the attachment sites of the largest ligament structures only could be determined from the MRI data. Due to the low contrast range in the MRI data between the sought structures and the surrounding tissue, it was not possible to localize the attachment sites of capsule structures or smaller ligament structures such as the ALL or the POL. The data and their segmentations were also subject to a certain inaccuracy due to the resolution, contrast range, and spacing of the MRI sectional images. Although this inaccuracy was not evaluated in the context of this work, other studies were able to show that the segmentation of long bones can be realized with a mean accuracy of 0.56 mm [228] and the cartilage surfaces of the knee with 0.22 mm [44]. According to a study by Rachmat *et al.*, however, the segmentation of ligament attachment sites is critical. On a knee specimen, they investigated the accuracy as well as the inter- and intra-observer reliability of the attachment site determination from MRI data. They found dependent on the individual structure inter-observer accuracies ranging from 5.0 mm to 23.4 mm and intra-observer accuracies from 4.1 mm to 31.8 mm relative to physical measurements [196]. When evaluating these investigations, however, it should be noted that an exact localization and definition of the attachment sites with physical measurements on the specimen is just as difficult due to the usually large irregular attachment areas. This was also shown in the course of own dissections on the specimens.

The transfer of the individual bone geometries and ligament attachments to the simulation model again required considerable manual adaptations of the model for each individual subject. With the integration of a morphing algorithm, a method could be integrated with which the ligament attachment sites of a generic model could be transferred to subject-specific bone models. This morphing algorithm based on radial basis functions worked reliably for the investigated ligaments. An influence of the type of radial basis function

and the number of reference points used for the morphing could not be found. The mean deviation of the prediction of 1.1 mm at a precision of 2.8 mm was in the range of an algorithm for estimation of the ligament attachment sites at CT data presented by Ascani *et al.* where the estimates were also compared to direct measurements on MRI data [15]. In another study, Pellikaan *et al.* also investigated a morphing algorithm to estimate muscle insertions. In comparison with *ex-vivo* insertions an accuracy of 15 mm [185] was found. Considering the investigations by Rachmat *et al.* which could show a low accuracy for the MRI based detection of the ligament attachment sites [196], it can be assumed that the estimation of the ligament attachment sites with an RBF function with less effort yields results in the range of manual segmentation.

No previous study further analyzed the effects of such inaccuracies. Within the scope of this work, a variation of the ligament attachments by a maximum of 5 mm per direction and attachment site showed a considerable influence on the simulation results when applying to the developed model. With regard to the calculation of the knee laxity as a result of an anteriorly directed load on the tibia, it was shown that the position of certain ligament attachments had a particularly large influence on the results. These investigations, therefore, suggest that subject-specific models of the knee joint are subject to a relevant modeling error due to the complexity of the ligament attachment sites. This poses considerable challenges with regard to the future clinical application of a subject-specific model. Only data from medical imaging would be available for such a model. In addition, it is not possible to determine the attachment site for some of the stabilizing structures using MRI data, so that these have to be estimated based on anatomical studies, which represents a further inaccuracy of the model. Accordingly, for a clinical application of a numerical model for the simulation of the joint laxity, a method would first have to be developed which allows a non-invasive recording of the ligament attachment sites with sufficient accuracy.

The extension of the multibody simulation model by a so-called Force Dependent Kinematic approach together with a contact model between femur and tibia, as well as between femur and the two menisci made it possible to model a femorotibial joint with five DOFs, in order to be able to predict joint laxity. The contact forces were calculated for the contact triangles of the meshes of femur and tibia. The sensitivity analysis of the mesh refinement showed that the mesh of the models can be reduced by 1/4 without influencing the calculations of the joint laxity. This may save computing time. The pressure module, which establishes the relationship between the penetration volume of the bodies in contact and the contact force, showed a considerable influence on the result of the joint laxity calculations with an inverse proportional magnification of the laxity with reduction of the pressure module. This behavior is plausible and can be explained by the fact that the force in individual ligaments is reduced due to a stronger penetration of the bone models as a result of a lower pressure module, which increases the laxity of the joint. With regard to subject-specific modeling, however, there is a fundamental problem that there is no physical equivalent for this pressure module. This makes a realistic and subject-individual mapping of the joint contact considerably more difficult. In addition, the sensitivity analysis of the pressure module showed that many values of this model parameter do not allow a successful calculation of joint laxity as the calculations are aborted by the system. This fact further limits the applicability of the contact model.

The initial position of the femorotibial joint was another parameter with a considerable

influence on the simulation results. A change of the initial joint position by 5 mm or 1.5° showed a considerable influence on the flexibility of the joint. In the present study, this influence was addressed by deriving the initial joint position from the MRI data. This or a similar approach is recommended to avoid inaccuracies in modeling in this context.

In addition to the sensitivity analysis, another major objective of this study was to evaluate the basic function of the simulation model and to test the suitability of the model for the numerical prediction of the subject-specific joint laxity. In order to realize a realistic function of the ligaments, a calibration of the ligaments based on the literature data was performed before the simulation of joint laxity. However, only limited information was available for the ligament calibration. Above all, the definition of the slack length of the individual ligaments posed a great challenge. Currently there are only very few publications in which the force within individual ligament structures was directly investigated [155, 157, 195]. However, also for these investigations of the cruciate ligaments, the ligament structures were first loosened in order to attach them to a load cell. Statements about the natural soft-tissue tension are, therefore, not feasible even with these investigations. For all modeled structures it was, therefore, only possible to fall back on studies in which the change in length of the ligaments during joint flexion was examined by means of medical imaging. Though, the length changes of the ligament structures give only vague indications of the actual slack lengths of the individual ligaments. This kind of studies were not available for all modeled ligament structures, so that for the capsule structures, the POL and OPL the flexion angle where the structures become slack had to be estimated. This limited access to functional properties of individual soft-tissue structures is an important aspect that prevents the modeling of further soft-tissue structures.

Nevertheless, following ligament calibration, plausible results were obtained with regard to joint kinematics for simulated joint flexion. The data from the simulations show a femoral rollback *i.e.* femorotibial translation equal to that of a healthy knee joint, with an almost linear increase in posterior translation of the tibia with increasing flexion angle. Regarding the axial rotation of the tibia, a very good agreement with the literature data was found in the range of 0-45°, with an internal rotation of the tibia of about 6° within the first 15° of flexion. For higher flexion angles, larger deviations could be found in direct comparison to the literature. It should be noted here that the literature data for large flexion angles of 60° and more vary widely. This can probably also be explained by the fact that the internal-external rotation laxity of the joint is greatest at flexion angles of 60° and more and, therefore, the kinematics of the joint is strongly influenced by boundary conditions. One reason for the deviation of the numerically predicted kinematic of the knee could be the missing femoropatellar joint which stabilizes the femorotibial joint by sliding the patella in femoral groove with increasing flexion.

When comparing the predicted changes in lengths of the ligaments during flexion motion with experimentally determined changes in length from the literature, similar patterns could be found for some ligaments. The increase in length of both bundles of the PCL from extension to flexion is in agreement with investigations by Belvedere *et al.* on ten human knee specimens. In the study an increase in length of 27 % and 15 % could be observed for the alPCL and pmPCL during flexion from 0° to 120° [22]. The shortening of the LCL observed in the simulations from 0° extension to 90° flexion is also in line with the investigations of Belvedere *et al.* In their study the LCL shortened from extension to 90° flexion by 15 %, while in the simulation a shortening of 9 % could be observed

[22]. The predicted length change of the ALL also shows a tendency to coincide with the investigations of Zens *et al.* on six cadaveric specimens [259]. They found an increase in the length from joint extension to 90° flexion in a range of 8 % to 22 %. In comparison to this, the results of the simulations showed an average increase of 17 %.

However, for the proportions of the MCL and the ACL there were larger differences compared to the literature data. In the Belvedere study, the measurement of the length changes of the two bundles of the ACL and the MCL showed a decrease in length from 0° to 90° flexion [22]. The numerical calculations, on the other hand, showed an increase in the length of the ligaments. Other studies by Hosseini *et al.* and Park *et al.*, who also examined the change in length of MCL in joint flexion, observed an increase or decrease in length from 0° to 90° flexion depending on the bundle [96, 180]. The deviations between the simulation and the literature data can possibly be explained by the abnormalities of joint kinematics at high flexion angles. Another explanation is provided by a sensitivity study on the length change patterns in insertion site selection [105]. The research group demonstrated using the ACL that an increase or decrease in ligament length from 0° to 90° flexion depends on the choice of the attachment site. A shift of the femoral attachment site by 6 mm to the anterior significantly changed the behavior of the length change pattern [105]. Since, according to current knowledge, a recording of the ligament attachment sites with a significantly better accuracy than 6 mm cannot be guaranteed, the investigations on the length changes of the ligaments, which are mostly based on MRI data, must be interpreted with caution.

When looking at the ligament forces, the OPL and the capsule showed themselves to be the most tense structures in extension. This is in accordance with biomechanical studies on human joint specimens investigating the function of posterior structures. Therein it could be shown that particularly the OPL and the posterior capsule prevent the joint from hyperextension [169, 27]. On the other hand, according to the simulation results, the posterior cruciate ligament is the most tense ligament in flexion. This is plausible as the *in-vitro* studies in the context of this dissertation showed the function of the PCL as primary restraint to posterior tibial translation especially at high flexion angles (section 6.2). The increase in tension of the ACL with increasing flexion angle is in contrast to two studies. On knee specimens in which a tensiometer was attached to the ligament attachment, the ligament forces were investigated without further joint loading. The investigations showed a tension of the ligament only in extension and for low flexion angles [155, 195]. However, a recent study by Markolf *et al.* using the same method but the knee joint additionally subjected to an axial load (500 N) during flexion, showed an increase in force in the anterior cruciate ligament with increasing flexion [157]. Accordingly, the tension of the ACL as well as the anterior translation of the tibia during flexion seems to be dependent on an axial load. Since passive flexion was also performed with a slight axial load (20 N) in the numerical calculations, this could to some extent explain the differences to the other two studies. In summary, a plausible model behavior could be demonstrated from this first indirect validation of the developed models, which allowed further investigations.

The laxity investigations on the model showed similar results compared to the *in-vitro* investigations in the area of scale. The RMSEs ranged from 0.4 mm to 6.9 mm for the translations and 1.0° to 6.9° for the rotations. Particularly noticeable were the considerably lower calculated laxity values for high flexion angles of 60° and 90° compared to the *in-vitro* results. These abnormalities were also found in other numerical studies [89, 251]. The

reason for this could be the considerable reduction of the ligaments to one to three bundles, which were calibrated in the same form. Together with a very simple attachment site definition, the ligament bundles in the form of non-linear springs may not adequately reflect the complex biomechanics of the ligaments. A more complex calibration of individual bundles within a ligament in order to reflect different functions of individual bundles over the range of motion could help in this respect. Another aspect that might explain the deviation of the predictions from the experimental values is the modeling of the ligaments based on literature data. The destructive *in-vitro* method made it impossible to determine representative mechanical ligament properties after extensive *in-vitro* investigations on the robot. The individual adaptation of the ligament properties would most likely have improved the accuracy of the model.

The results of the laxity examinations after removal of the menisci could only partially reflect the results observed in the *in-vitro* study. An influence on the anterior translation could not be determined, but there was an increase of the internal rotation after removal of the menisci, which could also be observed in the *in-vitro* experiments. The meniscus model in its current form is kept reduced in order to not further increase the instability of the numerical model. The mechanical function of the meniscus was realized exclusively by a contact modeling between femur and meniscus. The movement between tibia and meniscus was not considered. In addition, the selected pressure module for the meniscus is based only on a simple estimate, since there is no physical equivalent for this case either. As the joint model was essentially developed for the knee arthroplasty, in which the menisci are removed anyway except for the unicompartimental replacement, this simplification is acceptable. For investigations in which the menisci play a greater role, the model should be extended accordingly by a tibial contact model and the ligament structures of the menisci. In order to better consider the deformation of the menisci in the multibody simulation model, a modelling according to Guess *et al.* could also be useful, in which the meniscus geometry is divided into numerous small rigid bodies which are then held together by springs [79].

The removal of the anterior cruciate ligament in the simulation model essentially reflected the findings from the *in-vitro* investigations. A direct comparison of the results from the models with the experimentally determined data showed that the numerical simulation slightly overestimated the influence of the anterior cruciate ligament on anterior laxity. With an optimization of the ligament calibration by individually calibrating single bundles of a ligament and the addition of subject-specific ligament properties to the model, the model seems well suited for the fundamental investigation of knee laxity depending on the condition of the soft-tissue envelope. However, the removal of a ligament further increased the instability of the model, whereby only a maximum of five models could be successfully solved, depending on the loading direction and flexion angle.

The biggest issue with the developed model was the great instability of the model. The stability was influenced by numerical values of single simulation parameters like the pressure module, prevented a calibration of the ligament structures in three models, limited the laxity investigations in single loading directions and complicated the laxity investigations after removing the ACL. According to information from the manufacturer of the simulation platform, this problem is generally known. To solve the instability the Anybody Modelling software offers the possibility to increase the acceptable error in the calculation of the contact forces in order to solve the force dependent kinematics, but the calculations

of the joint laxity are significantly influenced by this. On the other hand, it is possible to supplement the DOFs of the model with a so-called gearing in order to harmonize the DOFs in their behavior. However, this measure also influences joint laxity. In order to control the instability observed, a detailed investigation of the mentioned options must be carried out to achieve a parameterization of the model that allows a robust calculation but does not significantly influence the joint laxity. Furthermore, the addition of further soft-tissue structures to the model could be helpful to increase the stability of the model, especially after removal of individual ligament structures. Since the mechanical properties of many smaller soft-tissue structures are still unknown, further *in-vitro* investigations on material samples will have to be carried out in future work.

The numerical model developed within the framework of this work is based on several simplifications of the real knee joint, so that some further limitations of the model itself and the studies carried out with it should not remain unmentioned. According to the findings from the sensitivity studies performed in this dissertation, it must be assumed that the way of modeling the ligaments has a considerable influence on the model accuracy. This aspect should be critically questioned in future studies and further investigated with regard to the goal of applying such a simulation model clinically. In this context, it is important to note that the ligament calibration for these studies has been greatly simplified. A calibration of the ligaments as performed for the model validation requires a computation time of about 24 hours. Parameter studies with 100 or 200 individual tests for each of which a new ligament calibration was necessary, these investigations would not have been possible within a reasonable period of time. Since the mechanical properties of many smaller structures are unknown in addition to the missing information on the ligament attachment sites, it was not possible to model all soft-tissue structures such as large parts of the joint capsule. Since these structures have a much smaller cross-section, it can be assumed that these structures are of secondary importance from a mechanical point of view and the influence of the missing soft-tissue structures is, therefore, negligible for the investigations carried out. The femoropatellar joint was not modelled in this thesis to limit the model complexity and not to enhance the instability of the FDK algorithm provided by Anybody. Since the patella is relevant for the function of the quadriceps muscle and the developed model deals exclusively with the passive structures, a negligible influence of the femoropatellar joint was assumed. Nevertheless, an influence of the missing patella on the kinematics of the numerical model cannot be excluded.

In summary, in this work subject-specific multibody simulation models could be developed, with which the laxity of the knee joint, especially in the area of low flexion angles, can be well reproduced. The presented procedure for the approximation of the ligament attachment sites represents a time-saving alternative to the segmentation of the attachment sites in MRI data. The instabilities of the models in the numerical solution have to be regarded as critical. In future work further investigations must show to what extent these instabilities can be reduced.

8 Conclusion and perspective

Even after decades of implant and tool development and the continuous improvement of surgical procedures, knee endoprosthetics fell short of expectations. The strong soft-tissue guidance and stabilization of the knee makes it difficult to restore complete joint function with natural kinematics. These challenges in endoprosthetics can only be met with a particularly strong focus on soft-tissue structures. To this day, the assessment and adaptation of the soft-tissue envelope in endoprosthetics is a subjective process that is strongly dependent on the surgeon. This dissertation addresses these resulting challenges, provides quantitative guidelines for soft-tissue balancing based on analyses of the natural knee joint and describes the adjustment ability of the knee laxity by adaptation of individual soft-tissue structures. Furthermore, investigations within the scope of the dissertation form the basis for a numerical tool to better understand the function of the ligaments and to better plan the soft-tissue balancing pre-operatively in the future.
The asymmetry of the soft-tissue structures quantified in the dissertation and the strong dependence of joint laxity on the flexion angle illustrate the complex construction and biomechanical function of the knee joint. This is not considered in the mechanical alignment and the associated balancing techniques which aim to achieve a symmetrical and equal joint gap in flexion and extension. From the data obtained, it can be concluded that a technique such as gap balancing greatly alters the laxity of the joint, possibly leading to unnatural joint function, especially in mid-flexion, and contributing to the lack of function of the joint replacement. The data also underlines that the evaluation of the joint laxity only at 0° and 90° of flexion is not sufficient to assess the function of the prosthesis. An additional quantitative evaluation at 30° and 60° flexion could significantly contribute to avoid postoperative instability of the joint. For surgeons who favor surgical techniques aimed at restoring natural joint laxity as well as possible, the data collected in the context of the dissertation provide quantitative target parameters for soft-tissue management for the first time.

The developed guidelines, together with the computer- and robot-supported instruments available today, with which the joint laxity can be quantified intra-operatively, provide the basic requirements for the reconstruction of natural joint laxity in knee arthroplasty procedures. The findings from the *in-vitro* investigations in the context of this dissertation show on the one hand that an intra-operative measurement of joint laxity is not biased by the surgical approach and on the other hand provide important information on which structures can be addressed in order to compensate for deviations from the desired joint laxity within the scope of soft-tissue management. The findings also show that, for example, the removal of the anterior cruciate ligament alters the stability of the joint in such a way that restoration of natural joint laxity is a goal that can no longer be achieved. By using prosthesis designs that allow the preservation of the anterior cruciate ligament together with a kinematic alignment approach, the goal of a knee arthroplasty with natural joint restraints could be achieved closest.

In the context of this dissertation, also a numerical knee model was developed to predict

the laxity of the knee joint using multibody dynamics. The radial basis functions based morphing method for the estimation of the ligament attachment sites, which was integrated into the model, is a robust method. It allows a good estimation of the ligament attachment sites with considerably less effort compared to a manual segmentation of the attachment sites from MRI data. The applied contact model allows a convincing simulation of the movement within the joint, but also leads to an inherently unstable model, so that in some situations no result can be calculated. The pressure module as essential parameter for the control of the joint contact has to be considered critical with regard to a later clinical application of the model since no physical equivalent exists for this parameter. The modeling of the ligaments and their calibration allow a good prediction of joint laxity for low flexion angles. In order to achieve a realistic behavior of the joint over the entire flexion range of the knee joint, a more complex modeling of the ligaments and an adapted calibration of individual bundles within a modelled ligament may be necessary. The achievements of this dissertation provide basic guidelines and recommendations to restore the soft-tissue restraints of the natural knee joint even with implantation of a knee prosthesis.

In the following the perspectives in research based on the findings of this dissertation are presented. The main focus is on the interaction between individual soft-tissue structures of the knee joint with regard to soft-tissue balancing and to advance the numerical knee model as a link between experimental research and clinical application of the knee joint arthroplasty. The numerical model built up in this dissertation is primarily the fundament for further developments. The focus of the following work must be first and foremost on improving the robustness of the model. The stabilization approaches mentioned in section 7.3 must be investigated in parameter studies to keep the influence on joint laxity as small as possible. With the implementation of a more complex ligament calibration, a more realistic representation of the ligament function over the entire range of motion of the knee can be realized. A further model validation should then provide information on this, whereby subject-specific models should be analysed after transferring also the mechanical properties of the ligaments from the specimens to the model. In the course of tissue characterization, as many individual structures as possible should be characterized in order to supplement the simulation model with additional soft-tissue structures. In further biomechanical investigations of joint specimens, the influence of individual bundles of the largest ligament structures on joint laxity should be further investigated. The data obtained could then provide further information on the function of individual ligament components at different flexion angles [1]. This would be an important contribution to model the ligament function more realistically in the numerical model, but above all these findings could contribute to a more targeted adaptation of the soft-tissue structures during joint arthroplasty procedures.

[1] The data obtained and the model created in this dissertation are completely documented and available to further researchers at the Laboratory for Biomechanics and Biomaterials at the Hannover Medical School.

Bibliography

[1] *Total Knee Replacement*. Springer London, London, 1991. OCLC: 863929913.

[2] https://emea.depuysynthes.com/binary/org/dpy_syn_emea/hcp/jointrecon-knee/products/pfcsigmatc3knee-system/pfcsigmatc3kneesystem1.png, accessed February 3, 2019.

[3] https://www.odtmag.com/contents/view_breaking-news/2018-03-09/smith-nephew-releases-journey-ii-xr-total-knee-arthroplasty, accessed February 3, 2019.

[4] https://www.strykermeded.com/media/1035/triathlonprimary.jpg, accessed February 3, 2019.

[5] M. P. Abdel, L. Pulido, E. P. Severson, and A. D. Hanssen. Stepwise surgical correction of instability in flexion after total knee replacement. *The Bone & Joint Journal*, 96-B(12):1644–1648, December 2014.

[6] J. H. Ahn, T. S. Bae, K. Kang, S. Y. Kang, and S. H. Lee. Longitudinal Tear of the Medial Meniscus Posterior Horn in the Anterior Cruciate Ligament–Deficient Knee Significantly Influences Anterior Stability. *The American Journal of Sports Medicine*, 39(10):2187–2193, October 2011.

[7] F. H. Albee. Original features in arthroplasty of the knee with improved prognosis. *Surgery*, (47):312–328, 1928.

[8] I. Alfred. Evaluierung einer nichtlinearen Morphing Methode für patienten-spezifische muskuloskelettale Modelle. Leibniz Universität Hannover. Master-thesis, March 2016.

[9] O. K. Alnachoukati, R. H. Emerson, E. Diaz, E. Ruchaud, and K. A. Ennin. Modern Day Bicruciate-Retaining Total Knee Arthroplasty: A Short-Term Review of 146 Knees. *The Journal of Arthroplasty*, 33(8):2485–2490, August 2018.

[10] T. O. Alonge and O. O. Oni. An investigation of the frequency of co-existence of osteophytes and circumscribed full thickness articular surface defects in the knee joint. *African Journal of Medicine and Medical Sciences*, 29(2):151–153, June 2000.

[11] S. Amiri and D. R. Wilson. A computational modeling approach for investigating soft tissue balancing in bicruciate retaining knee arthroplasty. *Computational and Mathematical Methods in Medicine*, 2012:652865, 2012.

[12] M. S. Andersen. Force-dependent kinematics – a method for simultaneous prediction of joint reaction forces, muscle forces and joint movements, 2014.

[13] C. J. Anderson, B. D. Westerhaus, S. D. Pietrini, C. G. Ziegler, C. A. Wijdicks, S. Johansen, L. Engebretsen, and R. F. LaPrade. Kinematic Impact of Anteromedial and Posterolateral Bundle Graft Fixation Angles on Double-Bundle Anterior

Cruciate Ligament Reconstructions. *The American Journal of Sports Medicine*, 38(8):1575–1583, August 2010.

[14] H. Asano, T. Muneta, and A. Hoshino. Stiffness of soft tissue complex in total knee arthroplasty. *Knee Surgery, Sports Traumatology, Arthroscopy*, 16(1):51–55, January 2008.

[15] D. Ascani, C. Mazzà, A. De Lollis, M. Bernardoni, and M. Viceconti. A procedure to estimate the origins and the insertions of the knee ligaments from computed tomography images. *Journal of Biomechanics*, 48(2):233–237, January 2015.

[16] K. K. Athwal, H. El Daou, B. Lord, A. J. Davies, W. Manning, F. Rodriguez y Baena, D. J. Deehan, and A. A. Amis. Lateral soft-tissue structures contribute to cruciate-retaining total knee arthroplasty stability: Lateral Structures with TKA. *Journal of Orthopaedic Research*, 35(9):1902–1909, September 2017.

[17] K. K. Athwal, P. E. Milner, G. Bellier, and A. A. Amis. Posterior capsular release is a biomechanically safe procedure to perform in total knee arthroplasty. *Knee surgery, sports traumatology, arthroscopy: official journal of the ESSKA*, August 2018.

[18] J. H. Bargren, J. D. Blaha, and M. A. Freeman. Alignment in total knee arthroplasty. Correlated biomechanical and clinical observations. *Clinical Orthopaedics and Related Research*, (173):178–183, March 1983.

[19] J. Beckmann, A. Steinert, C. Zilkens, A. Zeh, C. Schnurr, M. Schmitt-Sody, and M. Gebauer. [Partial replacement of the knee joint with patient-specific instruments and implants (ConforMIS iUni, iDuo)]. *Der Orthopade*, 45(4):322–330, April 2016.

[20] P. Beillas, G. Papaioannou, S. Tashman, and K. H. Yang. A new method to investigate in vivo knee behavior using a finite element model of the lower limb. *Journal of Biomechanics*, 37(7):1019–1030, July 2004.

[21] J. Bellemans, M. D. Ries, and J. M. K. Victor. *Total Knee Arthroplasty A Guide to Get Better Performance*. Springer Medizin, Berlin; Heidelberg, 2005. OCLC: 780901275.

[22] C. Belvedere, A. Ensini, A. Feliciangeli, F. Cenni, V. D'Angeli, S. Giannini, and A. Leardini. Geometrical changes of knee ligaments and patellar tendon during passive flexion. *Journal of Biomechanics*, 45(11):1886–1892, July 2012.

[23] M. G. Benedetti, F. Catani, T. W. Bilotta, M. Marcacci, E. Mariani, and S. Giannini. Muscle activation pattern and gait biomechanics after total knee replacement. *Clinical Biomechanics*, 18(9):871–876, November 2003.

[24] M. J. Bercik, A. Joshi, and J. Parvizi. Posterior Cruciate-Retaining Versus Posterior-Stabilized Total Knee Arthroplasty. *The Journal of Arthroplasty*, 28(3):439–444, March 2013.

[25] J. A. Bergfeld, S. M. Graham, R. D. Parker, A. Valdevit, and H. Kambic. A Biomechanical Comparison of Posterior Cruciate Ligament Reconstructions Using Single- and Double-Bundle Tibial Inlay Techniques. *The American Journal of Sports Medicine*, 33(7):976–981, July 2005.

[26] L. Bertozzi, R. Stagni, S. Fantozzi, and A. Cappello. Evaluation of a cruciate ligament model: sensitivity to the parameters during drawer test simulation. *Journal of Applied Biomechanics*, 24(3):234–243, August 2008.

[27] P. Bizot, A. Meunier, P. Christel, and J. Witvoët. [Experimental capsulo-ligamentar lesions of the knee during passive hyperextension. Biomechanical aspects. A lesional evaluation and consequences]. *Revue De Chirurgie Orthopedique Et Reparatrice De L'appareil Moteur*, 81(3):211–220, 1995.

[28] L. Blankevoort and R. Huiskes. Ligament-Bone Interaction in a Three-Dimensional Model of the Knee. *Journal of Biomechanical Engineering*, 113(3):263, 1991.

[29] D. V. Boguszewski, E. C. Cheung, N. B. Joshi, K. L. Markolf, and D. R. McAllister. Male-Female Differences in Knee Laxity and Stiffness: A Cadaveric Study. *The American Journal of Sports Medicine*, 43(12):2982–2987, December 2015.

[30] S. Brandsson, J. Karlsson, L. Swärd, J. Kartus, B. I. Eriksson, and J. Kärrholm. Kinematics and Laxity of the Knee Joint after Anterior Cruciate Ligament Reconstruction: Pre- and Postoperative Radiostereometric Studies. *The American Journal of Sports Medicine*, 30(3):361–367, May 2002.

[31] K. D. Brandt, M. Doherty, and S. Lohmander, editors. *Osteoarthritis*. Oxford medical publications. Oxford University Press, Oxford ; New York, 1998.

[32] A. M. J. Bull, O. Kessler, M. Alam, and A. A. Amis. Changes in knee kinematics reflect the articular geometry after arthroplasty. *Clinical Orthopaedics and Related Research*, 466(10):2491–2499, October 2008.

[33] R. Burnett, J. Stephen, and R. L. Barrack. Computer-assisted Total Knee Arthroplasty Is Currently of No Proven Clinical Benefit: A Systematic Review. *Clinical Orthopaedics and Related Research®*, 471(1):264–276, January 2013.

[34] D. B. Burr and E. L. Radin. Microfractures and microcracks in subchondral bone: are they relevant to osteoarthrosis? *Rheumatic Disease Clinics of North America*, 29(4):675–685, November 2003.

[35] D. L. Butler, M. D. Kay, and D. C. Stouffer. Comparison of material properties in fascicle-bone units from human patellar tendon and knee ligaments. *Journal of Biomechanics*, 19(6):425–432, 1986.

[36] S. van Buuren and K. Groothuis-Oudshoorn. mice: Multivariate imputation by chained equations in R. *Journal of statistical software*, pages 1–68, 2010.

[37] T. Calliess, P. Savov, M. Ettinger, and R. Karkosch. Knieprothesendesign und Kinematik: Unterschiede in Radien, Konformität und Rotation/Pivot. *Zeitschrift für Orthopädie und Unfallchirurgie*, June 2018.

[38] A. J. Carr, O. Robertsson, S. Graves, A. J. Price, N. K. Arden, A. Judge, and D. J. Beard. Knee replacement. *The Lancet*, 379(9823):1331–1340, April 2012.

[39] J. J. Cherian, B. H. Kapadia, S. Banerjee, J. J. Jauregui, K. Issa, and M. A. Mont. Mechanical, Anatomical, and Kinematic Axis in TKA: Concepts and Practical Applications. *Current Reviews in Musculoskeletal Medicine*, 7(2):89–95, June 2014.

[40] W.-S. Cho, S.-E. Byun, S.-J. Lee, and J. Yoon. Laxity after complete release of the medial collateral ligament in primary total knee arthroplasty. *Knee surgery, sports traumatology, arthroscopy: official journal of the ESSKA*, 23(6):1816–1823, June 2015.

[41] S. Claes, E. Vereecke, M. Maes, J. Victor, P. Verdonk, and J. Bellemans. Anatomy of the anterolateral ligament of the knee. *Journal of Anatomy*, 223(4):321–328, October 2013.

[42] H. D. Clarke and G. R. Scuderi. Flexion instability in primary total knee replacement. *The Journal of Knee Surgery*, 16(2):123–128, April 2003.

[43] C. W. Clary, C. K. Fitzpatrick, L. P. Maletsky, and P. J. Rullkoetter. The influence of total knee arthroplasty geometry on mid-flexion stability: An experimental and finite element study. *Journal of Biomechanics*, 46(7):1351–1357, April 2013.

[44] Z. A. Cohen, D. M. McCarthy, S. D. Kwak, P. Legrand, F. Fogarasi, E. J. Ciaccio, and G. A. Ateshian. Knee cartilage topography, thickness, and contact areas from MRI: in-vitro calibration and in-vivo measurements. *Osteoarthritis and Cartilage*, 7(1):95–109, January 1999.

[45] B. R. Coobs, R. F. LaPrade, C. J. Griffith, and B. J. Nelson. Biomechanical Analysis of an Isolated Fibular (Lateral) Collateral Ligament Reconstruction Using an Autogenous Semitendinosus Graft. *The American Journal of Sports Medicine*, 35(9):1521–1527, September 2007.

[46] R. Cristiani, E. Rönnblad, B. Engström, M. Forssblad, and A. Stålman. Medial Meniscus Resection Increases and Medial Meniscus Repair Preserves Anterior Knee Laxity: A Cohort Study of 4497 Patients With Primary Anterior Cruciate Ligament Reconstruction. *The American Journal of Sports Medicine*, 46(2):357–362, 2018.

[47] P. Damm, I. Kutzner, G. Bergmann, A. Rohlmann, and H. Schmidt. Comparison of in vivo measured loads in knee, hip and spinal implants during level walking. *Journal of Biomechanics*, 51:128–132, 2017.

[48] M. Damsgaard, J. Rasmussen, S. Tørholm Christensen, E. Surma, and M. de Zee. Analysis of musculoskeletal systems in the AnyBody Modeling System. *Simulation Modelling Practice and Theory*, 14(8):1100–1111, November 2006.

[49] D. R Diduch, J. N. Insall, R. Iorio, W. J. Long, and W. N. Scott. *Insall & Scott Surgery of the knee*. 2018. OCLC: 989482381.

[50] P. A. Dieppe and L. S. Lohmander. Pathogenesis and management of pain in osteoarthritis. *The Lancet*, 365(9463):965–973, March 2005.

[51] N. Diermann, T. Schumacher, S. Schanz, M. J. Raschke, W. Petersen, and T. Zantop. Rotational instability of the knee: internal tibial rotation under a simulated pivot shift test. *Archives of Orthopaedic and Trauma Surgery*, 129(3):353–358, March 2009.

[52] D. D. D'Lima, S. Patil, N. Steklov, J. E. Slamin, and C. W. Colwell. The Chitranjan Ranawat Award: in vivo knee forces after total knee arthroplasty. *Clinical Orthopaedics and Related Research*, 440:45–49, November 2005.

[53] D. D. D'Lima, S. Patil, N. Steklov, J. E. Slamin, and C. W. Colwell. Tibial Forces Measured In Vivo After Total Knee Arthroplasty. *The Journal of Arthroplasty*, 21(2):255–262, February 2006.

[54] D. D. D'Lima, C. Poole, H. Chadha, J. C. Hermida, A. Mahar, and C. W. Colwell. Quadriceps moment arm and quadriceps forces after total knee arthroplasty. *Clinical Orthopaedics and Related Research*, (392):213–220, November 2001.

[55] D. D. D'Lima, M. Trice, A. G. Urquhart, and C. W. Colwell. Tibiofemoral conformity and kinematics of rotating-bearing knee prostheses. *Clinical Orthopaedics and Related Research*, (386):235–242, May 2001.

[56] H. G. Dossett, N. A. Estrada, G. J. Swartz, G. W. LeFevre, and B. G. Kwasman. A randomised controlled trial of kinematically and mechanically aligned total knee replacements: Two-year clinical results. *The Bone & Joint Journal*, 96-B(7):907–913, July 2014.

[57] L. Dürselen, L. Claes, and H. Kiefer. The Influence of Muscle Forces and External Loads on Cruciate Ligament Strain. *The American Journal of Sports Medicine*, 23(1):129–136, January 1995.

[58] D. Eckhoff, C. Hogan, L. DiMatteo, M. Robinson, and J. Bach. Difference Between the Epicondylar and Cylindrical Axis of the Knee. *Clinical Orthopaedics and Related Research*, PAP, May 2007.

[59] J. A. Ewing, M. K. Kaufman, E. E. Hutter, J. F. Granger, M. D. Beal, S. J. Piazza, and R. A. Siston. Estimating patient-specific soft-tissue properties in a TKA knee: Estimating Properties Of TKA Knees. *Journal of Orthopaedic Research*, 34(3):435–443, March 2016.

[60] M. Ferle, R. Guo, and C. Hurschler. The Laxity of the Native Knee: A Meta-Analysis of in Vitro Studies. *The Journal of Bone and Joint Surgery*, 101(12):1119–1131, June 2019.

[61] C. B. Frank. Ligament structure, physiology and function. *Journal of Musculoskeletal & Neuronal Interactions*, 4(2):199–201, June 2004.

[62] T. Fridén, K. Sommerlath, N. Egund, J. Gillquist, and A. Ryd, L.and Lindstrand. Instability after anterior cruciate ligament rupture: Measurements of sagittal laxity compared in 11 cases. *Acta Orthopaedica Scandinavica*, 63(6):593–598, January 1992.

[63] J. Fuchs, M. Rabenberg, and C. Scheidt-Nave. Prävalenz ausgewählter muskuloskelettaler Erkrankungen: Ergebnisse der Studie zur Gesundheit Erwachsener in Deutschland (DEGS1). *Bundesgesundheitsblatt - Gesundheitsforschung - Gesundheitsschutz*, 56(5-6):678–686, May 2013.

[64] M. T. Gabriel, E. K. Wong, S. L-Y. Woo, M. Yagi, and R. E. Debski. Distribution of in situ forces in the anterior cruciate ligament in response to rotatory loads. *Journal of Orthopaedic Research*, 22(1):85–89, January 2004.

[65] H. R. Gadikota, Seon J. K., M. Kozanek, L. S. Oh, T. J. Gill, K. D. Montgomery, and G. Li. Biomechanical Comparison of Single-Tunnel—Double-Bundle and Single-Bundle Anterior Cruciate Ligament Reconstructions. *The American Journal of*

Sports Medicine, 37(5):962–969, May 2009.

[66] H. R. Gadikota, J. K. Seon, J.-L. Wu, T. J. Gill, and G. Li. The effect of isolated popliteus tendon complex injury on graft force in anterior cruciate ligament reconstructed knees. *International Orthopaedics*, 35(9):1403–1408, September 2011.

[67] H. R. Gadikota, J.-L. Wu, J. K. Seon, K. Sutton, T. J. Gill, and G. Li. Single-Tunnel Double-Bundle Anterior Cruciate Ligament Reconstruction With Anatomical Placement of Hamstring Tendon Graft. *The American Journal of Sports Medicine*, 38(4):713–720, April 2010.

[68] R. A. Gallo, S. C. Gamradt, C. J. Mattern, F. A. Cordasco, E. V. Craig, D. M. Dines, and R. F. Warren. Instability after reverse total shoulder replacement. *Journal of Shoulder and Elbow Surgery*, 20(4):584–590, June 2011.

[69] M. T. Galloway, E. S. Grood, J. N. Mehalik, M. Levy, S. C. Saddler, and F. R. Noyes. Posterior cruciate ligament reconstruction: an in vitro study of femoral and tibial graft placement. *The American journal of sports medicine*, 24(4):437–445, 1996.

[70] J. C. Gardiner and J. A. Weiss. Subject-specific finite element analysis of the human medial collateral ligament during valgus knee loading. *Journal of Orthopaedic Research: Official Publication of the Orthopaedic Research Society*, 21(6):1098–1106, November 2003.

[71] L. R. Garsden and J. E. Bullock-Saxton. Joint reposition sense in subjects with unilateral osteoarthritis of the knee. *Clinical Rehabilitation*, 13(2):148–155, April 1999.

[72] K. M. Ghosh, A. M. Merican, F. Iranpour, D. J. Deehan, and A. A. Amis. Length-change patterns of the collateral ligaments after total knee arthroplasty. *Knee Surgery, Sports Traumatology, Arthroscopy*, 20(7):1349–1356, July 2012.

[73] J. R. Giffin, K. J. Stabile, T. Zantop, T. M. Vogrin, S. L-Y. Woo, and C. D. Harner. Importance of Tibial Slope for Stability of the Posterior Cruciate Ligament—Deficient Knee. *The American Journal of Sports Medicine*, 35(9):1443–1449, September 2007.

[74] F. G. Girgis, J. L. Marshall, and A. Monajem. The cruciate ligaments of the knee joint. Anatomical, functional and experimental analysis. *Clinical Orthopaedics and Related Research*, (106):216–231, February 1975.

[75] KUKA Roboter GmbH. KUKA.RoboterSensorInterface 2.3 V1 for KUKA System Software 8.3, May 2013.

[76] M. T. Goldsmith, K. S. Jansson, S. D. Smith, L. Engebretsen, R. F. LaPrade, and C. A. Wijdicks. Biomechanical Comparison of Anatomic Single- and Double-Bundle Anterior Cruciate Ligament Reconstructions: An In Vitro Study. *The American Journal of Sports Medicine*, 41(7):1595–1604, July 2013.

[77] D. Goutallier, O. Manicom, and S. Van Driessche. [Total knee arthroplasty with bicruciate preservation: Comparison versus the same posterostabilized design at eight years follow-up]. *Revue De Chirurgie Orthopedique Et Reparatrice De L'appareil Moteur*, 94(6):585–595, October 2008.

[78] Y. Gu, J. D. Roth, S. M. Howell, and M. L. Hull. How Frequently Do Four Methods for Mechanically Aligning a Total Knee Arthroplasty Cause Collateral Ligament Imbalance and Change Alignment from Normal in White Patients?: AAOS Exhibit Selection. *The Journal of Bone and Joint Surgery-American Volume*, 96(12):e101–1–9, June 2014.

[79] T. M. Guess and S. Razu. Loading of the medial meniscus in the ACL deficient knee: A multibody computational study. *Medical Engineering & Physics*, 41:26–34, March 2017.

[80] T. M. Guess, G. Thiagarajan, M. Kia, and M. Mishra. A subject specific multibody model of the knee with menisci. *Medical Engineering & Physics*, 32(5):505–515, June 2010.

[81] R. Gunaratne, D. N. Pratt, J. Banda, D. P. Fick, R. J. K. Khan, and B. W. Robertson. Patient Dissatisfaction Following Total Knee Arthroplasty: A Systematic Review of the Literature. *The Journal of Arthroplasty*, 32(12):3854–3860, December 2017.

[82] C. M. Gupte, A. Bull, R. D. Thomas, and A. A. Amis. The meniscofemoral ligaments: Secondary restraints to the posterior drawer Analysis of anteroposterior and rotary laxity in the intact and posterior-cruciate-deficient knee. *Journal of Bone & Joint Surgery, British Volume*, 85(5):765–773, 2003.

[83] S. P. Hacker, A. Ignatius, and L. Dürselen. The influence of the test setup on knee joint kinematics – A meta-analysis of tibial rotation. *Journal of Biomechanics*, July 2016.

[84] F. W. Hagena, G. O. Hofmann, T. Mittlmeier, G. Wasmer, and M. Bergmann. The cruciate ligaments in knee replacement. *International Orthopaedics*, 13(1):13–16, 1989.

[85] C. Halewood, M. Risebury, N. P. Thomas, and A. A. Amis. Kinematic behaviour and soft tissue management in guided motion total knee replacement. *Knee Surgery, Sports Traumatology, Arthroscopy*, 22(12):3074–3082, December 2014.

[86] J. P. Halloran, A. J. Petrella, and P. J. Rullkoetter. Explicit finite element modeling of total knee replacement mechanics. *Journal of Biomechanics*, 38(2):323–331, February 2005.

[87] C. D. Harner, M. A. Janaushek, A. Kanamori, M. Yagi, T. M. Vogrin, and S. Woo. Biomechanical analysis of a double-bundle posterior cruciate ligament reconstruction. *The American journal of sports medicine*, 28(2):144–151, 2000.

[88] C. D. Harner, J. W. Xerogeanes, G. A. Livesay, G. J. Carlin, B. A. Smith, T. Kusayama, S. Kashiwaguchi, and S. L. Woo. The human posterior cruciate ligament complex: an interdisciplinary study. Ligament morphology and biomechanical evaluation. *The American Journal of Sports Medicine*, 23(6):736–745, December 1995.

[89] M. D. Harris, A. J. Cyr, A. A. Ali, C. K. Fitzpatrick, P. J. Rullkoetter, L. P. Maletsky, and K. B. Shelburne. A Combined Experimental and Computational Approach

to Subject-Specific Analysis of Knee Joint Laxity. *Journal of Biomechanical Engineering*, 138(8):081004, June 2016.

[90] B. Heinlein, I. Kutzner, F. Graichen, A. Bender, A. Rohlmann, A. M. Halder, A. Beier, and G. Bergmann. ESB Clinical Biomechanics Award 2008: Complete data of total knee replacement loading for level walking and stair climbing measured in vivo with a follow-up of 6-10 months. *Clinical Biomechanics (Bristol, Avon)*, 24(4):315–326, May 2009.

[91] M. Herbort, C. Domnick, M. J.s Raschke, S. Lenschow, T. Förster, W. Petersen, and T. Zantop. Comparison of Knee Kinematics After Single-Bundle Anterior Cruciate Ligament Reconstruction via the Medial Portal Technique With a Central Femoral Tunnel and an Eccentric Femoral Tunnel and After Anatomic Double-Bundle Reconstruction: A Human Cadaveric Study. *The American Journal of Sports Medicine*, 44(1):126–132, January 2016.

[92] M. Herbort, S. Lenschow, F. H. Fu, W. Petersen, and T. Zantop. ACL mismatch reconstructions: influence of different tunnel placement strategies in single-bundle ACL reconstructions on the knee kinematics. *Knee Surgery, Sports Traumatology, Arthroscopy*, 18(11):1551–1558, November 2010.

[93] M. Herbort, K. Tecklenburg, T. Zantop, M. J. Raschke, C. Hoser, M. Schulze, W. Petersen, and C. Fink. Single-Bundle Anterior Cruciate Ligament Reconstruction: A Biomechanical Cadaveric Study of a Rectangular Quadriceps and Bone–Patellar Tendon–Bone Graft Configuration Versus a Round Hamstring Graft. *Arthroscopy: The Journal of Arthroscopic & Related Surgery*, 29(12):1981–1990, December 2013.

[94] J. P. T. Higgins and S. G. Thompson. Quantifying heterogeneity in a meta-analysis. *Statistics in Medicine*, 21(11):1539–1558, June 2002.

[95] A. M. Hollister, S. Jatana, A. K. Singh, W. W. Sullivan, and A. G. Lupichuk. The axes of rotation of the knee. *Clinical Orthopaedics and Related Research*, (290):259–268, May 1993.

[96] A. Hosseini, W. Qi, T.-Y. Tsai, Y. Liu, H. Rubash, and G. Li. In vivo length change patterns of the medial and lateral collateral ligaments along the flexion path of the knee. *Knee surgery, sports traumatology, arthroscopy: official journal of the ESSKA*, 23(10):3055–3061, October 2015.

[97] S. M. Howell and M. L. Hull. Kinematic alignment in total knee arthroplasty. *Insall and Scott Surgery of the Knee. Philadelphia, PA: Elsevier*, pages 1255–1268, 2012.

[98] H. H. Huberti and W. C. Hayes. Patellofemoral contact pressures. The influence of q-angle and tendofemoral contact. *The Journal of Bone and Joint Surgery. American Volume*, 66(5):715–724, June 1984.

[99] J. C. Hughston and A. F. Eilers. The role of the posterior oblique ligament in repairs of acute medial (collateral) ligament tears of the knee. *The Journal of Bone and Joint Surgery. American Volume*, 55(5):923–940, July 1973.

[100] C. Hurschler. Experimental Methods for the Investigation of the Biomechanics of the Shoulder. 2004.

[101] N. Iizawa, A. Mori, T. Majima, H. Kawaji, S. Matsui, and S. Takai. Influence of the Medial Knee Structures on Valgus and Rotatory Stability in Total Knee Arthroplasty. *The Journal of Arthroplasty*, 31(3):688–693, March 2016.

[102] C. Imhauser, C. Mauro, D. Choi, E. Rosenberg, S. Mathew, J. Nguyen, Y. Ma, and T. Wickiewicz. Abnormal Tibiofemoral Contact Stress and Its Association With Altered Kinematics After Center-Center Anterior Cruciate Ligament Reconstruction: An In Vitro Study. *The American Journal of Sports Medicine*, 41(4):815–825, April 2013.

[103] E. Inderhaug, J. M. Stephen, A. Williams, and A. A. Amis. Biomechanical Comparison of Anterolateral Procedures Combined With Anterior Cruciate Ligament Reconstruction. *The American Journal of Sports Medicine*, 45(2):347–354, February 2017.

[104] J. Insall, A. J. Tria, and W. N. Scott. The total condylar knee prosthesis: the first 5 years. *Clinical Orthopaedics and Related Research*, (145):68–77, December 1979.

[105] T. Iwahashi, K. Shino, K. Nakata, N. Nakamura, Y. Yamada, H. Yoshikawa, and K. Sugamoto. Assessment of the "functional length" of the three bundles of the anterior cruciate ligament. *Knee surgery, sports traumatology, arthroscopy: official journal of the ESSKA*, 16(2):167–174, February 2008.

[106] H. Iwaki, V. Pinskerova, and M. A. Freeman. Tibiofemoral movement 1: the shapes and relative movements of the femur and tibia in the unloaded cadaver knee. *The Journal of Bone and Joint Surgery. British Volume*, 82(8):1189–1195, November 2000.

[107] W. L. Jaffe, J. M. Dundon, and T. Camus. Alignment and Balance Methods in Total Knee Arthroplasty. *The Journal of the American Academy of Orthopaedic Surgeons*, 26(20):709–716, October 2018.

[108] E. W. James, B. T. Williams, and R. F. LaPrade. Stress Radiography for the Diagnosis of Knee Ligament Injuries: A Systematic Review. *Clinical Orthopaedics and Related Research®*, 472(9):2644–2657, September 2014.

[109] J. Y. Jenny and G. Jenny. Preservation of anterior cruciate ligament in total knee arthroplasty. *Archives of Orthopaedic and Trauma Surgery*, 118(3):145–148, 1998.

[110] A.-R. Jo, E.-K. Song, K.-B. Lee, H.-Y. Seo, S.-K. Kim, and J.-K. Seon. A Comparison of Stability and Clinical Outcomes in Single-Radius Versus Multi-Radius Femoral Design for Total Knee Arthroplasty. *The Journal of Arthroplasty*, 29(12):2402–2406, December 2014.

[111] C. W. Jones and S. A. Jerabek. Current Role of Computer Navigation in Total Knee Arthroplasty. *The Journal of Arthroplasty*, 33(7):1989–1993, 2018.

[112] A. Kanamori, J. M. Lee, M. J. Haemmerle, T. M. Vogrin, and C. D. Harner. A biomechanical analysis of two reconstructive approaches to the posterolateral corner of the knee. *Knee Surgery, Sports Traumatology, Arthroscopy*, 11(5):312–317, September 2003.

[113] A. Kanamori, S. L-Y. Woo, C. B. Ma, J. Zeminski, T. W. Rudy, G. Li, and G. A.

Livesay. The forces in the anterior cruciate ligament and knee kinematics during a simulated pivot shift test: A human cadaveric study using robotic technology. *Arthroscopy: The Journal of Arthroscopic & Related Surgery*, 16(6):633–639, September 2000.

[114] A. I. Kapandji and S. Rehart. *Funktionelle Anatomie der Gelenke: schematisierte und kommentierte Zeichnungen zur menschlichen Biomechanik*. Georg Thieme Verlag, Stuttgart New York, NY, 6. auflage edition, 2016. OCLC: 905368102.

[115] Y. Kato, S. J. M. Ingham, A. Maeyama, P. Lertwanich, J. H. Wang, Y. Mifune, S. Kramer, P. Smolinski, and F. H. Fu. Biomechanics of the Human Triple-Bundle Anterior Cruciate Ligament. *Arthroscopy: The Journal of Arthroscopic & Related Surgery*, 28(2):247–254, February 2012.

[116] Y. Kato, A. Maeyama, P. Lertwanich, J. H. Wang, S. J. M. Ingham, S. Kramer, C. Q. A. Martins, P. Smolinski, and F. H. Fu. Biomechanical comparison of different graft positions for single-bundle anterior cruciate ligament reconstruction. *Knee Surgery, Sports Traumatology, Arthroscopy*, 21(4):816–823, April 2013.

[117] E. Kellis. Tibiofemoral joint forces during maximal isokinetic eccentric and concentric efforts of the knee flexors. *Clinical Biomechanics (Bristol, Avon)*, 16(3):229–236, March 2001.

[118] M. I. Kennedy, S. Claes, F. A. F. Fuso, B. T. Williams, M. T. Goldsmith, T. L. Turnbull, C. A. Wijdicks, and R. F. LaPrade. The Anterolateral Ligament: An Anatomic, Radiographic, and Biomechanical Analysis. *The American Journal of Sports Medicine*, 43(7):1606–1615, July 2015.

[119] N. I. Kennedy, R. F. LaPrade, M. T. Goldsmith, S. C. Faucett, M. T. Rasmussen, G. A. Coatney, L. Engebretsen, and C. A. Wijdicks. Posterior Cruciate Ligament Graft Fixation Angles, Part 2: Biomechanical Evaluation for Anatomic Double-Bundle Reconstruction. *The American Journal of Sports Medicine*, 42(10):2346–2355, October 2014.

[120] A. Keshmiri, G. Maderbacher, C. Baier, A. Benditz, J. Grifka, and F. Greimel. Kinematic alignment in total knee arthroplasty leads to a better restoration of patellar kinematics compared to mechanic alignment. *Knee Surgery, Sports Traumatology, Arthroscopy*, November 2018.

[121] A. Kido, G. Pap, K. Kawate, A. Roessner, and Y. Takakura. Disease-specific expression patterns of proteases in synovial tissues. *Pathology - Research and Practice*, 203(6):451–456, June 2007.

[122] R. H. P. Kilger, J. Stehle, J. A. Fisk, M. Thomas, K. Miura, and S. L-Y. Woo. Anatomical Double-Bundle Anterior Cruciate Ligament Reconstruction After Valgus High Tibial Osteotomy. *The American Journal of Sports Medicine*, 34(6):961–967, June 2006.

[123] R. H. P. Kilger, M. Thomas, S. Hanford, D. A. Alaseirlis, H. H. Paessler, and S. L-Y. Woo. The Effectiveness of Reconstruction of the Anterior Cruciate Ligament Using the Novel Knot/Press-Fit Technique. *The American Journal of Sports Medicine*, 33(6):856–863, June 2005.

[124] S.-J. Kim, H.-S. Kim, H.-K. Moon, W.-H. Chang, S.-G. Kim, and Y.-M. Chun. A Biomechanical Comparison of 3 Reconstruction Techniques for Posterolateral Instability of the Knee in a Cadaveric Model. *Arthroscopy: The Journal of Arthroscopic & Related Surgery*, 26(3):335–341, March 2010.

[125] Z. Knoll, L. Kocsis, and R. M. Kiss. Gait patterns before and after anterior cruciate ligament reconstruction. *Knee surgery, sports traumatology, arthroscopy: official journal of the ESSKA*, 12(1):7–14, January 2004.

[126] D. Kohn and F. Adam, editors. *Das Knie: 57 Tabellen*. Thieme, Stuttgart, 2000. OCLC: 247325630.

[127] E. Kondo, A. M. Merican, K. Yasuda, and A. A. Amis. Biomechanical Comparisons of Knee Stability After Anterior Cruciate Ligament Reconstruction Between 2 Clinically Available Transtibial Procedures: Anatomic Double Bundle Versus Single Bundle. *The American Journal of Sports Medicine*, 38(7):1349–1358, July 2010.

[128] E. Kondo, A. M. Merican, K. Yasuda, and A. A. Amis. Biomechanical Comparison of Anatomic Double-Bundle, Anatomic Single-Bundle, and Nonanatomic Single-Bundle Anterior Cruciate Ligament Reconstructions. *The American Journal of Sports Medicine*, 39(2):279–288, February 2011.

[129] E. Kondo, A. M. Merican, K. Yasuda, and A. A. Amis. Biomechanical Analysis of Knee Laxity With Isolated Anteromedial or Posterolateral Bundle–Deficient Anterior Cruciate Ligament. *Arthroscopy: The Journal of Arthroscopic & Related Surgery*, 30(3):335–343, March 2014.

[130] G. L. Kraft and D. H. Levinthal. Acrylic prosthesis replacing lower end of the femur for benign giant-cell tumor. *The Journal of Bone and Joint Surgery. American Volume*, 36(A:2):368–374, April 1954.

[131] H. W. Krutsch. Differentialstrategien zum Weichteil-Balancing bei der Knieendoprothetik in Abhängigkeit von der präoperativen Deformität. Differential strategies for soft tissue balancing in total knee arthroplasty regulated by the preoperative deformity. 2010.

[132] K. E. Kuettner, V. M. Goldberg, American Academy of Orthopaedic Surgeons, and American Academy of Orthopaedic Surgeons, editors. *Osteoarthritic disorders: workshop, Monterey, California, April 1994*. The Academy, Rosemont, IL, 1995.

[133] J. G. Kuhns and T. A. Potter. Nylon arthroplasty of the knee joint in chronic arthritis. *Surgery, Gynecology & Obstetrics*, 91(3):351–362, September 1950.

[134] S. D. Kwak, C. S. Ahmad, T. R. Gardner, R. P. Grelsamer, J. H. Henry, L. Blankevoort, G. A. Ateshian, and V. C. Mow. Hamstrings and iliotibial band forces affect knee kinematics and contact pattern. *Journal of Orthopaedic Research: Official Publication of the Orthopaedic Research Society*, 18(1):101–108, January 2000.

[135] R. F. LaPrade. The Anatomy of the Posterior Aspect of the KneeAn Anatomic Study. *The Journal of Bone and Joint Surgery (American)*, 89(4):758, April 2007.

[136] R. F. LaPrade, J. K. Wozniczka, M. P. Stellmaker, and C. A. Wijdicks. Analysis

of the Static Function of the Popliteus Tendon and Evaluation of an Anatomic Reconstruction. *The American Journal of Sports Medicine*, 38(3):543–549, March 2010.

[137] J. S. Lawrence, J. M. Bremner, and F. Bier. Prevalence in the population and relationship between symptoms and x-ray changes. *Annals Of The Rheumatic Diseases*, page 24.

[138] S. Lenschow, T. Zantop, A. Weimann, T. Lemburg, M. Raschke, M. Strobel, and W. Petersen. Joint kinematics and in situ forces after single bundle PCL reconstruction: a graft placed at the center of the femoral attachment does not restore normal posterior laxity. *Archives of Orthopaedic and Trauma Surgery*, 126(4):253–259, May 2006.

[139] P. Lertwanich, Y. Kato, C. A.Q. Martins, A. Maeyama, S. J.M. Ingham, S. Kramer, M. Linde-Rosen, P. Smolinski, and F. H. Fu. A Biomechanical Comparison of 2 Femoral Fixation Techniques for Anterior Cruciate Ligament Reconstruction in Skeletally Immature Patients: Over-the-Top Fixation Versus Transphyseal Technique. *Arthroscopy: The Journal of Arthroscopic & Related Surgery*, 27(5):672–680, May 2011.

[140] G. Li, L. E. DeFrate, H. Sun, and T. J. Gill. In vivo elongation of the anterior cruciate ligament and posterior cruciate ligament during knee flexion. *The American Journal of Sports Medicine*, 32(6):1415–1420, September 2004.

[141] X. Li, C. Wang, Y. Guo, and W. Chen. An Approach to Developing Customized Total Knee Replacement Implants. *Journal of Healthcare Engineering*, 2017:9298061, 2017.

[142] H.-C. Lim, Y.-C. Yoon, J.-H. Wang, and J.-H. Bae. Anatomical versus Non-Anatomical Single Bundle Anterior Cruciate Ligament Reconstruction: A Cadaveric Study of Comparison of Knee Stability. *Clinics in Orthopedic Surgery*, 4(4):249, 2012.

[143] P. Liu, J. Wang, Y. Xu, and Y. Ao. In situ forces and length patterns of the fibular collateral ligament under controlled loading: an in vitro biomechanical study using a robotic system. *Knee Surgery, Sports Traumatology, Arthroscopy*, 23(4):1018–1025, April 2015.

[144] M. K. Liukkonen, M. E. Mononen, P. Tanska, S. Saarakkala, M. T. Nieminen, and R. K. Korhonen. Application of a semi-automatic cartilage segmentation method for biomechanical modeling of the knee joint. *Computer Methods in Biomechanics and Biomedical Engineering*, 20(13):1453–1463, October 2017.

[145] J. Lo, O. Müller, M. Wünschel, S. Bauer, and N. Wülker. Forces in anterior cruciate ligament during simulated weight-bearing flexion with anterior and internal rotational tibial load. *Journal of Biomechanics*, 41(9):1855–1861, January 2008.

[146] B. R. Lord, H. El-Daou, B. M. Sabnis, C. M. Gupte, A. M. Wilson, and A. A. Amis. Biomechanical comparison of graft structures in anterior cruciate ligament reconstruction. *Knee Surgery, Sports Traumatology, Arthroscopy*, 25(2):559–568, February 2017.

[147] A. Lorenz, H. Röttgerkamp, E. Bobrowitsch, C. I. Leichtle, and U. G. Leichtle. Tibial rotation influences anterior knee stability — a robot-aided in-vitro study. *Clinical Biomechanics*, 32:131–137, February 2016.

[148] J. K. Loudon. Biomechanics and Pathomechanics of the Patellofemoral Joint. *International Journal of Sports Physical Therapy*, 11(6):820–830, December 2016.

[149] C.-F. Luo. Reference axes for reconstruction of the knee. *The Knee*, 11(4):251–257, August 2004.

[150] C. B. Ma, M. A. Janaushek, T. M. Vogrin, T. W. Rudy, C. D. Harner, and S. L.-Y. Woo. Significance of changes in the reference position for measurements of tibial translation and diagnosis of cruciate ligament deficiency. *Journal of Orthopaedic Research*, 18(2):176–182, 2000.

[151] C. B. Ma, A. Kanamori, T. M. Vogrin, S. L. Y. Woo, and C. D. Harner. Measurement of Posterior Tibial Translation in the Posterior Cruciate Ligament-Reconstructed Knee. *The American journal of sports medicine*, 31(6):843–848, 2003.

[152] G. Maderbacher, A. Keshmiri, B. Krieg, F. Greimel, J. Grifka, and C. Baier. Kinematic component alignment in total knee arthroplasty leads to better restoration of natural tibiofemoral kinematics compared to mechanic alignment. *Knee Surgery, Sports Traumatology, Arthroscopy*, August 2018.

[153] F. Margheritini, C. S. Mauro, J. A. Rihn, K. J. Stabile, S. L-Y. Woo, and C. D. Harner. Biomechanical Comparison of Tibial Inlay Versus Transtibial Techniques for Posterior Cruciate Ligament Reconstruction. *The American Journal of Sports Medicine*, 32(3):587–593, April 2004.

[154] G. Marinozzi, S. Pappalardo, and R. Steindler. Human knee ligaments: mechanical tests and ultrastructural observations. *Italian Journal of Orthopaedics and Traumatology*, 9(2):231–240, June 1983.

[155] K. L. Markolf, J. F. Gorek, J. M. Kabo, and M. S. Shapiro. Direct measurement of resultant forces in the anterior cruciate ligament. An in vitro study performed with a new experimental technique. *The Journal of Bone and Joint Surgery. American Volume*, 72(4):557–567, April 1990.

[156] K. L. Markolf, A. Graff-Radford, and H. C. Amstutz. In vivo knee stability. A quantitative assessment using an instrumented clinical testing apparatus. *The Journal of Bone and Joint Surgery. American Volume*, 60(5):664–674, July 1978.

[157] K. L. Markolf, S. R. Jackson, B. Foster, and D. R. McAllister. ACL forces and knee kinematics produced by axial tibial compression during a passive flexion-extension cycle: ACL BIOMECHANICS PRODUCED BY AXIAL COMPRESSION. *Journal of Orthopaedic Research*, 32(1):89–95, January 2014.

[158] K. L. Markolf, S. Park, S. R. Jackson, and D. R. McAllister. Contributions of the Posterolateral Bundle of the Anterior Cruciate Ligament to Anterior-Posterior Knee Laxity and Ligament Forces. *Arthroscopy: The Journal of Arthroscopic & Related Surgery*, 24(7):805–809, July 2008.

[159] P. Massin. How does total knee replacement technique influence polyethylene wear?

Orthopaedics & Traumatology: Surgery & Research, 103(1):S21–S27, February 2017.

[160] T. Matsumoto, H. Muratsu, N. Tsumura, K. Mizuno, M. Kurosaka, and R. Kuroda. Soft Tissue Balance Measurement in Posterior-Stabilized Total Knee Arthroplasty With a Navigation System. *The Journal of Arthroplasty*, 24(3):358–364, April 2009.

[161] G. Matziolis, D. Krocker, U. Weiss, S. Tohtz, and C. Perka. A Prospective, Randomized Study of Computer-Assisted and Conventional Total Knee Arthroplasty: Three-Dimensional Evaluation of Implant Alignment and Rotation. *The Journal of Bone & Joint Surgery*, 89(2):236–243, February 2007.

[162] M. J. Maynard, X. Deng, T. L. Wickiewicz, and R. F. Warren. The popliteofibular ligament. Rediscovery of a key element in posterolateral stability. *The American Journal of Sports Medicine*, 24(3):311–316, June 1996.

[163] M. M. McCarthy, S. Tucker, J. T. Nguyen, D. W. Green, C. W. Imhauser, and F. A. Cordasco. Contact Stress and Kinematic Analysis of All-Epiphyseal and Over-the-Top Pediatric Reconstruction Techniques for the Anterior Cruciate Ligament. *The American Journal of Sports Medicine*, 41(6):1330–1339, June 2013.

[164] A. Menschick. Mechanik des Kniegelenkes. Teil 1. (112):481–495, 1974.

[165] A. M. Merican, K. M. Ghosh, F. Iranpour, D. J. Deehan, and Andrew A. Amis. The effect of femoral component rotation on the kinematics of the tibiofemoral and patellofemoral joints after total knee arthroplasty. *Knee Surgery, Sports Traumatology, Arthroscopy*, 19(9):1479–1487, September 2011.

[166] J. W.-P. Michael, K. U. Schlüter-Brust, and P. Eysel. The Epidemiology, Etiology, Diagnosis, and Treatment of Osteoarthritis of the Knee. *Deutsches Aerzteblatt Online*, March 2010.

[167] C. E. Milner. Is gait normal after total knee arthroplasty? Systematic review of the literature. *Journal of Orthopaedic Science: Official Journal of the Japanese Orthopaedic Association*, 14(1):114–120, January 2009.

[168] K. Miura, S. L.-Y. Woo, R. Brinkley, Y.-C. Fu, and S. Noorani. Effects of Knee Flexion Angles for Graft Fixation on Force Distribution in Double-Bundle Anterior Cruciate Ligament Grafts. *The American Journal of Sports Medicine*, 34(4):577–585, April 2006.

[169] P. M. Morgan, R. F. LaPrade, F. A. Wentorf, J. W. Cook, and A. Bianco. The Role of the Oblique Popliteal Ligament and Other Structures in Preventing Knee Hyperextension. *The American Journal of Sports Medicine*, 38(3):550–557, March 2010.

[170] V. Musahl, A. Plakseychuk, A. Vanscyoc, T. Sasaki, R. E. Debski, P. J. Mcmahon, and F. H. Fu. Varying Femoral Tunnels Between the Anatomical Footprint and Isometric Positions. *The American Journal of Sports Medicine*, 33(5):712–718, May 2005.

[171] T. Nagura, C. O. Dyrby, E. J. Alexander, and T. P. Andriacchi. Mechanical loads at the knee joint during deep flexion. *Journal of Orthopaedic Research*, 20(4):881–886, July 2002.

[172] D. Nam, R. M. Nunley, and R. L. Barrack. Patient dissatisfaction following total knee replacement: a growing concern? *Bone Joint J*, 96(11 Supple A):96–100, 2014.

[173] P. C. Noble, M. A. Conditt, K. F. Cook, and K. B. Mathis. The John Insall Award: Patient Expectations Affect Satisfaction with Total Knee Arthroplasty:. *Clinical Orthopaedics and Related Research*, 452:35–43, November 2006.

[174] F. R. Noyes, D. L. Butler, E. S. Grood, R. F. Zernicke, and M. S. Hefzy. Biomechanical analysis of human ligament grafts used in knee-ligament repairs and reconstructions. *The Journal of Bone and Joint Surgery. American Volume*, 66(3):344–352, March 1984.

[175] OECD. *Health at a Glance 2017: OECD Indicators*. Health at a Glance. OECD, November 2017.

[176] M. W. Pagnano, A. D. Hanssen, D. G. Lewallen, and M. J. Stuart. Flexion instability after primary posterior cruciate retaining total knee arthroplasty. *Clinical Orthopaedics and Related Research*, (356):39–46, November 1998.

[177] G. Pap, A. Machner, and F. Awiszus. Messung der Kniegelenkskinästhesie zur Bestimmung von Propriozeptionsdefiziten bei Varusgonarthrose. *Zeitschrift fr Rheumatologie*, 57(1):5–10, March 1998.

[178] G. Pap, A. Machner, and F. Awiszus. Strength and voluntary activation of the quadriceps femoris muscle at different severities of osteoarthritic knee joint damage. *Journal of Orthopaedic Research*, 22(1):96–103, January 2004.

[179] M. A. Parentis, M. N. Rumi, G. S. Deol, M. Kothari, W. M. Parrish, and V. D. Pellegrini. A comparison of the vastus splitting and median parapatellar approaches in total knee arthroplasty. *Clinical Orthopaedics and Related Research*, (367):107–116, October 1999.

[180] S. E. Park, L. E. DeFrate, J. F. Suggs, T. J. Gill, H. E. Rubash, and G. Li. The change in length of the medial and lateral collateral ligaments during in vivo knee flexion. *The Knee*, 12(5):377–382, October 2005.

[181] S. E. Park, B. D. Stamos, L. E. DeFrate, T. J. Gill, and G. Li. The Effect of Posterior Knee Capsulotomy on Posterior Tibial Translation during Posterior Cruciate Ligament Tibial Inlay Reconstruction. *The American Journal of Sports Medicine*, 32(6):1514–1519, September 2004.

[182] E. M. Parsons, A. O. Gee, C. Spiekerman, and P. R. Cavanagh. The Biomechanical Function of the Anterolateral Ligament of the Knee. *The American Journal of Sports Medicine*, 43(3):669–674, March 2015.

[183] S. Patil, A. Bunn, W. D. Bugbee, C. W. Colwell, and D. D. D'Lima. Patient-specific implants with custom cutting blocks better approximate natural knee kinematics than standard TKA without custom cutting blocks. *The Knee*, 22(6):624–629, December 2015.

[184] A. W. Pearsall and J. M. Hollis. The Effect of Posterior Cruciate Ligament Injury and Reconstruction on Meniscal Strain. *The American Journal of Sports Medicine*, 32(7):1675–1680, October 2004.

[185] P. Pellikaan, M. M. van der Krogt, V. Carbone, R. Fluit, L. M. Vigneron, J. Van Deun, N. Verdonschot, and H. F. Koopman. Evaluation of a morphing based method to estimate muscle attachment sites of the lower extremity. *Journal of Biomechanics*, 47(5):1144–1150, March 2014.

[186] W. Petersen, S. Loerch, S. Schanz, M. Raschke, and T. Zantop. The Role of the Posterior Oblique Ligament in Controlling Posterior Tibial Translation in the Posterior Cruciate Ligament-Deficient Knee. *The American Journal of Sports Medicine*, 36(3):495–501, November 2007.

[187] W. Petersen, H. Tretow, A. Weimann, M. Herbort, F. H. Fu, M. Raschke, and T. Zantop. Biomechanical Evaluation of Two Techniques for Double-Bundle Anterior Cruciate Ligament Reconstruction. *The American Journal of Sports Medicine*, 35(2):228–234, February 2007.

[188] L. A. Pottenger, F. M. Phillips, and L. F. Draganich. The effect of marginal osteophytes on reduction of varus-valgus instability in osteoarthritic knees. *Arthritis and Rheumatism*, 33(6):853–858, June 1990.

[189] A. J. Price, J. L. Rees, D. Beard, E. Juszczak, S. Carter, S. White, R. de Steiger, C. A. F. Dodd, M. Gibbons, P. McLardy-Smith, J. W. Goodfellow, and D. W. Murray. A mobile-bearing total knee prosthesis compared with a fixed-bearing prosthesis: A Multicentre Single-Blind Randomized Controlled Trial. *The Journal of Bone and Joint Surgery. British volume*, 85-B(1):62–67, January 2003.

[190] J. W. Pritchett. Anterior cruciate-retaining total knee arthroplasty. *The Journal of Arthroplasty*, 11(2):194–197, February 1996.

[191] J. W. Pritchett. Patients prefer a bicruciate-retaining or the medial pivot total knee prosthesis. *The Journal of Arthroplasty*, 26(2):224–228, February 2011.

[192] P. P. Provenzano and R. Vanderby. Collagen fibril morphology and organization: Implications for force transmission in ligament and tendon. *Matrix Biology*, 25(2):71–84, March 2006.

[193] A. Race and A. A. Amis. Loading of the two bundles of the posterior cruciate ligament: an analysis of bundle function in AP drawer. *Journal of biomechanics*, 29(7):873–879, 1996.

[194] A. Race and A. A. Amis. PCL reconstruction. *J Bone Joint Surg Br*, 80(1):173–179, 1998.

[195] H. H. Rachmat, D. Janssen, G. J. Verkerke, R. L. Diercks, and N. Verdonschot. In-situ mechanical behavior and slackness of the anterior cruciate ligament at multiple knee flexion angles. *Medical Engineering & Physics*, 38(3):209–215, March 2016.

[196] H. H. Rachmat, D. Janssen, W. J. Zevenbergen, G. J. Verkerke, R. L. Diercks, and N. Verdonschot. Generating finite element models of the knee: How accurately can we determine ligament attachment sites from MRI scans? *Medical Engineering & Physics*, 36(6):701–707, June 2014.

[197] A. A. Rahnemai-Azar, R. M. Miller, D. Guenther, F. H. Fu, B. P. Lesniak, V. Musahl, and R. E. Debski. Structural Properties of the Anterolateral Capsule and Iliotibial

Band of the Knee. *The American Journal of Sports Medicine*, 44(4):892–897, April 2016.

[198] M. T. Rasmussen, M. Nitri, B. T. Williams, S. G. Moulton, R. Serra Cruz, G. J. Dornan, M. T. Goldsmith, and R. F. LaPrade. An In Vitro Robotic Assessment of the Anterolateral Ligament, Part 1: Secondary Role of the Anterolateral Ligament in the Setting of an Anterior Cruciate Ligament Injury. *The American Journal of Sports Medicine*, 44(3):585–592, March 2016.

[199] R. J. Reynolds, P. S. Walker, and J. Buza. Mechanisms of anterior-posterior stability of the knee joint under load-bearing. *Journal of Biomechanics*, 57:39–45, May 2017.

[200] M. A. Ritter, K. E. Davis, J. B. Meding, J. L. Pierson, M. E. Berend, and R. A. Malinzak. The effect of alignment and BMI on failure of total knee replacement. *The Journal of Bone and Joint Surgery. American Volume*, 93(17):1588–1596, September 2011.

[201] A. Roaas and G. B. Andersson. Normal range of motion of the hip, knee and ankle joints in male subjects, 30-40 years of age. *Acta Orthopaedica Scandinavica*, 53(2):205–208, April 1982.

[202] J. R. Robinson, A. M. J. Bull, R. R. deW. Thomas, and A. A. Amis. The Role of the Medial Collateral Ligament and Posteromedial Capsule in Controlling Knee Laxity. *American Journal of Sports Medicine*, 34(11):1815–1823, July 2006.

[203] J. D. Roth, S. M. Howell, and M. L. Hull. Native Knee Laxities at 0°, 45°, and 90° of Flexion and Their Relationship to the Goal of the Gap-Balancing Alignment Method of Total Knee Arthroplasty. *J Bone Joint Surg Am*, 97(20):1678–1684, October 2015.

[204] J. D. Roth, S. M. Howell, and M. L. Hull. An Improved Tibial Force Sensor to Compute Contact Forces and Contact Locations In Vitro After Total Knee Arthroplasty. *Journal of Biomechanical Engineering*, 139(4):041001, February 2017.

[205] K. S. Rudolph, M. J. Axe, T. S. Buchanan, J. P. Scholz, and L. Snyder-Mackler. Dynamic stability in the anterior cruciate ligament deficient knee. *Knee Surgery, Sports Traumatology, Arthroscopy*, 9(2):62–71, March 2001.

[206] T. W. Rudy, G. A. Livesay, SL-Y. Woo, and F. H. Fu. A combined robotic/universal force sensor approach to determine in situ forces of knee ligaments. *Journal of biomechanics*, 29(10):1357–1360, 1996.

[207] T. Saari, R. Tranberg, R. Zügner, J. Uvehammer, and J. Kärrholm. Changed gait pattern in patients with total knee arthroplasty but minimal influence of tibial insert design: Gait analysis during level walking in 39 TKR patients and 18 healthy controls. *Acta Orthopaedica*, 76(2):253–260, January 2005.

[208] M. Sakane, G. A. Livesay, R. J. Fox, T. W. Rudy, T. J. Runco, and S. Woo. Relative contribution of the ACL, MCL, and bony contact to the anterior stability of the knee. *Knee Surgery, Sports Traumatology, Arthroscopy*, 7(2):93–97, 1999.

[209] R. G. Sargent. Verification and validation of simulation models. In *2007 Winter Simulation Conference*, pages 124–137, Washington, DC, USA, December 2007.

IEEE.

[210] B. Schliemann, S. Lenschow, C. Domnick, M. Herbort, J. Häberli, M. Schulze, D. Wähnert, M. J. Raschke, and C. Kösters. Knee joint kinematics after dynamic intraligamentary stabilization: cadaveric study on a novel anterior cruciate ligament repair technique. *Knee Surgery, Sports Traumatology, Arthroscopy*, 25(4):1184–1190, April 2017.

[211] J. H. Schwab, G. J. Haidukewych, A. D. Hanssen, D. J. Jacofsky, and M. W. Pagnano. Flexion instability without dislocation after posterior stabilized total knees. *Clinical Orthopaedics and Related Research*, 440:96–100, November 2005.

[212] M. Schünke. *Funktionelle Anatomie: Topographie und Funktion des Bewegungssystems*. Thieme, Stuttgart, 2000. OCLC: 50466227.

[213] M. Schünke, E. Schulte, and U. Schumacher. *Allgemeine Anatomie und Bewegungssystem*. Number LernAtlas der Anatomie / Michael Schünke, Erik Schulte, Udo Schumacher ; Illustrationen von Markus Voll, Karl Wesker[...] in Prometheus. Georg Thieme Verlag, Stuttgart New York, 5., vollständig überarbeitete auflage edition, 2018. OCLC: 1053821781.

[214] G. R. Scuderi. *Knee arthroplasty handbook techniques in total knee and revision arthroplasty ; with 75 fig.* Springer, New York, 2006.

[215] G. R. Scuderi and T. Kochhar. Management of Flexion Contracture in Total Knee Arthroplasty. *The Journal of Arthroplasty*, 22(4):20–24, June 2007.

[216] J. K. Sekiya, M. J. Haemmerle, K. J. Stabile, T. M. Vogrin, and C. D. Harner. Biomechanical Analysis of a Combined Double-Bundle Posterior Cruciate Ligament and Posterolateral Corner Reconstruction. *The American Journal of Sports Medicine*, 33(3):360–369, March 2005.

[217] K. Shino, M. Inoue, S. Horibe, H. Nakamura, and K. Ono. Measurement of anterior instability of the knee. A new apparatus for clinical testing. *The Journal of Bone and Joint Surgery. British volume*, 69-B(4):608–613, August 1987.

[218] S. J. Shultz, Y. Shimokochi, A.-D. Nguyen, R. J. Schmitz, B. D. Beynnon, and D. H. Perrin. Measurement of varus-valgus and internal-external rotational knee laxities in vivo–Part I: assessment of measurement reliability and bilateral asymmetry. *Journal of Orthopaedic Research: Official Publication of the Orthopaedic Research Society*, 25(8):981–988, August 2007.

[219] J. A. Sim, H. R. Gadikota, G. Li, J.-S.and Li, and T. J. Gill. Biomechanical Evaluation of Knee Joint Laxities and Graft Forces After Anterior Cruciate Ligament Reconstruction by Anteromedial Portal, Outside-In, and Transtibial Techniques. *The American Journal of Sports Medicine*, 39(12):2604–2610, December 2011.

[220] L. A. Stewart, M. Clarke, M. Rovers, R. D. Riley, M. Simmonds, G. Stewart, and J. F. Tierney. Preferred Reporting Items for a Systematic Review and Meta-analysis of Individual Participant Data: The PRISMA-IPD Statement. *JAMA*, 313(16):1657, April 2015.

[221] J. E. Stoddard, D. J. Deehan, A. M. J. Bull, A. W. McCaskie, and A. A. Amis.

The kinematics and stability of single-radius versus multi-radius femoral components related to Mid-range instability after TKA. *Journal of Orthopaedic Research*, 31(1):53–58, January 2013.

[222] J. F. Suggs, G. Li, S. E. Park, S. Steffensmeier, H. E. Rubash, and A. A Freiberg. Function of the anterior cruciate ligament after unicompartmental knee arthroplasty. *The Journal of Arthroplasty*, 19(2):224–229, February 2004.

[223] T. Sugita and A. A. Amis. Anatomic and biomechanical study of the lateral collateral and popliteofibular ligaments. *The American Journal of Sports Medicine*, 29(4):466–472, August 2001.

[224] T. Takahashi, J. Ansari, and H: Pandit. Kinematically Aligned Total Knee Arthroplasty or Mechanically Aligned Total Knee Arthroplasty. *The Journal of Knee Surgery*, February 2018.

[225] P. S. Trent, P. S. Walker, and B. Wolf. Ligament length patterns, strength, and rotational axes of the knee joint. *Clinical Orthopaedics and Related Research*, (117):263–270, June 1976.

[226] A. G. Tsai, C. A. Wijdicks, M. P. Walsh, and R. F. LaPrade. Comparative Kinematic Evaluation of All-Inside Single-Bundle and Double-Bundle Anterior Cruciate Ligament Reconstruction. *The American Journal of Sports Medicine*, 38(2):263–272, February 2010.

[227] H. Tsukada, Y. Ishibashi, E. Tsuda, A. Fukuda, Y. Yamamoto, and S. Toh. Biomechanical Evaluation of an Anatomic Double-Bundle Posterior Cruciate Ligament Reconstruction. *Arthroscopy: The Journal of Arthroscopic & Related Surgery*, 28(2):264–271, February 2012.

[228] J. Van den Broeck, E. Vereecke, R. Wirix-Speetjens, and J. Vander Sloten. Segmentation accuracy of long bones. *Medical Engineering & Physics*, 36(7):949–953, July 2014.

[229] A. Verneuil. *De la création d'une fausse articulation par section ou résection partielle de l'os maxillaire inférieur, comme moyen de remédier à l'ankylose vraie ou fausse de la machoire inférieure.* Rignoux, Paris, 1860.

[230] W. Viechtbauer. Conducting meta-analyses in R with the metafor package. *J Stat Softw*, 36(3):1–48, 2010.

[231] T. M. Vogrin, J. Höher, A. \AArøen, S. LY Woo, and C. D. Harner. Effects of sectioning the posterolateral structures on knee kinematics and in situ forces in the posterior cruciate ligament. *Knee Surgery, Sports Traumatology, Arthroscopy*, 8(2):93–98, 2000.

[232] B. Walldius. Arthroplasty of the knee using an endoprosthesis. *Acta Orthopaedica Scandinavica. Supplementum*, 24:1–112, 1957.

[233] C. J. Wang and P. S. Walker. Rotatory laxity of the human knee joint. *The Journal of Bone and Joint Surgery. American Volume*, 56(1):161–170, January 1974.

[234] D. C. Wascher, K. L. Markolf, M. S. Shapiro, and G. A. Finerman. Direct in vitro

measurement of forces in the cruciate ligaments. Part I: The effect of multiplane loading in the intact knee. *The Journal of Bone and Joint Surgery. American Volume*, 75(3):377–386, March 1993.

[235] H. T. Weiler, G. Pap, and F. Awiszus. The role of joint afferents in sensory processing in osteoarthritic knees. *Rheumatology (Oxford, England)*, 39(8):850–856, August 2000.

[236] A. Weimann, I. Schatka, M. Herbort, A. Achtnich, T. Zantop, M. Raschke, and W. Petersen. Reconstruction of the Posterior Oblique Ligament and the Posterior Cruciate Ligament in Knees With Posteromedial Instability. *Arthroscopy: The Journal of Arthroscopic & Related Surgery*, 28(9):1283–1289, September 2012.

[237] L. M. Westover, N. Sinaei, J. C. Küpper, and J. L. Ronsky. Quantifying in vivo laxity in the anterior cruciate ligament and individual knee joint structures. *Computer Methods in Biomechanics and Biomedical Engineering*, 19(14):1567–1577, November 2016.

[238] L. A. Whiteside. Selective ligament release in total knee arthroplasty of the knee in valgus. *Clinical Orthopaedics and Related Research*, (367):130–140, October 1999.

[239] C. A. Wijdicks, D. T. Ewart, D. J. Nuckley, S. Johansen, L. Engebretsen, and R. F. Laprade. Structural properties of the primary medial knee ligaments. *The American Journal of Sports Medicine*, 38(8):1638–1646, August 2010.

[240] C. A. Wijdicks, N. I. Kennedy, M. T. Goldsmith, B. M. Devitt, M. P. Michalski, A. Årøen, L. Engebretsen, and R. F. LaPrade. Kinematic Analysis of the Posterior Cruciate Ligament, Part 2: A Comparison of Anatomic Single- Versus Double-Bundle Reconstruction. *The American Journal of Sports Medicine*, 41(12):2839–2848, December 2013.

[241] C. A. Wijdicks, M. P. Michalski, M. T. Rasmussen, M. T. Goldsmith, N. I. Kennedy, M. Lind, L. Engebretsen, and R. F. LaPrade. Superficial Medial Collateral Ligament Anatomic Augmented Repair Versus Anatomic Reconstruction: An In Vitro Biomechanical Analysis. *The American Journal of Sports Medicine*, 41(12):2858–2866, December 2013.

[242] F. C. Wilson. Total replacement of the knee in rheumatoid arthritis. A prospective study of the results of treatment with the Walldius prosthesis. *The Journal of Bone and Joint Surgery. American Volume*, 54(7):1429–1443, October 1972.

[243] W. T. Wilson, A. H. Deakin, A. P. Payne, F. Picard, and S. C. Wearing. Comparative analysis of the structural properties of the collateral ligaments of the human knee. *The Journal of Orthopaedic and Sports Physical Therapy*, 42(4):345–351, April 2012.

[244] D. C. Wirtz, editor. *Knie*. Number Bd. 3 in AE-Manual der Endoprothetik. Springer, Heidelberg, 2011. OCLC: 682148329.

[245] S. Woo, R. E. Debski, J. D. Withrow, and M. A. Janaushek. Biomechanics of Knee Ligaments. *The American Journal of Sports Medicine*, 27(4):533–543, July 1999.

[246] S. Woo, A. Kanamori, J. Zeminski, M. Yagi, C. Papageorgiou, and F. H. Fu. The effectiveness of reconstruction of the anterior cruciate ligament with hamstrings and

patellar tendon: a cadaveric study comparing anterior tibial and rotational loads. *JBJS*, 84(6):907–914, 2002.

[247] S. L. Woo, J. M. Hollis, D. J. Adams, R. M. Lyon, and S. Takai. Tensile properties of the human femur-anterior cruciate ligament-tibia complex. The effects of specimen age and orientation. *The American Journal of Sports Medicine*, 19(3):217–225, June 1991.

[248] Y. Xu, J. Liu, S. Kramer, C. Martins, Y. Kato, M. Linde-Rosen, P. Smolinski, and F. H. Fu. Comparison of In Situ Forces and Knee Kinematics in Anteromedial and High Anteromedial Bundle Augmentation for Partially Ruptured Anterior Cruciate Ligament. *The American Journal of Sports Medicine*, 39(2):272–278, February 2011.

[249] M. Yagi, E. K. Wong, A. Kanamori, R. E. Debski, F. H. Fu, and S. Woo. Biomechanical Analysis of an Anatomic Anterior Cruciate Ligament Reconstruction. *The American Journal of Sports Medicine*, 30(5):660–666, September 2002.

[250] Y. Yamamoto, W.-H. HsuMD, S. L-Y. Woo, A. H. Van Scyoc, Y. Takakura, and R. E. Debski. Knee Stability and Graft Function After Anterior Cruciate Ligament Reconstruction. *The American Journal of Sports Medicine*, 32(8):1825–1832, December 2004.

[251] Z. Yang, A. C. Wickwire, and R. E. Debski. Development of a subject-specific model to predict the forces in the knee ligaments at high flexion angles. *Medical & Biological Engineering & Computing*, 48(11):1077–1085, November 2010.

[252] S. Zaffagnini, C. Signorelli, T. Bonanzinga, A. Grassi, H. Galán, I. Akkawi, L. Bragonzoni, F. Cataldi, and M. Marcacci. Does meniscus removal affect ACL-deficient knee laxity? An in vivo study. *Knee Surgery, Sports Traumatology, Arthroscopy*, 24(11):3599–3604, November 2016.

[253] G. Zamarra, M. B. Fisher, S. L-Y. Woo, and G. Cerulli. Biomechanical evaluation of using one hamstrings tendon for ACL reconstruction: a human cadaveric study. *Knee Surgery, Sports Traumatology, Arthroscopy*, 18(1):11–19, January 2010.

[254] T. Zantop, N. Diermann, T. Schumacher, S. Schanz, F. H. Fu, and W. Petersen. Anatomical and Nonanatomical Double-Bundle Anterior Cruciate Ligament Reconstruction: Importance of Femoral Tunnel Location on Knee Kinematics. *The American Journal of Sports Medicine*, 36(4):678–685, April 2008.

[255] T. Zantop, M. Herbort, M. J. Raschke, F. H. Fu, and W. Petersen. The Role of the Anteromedial and Posterolateral Bundles of the Anterior Cruciate Ligament in Anterior Tibial Translation and Internal Rotation. *The American Journal of Sports Medicine*, 35(2):223–227, February 2007.

[256] T. Zantop, T. Schumacher, N. Diermann, S. Schanz, M. J. Raschke, and W. Petersen. Anterolateral rotational knee instability: role of posterolateral structures. *Archives of Orthopaedic and Trauma Surgery*, 127(9):743–752, October 2007.

[257] T. Zantop, T. Schumacher, S. Schanz, M. J. Raschke, and W. Petersen. Double-bundle reconstruction cannot restore intact knee kinematics in the ACL/LCL-deficient knee. *Archives of Orthopaedic and Trauma Surgery*, 130(8):1019–1026, August 2010.

[258] I. M. Zeller, A. Sharma, W. B. Kurtz, M. R. Anderle, and R. D. Komistek. Customized versus Patient-Sized Cruciate-Retaining Total Knee Arthroplasty: An In Vivo Kinematics Study Using Mobile Fluoroscopy. *The Journal of Arthroplasty*, 32(4):1344–1350, 2017.

[259] M. Zens, P. Niemeyer, J. Ruhhammer, A. Bernstein, P. Woias, H. O. Mayr, N. P. Südkamp, and M. J. Feucht. Length Changes of the Anterolateral Ligament During Passive Knee Motion: A Human Cadaveric Study. *The American Journal of Sports Medicine*, 43(10):2545–2552, October 2015.

List of figures

List of tables

9 Curriculum Vitae

Persönliche Daten

Name:	Manuel Ferle (geb. Krämer)
Anschrift:	Arnulfstraße 8c, 83026 Rosenheim
Telefon:	+49 157 326 634 87
Email:	manuel.ferle@posteo.de

Akademische Laufbahn

10/2015 – heute	**Leibniz Universität Hannover** Promotion, Dr.-Ing. Maschinenbau
04/2011 – 10/2012	**Leibniz Universität Hannover** Master of Science, Biomedizinische Technik
03/2008 – 03/2011	**Ostbayerische Technische Hochschule Regensburg** Bachelor of Engineering, Maschinenbau
10/2005 – 08/2007	**Ostbayerische Technische Hochschule Regensburg** Mechatronik, ohne Abschluss

Beruflicher Werdegang

05/2019 – heute	**Endolab Mechanical Engineering GmbH** Leitung der Forschung und Entwicklung
11/2012 – 03/2019	**Medizinische Hochschule Hannover** Labor für Biomechanik und Biomaterialien Wissenschaftlicher Mitarbeiter
08/2011 – 10/2012	**Medizinische Hochschule Hannover** Labor für Biomechanik und Biomaterialien Wissenschaftliche Hilfskraft

03/2011 – 05/2011	**Ostbayerische Technische Hochschule Regensburg** Labor Materialflusstechnik und Robotik Wissenschaftliche Hilfskraft
05/2010 – 09/2010	**Ostbayerische Technische Hochschule Regensburg** Labor Windkanal/Strömungsmesstechnik Wissenschaftliche Hilfskraft

Auszeichnungen und Engagement

2019	**Deutsche Gesellschaft für Biomechanik** Young Investigator Award, 3. Platz
2017	**Deutsche Gesellschaft für Biomechanik** Young Investigator Award, 3. Platz
2012	**Leibniz Universität Hannover** Master of Science, Abschluss mit Auszeichnung
Gutachtertätigkeiten	IEEE/ASME Transaction on Mechatronics, International Orthopaedics, Journal of Biomechanics, The International Journal of Medical Robotics and Computer Assisted Surgery, Zeitschrift für Medizinische Physik

Patent

DE102016105208B3	Medizinisches Instrumentarium Tobias Ortmaier, Lüder Kahrs, Samuel Müller, Henning Windhagen, Manuel Krämer, Christof Hurschler, 06.07.2017

Publikationen

Vagstad T, Klungsøyr PJ, Drogset JO, Nebel D, **Ferle M**, Hurschler C, Klungsøyr JA. The novel arthroscopic subscapular sling procedure grants better stability than an arthroscopic Bankart repair in a cadaveric study. *Knee Surgery, Sports Traumatology, Arthroscopy.* 2019; Epub ahead of print.

Ferle M, Guo R, Hurschler C. The Laxity of the Native Knee: A Meta-Analysis of in Vitro Studies. *Journal of Bone and Joint Surery.* 2019; 101(12):1119-31.

Pastor MF, **Ferle M**, Hagenah J, Ellwein A, Wellmann M, Smith T. The stabilization effect of the conjoint tendon in reverse total shoulder arthroplasty. *Clinical Biomechanics.* 2019; 63:179-184.

Decker S, Meyer M, Müller CW, Krettek C, **Ferle M**. Cement augmentation as revision strategy for loosened thick-diameter non-fenestrated iliac screws - A biomechanical analysis. *Clinical Biomechanics*. 2019; 65:41-44.

Ferle M, Pastor MF, Hagenah J, Hurschler C, Smith T. Effect of humeral neck-shaft angle and glenosphere lateralization on stability of reverse shoulder arthroplasty: a cadaveric study. *Journal of Shoulder and Elbow Surgery*. 2019: 28(5):966-73.

Pastor MF, **Krämer M**, Schwarze M, Hurschler C, Smith T, Wellmann M. The effect of rotator cuff malreduction on tendon tension: an evaluation of a custom-made digital tensiometer clamp. *Archives of Orthopaedic and Trauma Surgery*. 2018; 138(2):219-25.

Schmiddem U, Hawi N, Liodakis E, Dratzidis A, **Krämer M**, Hurschler C, u. a. Monocortical fixation of the coracoid in the Latarjet procedure is significantly weaker than bicortical fixation. *Knee Surgery, Sports Traumatology, Arthroscopy*. 2018; 27(1):239-244.

Krämer M, Müller CW, Hermann M, Decker S, Springer A, Overmeyer L, u. a. Design considerations for a novel shapememory- plate osteosynthesis allowing for non-invasive alteration of bending stiffness. *Journal of the Mechanical Behavior of Biomedical Materials*. 2017; 75:558-66.

Müller S, Ahmad I, **Krämer M**, Utz M, Gaa J, Kahrs LA, u. a. Design considerations for patient-specific surgical templates for total hip arthroplasty with respect to acetabular cartilage. Biomedical Engineering / Biomedizinische Technik. 2017; 62(3).

Hawi N, Dratzidis A, **Krämer M**, Suero EM, Liodakis E, Hurschler C, u. a. Biomechanical evaluation of the simple cinch stitch for arthroscopic rotator cuff repair. *Clinical Biomechanics*. 2016; 36:21-5.

Krämer M, Bäunker A, Wellmann M, Hurschler C, Smith T. Implant impingement during internal rotation after reverse shoulder arthroplasty. The effect of implant configuration and scapula anatomy: A biomechanical study. *Clinical Biomechanics*. 2016; 33:111-6.

Krämer M, Schilling M, Eifler R, Hering B, Reifenrath J, Besdo S, u. a. Corrosion behavior, biocompatibility and biomechanical stability of a prototype magnesium-based biodegradable intramedullary nailing system. *Materials Science and Engineering:C*. 2016; 59:129-35.

Liodakis E, Dratzidis A, **Krämer M**, Hurschler C, Krettek C, Hawi A, u. a. The lasso-loop, lasso-mattress and simplecinch stitch for arthroscopic rotator cuff repair: are there biomechanical differences? *Archives of Orthopaedic and Trauma Surgery*. 2016; 136(11):1581-5.

Pastor MF, **Krämer M**, Hurschler C, Claassen L, Wellmann M, Smith T. Transfer of the long head of biceps to the conjoint tendon. A biomechanical study. *Clinical Biomechanics*. 2016; 32:80-4.

Pastor MF, **Krämer M**, Wellmann M, Hurschler C, Smith T. Anterior stability of the reverse shoulder arthroplasty depending on implant configuration and rotator cuff condition. *Archives of Orthopaedic and Trauma Surgery*. 2016; 136(11):1513-9.

Schröter S, **Krämer M,** Welke B, Hurschler C, Russo R, Herbst M, u. a. The effect of the arthroscopic augmentation of the subscapularis tendon on shoulder instability and range of motion: A biomechanical study. *Clinical Biomechanics*. 2016; 38:75-83.

Smith T, Bäunker A, **Krämer M**, Hurschler C, Kaufmann M, Pastor M, u. a. Biomechanical evaluation of inferior scapula notching of reverse shoulder arthroplasty depending on implant configuration and scapula neck anatomy. *International Journal of Shoulder Surgery*. 2015; 9(4):103.

Decker S, **Krämer M**, Marten AK, Pfeifer R, Wesling V, Neunaber C, u. a. A nickel-titanium shape memory alloy plate for contactless inverse dynamization after internal fixation in a sheep tibia fracture model: A pilot study. *Technology and Health Care*. 2015; 23(4):463-74.

Moroder P, Runer A, **Krämer M**, Fierlbeck J, Niederberger A, Cotofana S, u. a. Influence of Defect Size and Localization on the Engagement of Reverse Hill-Sachs Lesions. *The American Journal of Sports Medicine*. 2015; 43(3):542-8.

Müller CW, Pfeifer R, Meier K, Decker S, Reifenrath J, Gösling T, u. a. A Novel Shape Memory Plate Osteosynthesis for Noninvasive Modulation of Fixation Stiffness in a Rabbit Tibia Osteotomy Model. *BioMed Research International*. 2015; 2015:1-8.

Rosenheim, 3. Dezember 2019

A Appendix - Soft tissue laxity of the healthy knee joint

A.1 Search strategy used for literature search in the meta-analysis

Pubmed

("1996/01/01"[PDAT] : "2016/12/31"[PDAT]) AND (("posteromedial"[All Fields] OR "posterolateral"[All Fields] OR "medial"[All Fields] OR "lateral"[All Fields] OR "varus"[All Fields] OR "valgus"[All Fields] OR "anterior"[All Fields] OR "posterior"[All Fields] AND ("structures"[All Fields] OR "ligament"[All Fields]) AND ("in vitro techniques"[MeSH Terms] OR ("vitro"[All Fields] AND "techniques"[All Fields]) OR "in vitro techniques"[All Fields] OR "vitro"[All Fields] OR "in vitro"[All Fields]) AND ("knee"[MeSH Terms] OR "knee"[All Fields] OR "knee joint"[MeSH Terms] OR ("knee"[All Fields] AND "joint"[All Fields]) OR "knee joint"[All Fields])) OR ("cadaveric"[All Fields] AND "knee"[All Fields] AND "ligament"[All Fields] AND "biomechanical"[All Fields])) OR ("in vitro"[All Fields] AND "laxity"[All Fields] AND ("ligaments"[MeSH Terms] OR "ligaments"[All Fields] OR "ligament"[All Fields]) AND "knee"[All Fields])

Web of Science

PY=(1996-2016) AND TI=(posteromedial OR posterolateral OR medial OR lateral OR varus OR valgus OR anterior OR posterior) AND TI=(structures OR Ligament) AND TI=(vitro OR in-vitro OR biomechanica OR cadaveric) AND TI=(knee OR knee joint) OR TI=(laxity and knee)

A.2 Details of the included studies

Table A.1: Baseline characteristics of all studies included in the meta-analysis

No.	Lead author	Year	Sample size	Mean age	Age range	Sex (m/f)	Specimen condition	Thawing time	Storage temp.	Test rig design	Coordinate System
1	Ahn, J.H. [6]	2011	10	58	34-74	6/4	Y	ON	-20	CTD	N
2	Anderson, C.J. [13]	2010	12	50.9	26-66	NR	Y	ON	-20	CTD	Y
3	Bergfeld, J.A. [25]	2005	8	48.5	37-63	4/4	Y	ON	NR	MTM	Y
4	Boguszewski, D.V. [29]	2015	47	31.3	16-45	22/25	Y	NR	NR	RTD	Y
5	Diermann, N. [51]	2009	7	NR	62-78	NR	Y	24	-20	RTD	N
6	Fukubayashi, T.	1982	9	NR	54-80	NR	Y	NR	-20	MTM	N
7	Gabriel, M.T. [64]	2004	10	50	46-66	NR	Y	24	-20	RTD	N
8	Gadikota, H.R. [65]	2009	8	NR	NR	NR	Y	24	NR	RTD	N
9	Gadikota, H.R. [67]	2010	9	55	47-60	7/2	Y	24	-20	RTD	N
10	Gadikota, H.R. [66]	2011	8	NR	NR	6/2	Y	24	-20	RTD	N
11	Galloway, M.T. [69]	1996	6	NR	NR	NR	Y	12-18	-15	CTD	N
12	Goldsmith, M.T. [76]	2013	18	46.7	16-58	6/3	Y	NR	NR	RTD	Y
13	Giffin, J.R. [73]	2007	10	NR	38-71	NR	Y	24	NR	RTD	N
14	Gupte, C.M. [82]	2003	8	NR	NR	NR	N	NR	-20	MTM	Y
15	Harner, C.D. [87]	2000	10	NR	39-73	NR	Y	24	NR	RTD	N
16	Herbort, M.[92]	2010	9	NR	53-78	NR	Y	24	-20	RTD	N
17	Herbort, M. [93]	2013	9	NR	52-76	NR	N	24	-20	RTD	N
18	Herbort, M. [91]	2016	10	76.3	63-86	NR	Y	24	-20	RTD	N
19	Imhauser, C. [102]	2013	11	38	21-58	9/2	Y	36	NR	RTD	Y
20	Inderhaug, E. [103]	2017	12	57	41-63	6/6	N	24	-20	CTD	Y
21	Kanamori, A. [113]	2000	12	NR	42-69	NR	Y	24	NR	RTD	N

Table A.1: Baseline characteristics of all studies included in the meta-analysis

No.	Lead author	Year	Sample size	Mean age	Age range	Sex (m/f)	Specimen condition	Thawing time	Storage temp.	Test rig design	Coordinate System
22	Kanamori, A. [112]	2003	10	NR	40-60	NR	Y	24	-20	RTD	N
23	Kato, Y. [115]	2012	18	53.5	NR	13/5	Y	ON	-20	RTD	N
24	Kato, Y. [116]	2013	16	NR	NR	NR	Y	24	-20	RTD	N
25	Kilger, R.H.P. [123]	2005	8	53.5	NR	NR	Y	ON	-20	RTD	N
26	Kilger, R.H.P. [122]	2006	10	45	NR	NR	Y	ON	-20	RTD	N
27	Kim, S.-J. [124]	2010	36	75.7	68-84	NR	Y	24	-20	CTD	N
28	Kennedy, N.I. [119]	2014	9	52.3	29-63	6/3	Y	24	-20	RTD	Y
29	Kennedy, N.I. [119]	2014	9	52.3	29-63	6/3	Y	24	-20	RTD	Y
30	Kondo, E. [127]	2010	8	62.1	31-72	NR	N	24	-20	RTD	Y
31	Kondo, E. [128]	2011	8	59	49-71	NR	N	NR	NR	RTD	Y
32	Kondo, E. [129]	2014	14	61	31-72	NR	N	24	-20	RTD	Y
33	LaPrade, R.F. [136]	2010	11	64	43-76	NR	Y	ON	-20	CTD	N
34	Lenschow, S. [138]	2006	10	NR	49-78	NR	N	12	-20	RTD	N
35	Lertwanich, P. [139]	2011	10	57	48-65	NR	Y	24	-20	RTD	N
36	Liu, P. [143]	2013	6	46	20-58	NR	Y	24	-20	RTD	Y
37	Lim, H.-C. [142]	2012	14	63.4	59-83	NR	Y	NR	-20	CTD	Y
38	Lord, B.R. [146]	2017	9	66	54-78	4/5	Y	NR	NR	RTD	N
39	Lorenz, A. [147]	2016	10	71	NR	NR	Y	12	NR	RTD	Y
40	Ma, C.B. [150]	2000	36	NR	36-76	NR	Y	24	NR	RTD	N
41	Ma, C.B. [151]	2003	10	NR	36-65	NR	Y	24	-20	RTD	N
42	Margheritini, F. [153]	2004	10	NR	34-80	NR	Y	18	-20	RTD	N

Table A.1: Baseline characteristics of all studies included in the meta-analysis

No.	Lead author	Year	Sample size	Mean age	Age range	Sex (m/f)	Specimen condition	Thawing time	Storage temp.	Test rig design	Coordinate System
43	Markolf, K.L. [158]	2008	12	36.6	17-46	12/-	N	NR	NR	CTD	N
44	McCarthy, M.M. [163]	2013	10	55.1	45-61	NR	Y	24	NR	RTD	Y
45	Miura, K. [168]	2006	10	43.3	29-52	NR	Y	24	-20	RTD	N
46	Musahl, V. [170]	2005	10	49	35-69	NR	Y	NR	NR	RTD	N
47	Park, S.E. [181]	2004	6	NR	52-76	5/1	Y	NR	NR	RTD	N
48	Parsons, E.M. [182]	2015	11	76.3	35-92	NR	Y	24	-30	RTD	Y
49	Pearsall, A.W. [184]	1996	7	70.6	35-76	NR	N	NR	-20	CTD	Y
50	Petersen, W. [187]	2007	10	NR	54-74	NR	N	12	-20	RTD	N
51	Petersen, W. [186]	2008	10	NR	61-73	6/4	Y	NR	-20	RTD	N
52	Race, A. [194]	1998	8	60	43-81	NR	N	NR	-20	MTM	Y
53	Rasmussen, M.T. [198]	2016	10	49.3	41-64	10/-	Y	24	-20	RTD	Y
54	Robinson, J.R.[202]	2006	14	78	NR	NR	Y	NR	-20	MTM	Y
55	Roth, J.D. [203]	2016	10	69	52-93	6/4	Y	NR	NR	CTD	Y
56	Rudy, T.W. [206]	2000	10	NR	63-86	NR	N	24	NR	RTD	Y
57	Sakane, M. [208]	1999	10	NR	71-80	NR	N	NR	NR	RTD	N
58	Schliemann, B. [210]	2017	8	78	61-81	NR	N	24	-20	RTD	N
59	Sekiya, J.K. [216]	2005	10	NR	38-71	NR	Y	24	NR	RTD	N
60	Sim, J.A. [219]	2011	8	56.4	46-77	NR	Y	24	-20	RTD	N
61	Suggs, J.F. [222]	2004	7	73.1	NR	NR	N	NR	NR	RTD	Y
62	Tsai, A.G. [226]	2010	14	54	42-65	NR	Y	ON	-20	CTD	Y
63	Tsukada, H. [227]	2012	8	63.8	52-77	NR	Y	24	-80	MTM	N

Table A.1: Baseline characteristics of all studies included in the meta-analysis

No.	Lead author	Year	Sample size	Mean age	Age range	Sex (m/f)	Specimen condition	Thawing time	Storage temp.	Test rig design	Coordinate System
64	Vogrin, T.M. [231]	2000	10	NR	52-86	NR	Y	24	-20	RTD	N
65	Weimann, A. [236]	2012	10	72	55-78	06. Apr	Y	12	-20	MTM	N
66	Wijdicks, C.A. [240]	2013	18	52.6	40-59	NR	Y	24	NR	RTD	Y
67	Wijdicks, C.A. [241]	2013	18	54.8	51-59	10/8	Y	NR	NR	RTD	N
68	Woo, S.L. [246]	2002	12	37	NR	NR	Y	ON	-20	RTD	Y
69	Xu, J. [248]	2011	7	NR	NR	NR	Y	24	-20	RTD	N
70	Yagi, M. [249]	2002	10	NR	44-60	NR	Y	24	NR	RTD	N
71	Yamamoto, Y. [250]	2004	10	48.6	39-55	NR	Y	24	-20	RTD	N
72	Zamarra, G. [253]	2010	10	54	42-64	NR	Y	24	-20	RTD	N
73	Zantop, T. [255]	2007	10	NR	59-78	NR	Y	24	-20	RTD	N
74	Zantop, T. [256]	2007	10	NR	53-71	NR	Y	12	-20	RTD	N
75	Zantop, T. [254]	2008	12	NR	62-78	NR	Y	24	-20	RTD	Y
76	Zantop, T. [257]	2010	10	NR	52-74	NR	Y	24	-20	RTD	N

Table A.2: Overview of the loads and degrees of freedom applied in the single directions of all included studies.

			Applied forces						**Degrees of freedom**					
No.	Lead author	Year	Anterior / N	Posterior / N	Varus / Nm	Valgus / Nm	Internal / Nm	External / Nm	Anterior	Posterior	Varus	Valgus	Internal	External
1	Ahn, J.H.	2011	134						4					
2	Anderson, C.J.	2010	88			10	5		5			5	5	
3	Bergfeld, J.A.	2005		100						4				
4	Boguszewski, D.V.	2015	134	134	10	10	5	5	3	3	3	3	3	3
5	Diermann, N.	2009	134						NR					
6	Fukubayashi, T.	1982	125	125					3	3				
7	Gabriel, M.T.	2004	134						5					
8	Gadikota, H.R.	2009	134						5					
9	Gadikota, H.R.	2010	134						NR					
10	Gadikota, H.R.	2011			10						NR			
11	Galloway, M.R.	1996		100						5				
12	Goldsmith, M.T.	2013	88		10	10	5	5	5		5	5	5	5
13	Giffin, J.R.	2007	134	134					5	5				
14	Gupte, C.M.	2003	100	100			5	5	5	5			NR	NR
15	Harner, C.D.	2000		134						5				
16	Herbort, M.	2010	134						5					
17	Herbort, M.	2013	134						5					
18	Herbort, M.	2016	134						5					
19	Imhauser, C.	2013	134						5					
20	Inderhaug, E.	2017	90				5		5				5	

Table A.2: Overview of the loads and degrees of freedom applied in the single directions of all included studies.

			Applied forces						**Degrees of freedom**					
No.	Lead author	Year	Anterior / N	Posterior / N	Varus / Nm	Valgus / Nm	Internal / Nm	External / Nm	Anterior	Posterior	Varus	Valgus	Internal	External
21	Kanamori, A.	2000					10						5	
22	Kanamori, A.	2003		134				10		5				5
23	Kato, Y.	2012	89						5					
24	Kato, Y.	2013	89						5					
25	Kilger, R.H.P.	2005	134						5					
26	Kilger, R.H.P.	2006	134						5					
27	Kim, S.-J.	2010			3			5			NR			NR
28	Kennedy, N.I.	2014		134		10	5	5		5		5	5	5
29	Kennedy, N.I.	2014		134		10	5	5		5		5	5	5
30	Kondo, E.	2010	90				5		5				5	
31	Kondo, E.	2011	90	90			5	5	5	5			5	5
32	Kondo, E.	2014	90	90			5	5	5	5			5	5
33	LaPrade, R.F.	2010	88	88	10		5	5	NR	NR	NR		NR	NR
34	Lenschow, S.	2006		134						4				
35	Lertwanich, P.	2011	89						5					
36	Liu, P.	2013			10		5	5			5		5	5
37	Lim, H.-C.	2012	NR				NR		NR				NR	
38	Lord, B.R.	2017	90				5	5	4				4	4
39	Lorenz, A.	2016					4	4					5	5
40	Ma, C.B.	2000	134	134					5	5				

Table A.2: Overview of the loads and degrees of freedom applied in the single directions of all included studies.

			Applied forces						**Degrees of freedom**					
No.	Lead author	Year	Anterior / N	Posterior / N	Varus / Nm	Valgus / Nm	Internal / Nm	External / Nm	Anterior	Posterior	Varus	Valgus	Internal	External
41	Ma, C.B.	2003		134						5				
42	Margheritini, F.	2004		134						5				
43	Markolf, K.L.	2008	100				5		NR				NR	
44	McCarthy, M.M.	2013	134						5					
45	Miura, K.	2006	134						5					
46	Musahl, V.	2005	134						5					
47	Park, S.E.	2004		130						5				
48	Parsons, E.M.	2015	134				5		NR				NR	
49	Pearsall, A.W.	1996		100						1				
50	Petersen, W.	2007	134						NR					
51	Petersen, W.	2008		134						NR				
52	Race, A.	1998	100	100					4	4				
53	Rasmussen, M.T.	2016	88				5		NR				NR	
54	Robinson, J.R.	2006	150	150		5	5	5	5	5		NR	NR	NR
55	Roth, J.D.	2016	45	45	5	5	3	3	NR	NR	NR	NR	NR	NR
56	Rudy, T.W.	2000	100						5					
57	Sakane, M.	1999	110	110					5	5				
58	Schliemann, B.	2017	134						5					
59	Sekiya, J.K.	2005		134				5		5				5
60	Sim, J.A.	2011	134						5					

Table A.2: Overview of the loads and degrees of freedom applied in the single directions of all included studies.

			Applied forces						**Degrees of freedom**					
No.	Lead author	Year	Anterior / N	Posterior / N	Varus / Nm	Valgus / Nm	Internal / Nm	External / Nm	Anterior	Posterior	Varus	Valgus	Internal	External
61	Suggs, J.F.	2004	130	130					5	5				
62	Tsai, A.G.	2010	88	88	10	10	5	5	5	5	5	5	5	5
63	Tsukada, H.	2012		100						4				
64	Vogrin, T.M.	2000		134				5		5				5
65	Weimann, A.	2012		134						NR				
66	Wijdicks , C.A.	2013				10	5	5				NR	NR	NR
67	Wijdicks , C.A.	2013		134	10	10	5	5		5	5	5	5	5
68	Woo, S.L.	2002	134						5					
69	Xu, J.	2011	89						5					
70	Yagi, M.	2002	134						5					
71	Yamamoto, Y.	2004	134						5					
72	Zamarra, G.	2010	134						5					
73	Zantop, T.	2007	134						NR					
74	Zantop, T.	2007	134						5					
75	Zantop, T.	2008	134						NR					
76	Zantop, T.	2010	134						NR					

A.3 Supplementary material to the results

Table A.3: Asymmetry in laxity dependent on the flexion angle for the direction: anterior-posterior, varus-valgus, and internal-external rotation. Mean differences, the 95% confidence Interval (CI) and the p values are shown.

	anterior - posterior translation			**varus - valgus rotation**			**internal - external rotation**		
Flexion / deg	Mean dif. / mm	95% CI	*p* value	Mean dif. / mm	95% CI	*p* value	Mean dif. / mm	95% CI	*p* value
0	-2.64	-2.95, -2.33	<0.001	-0.17	-0.34, 0.005	0.041	1.52	0.24, 2.80	0.02
15	-0.27	-0.59, 0.06	0.10						
30	-0.77	-1.09, -0.45	<0.001	-1.85	-2.20, -1.50	<0.001	3.31	2.03, 4.59	<0.001
60	-0.73	-1.05, -0.41	<0.001	-1.38	-1.68, -1.08	<0.001	1.63	0.29, 2.97	0.02
90	-0.92	-1.25, -0.58	<0.001	0.10	-0.37, 0.16	0.045	-1.44	-2.76, -0.13	0.03

Table A.4: Change in laxity dependent on the flexion angle for the anterior and posterior direction. Mean differences, the 95% confidence Interval (CI) and the p values are shown.

	anterior translation			**posterior translation**		
Change in flexion / deg	Mean dif. / mm	95% CI	p value	Mean dif. / mm	95% CI	p value
0:15	1.74	1.55, 1.92	<0.001	0.57	0.411, 0.73	<0.001
0:30	2.55	2.23, 2.76	<0.001	0.55	0.38, 0,72	<0.001
0:60	1.71	1.50, 1.92	<0.001	-1.12	-1.28, -0.95	<0.001
0:90	0.94	0.74, 1.14	<0.001	-0.35	-0.54, -0.17	<0.001
15:30	0.81	0.58, 1.04	<0.001	-0.02	-0.18, 0.15	0.84
15:60	-0.02	-0.26, 0.21	0.85	-1.69	-1.85,-1.52	<0.001
15:90	-0.8	-1.03,-0.57	<0.001	-0.92	-1.1, -0.74	<0.001
30:60	-0.84	-1.08, -0.59	<0.001	-1.67	-1.82, -1.52	<0.001
30:90	-0.16	-1.85, -1.38	<0.001	-0.90	-1.090, -0.72	<0.001
60:90	-0.78	-1.02, -0.54	<0.001	0.77	0.58, 0.95	<0.001

Table A.5: Change in laxity dependent on the flexion angle for the varus and valgus rotation. Mean differences, the 95% confidence Interval (CI) and the p values are shown.

	varus rotation			**valgus rotation**		
Change in flexion / deg	Mean dif. / mm	95% CI	p value	Mean dif. / mm	95% CI	p value
0:30	2.42	2.14, 2.71	<0.001	3.47	3.24, 3.7	<0.001
0:60	2.24	1.94, 2.55	<0.001	2.4	2.14, 2.66	<0.001
0:90	1.61	1.30, 1.91	<0.001	4.25	3.88, 4.61	<0.001
30:60	-0.18	-0.51, 0.15	0.28	-1.076	-1.30, -0.84	<0.001
30:90	-0.82	-1.18, -0.46	<0.001	0.78	0.38, 1.18	<0.001
60:90	-0.64	-1, -0.28	<0.001	1.85	1.43, 2.26	<0.001

Table A.6: Change in laxity dependent on the flexion angle for the internal and external rotation. Mean differences, the 95% confidence Interval (CI) and the p values are shown.

	internal rotation			**external rotation**		
Change in flexion /deg	Mean dif. / mm	95% CI	p value	Mean dif. / mm	95% CI	p value
0:30	6.56	5.93, 7.19	<0.001	4.96	4.12, 5.81	<0.001
0:60	5.60	4.95, 6.26	<0.001	7.31	6.46, 8.16	<0.001
0:90	1.62	1.01, 2.24	<0.001	6.42	5.5, 7.35	<0.001
30:60	-0.96	-1.69, -0.23	0.01	2.35	1.43, 3.26	<0.001
30:90	-4.94	-5.64, -4.24	<0.001	1.45	0.46, 2.44	0.004
60:90	-3.98	-4.67, -3.27	<0.001	-0.89	-1.87, 0.09	0.075

Table A.7: Mean values and standard deviations (SD) of the anterior joint laxity with regard to the flexion angle. One column showing values of all data and one data of the most often used testing method.

	All data		**134 N, RTD**	
Flexion angle / deg	Mean tranlsation / mm	SD / mm	Mean tranlsation / mm	SD / mm
0	4.31	1.45	4.48	1.47
15	6.52	2.13	7.01	2.30
30	7.38	2.28	8.28	2.52
60	6.54	2.28	7.48	2.49
90	5.79	2.22	6.55	2.60

Table A.8: Mean values and standard deviations (SD) of the posterior joint laxity with regard to the flexion angle. One column showing values of all data and one data of the most often used testing method.

	All data		**134 N, RTD**	
Flexion angle / deg	Mean tranlsation / mm	SD / mm	Mean tranlsation / mm	SD / mm
0	5.51	1.46	6.35	1.73
15	5.57	1.44	6.18	1.36
30	5.99	1.71	6.25	2.17
60	4.74	1.58	5.04	1.96
90	5.01	1.62	5.49	1.97

Table A.9: Mean values and standard deviations (SD) of the varus joint laxity with regard to the flexion angle. One column showing values of all data and one data of the most often used testing method.

	All data		**134 N, RTD**	
Flexion angle / deg	Mean tranlsation / mm	SD / mm	Mean tranlsation / mm	SD / mm
0	2.49	1.05	2.38	0.86
30	4.30	1.26	3.70	1.34
60	4.53	1.33	4.66	1.34
90	4.92	1.33	4.72	1.38

Table A.10: Mean values and standard deviations (SD) of the valgus joint laxity with regard to the flexion angle. One column showing values of all data and one data of the most often used testing method.

	All data		**134 N, RTD**	
Flexion angle / deg	Mean tranlsation / mm	SD / mm	Mean tranlsation / mm	SD / mm
0	3.00	0.65	3.38	0.65
30	5.45	1.80	5.13	1.97
60	6.96	2.96	6.65	3.37
90	6.67	2.45	6.43	3.17

Table A.11: Mean values and standard deviations (SD) of the internal rotation joint laxity with regard to the flexion angle. One column showing values of all data and one data of the most often used testing method.

	All data		**134 N, RTD**	
Flexion angle / deg	Mean tranlsation / mm	SD / mm	Mean tranlsation / mm	SD / mm
0	10.98	3.36	11.12	4.50
30	18.27	5.46	18.50	6.08
60	19.39	5.88	20.44	6.66
90	18.09	5.86	18.08	6.37

Table A.12: Mean values and standard deviations (SD) of the external rotation joint laxity with regard to the flexion angle. One column showing values of all data and one data of the most often used testing method.

	All data		**134 N, RTD**	
Flexion angle / deg	Mean tranlsation / mm	SD / mm	Mean tranlsation / mm	SD / mm
0	11.66	4.30	12.00	4.35
30	17.00	4.93	16.04	5.22
60	17.63	5.69	18.45	5.99
90	17.84	5.71	18.28	5.97

B Appendix - In-vitro analysis of the balancing capacity of the human knee in arthroplasty procedures

Table B.1: Laxity of the knee joint in physiologic condition in anterior, posterior, inferior (translation and varus-valgus rotation (VV)) direction and varus, valgus, internal and external rotation in dependence on the flexion angle. Mean and standard deviations (SD) are presented.

	Laxity depending on the flexion angle (mean $\pm SD$)			
Direction	0°	30°	60°	90°
Anterior / mm	3.5 ± 1.9	6.9 ± 3.6	5.5 ± 2.7	4.4 ± 2.1
Posterior / mm	5.3 ± 2.0	6.7 ± 2.2	6.2 ± 3.1	5.7 ± 3.3
Inferior / mm	0.6 ± 0.5	2.2 ± 0.9	2.9 ± 2.0	2.9 ± 2.2
Inferior VV / deg	0.1 ± 0.9	1.1 ± 1.7	2.6 ± 2.7	3.1 ± 2.9
Varus / deg	1.8 ± 1.1	4.5 ± 1.6	6.0 ± 3.1	7.0 ± 4.4
Valgus / deg	1.7 ± 1.3	3.5 ± 1.8	3.4 ± 2.8	2.6 ± 1.9
Internal / deg	7.2 ± 4.5	18.9 ± 5.2	17.8 ± 6.4	16.5 ± 7.0
External / deg	10.2 ± 6.2	17.5 ± 4.5	18.9 ± 6.5	20.2 ± 7.7

Table B.2: Laxity of the knee joint after surgical approach in anterior, posterior, inferior (translation and varus-valgus rotation (VV)) direction and varus, valgus, internal and external rotation in dependence on the flexion angle. Mean and standard deviations (SD) are presented.

	Laxity depending on the flexion angle (mean $\pm SD$)			
Direction	0°	30°	60°	90°
Anterior / mm	3.5 ± 2.9	8.2 ± 4.7	7.0 ± 4.4	5.5 ± 3.0
Posterior / mm	5.2 ± 2.6	6.9 ± 2.5	6.0 ± 2.6	6.0 ± 3.2
Inferior / mm	0.7 ± 0.6	2.4 ± 1.2	2.9 ± 1.9	3.1 ± 2.0
Inferior VV / deg	-0.4 ± 0.6	-0.3 ± 1.9	0.5 ± 3.7	1.6 ± 1.1
Varus / deg	1.7 ± 1.2	4.4 ± 1.5	5.8 ± 3.2	6.9 ± 4.1
Valgus / deg	1.6 ± 1.1	3.3 ± 1.4	3.0 ± 1.2	3.3 ± 3.8
Internal / deg	7.3 ± 5.5	20.8 ± 6.1	20.7 ± 7.7	19.0 ± 8.2
External / deg	9.2 ± 6.7	17.2 ± 3.8	18.9 ± 5.6	20.8 ± 6.9

Table B.3: Laxity of the knee joint in menisci deficient condition in anterior, posterior, inferior (translation and varus-valgus rotation (VV)) direction and varus, valgus, internal and external rotation in dependence on the flexion angle. Mean and standard deviations (SD) are presented.

	Laxity depending on the flexion angle (mean $\pm SD$)			
Direction	0°	30°	60°	90°
Anterior / mm	3.9 ± 2.9	10.0 ± 5.2	8.7 ± 6.0	7.6 ± 5.6
Posterior / mm	6.1 ± 3.0	6.3 ± 2.1	5.5 ± 2.5	5.5 ± 2.7
Inferior / mm	0.9 ± 0.7	3.1 ± 1.2	3.6 ± 1.8	4.1 ± 2.2
Inferior VV / deg	-0.7 ± 0.9	-1.6 ± 2.0	-1.0 ± 3.6	0.2 ± 5.1
Varus / deg	2.1 ± 1.4	4.4 ± 1.8	5.7 ± 2.6	7.6 ± 2.8
Valgus / deg	2.1 ± 1.6	4.3 ± 1.9	4.1 ± 2.0	3.7 ± 2.0
Internal / deg	8.5 ± 6.0	23.4 ± 7.2	24.3 ± 9.1	23.3 ± 9.2
External / deg	10.6 ± 7.3	17.1 ± 5.7	18.0 ± 5.6	19.4 ± 5.5

Table B.4: Laxity of the knee joint in menisci and ACL deficient condition in anterior, posterior, inferior (translation and varus-valgus rotation (VV)) direction and varus, valgus, internal and external rotation in dependence on the flexion angle. Mean and standard deviations (SD) are presented.

	Laxity depending on the flexion angle (mean $\pm SD$)			
Direction	0°	30°	60°	90°
Anterior / mm	8.3 ± 4.4	18.5 ± 5.0	15.6 ± 7.1	13.0 ± 7.1
Posterior / mm	6.6 ± 2.7	6.4 ± 2.2	5.3 ± 2.6	5.8 ± 3.3
Inferior / mm	1.3 ± 0.9	3.4 ± 1.5	4.2 ± 2.3	4.5 ± 2.2
Inferior VV / deg	-0.6 ± 1.0	-1.4 ± 2.2	-1.1 ± 3.8	0.0 ± 5.3
Varus / deg	2.3 ± 1.7	4.2 ± 2.3	5.4 ± 3.2	7.0 ± 3.6
Valgus / deg	2.1 ± 1.5	3.8 ± 2.2	3.7 ± 2.3	4.6 ± 5.3
Internal / deg	9.5 ± 7.1	22.4 ± 10.4	22.8 ± 11.7	21.7 ± 11.7
External / deg	10.2 ± 7.2	15.6 ± 7.5	16.7 ± 7.7	18.2 ± 8.0

C Appendix - Investigation of an in-silico model for laxity analysis of the knee joint

C.1 Accuracy and sensitivity analysis

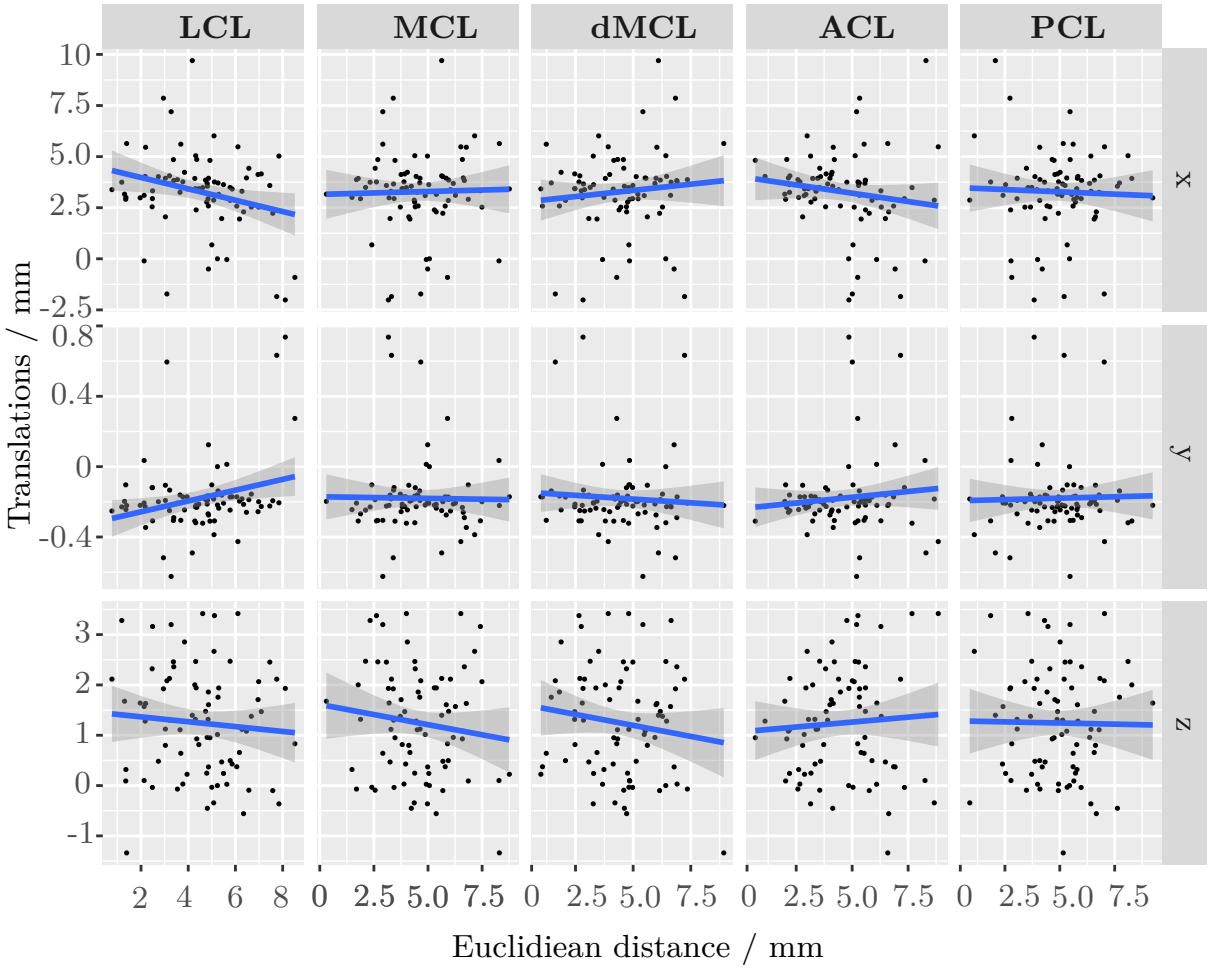

Figure C.1: Correlation of the Euclidean distances of femoral ligament attachment sites of single ligaments and the translations of the joint following an anterior load of 134 N. The Euclidean distances describe the deviations from the ligament attachment sites determined from MRI data.

C.2 Model validation

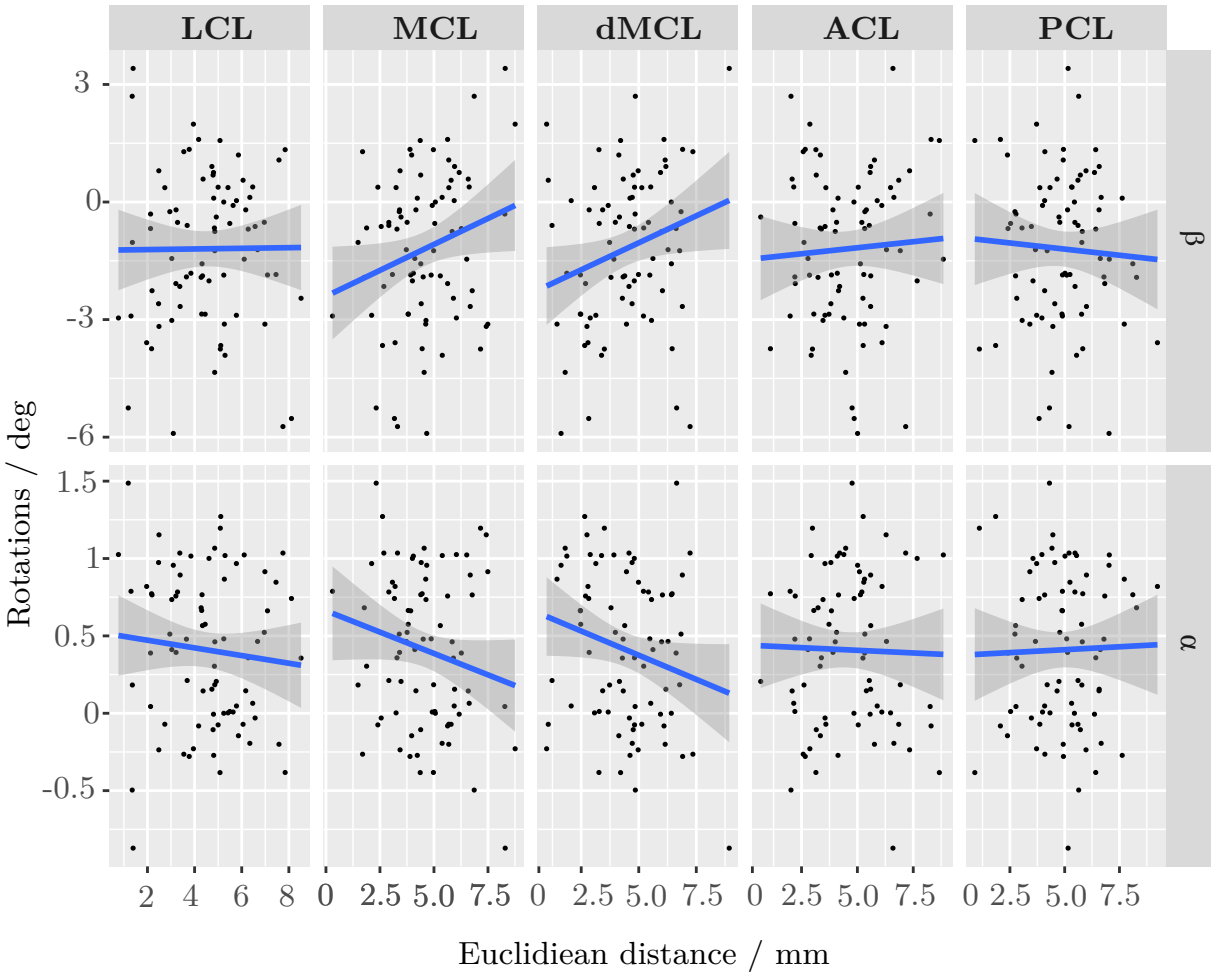

Figure C.2: Correlation of the Euclidean distances of femoral ligament attachment sites of single ligaments and the rotations of the joint following an anterior load of 134 N. The Euclidean distances describe the deviations from the ligament attachment sites determined from MRI data.

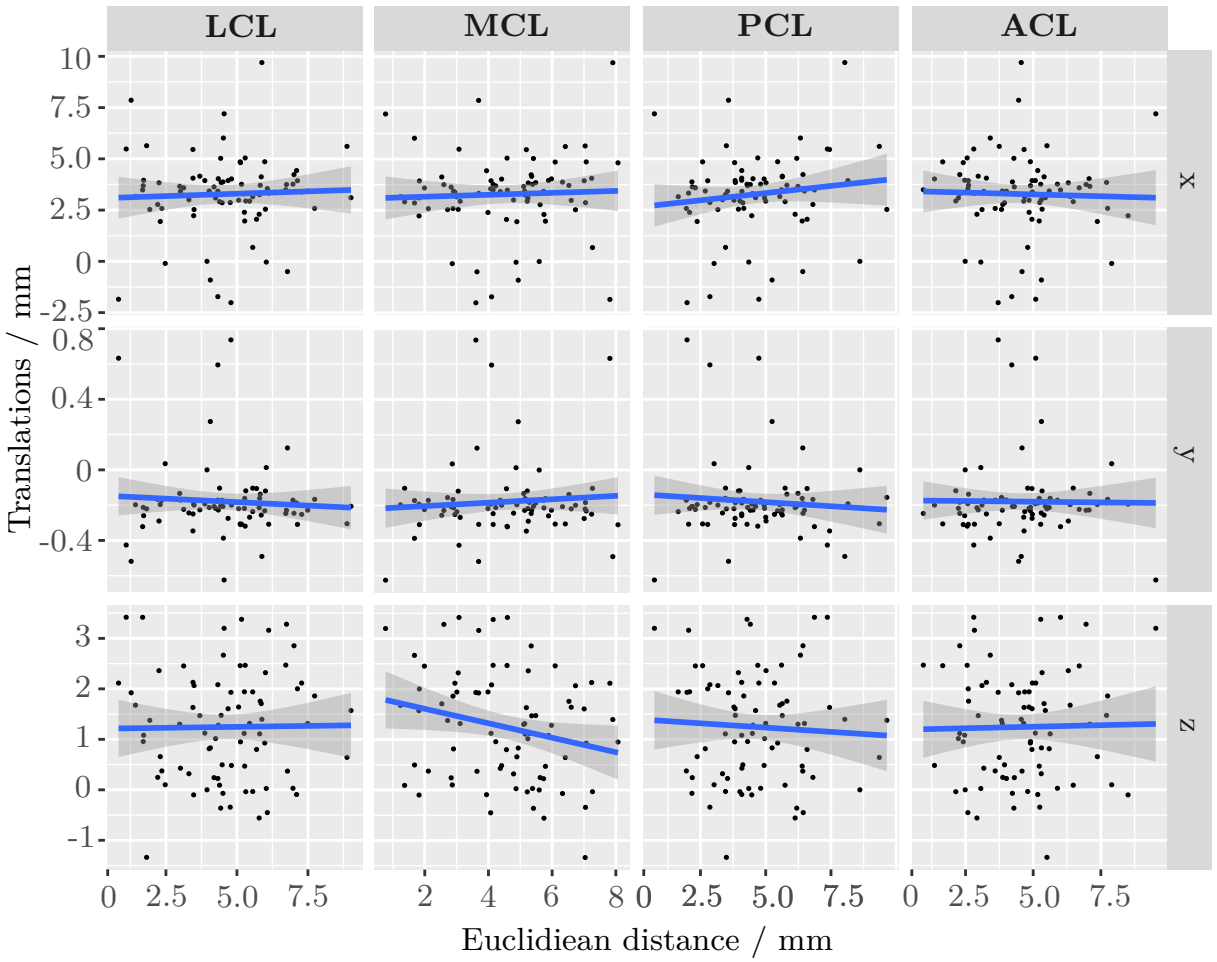

Figure C.3: Correlation of the Euclidean distances of tibial ligament attachment sites of single ligaments and the translations of the joint following an anterior load of 134 N. The Euclidean distances describe the deviations from the ligament attachment sites determined from MRI data.

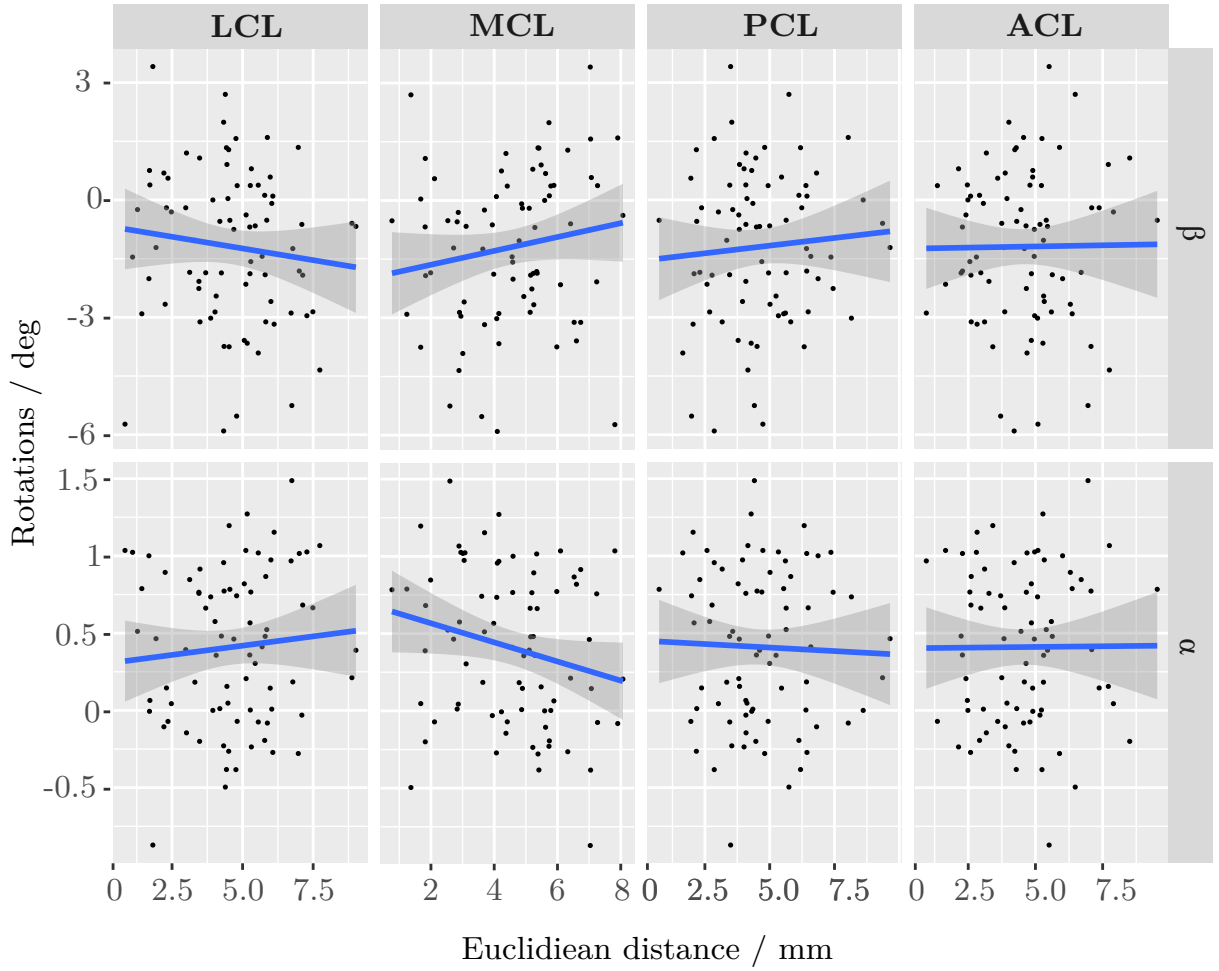

Figure C.4: Correlation of the Euclidean distances of tibial ligament attachment sites of single ligaments and the rotations of the joint following an anterior load of 134 N. The Euclidean distances describe the deviations from the ligament attachment sites determined from MRI data.

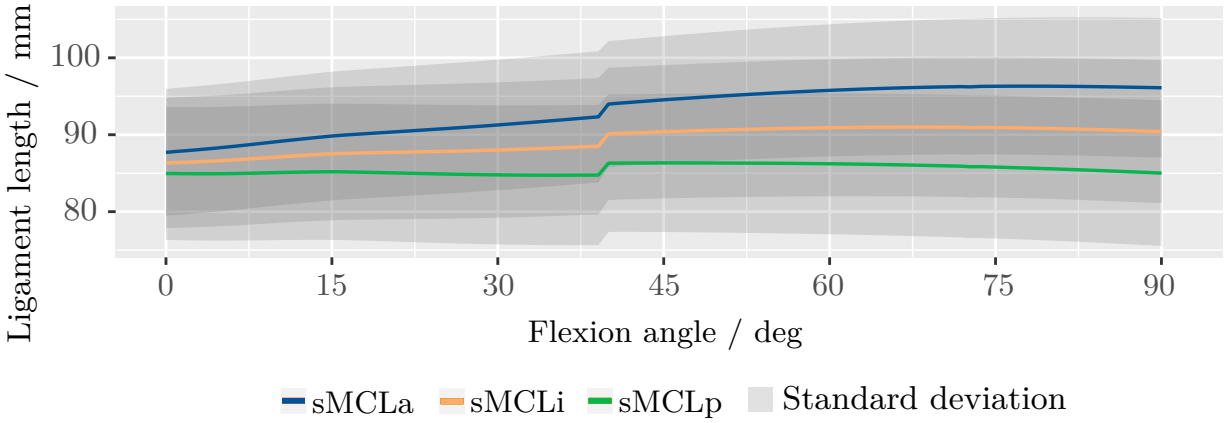

Figure C.5: Ligament length during knee flexion from 0 to 90°. Length of the anterior (sMCLa), intermediate (sMCLi), and posterior (sMCLp) bundle is given. Grey bands represent standard deviation.

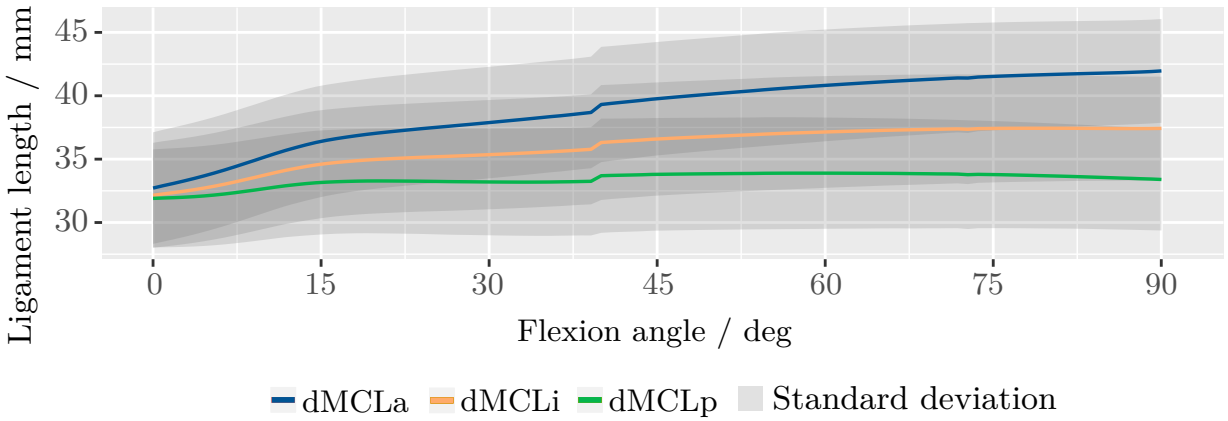

Figure C.6: Ligament length during knee flexion from 0 to 90°. Length of the anterior (dMCLa), intermediate (dMCLi), and posterior (dMCLp) bundle is given. Grey bands represent standard deviation.

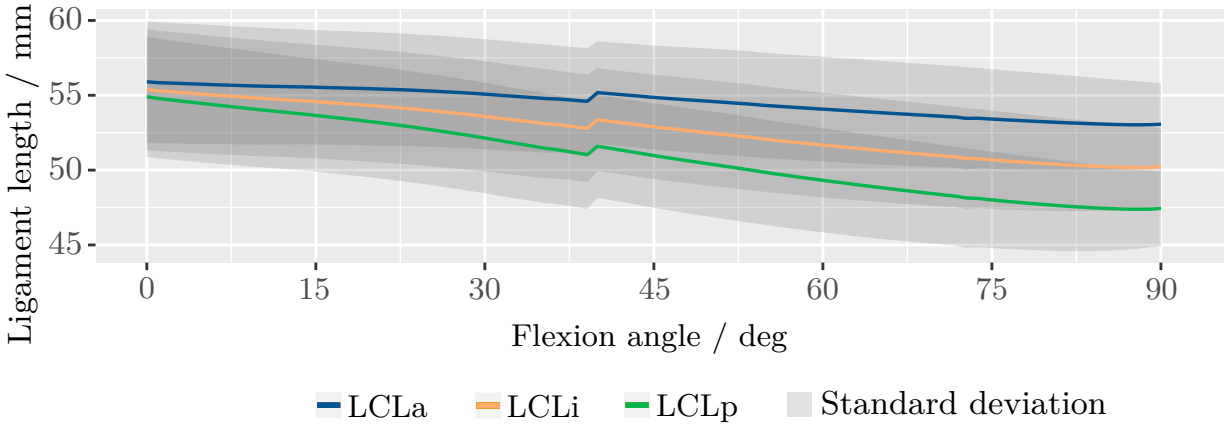

Figure C.7: Ligament length during knee flexion from 0 to 90°. Length of the anterior (LCLa), intermediate (LCLi), and posterior (LCLp) bundle is given. Grey bands represent standard deviation.

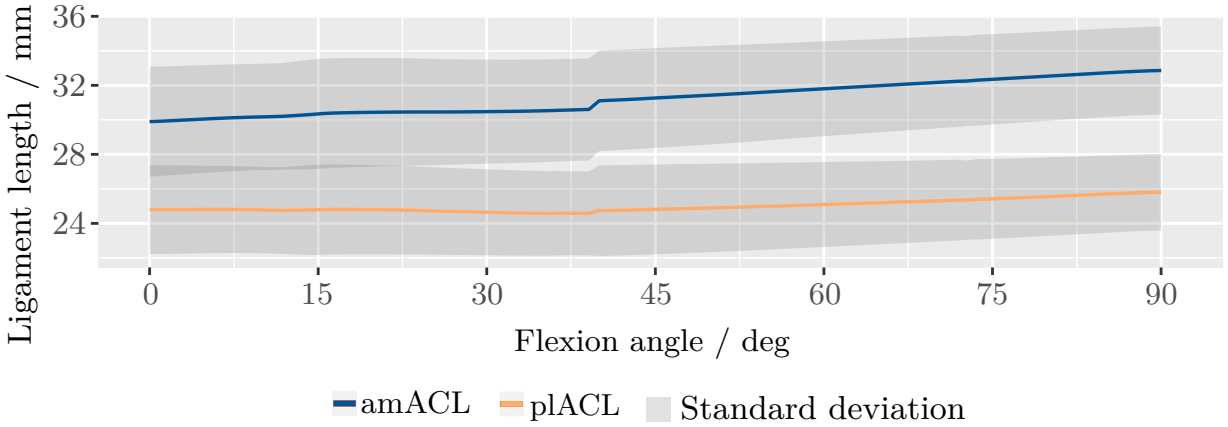

Figure C.8: Ligament length during knee flexion from 0 to 90°. Length of the anteromedial (amACL) and posterolateral (plACL) bundle is given. Grey bands represent standard deviation.

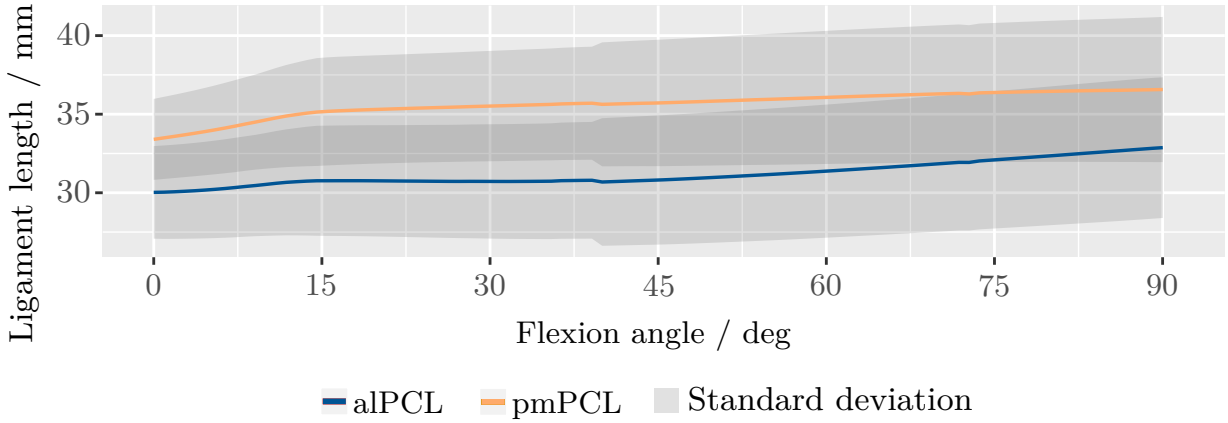

Figure C.9: Ligament length during knee flexion from 0 to 90°. Length of the anterolateral (alpCL) and posteromedial (pmPCL) bundle is given. Grey bands represent standard deviation.

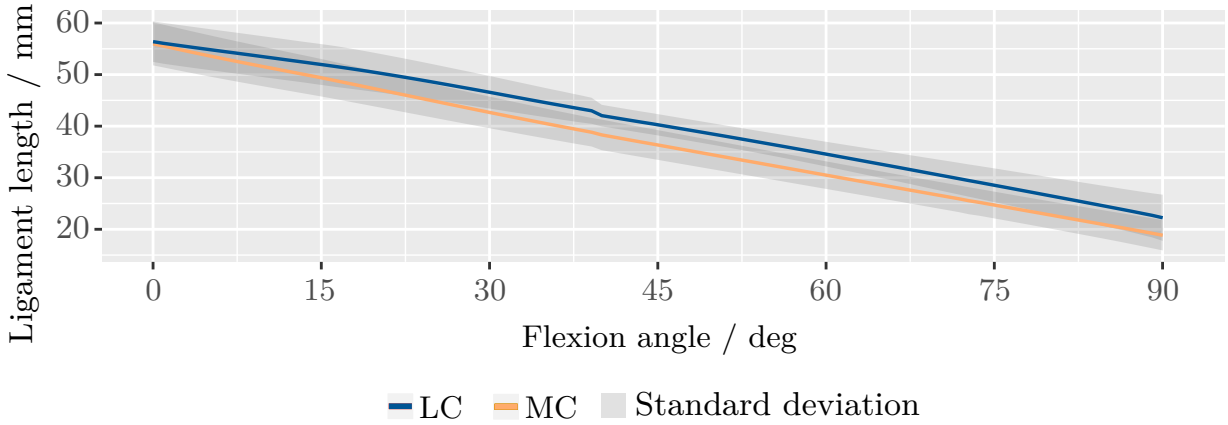

Figure C.10: Ligament length during knee flexion from 0 to 90°. Length of the medial (MC) and lateral (LC) capsule is given. Grey bands represent standard deviation.

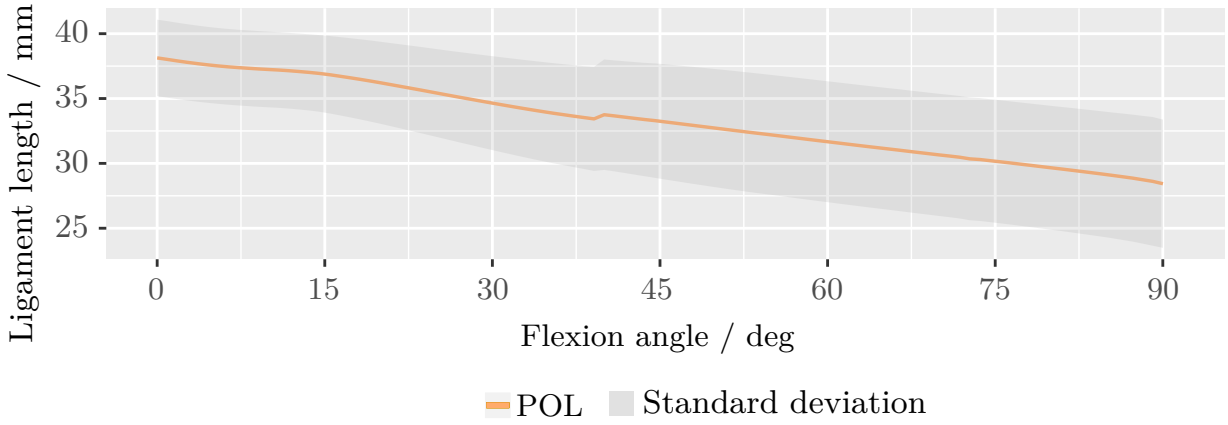

Figure C.11: POL length during knee flexion from 0 to 90°. Grey band represents standard deviation.

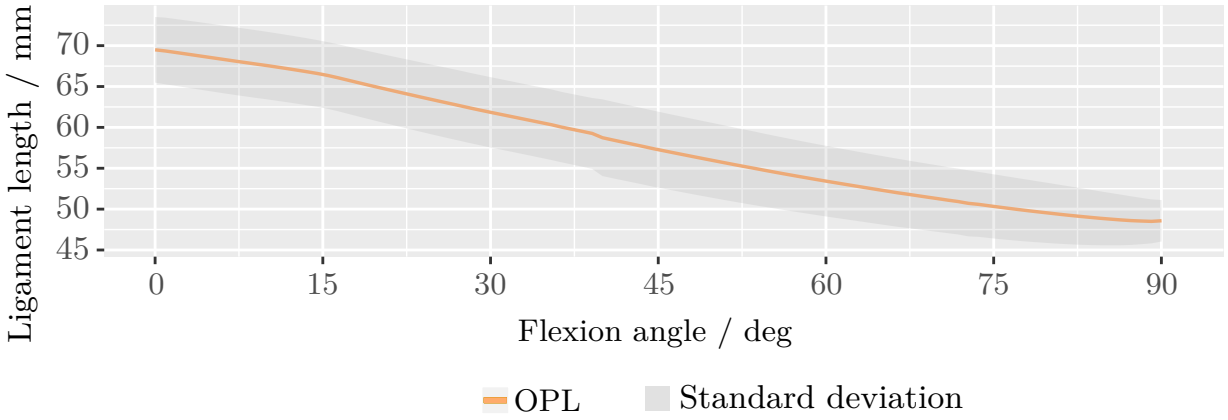

Figure C.12: OPL length during knee flexion from 0 to 90°. Grey band represents standard deviation.

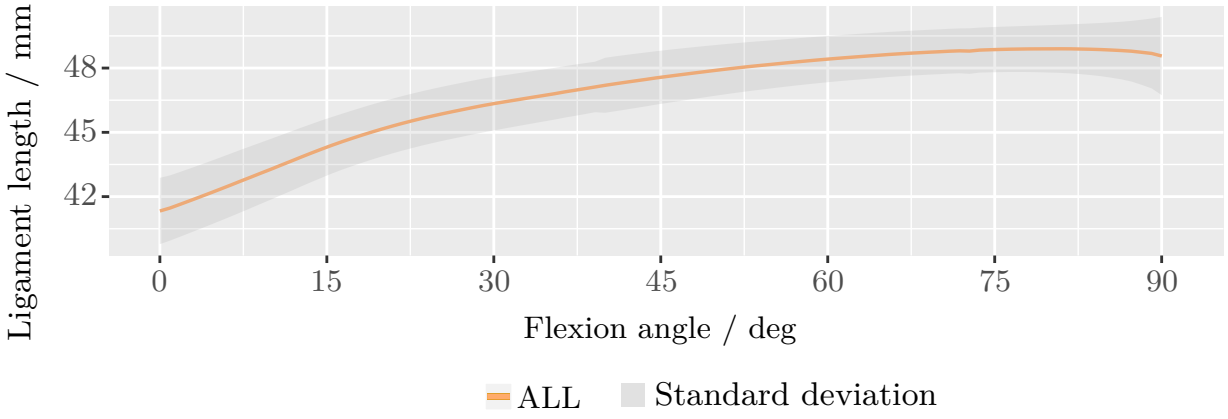

Figure C.13: ALL length during knee flexion from 0 to 90°. Grey band represents standard deviation.